

ANALYTICAL PYROLYSIS OF COAL
DEVELOPMENT OF A THERMAL DEGRADATION PROFILE

S.A. Liebman, C. Witterson, W.A. Bowe, E. J. Levy
Chemical Data Systems, Inc.
Box 74
Oxford, PA 19363

The challenge to obtain comprehensive analytical information on fossil fuels has led to the development of advanced methods in analytical pyrolysis. Extension of material science characterization techniques to coal and shales has permitted compositional data (elemental and structural) to be obtained on the solid and generated volatiles. CDS instrumentation has been successfully applied in both material sciences (1) and fossil fuel studies (2-4) with emphasis on the simulation of process conditions coupled to on-line gas chromatographic (GC) analysis. Analytical pyrolysis coupled with advanced concentrator technology is now applied to fossil fuels to provide a more complete range of information in a cost-effective manner.

Development of a thermal degradation profile involves application of controlled thermal inputs under inert and reactive atmospheres within the range of realistic process conditions. Experimental design for the coal and shales has utilized the Pyroprobe 123 system coupled to a modern GC unit with capillary column capabilities. Evolved volatiles are produced from either pulsed pyrolysis or programmed heating throughout chosen temperature intervals between 100-1000°C. Both inert and reactive atmospheres influence the nature and amount of evolved volatiles. The latter are trapped on a concentrator trap that is integral to the 123 system; the volatiles are then thermally desorbed as a sharp pulse into the GC. Since these data are obtained from weighed (milligram) amounts of coal shale samples, mass balance calculations may be obtained under the full range of imposed thermal/reactive treatments.

Figure 1 shows the FID/GC chromatogram of volatiles evolved from 5 mg of coal under an (a) oxidative (air) and (b) inert (helium) atmosphere in the low-temperature range (held at 275°C for 10 minutes). This analysis of the volatiles illustrates the type of GC pattern which, when coupled with identification and quantitation, provide the needed detailed structural information. Selected reference compounds and internal standardization procedures allow specific monitoring of substances and their fate under the chosen conditions, i.e. water, entrapped gases, etc.

In addition to the low-level thermal processing of fossil fuel samples under inert, oxidation, or reductive atmospheres, higher temperatures at varying rates may be imposed upon the samples. In Figure 2, pyrolysis patterns are shown from a coal sample treated at 60°/min to 1000°C for 32 min. under an (a) air and (b) helium atmosphere. The evolved volatiles were collected in the internal Tenax trap and subsequently thermally desorbed into the capillary GC system under the conditions given in Table 1. Other workers have shown that 1-alkene/alkane ratios are correlated to process yields from oil shales (5).

Previous studies in material sciences with complex polymer formulations for smoke, flammability, and toxicity studies have also shown that oxidative thermal treatments markedly alter the generation and reaction of polyenyl free-radicals in the solid phase (6). Certain organic/inorganic matrices produce increased cross-linking and char when pyrolyzed under oxidative (combustive) atmospheres, while increased chain-scission and greater volatilization resulted from degradation under inert (pyrolytic) atmospheres. Conjugated aromatic structures are dramatically affected by these factors.

Further studies to control and optimize the thermal degradation pathways of complex organic systems have shown that certain inorganic additives are very effective. The role of transition-metal compounds has been studied extensively (7) as smoke suppressant additives that promote extensive cross-linking in the solid phase by a proposed "reductive coupling" mechanism (7b). Hence, screening of such additives to effect the desired chain-scission and volatilization is directly accomplished by the analytical pyrolysis method. Thereby, addition of selected inorganics or organometallics to the coal or shale matrix permits optimization of degradation pathways in coal gasification, denitrification, or desulfurization processes. Illustrations will be shown to demonstrate this role of analytical pyrolysis.

Finally, in concert with the detailed monitoring of key products and the chromatographic patterns as a function of these thermal/reactive treatments, the overall elemental composition of coal and shales is important data. A unique capability of CDS instrumentation is shown in Figure 3 with the simultaneous determination of CHNS content of a typical coal sample. This analysis is accomplished by on-line reaction GC to effect standard microchemical conversions of the volatiles generated from the coal sample (heated to 1300°C in oxygen). With such data, effective N or S removal treatments may be monitored in concert with the volatile composition, since only a few milligrams are needed for these analyses.

In summary, it can be demonstrated that valuable information is generated in laboratory scale by simulation and analysis of realistic process variables of temperature, atmosphere, and catalytic additives. This data should aid on-going coal conversion process technologies as the thermal degradation profile is further developed.

References

1. S. A. Liebman, C. R. Foltz, C. I. Sanders, W. E. Beakes, T. C. Creighton, ACS 172nd Nat. Mtg., Org. Coatings & Plastics Div., San Francisco, CA Aug. 1976 "Thermal Degradation Profile of Materials with Scaling and Simulation"
2. C. S. Giam, R. E. Goodwin, P. Y. Giam, K. F. Rion, S. G. Smith, Anal. Chem. 49 1540 (1977) "Characterization of Lignites by PGC"
3. J. L. Glajch, J. A. Lubkowitz, J. Chromat. 168, 355 (1979)
4. B. K. Hovsepian, N. Amer. Thermal Anal. Soc., 12 (1980) "Anal. Pyrolysis of Fossil Fuels Using Flash Pyrolysis as a Scouting Technique".
5. T. T. Coburn, R. E. Bozak, J. E. Clarkson, J. H. Campbell, Anal. Chem., 50 958 (1978) "Correlation of Shale Oil 1-alkene/alkane Ratio with Process Yield"
6. a) S. A. Liebman, J. F. Reuwer, K. A. Gollatz, C. D. Nauman, J. Polym. Sci., Part A-1, 9 1823 (1971) Part I.
b) S. A. Liebman, D. H. Ahlstrom, E. J. Quinn, A. G. Geigley, J. T. Meluskey, Ibid. 1921 (1971) Part II.
7. a) N. J. Kroenke, J. Appl. Polym. Sci., in press.
b) R. P. Lattimer, W. J. Kroenke, Ibid.

Table 1

320 Concentrator

Sample: 5 mg coal in quartz tube/coil
Pyroprobe
Sampling: Desorber Purge 1 min., no heat
Desorber Heat 250°C for 15 min.
24" x 1/8" OD SS Tenax Trap -
20 ml/min He (or air)
Injection: Backflush Trap A at 60 ml/min.
He (split flow) at 265°C for 5
min to GC
Recondition: Backflush Trap A at 25 ml/min
He at 265°C for 10 min.

Pyrolysis

Sampling: Pyroprobe: 1000°C at 60°/min
for 30 min
Desorber Purge 1 min, no heat
Desorber Heat 250°C for 32 min,
20 ml/min He (or air)
Injection: As above
Recondition: As above

GC Analysis - Perkin Elmer, Sigma II, FID

Column: 25 x .21 mm ID flexible fused
silica WCOT OV-101
Oven: 40°C, 2 min, then 10°/min to 275°C,
10 min
Split flow: 60 ml/min He; split ratio,
60:1
Detector: Att'n x 10⁻¹² as noted
Chart: 1 cm/min

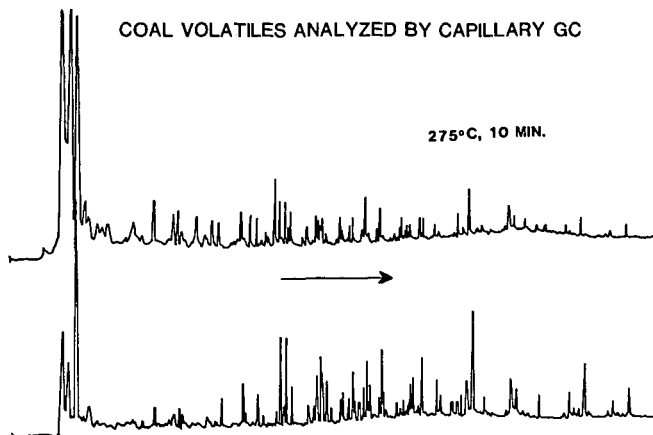


Figure 1 - Coal Volatiles Analyzed by Capillary GC - Thermal Treatment at Low Temperature (275°C, 10 min) in (a) air (b) helium

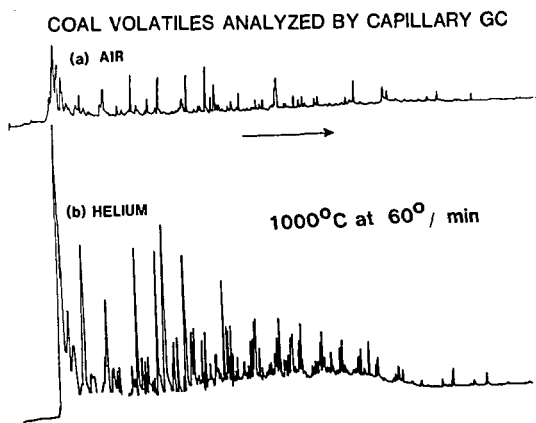


Figure 2 - Coal Volatiles Analyzed by Capillary GC - Thermal Treatment at high temperature (100° to 1000°C at 60°/min) in (a) air (b) helium

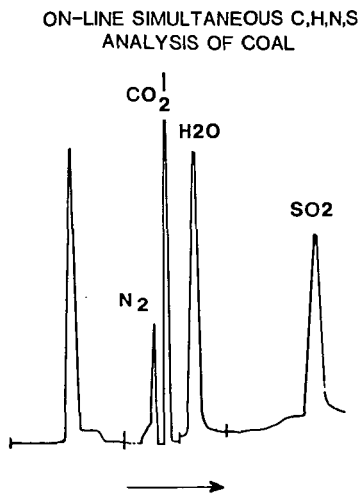


Figure 3 - On-line, Simultaneous Elemental C, H, N, S, Analysis of coal

COAL PYROLYSIS AT HIGH TEMPERATURE*

P. R. Solomon and D. G. Hamblen

Advanced Fuel Research, Inc.
87 Church Street, East Hartford, CT 06108
and

G. J. Goetz and N. Y. Nsakala

Kreisinger Development Laboratory
Combustion Engineering, Inc., Windsor, CT 06095

INTRODUCTION

This paper considers the application of a recently developed pyrolysis model to the high temperature rapid pyrolysis of coal in an entrained flow reactor. The model is based on experiments using a heated grid pyrolysis apparatus, which have helped to establish a relationship between the chemical structure of a coal and its pyrolysis products (1-9). The relationship has been incorporated into a kinetic model of thermal decomposition (1-6) which has the following general features: 1) The time and temperature dependent evolution of the products of thermal decomposition are predicted using a general set of kinetic parameters and a knowledge of the coal's structural composition; 2) the evolution of a species results from the thermal decomposition of a particular structural element within the coal at a kinetic rate which depends on the type of element but which is relatively insensitive to coal rank; 3) much of the needed structural information can be obtained from quantitative Fourier Transform Infrared (FTIR) analysis of the coal and pyrolysis products. The model has proved successful in simulating the results of vacuum thermal decomposition experiments in a heated grid for a variety of bituminous coals and lignites.

The heated grid experiment has advantages over other pyrolysis experiments in achieving good mass and elemental balances and in allowing the primary pyrolysis products to be observed with minimal secondary reactions. It has the distinct disadvantage, however, that the heating of the coal is slower than in practical devices and it is very difficult to measure or estimate the time-temperature history of the coal. While the general concepts of the thermal decomposition model and the relative magnitude of kinetic rates appear to be valid, the exact kinetic rates especially at high temperatures are uncertain. To improve the kinetic data, other experiments are needed. In one approach which has recently been reported, coal is dropped into a hot furnace and the evolving gases are monitored in-situ with a FTIR (10). This experiment verified the general features of the model but yielded higher kinetic rates. The experiment could only follow events on a time scale longer than a few hundred milliseconds due to the limit imposed by the FTIR scanning rate. Data was presented for temperatures between 500° and 800° C.

In the present investigation, results are extended to temperatures up to 1470° C and higher rates using pyrolysis experiments performed in an entrained flow reactor at Combustion Engineering. In this experiment coal is injected into a hot gas stream and after a variable residence time of 0 to 450 milliseconds, the reaction is quenched. The pyrolysis gas compositions were determined and the chars were analyzed by FTIR, elemental analysis and optical microscopy to determine the changes in char chemistry and physical appearance. The time-temperature histories of the solid particles have been calculated to provide input to the pyrolysis model. The pyrolysis model was successful in simulating the reactor data after adjustment to the kinetic rates at high temperatures.

*Work supported under EPRI contracts RP1654-6 and RP1654-7

EXPERIMENTAL

Combustion Engineering's Drop Tube Furnace System (DTFS) is similar in design to the reactors described by Nsakala et. al. (11) and Badzioch and Hawksley (12). The DTFS (Fig. 1) is comprised of a 2.54 cm inner diameter preheater, a 5.08 cm inner diameter test furnace, a fuel feeding system, and a gas analysis system. Both furnaces are powered with silicon carbide (SiC) heating elements.

The conditions of this particular experiment were as follows follows: 1) A 200 x 400 mesh size fraction of Pittsburgh seam coal was introduced by screw feeding through a water-cooled probe into the test furnace reaction zone; 2) The primary stream (comprised of the fuel fed at a rate of 1 gram/min and 15% CO₂/85% N₂ carrier gas fed at 2 liters/min) was allowed to mix rapidly with a preheated down-flowing secondary gas (15% CO₂/85% N₂) stream (fed at 28 liters/min); 3) After a variable distance (zero to 40.6 cm) the pyrolysis products were aspirated in a water-cooled probe to quench all the reactions; 4) The solids were separated from gaseous products in a small cyclone; 5) A portion of the gas sample was analyzed on-line to determine NO_x, O₂, CO, CO₂ and SO₂ concentrations; and 6) Solid samples were analyzed by FTIR; ultimate analysis and optical microscopy. Experiments were performed with furnace wall temperatures of 1370 and 1470°C. Free fall velocities of particles in these experiments were small compared with gas velocities; hence it was assumed that the particles traveled at the same velocities as the gas. Maximum residence times in the reaction zone varied from 0.342 to 0.453 sec for the higher and lower temperature, respectively.

PYROLYSIS RESULTS

The physical and chemical changes occurring during pyrolysis are characterized by the data illustrated in Figs. 2, 3, 5 and 6. Figure 2 follows the infrared spectra of solid samples collected at various positions in the reactor. The techniques for preparing and analyzing the FTIR spectra have been presented previously (2). The figure presents the absorbance from 1 mg of sample in a KBr pellet or 1 mg/1.33 cm². The data are for a wall temperature of 1370°C. The results indicate that no changes occur for the first 5 cm in the reactor. Between 5 and 10 cm the absorbance in the aliphatic stretch region at 2900 cm⁻¹ decreases, indicating a decreasing concentration of aliphatic C-H bonds which goes to zero at 20 cm. The behavior of the aromatic stretch region at 3050 cm⁻¹ indicates that the aromatic C-H concentration starts to decrease between 10 and 20 cm. The behavior of the region near 1200 cm⁻¹ indicates that the density of O-C bonds is not decreased during the initial stage of pyrolysis. The FTIR spectra for the 1470°C wall temperature are similar except that the aliphatic C-H concentration goes to zero at 10 cm and the aromatic C-H concentration at 10 cm is about the same as it is for 20 cm in the lower temperature run.

The samples were examined optically to determine physical change occurring during pyrolysis. In agreement with the FTIR results, little happens to the samples collected at 5 cm or less. At 10 cm however, the particles are observed to have become substantially swollen. By 20 cm they are well formed structures which look like foamy soap bubbles. The wall thickness in these bubbles appears to be about 1 micron. At 30 and 40 cm the bubbles appear to be more opaque and have shrunk slightly. Results for the 1370°C run showing samples collected at zero and 20 cm are presented in Fig. 3. The long dimension of the photomicrograph is 1.9 mm. The swelling increases the diameter by a factor of about 4.

CALCULATION OF TIME-TEMPERATURE HISTORIES

Calculations were made of the following quantities: 1) the average gas temperatures in the preheater, the experimental section and the collection probe; 2) the radially dependent gas temperature in the experimental section; 3) the coal particle temperatures and 4) the temperature of a thermocouple at positions along the reactor

center line. The calculations include a model for the particle swelling which is found to produce a rapid temperature rise because of the increase in surface area for absorbing radiation.

To determine both radial and longitudinal temperature profiles, calculations were performed numerically on a PDP/11 computer by considering tubular shells at progressive cross sections of the flow path. The radial gas temperatures are calculated for the primary gas core, and for n concentric rings of gas. The total calculation proceeds as follows: starting at the inlet, with the particle temperature set equal to the primary gas temperature, $n-1$ concentric gas rings set equal to the secondary gas temperature, and the outer ring fixed at the wall temperature, a system of differential equations are integrated using a Runge-Kutta integration scheme to determine the temperature of each element at the next time increment. (Note-The differential equations include: a) radiative heat transfer between the coal particles and the wall including the effects of the cold injector and collector; b) convective heat transfer between the coal and the core gas c) conductive heat transfer within the gas; and d) the heat capacities of the coal and gas). Using these new temperatures, an average temperature for the gas is calculated (the temperature after complete mixing), and this average temperature is used to calculate an average velocity, which in turn is used to calculate the axial position of the particles and the gas. The results of the calculations were compared with standard predictions for heat transfer in a pipe (13) and it was found that under the particular conditions of the experiment the additional heat transfer due to convection and turbulence (even in the collection tube) could be neglected. The general conclusion from these calculations is that the particle temperature is dominated by radiation from the hot furnace walls. The particles heat rapidly and achieve temperatures close to the wall temperatures. The local gas around the particles (e.g. the primary gas stream) is heated by conduction from the particles but the secondary gas stream is not well coupled to the particles. For this reason mixing effects appeared to be of minor importance for calculating particle temperatures in the reactor section.

The results of the calculation for the collection probe at 5 and 10 cm are shown in Fig. 4. For the 5 cm case the particle temperature rises rapidly, driven by radiative heating. The primary gas temperature also rises rapidly (much faster than in the absence of the coal) due to heat transfer from the coal. The average gas temperature is dominated by the secondary gas which is not well coupled to the coal particles and thus heats as in the case for no coal. The temperature for the coal and the gas is assumed to fall in the smaller diameter collection probe at a uniform temperature due to turbulent mixing. To cool below reaction temperatures takes about 20 milliseconds.

The particle volume is assumed to increase with the volume of evolved gases until it has reached four times its original diameter, which appeared to be the experimentally observed limit. According to the prediction at the 5 cm collection point the particle diameter starts to change slightly for the higher wall temperature experiment but not for the lower wall temperature. The volatile yield corresponding to this change would be less than 1%. These results are in agreement with the chemical and FTIR measurements of the samples for 5 cm and less which show no measurable change from the raw coal and with the visual observation of the 5 cm sample which shows some slight particle swelling for small particles in the high temperature wall case.

By 10 cm the coal for both wall temperatures has come to within 100 kelvins of the wall temperature. The coal temperature exceeds the average gas temperature because of the better radiation coupling to the wall. The particle swelling is complete for both wall temperatures in agreement with the visual observation of the samples for 10 cm and greater.

PYROLYSIS MODEL

The pyrolysis model assumes a coal structure consisting of highly substituted aromatic ring clusters containing heteroatoms linked by relatively weak aliphatic bridges. Evidence suggests that during thermal decomposition these weak links break, releasing the clusters and attached bridge fragment which comprise the tar. Simultaneous with the evolution of tar molecules is the competitive cracking of bridge fragments, substituted groups and ring clusters to form the light molecular species of the gas. The quantity of each gas species depends on the functional group distribution in the original coal. At low temperatures there is very little rearrangement of the aromatic ring structure. There is, however, decomposition of the substituted groups and aliphatic (or hydroaromatic) structures resulting in CO_2 release from the carboxyl, H_2O from hydroxyl, hydrocarbon gases from aliphatics, H_2S from mercaptans and some HCN and CO from weakly bound nitrogen and oxygen groups. At high temperature there is breaking and rearrangement of the aromatic rings. In this process, H_2 is released from the aromatic hydrogen, CS_2 from the thiophenes, HCN from ring nitrogen and additional CO from tightly bound ether linkages. As this process continues the char becomes more graphitic.

A striking feature of thermal decomposition which was observed for a variety of coals is that the temperature dependent evolution rate of a particular species is similar for all coals. This is true even though the amount of the species may vary substantially from one coal to another. These rates characterize the thermal decomposition of the various functional groups. They depend on the nature of the functional group but appear insensitive to coal rank. The differences between coals may be attributed to differences in the mix of functional groups.

The mathematical description of the pyrolysis model has been presented previously (1-6). The evolution of tar and light species provide two different mechanisms for removal of a functional group from the coal; evolution as a part of a tar molecule and evolution as a distinct species with cracking of the molecule. To model these two paths with one path yielding a product which is similar in composition to the parent coal, the coal is represented as a rectangular area with X and Y dimensions. The Y dimension is divided into fractions according to the chemical composition of the coal. Y_i^0 represents the initial fraction of a particular component (carboxyl, aromatic hydrogen, etc) and $\sum Y_i^0 = 1$. The evolution of each component into the gas (carboxyl into CO_2 , aromatic hydrogen into H_2 , etc) is represented by the first order diminishing of the Y_i dimension, $Y_i = Y_i^0 \exp(-k_i t)$. The X dimension is divided into a potential tar forming fraction X^0 and a non-tar forming fraction $1 - X^0$ with the evolution of the tar being represented by the first order diminishing of the X dimension $X = X^0 \exp(-k_t t)$. The amount of a particular component in the char is $(1 - X^0 + X)Y_i$ and the amounts in the gas and tar may be obtained by integration. In the heated grid experiment the products cool upon evolution so they undergo no further reactions. In the present experiment, the evolved products continue to react. Under these conditions it has been assumed that the decomposition of a component occurs at the same rate in the evolved product as it does in the char.

The coal compositional parameters for the Pittsburgh seam coal and the kinetic rates used in the simulation are presented in Table I. Most of the composition parameters have been obtained from elemental and FTIR analysis. The carboxyl, CO-loose and N-loose have been estimated from the parameters of a previously run Pittsburgh seam coal (5) by assuming that these components represented the same fraction of the oxygen and nitrogen in both coals. The split of the N and CO into loose and tight groups conforms to the experimental observation that these components have at least two distinct evolution rates which presumably indicate distinct chemical species. The tar was estimated from the previously measured coal, but decreased by 30% to

account for the decrease in going from vacuum to 1 atmosphere (see Ref. 9). The kinetic rates have been modified from those most recently presented (5). 1) The H_2 and CO-tight rates have been increased at high temperature to match the new experimental data. 2) The rates for the other species appeared to be adequate at high temperature. However, the recent experiments by Freihaut et al (10) suggest that they are low in the range 500-800°C. The rates of Table I are a compromise between these observations and the heated grid data. 3) The rates have also been simplified by using the same rate for tar, N-loose, CO-loose, carboxyl and hydroxyl instead of 5 slightly different rates.

RESULTS

The theory and experiment are compared in Figs. 5 and 6 for the two temperatures (1370°C and 1470°C) which were measured. Fig. 5a and 5b illustrate the char composition. The model predicts that little happens for the first 5 cm for both temperatures. At 10 cm and longer there are substantial changes especially in the hydrogen and oxygen. The model predicts a rapid decrease in the aliphatic hydrogen followed by a slower decrease in the aromatic hydrogen. This behavior is confirmed by the FTIR spectra. The model prediction for oxygen indicates an initial rapid evolution of CO_2 , H_2O and CO-loose and a slower evolution of CO-tight from ether groups. The FTIR spectra (Fig. 2) show a rapid decrease in the OH concentration indicated by the decrease in the broad peak between 3600 and 2200 cm^{-1} and the sharp peak at 1600 cm^{-1} which is attributed to an aromatic ring stretch enhanced by attached hydroxyl groups (2). (Note- The decrease in the broad band is confused by the persistence of a narrower KBr- H_2O peak at 3400 cm^{-1} . This occurs because much less sample is used for the high carbon content chars so that scaling the spectra to 1 mg/1.33 cm^2 enhances the contribution from the KBr.) As the char oxygen decreases, the CO concentration increases in agreement with the data in Figs. 5c, and 5d. Predictions for CO_2 and H_2O produced in pyrolysis are also presented. These predictions do not include secondary gas-char reactions.

Figures 6a and 6b show predictions for four additional evolved species. The stable products from the evolution of the hydrocarbons are H_2 and soot. This was observed in the heated grid experiments (3,5). The methane and acetylene are predicted to be short lived due to thermal cracking to soot and hydrogen.

Figures 6c and 6d show the overall product distribution. The experimental points are obtained using the ash tracer method (14). Unfortunately, soot may be included in varying amounts with the char. This would tend to underestimate the char concentration by a varying amount.

CONCLUSION

A pyrolysis model which was developed to simulate coal pyrolysis in a heated grid appears to be successful in simulating the high temperature pyrolysis of coal in an entrained flow reactor. The model relates evolved products to the coal structure. The structure parameters for the coal were input on the basis of the parameters obtained for a similar coal in the heated grid. No adjustments of these structure parameters were made in making the simulation. The kinetic parameters were modifications of the parameters derived from the heated grid experiments. Major changes were made in the aromatic hydrogen and CO-tight rates at high temperatures. The exponential and preexponential factors for these two components were adjusted to increase the rate in the range 1370-1470°C but held its value close to the original rates at lower temperature so that a fit is still obtained for the heated grid data.

The rates for aliphatics, tar, hydroxyl, CO-loose, N-loose and carboxyl received minor adjustments and so still fit the heated grid data.

The rates with the greatest uncertainty are those for olefin, acetylene and soot for which there is no data from the present experiment. The soot rate (the rate for

conversion of aliphatic to soot) is the highest rate in the simulation. It dominates the initial fast change in the coal. Additional experimental work is needed to sort out the effects of the aliphatic evolution and subsequent cracking to olefins, acetylene and soot.

ACKNOWLEDGEMENT

The authors wish to acknowledge the contributions of Dr. Joseph Yerushalmi (formerly of EPRI) and Dr. George Quentin of EPRI who were instrumental in bringing together the experimental and theoretical work.

REFERENCES

1. Solomon, P. R. and Colket, M. B., *Fuel*, 57, 749, (1978),.
2. Solomon, P. R., ACS Div. of Fuel Chemistry, Preprints, 24, #2, 184 and *Advances in Chemistry*, to be published, (1979),.
3. Solomon, P. R., ACS Div. of Fuel Chemistry Preprints, 24, #3, 154, (1979a),.
4. Solomon, P. R. and Colket, M. B., 17th Symposium (International) on Combustion, P. 131, the Combustion Institute, Pittsburgh, PA, (1979).
5. Solomon, P. R. and Hamblen, D. G., Understanding Coal Using Thermal Decomposition and Fourier Transform Infrared Spectroscopy, Presented at the Conference on the Chemistry and Physics of Coal Utilization, Morgantown, West Virginia, June 2-4, (1980) .
6. Solomon, P. R., *Fuel*, 60, 3, (1981),.
7. Suuberg, E. M. et al, *Ind. Eng. Chem. Process Design Develop.* 17,37, (1978),.
8. Suuberg, E. M., Peters, W. A. and Howard, J. B., Seventeenth Symposium (International) on Combustion, p. 117, The Combustion Institute, Pittsburgh, PA, (1979).
9. Suuberg, E. M., Peters, W. A. and Howard, J. B., *Am. Chem. Soc. Dir. Petrol. Chem. Preprints*, 23, (1), 175, (1977).
10. Freihaut, J. D., Solomon, P. R. and Seery, D. J., ACS, Division of Fuel Chemistry Preprints, 25, Sept., (1980).
11. Nsakala, N.-Y., Essenhigh, R. H. and Walker, P. L., Jr., *Combustion Sci. Technol.*, 16, 153, (1977).
12. Badzioch, S. and Hawksley, P. G., *W. Ind. Eng. Chem. Process Des. Dev.*, 9, 521, (1970).
13. *Heat Transfer*, Alan J. Chapman, Macmillan Publish. Co., (1980).
14. Kobayashi, H., Howard, J. B. and Sarofim, A. F., Sixteenth Symposium (International) on Combustion, The Combustion Institute, Pittsburgh, PA, 411, (1971).

TABLE I
Kinetic Rates and
Functional Group Composition for a Pittsburgh Seam Bituminous

Composition Parameter (dmmf)	Pittsburgh Seam Bituminous	Kinetic Rates	
C	.853		
H	.057		
N	.017		
S(organic)	.021		
O	.052		
S(mineral)	.014*		
CO ₂ - Carboxyl	.006	k ₁ = 5400	exp (-8850/T)
H ₂ O - 9/17 Hydroxyl	.010	k ₂ = 5400	exp (-8550/T)
CO - Ether Loose	.006	k ₃ = 5400	exp (-8850/T)
CO - Ether Tight	.062	K ₄ = 2.15 x 10 ¹⁶	exp (-57000/T)
N - Nitrogen Loose	.003	k ₅ = 5400	exp (-8850/T)
N - Nitrogen Tight	.014	k ₆ = 290	exp (-13000/T)
CH _{1.8} - Aliphatic	.276	k ₇ = 19000	exp (-11000/T)
H _{1.8} - Aromatic H	.020	K ₈ = 40644	exp (-14085/T)
C - Non Volatile	.582	K ₉ = 0	
S - Organic	.021		
Total	1.000		
Tar	.30	K _t = 5400	exp (-8850/T)
Olefins		K _o = 2 x 10 ⁹	exp (-24000/T)
Acetylene		K _a = 1 x 10 ¹⁶	exp (-50000/T)
Soot		K _s = 4 x 10 ¹⁹	exp (-60000/T)

*Dry

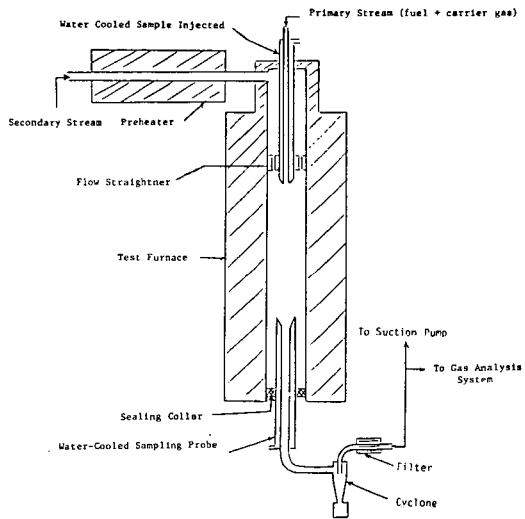


FIGURE 1 SCHEMATIC OF THE COMBUSTION ENGINEERING DROP TUBE FURNACE SYSTEM.

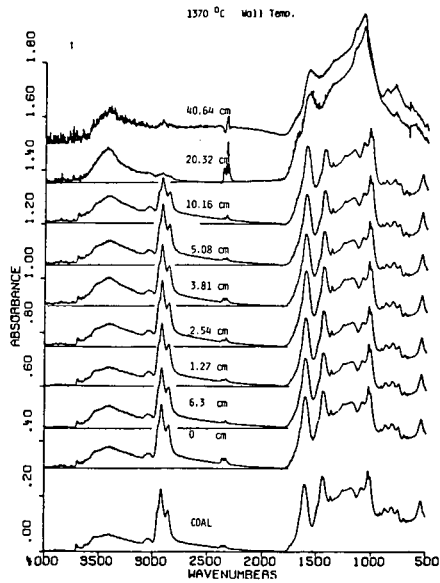
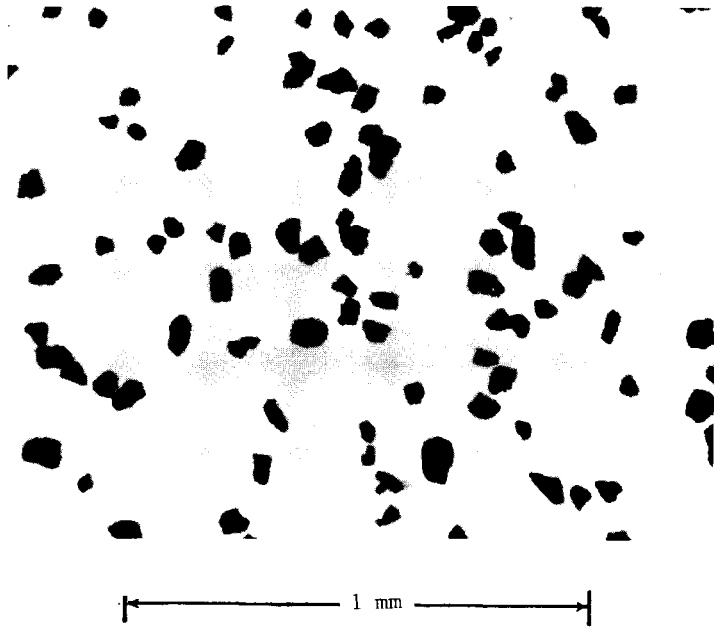


FIGURE 2. INFRARED SPECTRA OF CHARS COLLECTED IN THE DTFS

a). Char Samples at 0 cm.



b). Char Samples at 20 cm.

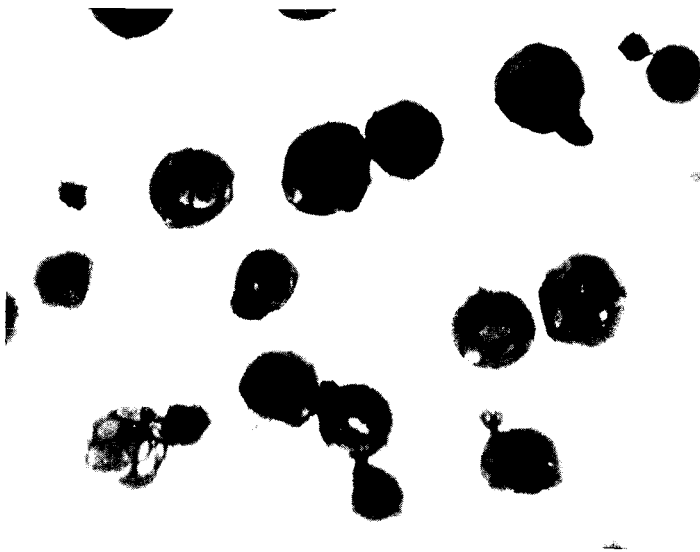


FIGURE 3. PHOTOMICROGRAPHS OF CHAR SAMPLES FROM THE DTFS

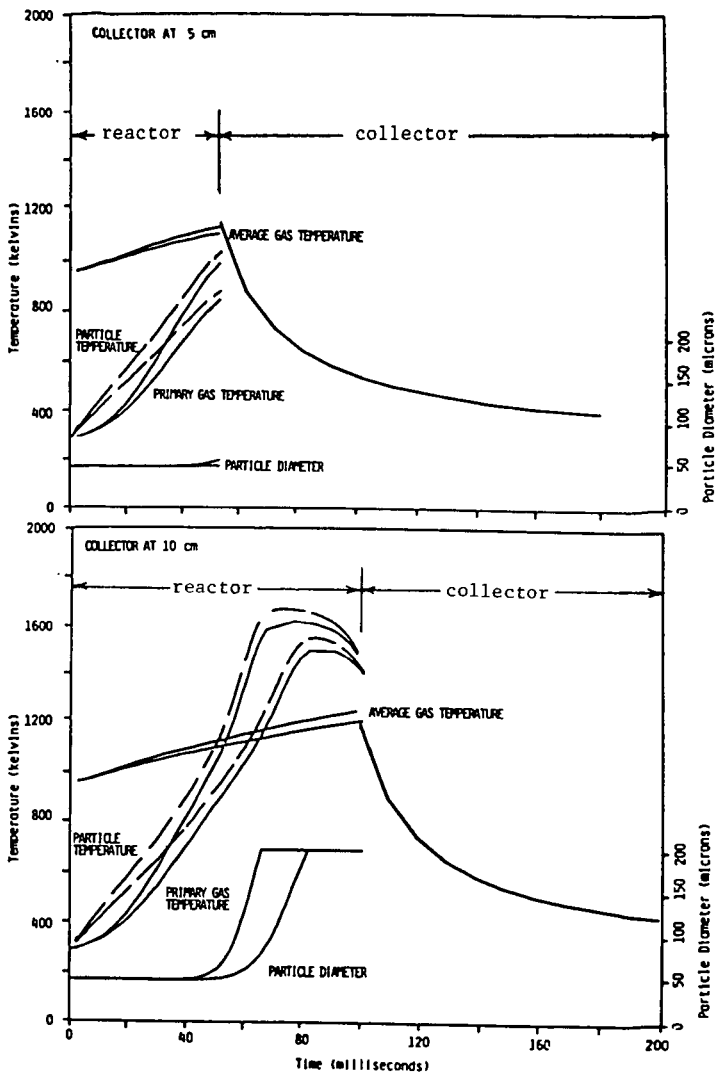
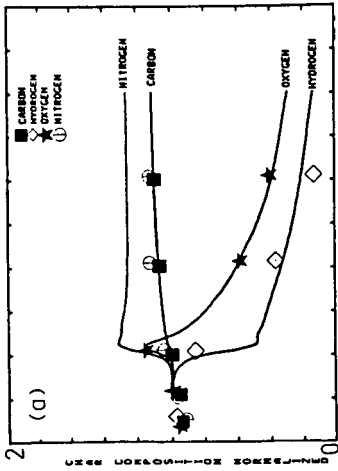


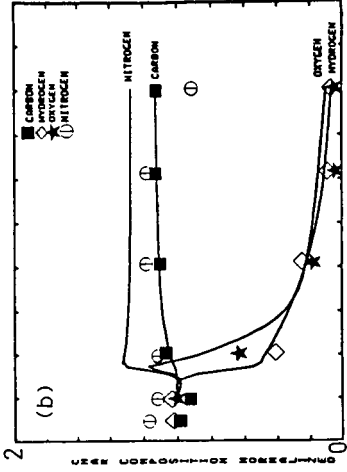
FIGURE 4.

TIME HISTORY OF TEMPERATURE AND PARTICLE DIAMETERS IN THE DTFS. Dashed lines are particle temperatures. Solid lines are the primary gas temperatures, average gas temperatures and particle diameter. A pair of curves is presented for each property. The upper curve is for a 1744 K wall temperature and the lower curve is for 1644 K.

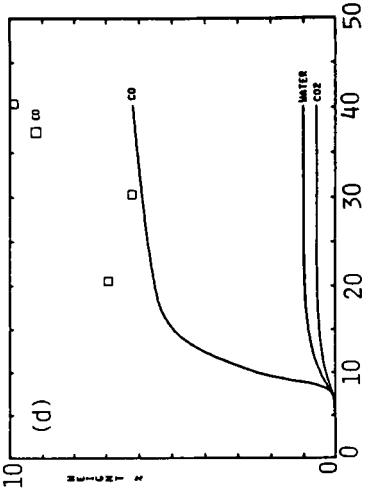
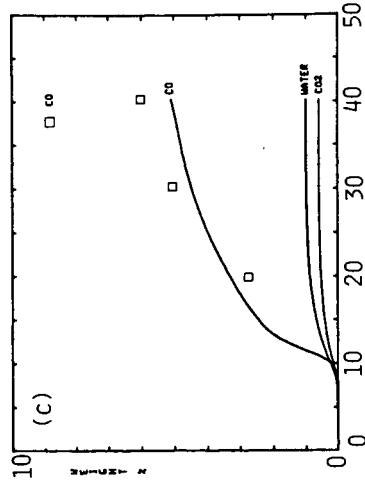
1644K



1744K

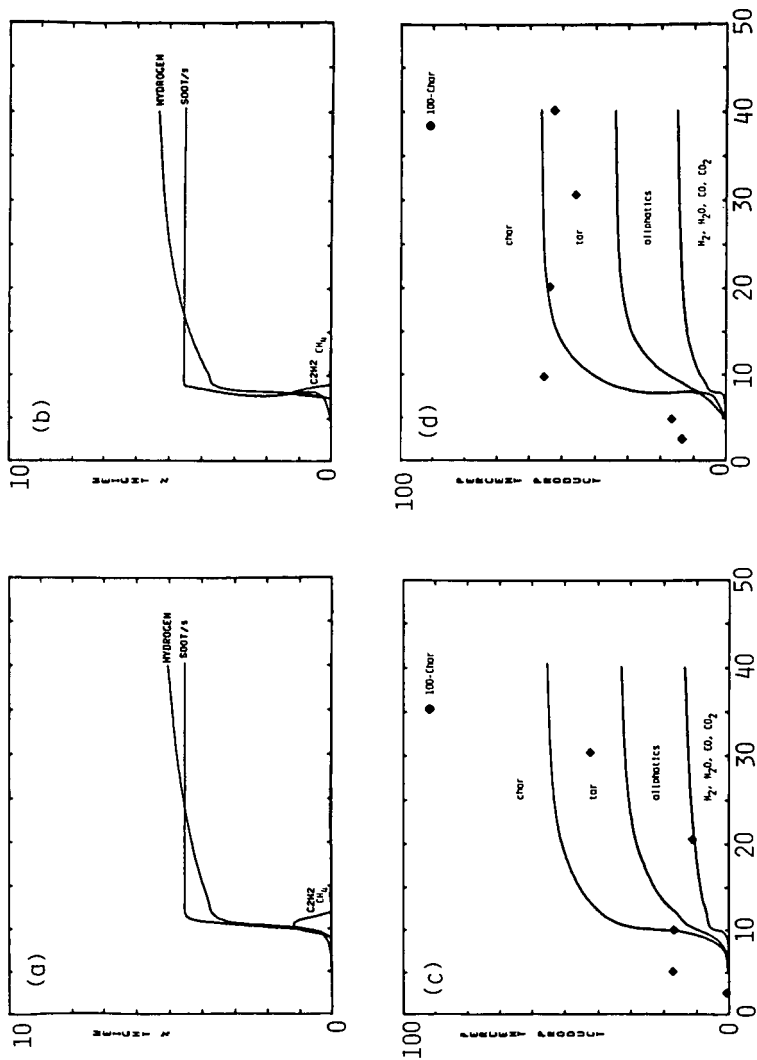


16



Distance into Reactor (cm)

FIGURE 5. PYROLYSIS PRODUCT DISTRIBUTION. Lines are predictions, symbols are experimental data. In a and b the char composition is normalized by the composition of the parent coal.



Distance into Reactor (cm)

FIGURE 6. PYROLYSIS PRODUCT DISTRIBUTION. Lines are predictions, symbols are experimental data. In c and d the symbols are for 100% - % char to correspond to the upper line.

EVOLUTION OF FUEL NITROGEN DURING
THE VACUUM THERMAL DEVOLATILIZATION OF COAL

J. D. Freihaut and D. J. Seery

United Technologies Research Center
East Hartford, CT 06108

Introduction

The fate of fuel nitrogen during the combustion or gasification of coal is a matter of practical and fundamental concern. During coal combustion, NO_x is known to form via HCN species released from the nitrogen-containing molecular components of the coal. During gasification processes, the release of nitrogen-containing fused ring compounds in evolved tar species is a matter of environmental concern. Since the thermal decomposition of the parent coal is an initial phase in both combustion and gasification, it is necessary to develop a knowledge of the fate of fuel nitrogen during thermal decomposition.

This study contains results of an investigation of the evolution of fuel nitrogen during the vacuum thermal decomposition of coal. Results are shown for variations with coal characteristics and apparent thermal history. Apparent heating rates of 75 C/sec to 2000 C/sec and final temperatures of 500 C to 1780 C were utilized. A variety of coals were investigated ranging in rank from a lignite to an anthracite.

The results indicate that nitrogen distribution in the volatiles is a sensitive function of the chemical characteristics of the parent coal. This distribution of nitrogen in the light gas, tar and char products of vacuum devolatilized coal is highly dependent on rank of the parent coal. Variations in nitrogen evolution with coal characteristics are most readily apparent in several aspects: (1) the coal nitrogen released with the tar species; (2) the release of nitrogen contained in primary tars as HCN upon secondary thermal decomposition reactions of the primary tars; (3) the retention of nitrogen in the char species.

Experimental Design

Figure 1 represents schematically the apparatus employed to perform the thermal decomposition experiments. The procedure involves placing small samples (20-50 mg) of finely ground coal (-100+325 mesh) between the folds of a fine mesh screen.

Stainless steel is used for final temperatures between 500 C and 1000 C. Tungsten is used for temperatures between 1000 C and 1780 C. The grid is driven to a predetermined temperature via the preset control circuitry. The apparent heating rate is monitored by a thermocouple bead placed between the folds of the screen.

Light gases are immediately vented through a glass wool filter into a 61 cm long infrared cell in a Fourier Transform Infrared Spectrometer. The cell was calibrated for mixtures of HCN (200, 100, 50 and 25 ppm) diluted in N₂ to a total pressure of 400 torr to avoid the uncertainties of pressure broadening by mixtures. At the end of a devolatilization run the cell and reactor chamber are filled with nitrogen to give a total pressure of 400 torr and simulate the calibration.

The control circuit in this investigation operated a Harrison power supply Model 6269A in the current program mode. In this mode heating rate and final temperature are coupled over the entire final temperature range. The coupling between heating rate and final temperature for the two screen materials can be described by a simple equation of the form $\log(\dot{T}) = mT + B$, where the parameters for each screen are given in Table I. The coupling between heating rate and final temperature is logarithmic in a manner analogous to Newton's law of heating/cooling. For the stainless steel screen the final temperature of 530 C is associated with a heating rate of ~ 100 C/sec while a final temperature of 1000 C is associated with a heating rate of 600 C/sec. The maximum heating rate obtained for the tungsten screen was ~ 2000 C/sec for a final temperature of 1780 C.

Chemical Structure Characteristics of the Coals

The coals examined in this investigation are the same as those previously reported in an investigation of tar yields and characteristics obtained from the devolatilization of the coal.¹ Detailed elemental analyses for the coals are given in Table II. Figure 2 represents the location of the coals on the coalification band as revealed by H/C and O/C values. The position of the Western bituminous coals relative to the Eastern bituminous coals reflects the differences in rank and, indirectly, geologic sources. This figure also reveals the maximum tar yields obtained from these coals. These yields are important characteristics of the devolatilization behavior of a coal as is the variation in tar yield with apparent thermal drive.¹

Figure 3 illustrates the infrared structural characteristics of the coals. Variations in infrared structural characteristics of a coal with its elemental

composition (position on the coalification band) have been previously discussed.^{2,3,4,5} The relationship of the tar yields and temperature sensitivity of tar yields to infrared structural characteristics of the parent coal has also been previously discussed.¹ Proceeding from the low rank side of the coalification band to the high rank side there is an apparent maximum in aliphatic hydrogen absorption ($\sim 3000 - 2750 \text{ cm}^{-1}$) around the location of the Utah bituminous coal ($\text{H/C} = 0.85$, $\text{O/C} = 0.13$). Such an apparent maximum is indirectly observed in the spectra of Fig. 3, normalized with respect to 1 mg of coal in a KBr pellet. It is more directly observable in plots of integrated absorbance versus sample size for each of the coals. The slopes of such plots give apparent extinction coefficients for each coal. The aliphatic extinction coefficient for the Utah coal is about 24% greater than that of the Pittsburgh seam bituminous coal. Its total hydrogen content is only about 3% greater. The greater apparent aliphatic hydrogen in the Utah bituminous coal reflects not only a difference in the amount of hydrogen present as aliphatic hydrogen, but also the nature and distribution of the molecular species to which the aliphatic hydrogen functional groups are attached.⁶

In proceeding through the coalification band it is also noted that the resolution of the aromatic hydrogen peaks ($\sim 3040 \text{ cm}^{-1}$, $680-920 \text{ cm}^{-1}$) increases with rank. This increase in resolution is reflected in the apparent aromatic hydrogen absorption coefficients of the coals. The integrated area absorption coefficients for aromatic hydrogen generally increase with rank for these coals. If the strength of the bands associated with aromatic hydrogen absorption is an indication of the aromaticity of the coal, then the spectra of these coals indicate a consistent increase in aromaticity with rank as reflected by the position on the coalification band diagram (Fig. 2).

These structural considerations are important because they lead to general understanding of the relationship between chemical structural characteristics of a coal and its primary devolatilization behavior. A previous report demonstrated that the influence of chemical structure on devolatilization for subbituminous and bituminous coals is most clearly reflected in the primary (vacuum, disperse phase, small particle size) tar yields and tar characteristics.¹ This report demonstrates that the nitrogen distribution in the primary volatiles and char residual can also be related to structural characteristics of the parent coal.

Nitrogen Distribution in the Devolatilization Products
Coal Nitrogen in the Char, Tar, Light Gas Species

Typical mass fraction distributions of the coal nitrogen in the devolatilization products are listed in Table III. Typical distributions are illustrated in Figs. 4-7. The data indicates that little (< 5%) of the coal nitrogen is evolved as HCN in those runs characterized by final temperatures of 700 C and below. In the 500 C to 700 C final temperature runs, most of the volatile nitrogen is in the tar species. As the thermal drive is increased (final temperatures - 700 C to - 950 C) HCN becomes a greater component in the volatiles nitrogen. The temperature dependence of the HCN evolution in this temperature range is coal dependent. The subbituminous and Western bituminous coals, for example, give sharper increases in HCN evolution with respect to final temperature than the Pittsburgh bituminous or Alabama bituminous.

For all of the samples examined except the anthracite, more of the coal nitrogen is evolved as an element of the tar species than as HCN in the < 1000 C runs. In the range of conditions, the retention of coal nitrogen in the char residue is similar for the subbituminous and Western bituminous coals. The fraction of coal nitrogen retained in the char is approximately the same for the same final temperature. The temperature dependent nitrogen retention in the chars of the Eastern bituminous coals (high volatile A Pittsburgh seam, Alabama medium volatile) is appreciably different than those of the subbituminous and Western bituminous coals. The chars of the Pittsburgh seam show less nitrogen variations with final temperature. The medium volatile bituminous chars show nitrogen variation with temperature similar to that of the Western bituminous but at higher levels of mass fraction retention.

Mass Fractions of Coal Nitrogen in Tar

All of the coals show substantial increases in nitrogen evolved as HCN for final temperatures above 950 C. A portion of this increase is the result of secondary cracking reactions of primary tar vapors under the conditions of increased thermal drive. As noted above, a previous study¹ on tar yields revealed that tar yields can be substantially modified by increasing the heating rate of the coal. Reduction in the tar yields by an increase in thermal drive results in a corresponding reduction in the coal nitrogen evolved in the tar. Cracking of the nitrogen - containing tar species results in the evolution of the nitrogen as HCN. The relationship between the coal nitrogen and the evolved tar species is illustrated in Figs. 8-10..

Figure 8 shows the fractions of Utah bituminous coal mass and coal nitrogen evolved as tar and as an element of the tar species for various final temperatures. Figure 9 shows plots of the mass fraction of coal evolved as tar versus the mass fraction of coal nitrogen evolved as tar, irrespective of thermal drive conditions. As the tar species are reduced by increasing the thermal drive, nitrogen is released as HCN from the tar cracking process.

Mass Fractions as CHAR

Figures 10 and 11 plot the mass fraction of the coal evolved as char versus the mass fraction of the coal nitrogen evolved as char nitrogen. As with the tar plots, upon elimination of the thermal history parameter, there is an obvious similarity in the nitrogen evolution of the subbituminous and bituminous coals. The plots indicate that the main phase of the devolatilization process is characterized by nitrogen retention in the char in proportion to the fraction of coal mass evolved as char. At mass fractions of char greater than ~ 0.5 (characterized by runs of 950 C final temperature and less) all of the chars lost retained nitrogen at a rate much greater than additional mass loss.

Phenomenological Description of Nitrogen Evolution

A phenomenological description of the evolution of coal nitrogen during vacuum devolatilization emerges from the investigation. For final temperatures of 950 C and less and apparent heating rates of 600 C/sec and less, the tar and char species generally contain 0.7 or more of the coal nitrogen. In this range of conditions, tar removes coal nitrogen in proportion to the mass fraction of coal evolved as tar. Char retains nitrogen in proportion to the mass fraction of coal evolved as char. The balance of the coal nitrogen evolves predominantly as HCN. Small but observable amounts of NH_3 are produced at low final temperatures. More NH_3 appears to be formed from low rank coals.

The distribution of the coal nitrogen in the tar, char or light gases produced during devolatilization is dependent on the rank of the parent coal in a manner analogous to the distribution of coal mass as tar, char or light gases. An increase in the fraction of volatiles evolved as tar with increase in rank results in a proportionate increase in nitrogen evolution as an element of the tar species. A decrease in tar yield with increase in thermal drive, results in a proportionate decrease in coal nitrogen evolved as tar. As the tar yield decreases, the tar nitrogen is evolved as HCN. Higher rank coals appear to produce tars more thermally stable than lower rank coals (See Reference 1).

For final temperatures greater than 950 C and heating rates in excess of 600 C/sec, Western bituminous and subbituminous coals display tar yield reductions as great as 50-60% of the maximum tar yield. The coal nitrogen evolved as tar is proportionately reduced. At volatile yields greater than ~ 0.5 of the parent coal the primary form of nitrogen evolution from the char is HCN. At these levels of conversion little increase in total volatiles by mass is observed while substantial reductions in char nitrogen levels are observed.

Relationship of Nitrogen Devolatilization Behavior to Coal Structural Characteristics, Structural Models

The chemical nature of the nitrogen distribution in the mix of molecular species present in the parent coal is indicated by the following phenomenological observations: (1) non-preferential evolution of coal nitrogen as char, tar or light gas during the devolatilization process; (2) the nitrogen distribution in the devolatilization products (tar, char, light gas) varies with rank and thermal drive as does the distribution of coal mass as char, tar and light gas; (3) HCN is the dominant nitrogen-containing light gas observed in rapid-heating; disperse phase devolatilization.

In the context of related investigations and a previous report on tar yields/ characteristics, the observations indicate: (1) nitrogen is uniformly distributed throughout the mix of molecular species present in the parent coal, irrespective of rank; (2) the primary type of nitrogen-bonding present in the parent coal is as a heteroatom in an aromatic ring system, i.e., pyridine-type; (3) variations with rank in the nitrogen distributions in the devolatilization products can be understood on the basis of a shift with rank in a condensation frequency function (the distribution of molecular species as characterized by the number of fused rings/ structure).

This devolatilization study as well as others indicate^{7,8} that HCN is the principal nitrogen-containing light gas evolved during disperse phase, rapid-heating coal devolatilization. Studies performed by Houser,⁹ et. al. and Axworthy,¹⁰ et. al. indicate HCN is the principal light gas evolved from the thermal decomposition of pyridine-type nitrogen compounds. In addition, recent studies performed by Deno, et. al.¹¹ indicate that the nitrogen present in the parent coal is found as an heteroatom in aromatic ring structures. Taking into account the known highly aromatic nature of coals, the data of this study indicate that the primary form of nitrogen appears to be as a heteroatom in aromatic ring structures.

As noted in an earlier report,¹ distinguishing features of the devolatilization behavior of a coal are its maximum tar yield and the sensitivity of tar yield to the conditions of thermal drive. It was shown, for example, that the Pittsburgh seam bituminous coal gave a maximum tar yield ~ 40% greater than the Utah bituminous coal, ~ 50% greater than either the Colorado bituminous or Alabama bituminous coals, ~ 85% greater than the two subbituminous coals. Only a small fraction of the lignite was evolved as tar and the anthracite gave only light gases. The Pittsburgh seam coal (HVA) and Alabama bituminous coal (MVB) gave tar yields which were relatively insensitive to changes in thermal drive by comparison to the Western bituminous and subbituminous coals. Total vacuum volatile yields do not vary significantly with rank until coals with characteristics of the medium volatile bituminous coal. This report indicates that the nitrogen distribution in the devolatilization products reflects these patterns.

Thus moving along the coalification band from the low rank to the high rank side, the tar yield becomes a greater fraction of the total volatiles evolved and the primary tars formed appear to be more thermally stable. Correspondingly, more of the parent coal nitrogen is evolved as tar and is retained by the thermally stable tars of these coals.

The devolatilization data, indicate that an increase in a condensation index (shift to a higher average number of the frequency function describing #fused rings/molecular species) and aromaticity of coal with position on the coalification band provides a reasonable explanation of changes in behavior with rank. The chemical nature of the nitrogen distribution in the parent coal forces the coal nitrogen devolatilization behavior to reflect the coal mass devolatilization behavior.

The variation in devolatilization behavior with rank appears to support some earlier attempts to develop a model of coal constitution based on the average number of fused rings in a molecular unit (lamella) of the coal. A model such as suggested by Ayre and Essenhig¹² and latter modified by Scaroni and Essenhig¹³ appears able to provide a reasonable explanation of behavior with some qualifications. The data of this study indicate a change in devolatilization behavior with respect to total yield at a carbon content lower than 90%. The data also indicates a change in devolatilization behavior with respect to the yields and characteristics much lower than 90%. It is believed that a statistical function of the type described above showing a pronounced shift in characteristics in the 82-85% carbon level would more adequately reflect behavior observed in these studies.

The devolatilization data of this study and the previous tar study indicate that coal does behave as if it devolatilizes in two stages. The main stage (mass fraction conversions of ~ .4-.5) of volatile evolution requires relatively low final temperatures and is followed by a second stage of volatile evolution requiring temperatures in excess of 1000 C for appreciable rates. The coal nitrogen does evolve as if it were contained in two components. The two-component hypothesis of coal constitution was first noted by Clark and Wheeler¹⁴ and later emphasized by Essenhigh and Howard¹⁵ to explain devolatilization behavior.

However, rather than identifying the easily evolved volatile matter as being generated by the weakly bonded amorphous material associated with stacked ring structures, the data suggest the easily evolved nitrogen to be associated with ring structures susceptible to thermal cracking and/or volatilization at temperatures of 950 C or below. Variations with rank in easily evolved nitrogen expelled as tar or HCN reflect variations in the ring size distribution function with rank characteristics. The Pittsburgh seam bituminous coal evolves more coal nitrogen as tar than the Utah bituminous coal because its parent nitrogen is contained in ring structures more thermally stable, that is, of greater degree of ring condensation and having fewer associated functional groups. For the same reason, the Alabama bituminous (medium volatile) coal initially expels most of its nitrogen as tar. The Alabama bituminous yields less total volatiles than the high volatile bituminous coals because a greater fraction of its nitrogen is associated with non-volatile ring structures. That is it contains a large fraction of structures too large to be volatilized before char-incorporating secondary reactions "polymerize" the species in the char matrix.

This study on nitrogen evolution and the previous study dealing with tar yields and characteristics obtained from a variety of coals indicates:

1. In vacuum devolatilization conditions, coal behaves as if it contains two volatile components, as previously noted.
2. Lignite to high volatile bituminous coals can be differentiated with respect to devolatilization yields, primarily tar yield and characteristics.
3. Coal nitrogen distribution in the volatile products for subbituminous coals and higher ranks reflects the coal mass distribution in the volatile products.

4. Coal nitrogen for subbituminous and higher rank coals behaves as if it were incorporated as an heteroatom in the aromatic ring system of the parent coal.
5. As previously noted, variations in devolatilization behavior with rank appear to reflect a variation in the degree of ring condensation present in the coal matrix.
6. Variations in devolatilization behavior (more specifically, tar and nitrogen evolution) with rank reflect a shift in the characteristics of a ring-size distribution function with rank.

TABLE I

COUPLING BETWEEN FINAL TEMPERATURE AND HEATING RATE

<u>Screen Material</u>	<u>m</u>	<u>b</u>	<u>T Range, °C</u>
Stainless steel	1.96×10^{-3}	0.92	530 - 950
Tungsten	6.50×10^{-4}	2.16	1000 - 1750

REFERENCES

1. Freihaut, J. D. and Seery, D. J., Amer. Chem. Soc. Div. of Fuel Chem. Preprints, 26, No. 2, 133 (1981).
2. Brown, J. K. and Hirsch, P. B., Nature, 175, 229 (1955).
3. Fujii, S., Osawa, Y., and Sugimura, H., Fuel, 49, 68 (1970).
4. Solomon, P. R., Amer. Chem. Soc. Div. of Fuel Chem. Preprints, 24, No. 3, 184 (1979) and Advances in Chemistry (to be published).
5. Painter, P. C., et. al. Applied Spectroscopy (to be published).
6. Bellamy, L. J. The Infrared Spectra of Complex Molecules, John Wiley & Sons, New York (1975).
7. Pohl, J. H. and Sarofim, A. F., Sixteenth Symp (Intern) on Combustion, The Combustion Institute, Pittsburgh, 491 (1979).
8. Blair, D. W., Wendt, J. D. L., and Bartok, N., Sixteenth Symp (Intern) on Combustion, The Combustion Institute, Pittsburgh, 475 (1977).
9. Houser, T. J., et. al., Int. Jr. of Chem. Kinetics, XII, 555 (1980).
10. Axworthy, A.E., et. al., Fuel, 57, 29 (1978).
11. Deno, N. C., Pennsylvania State U., Dept. of Chem, Private Communication.
12. Ayre, J. L. and Essenhigh, R. H. Sheffield Univ. Fuel Soc. Jr., 8, 44 (1957).
13. Scaroni, A. W. and Essenhigh, R. H., Amer. Chem. Soc. Div. of Fuel Chem.. Preprints, 23, No. 4, 124 (1978).
14. Clark, A. H. and Wheeler, R. V., Trans. Chem. Soc., 103, 1754 (1913).
15. Essenhigh, R. H. and Howard, J. B., The Pennsylvania State U., Studies, 31 (1971).

TABLE II

ELEMENTAL ANALYSIS (DMMF)

	Mon Lig(L)	WY Sub(S1)	WY Sub(S2)	Utah Bit(UB)	Col Bit(CB)	Pitt Bit(PB)	Ala Bit(AB)	Anth. (AN)
C	0.6827	0.7540	0.7550	0.7818	0.8100	0.8197	0.8497	0.9369
H	0.0457	0.0490	0.0517	0.0552	0.0553	0.0536	0.0463	0.0259
O	0.2547	0.1807	0.1699	0.1386	0.1119	0.0936	0.0818	0.0189
N	0.0102	0.0128	0.0171	0.0169	0.0163	0.0142	0.0173	0.0108
S _o	0.0067	0.0035	0.0063	0.0076	0.0064	0.0109	0.0052	0.0072
H/C	0.803	0.780	0.822	0.847	0.819	0.785	0.654	0.332
O/C	0.280	0.180	0.169	0.133	0.104	0.086	0.072	0.015

TABLE III - 1

NITROGEN DISTRIBUTIONS IN DEVOLATILIZATION PRODUCTS

Subbituminous 2 (SUB B)

$T_f(^{\circ}\text{C})$	$f^{\text{N}}_{\text{CHAR}}$	$f^{\text{N}}_{\text{tar}}$	$f^{\text{N}}_{\text{HCN}}$	Σf^{N}
520	0.99	0.05	---	1.04
600	0.76	0.24	0.01	1.01
745	0.67	0.19	0.10	0.96
820	0.63	0.28	0.17	1.00
890	0.57	0.22	0.21	1.00
945	0.57	0.12	0.20	0.89
950	0.53	0.11	0.30	0.94
1040	0.48	0.17	0.30	0.95
1090	0.40	0.14	0.40	0.94
1160	0.31	0.07	0.63	1.01
1240	0.28	0.06	0.65	0.99
1365	0.17	0.06	0.66	0.89
1390	0.08	0.04	0.61	0.73
1600	0.10	0.04	0.54	0.68
1700	0.08	0.04	0.92	1.03
1780	---	0.03	0.87	0.90

TABLE III - 2

NITROGEN DISTRIBUTIONS IN DEVOLATILIZATION PRODUCTS

Utah Bituminous (HVB)

$T_f(^{\circ}\text{C})$	$f^{\text{N}}_{\text{CHAR}}$	$f^{\text{N}}_{\text{tar}}$	$f^{\text{N}}_{\text{HCN}}$	Σf^{N}
530	0.81	0.04	0.01	0.86
595	0.66	0.22	0.01	0.89
745	0.58	0.26	0.08	0.92
790	0.57	0.27	0.09	0.93
880	0.49	0.25	0.17	0.91
915	0.48	0.24	0.17	0.89
935	0.51	0.30	0.13	0.94
1020	0.42	0.29	0.16	0.87
1090	0.40	0.24	0.25	0.89
1160	0.44	0.22	0.38	1.04
1240	0.30	0.21	0.51	1.02
1390	0.20	---	0.61	0.81
1600	0.20	0.10	0.67	0.97
1700	0.13	0.06	0.72	0.91
1780	0.10	0.05	0.96	1.11

TABLE III - 3

NITROGEN DISTRIBUTIONS IN DEVOLATILIZATION PRODUCTS

Pittsburgh Bituminous (HVA)

$T_f(^{\circ}\text{C})$	$f_{\text{CHAR}}^{\text{N}}$	$f_{\text{tar}}^{\text{N}}$	$f_{\text{HCN}}^{\text{N}}$	Σf^{N}
565	0.61	0.49	0.01	1.11
585	0.61	0.38	0.01	1.00
618	0.58	0.45	0.00	1.03
735	0.55	0.41	0.05	1.01
745	0.59	0.41	0.05	1.05
775	0.52	0.41	0.06	0.99
830	0.53	0.39	0.09	1.01
855	0.54	0.43	0.10	1.07
915	0.46	0.36	0.10	0.96
935	0.55	0.36	0.08	1.09
1040	0.44	0.40	0.10	0.94
1090	0.50	0.60	0.12	1.21
1107	0.41	0.40	0.24	1.04
1125	0.39	0.39	0.17	0.95
1165	0.46	0.43	0.22	1.11
1220	0.32	0.28	0.20	0.80
1220	0.39	0.36	0.33	1.08
1300	0.29	0.54	0.30	1.13
1450	0.33	0.19	0.33	0.85
1450	0.26	0.30	0.37	0.93
1700	0.04	---	0.43	0.47
1780	0.06	0.15	0.28	0.49

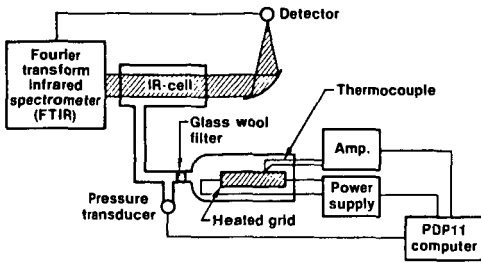


Fig. 1 Heated Grid Apparatus

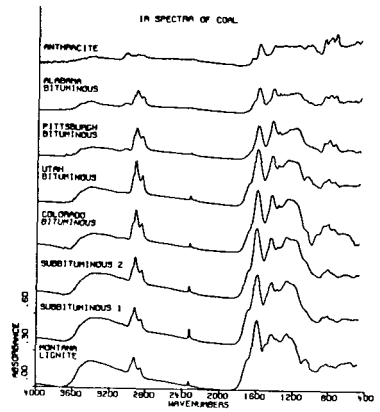


Fig. 3 IR Spectra of Coals

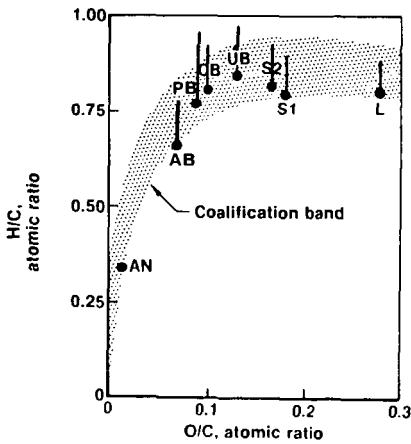


Fig. 2 Coal Band Location

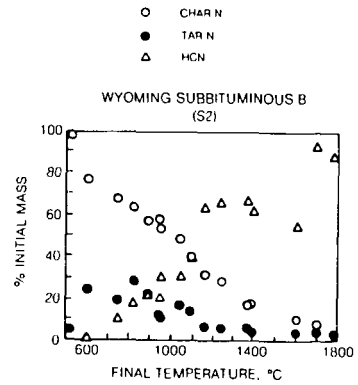


Fig. 4 Nitrogen Distribution: Subbituminous Coal

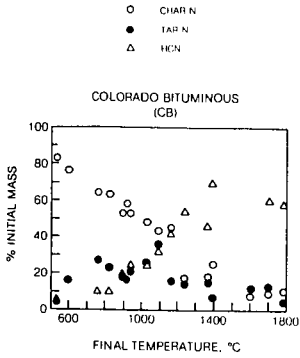


Fig. 5 Nitrogen Distribution: Colorado Bituminous Coal

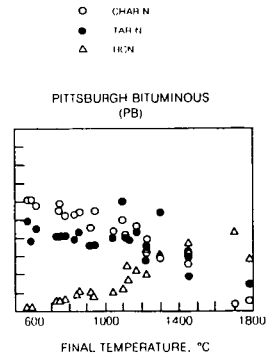


Fig. 7 Nitrogen Distribution in Pittsburgh Bituminous Coal Devolatilization Products

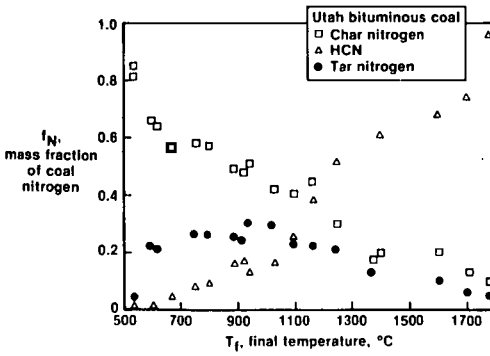


Fig. 6 Nitrogen Distribution: Utah Bituminous Coal

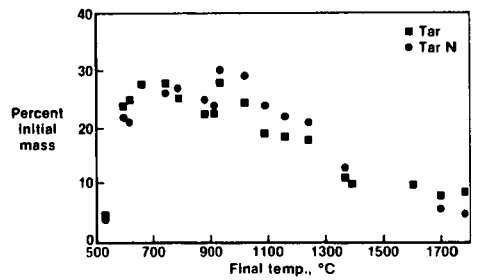


Fig. 8 Mass Fraction of Coal Mass and Coal Nitrogen vs. Final Temperature for Utah Bituminous Coal

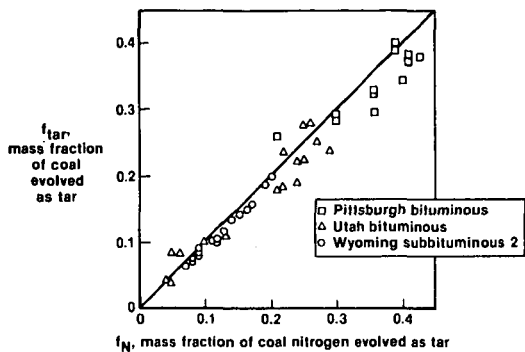


Fig. 9 Mass Fraction of Coal as Tar vs. Fraction of Coal Nitrogen as Tar

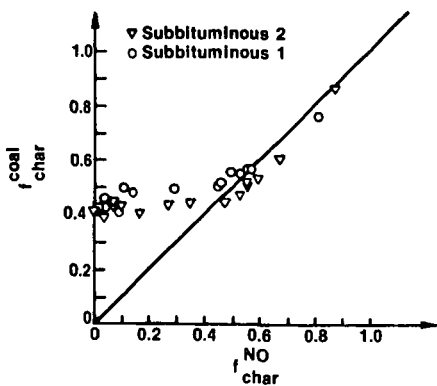


Fig. 10 Mass Fraction of Coal as Char vs. Fraction of Coal Nitrogen as Char

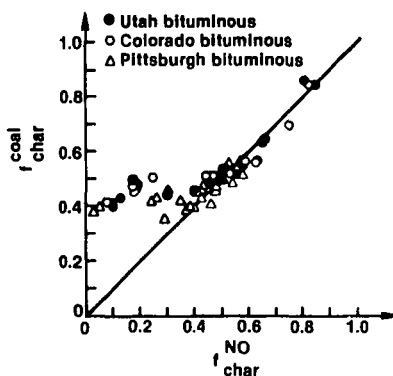


Fig. 11 Mass Fraction of Coal as Char vs. Fraction of Coal Nitrogen as Char

MINERAL MATTER EFFECTS ON THE RAPID PYROLYSIS AND
HYDROPYROLYSIS OF A BITUMINOUS COAL

Howard D. Franklin, William A. Peters, Jack B. Howard

Department of Chemical Engineering and Energy Laboratory,
Massachusetts Institute of Technology, Cambridge, Mass. 02139

Previous research at M.I.T. on rapid coal pyrolysis has dealt with the kinetics of evolution of individual products as a function of temperature, pressure, particle size, reactive gas, and coal type (1-5). Studies elsewhere have shown that constituents of coal mineral matter affect significantly other types of coal conversion reactions (6-14). Specifically, clays found in coal have been shown to affect coal carbonization (6), and to catalyze H_2 transfer to coal and coal model compounds (7,8). Pyrite, an important mineral in Eastern U.S. coals, is a strong catalyst for coal hydroliquefaction (7-11), while calcite promotes steam and CO_2 gasification of coal (12,13). Even quartz, though chemically inert, affects hydroliquefaction by acting as a diluent to agglomeration (14). Despite this importance of mineral content in coal thermochemistry, little work has been done on additive effects on rapid coal pyrolysis. Therefore this study was conducted to determine systematically how the important minerals present in coal influence the yields of individual devolatilization products.

EXPERIMENTAL

The coal used, described in Table 1, was a Pittsburgh No. 8 Seam bituminous coal from the Ireland Mine of the Consolidation Coal Company. Mineralogical analysis was by Fourier Transform Infrared Analysis (FTIR) of the low temperature ash of the coal (15). Pyrite content was not measured directly, but the pyrite-by-difference value agrees well with measured pyritic sulfur values for other samples from the same mine (16). The coal was ground to -270+325 US mesh (45-53 μ m) and a fraction of this raw sample was retained to obtain pyrolysis data on whole coal. The remainder of the sample was extracted with concentrated HF and HCl to remove its native clays, calcite, and quartz, and was then subjected to float-sink separation in a 2.50 specific gravity fluid to remove pyrite. The resulting demineralized coal contained 4.3% by weight mineral matter, most of it pyrite.

Mineral additives representing each of the major mineral constituents of this coal were studied. These are listed in Table 2. Acid-treated montmorillonite, prepared by extracting with HCl a portion of the montmorillonite sample, was used to study the effect of solid acidity on possible clay catalysis of pyrolysis. Shale was obtained from the Pittsburgh No. 8 Seam, and is representative of the native clays found in this coal. All mineral additives were ground to 2-40 μ m grain size, and added to the coal by co-slurrying with water in concentrated suspension for 24 hours.

At high temperatures and under the reducing conditions of coal pyrolysis, calcite and pyrite will decompose to CaO and pyrrhotite (FeS_{1+x} , $0 < x < 0.3$) respectively. In order to determine whether the extent of contact with the coal affects the catalytic properties of these particular minerals, additional sources of CaO and pyrrhotite were tried as well. $FeSO_4$, which is completely water

soluble, was added to the coal by impregnation from solution. Under pyrolysis conditions it should decompose to pyrrhotite. CaO was added in a manner similar to that for the mineral additives.

The pyrolysis apparatus and procedures have been described previously (2,17,18). Briefly, a thin horizontal layer of coal is sandwiched between the folds of a 325 US mesh stainless steel screen and held between two electrodes in either a length of glass pipe or a stainless steel pressure vessel. The coal is heated by electrically heating the screen. The vessel and its gaseous contents remain close to room temperature throughout the run and thus the volatiles are quenched almost instantaneously on escape from the coal particles. The entire time-temperature history of the sample is recorded by use of a chromel-alumel thermocouple (75 μm bead diameter) positioned within the folds of the screen alongside the coal particles. Heat transfer calculations show that at pressures of 1 atm and heating rates of 1000 K/s or less, coal particles and thermocouple beads 80 μm or less in diameter closely follow the temperature of the screen and are spatially isothermal.

All the reaction products were collected. Gases and low boiling liquids were trapped on lipophilic sorbents and subsequently analyzed by gas chromatography. Char was determined gravimetrically, and was further characterized by elemental analysis. Tar (room temperature condensibles) was collected on a filter at the reactor outlet and by a methylene chloride wash of the reactor internals, and its yield was determined gravimetrically. Total material balances usually exceeded 95%.

All runs were performed at heating rates of about 1000 K/s with holding times of 0 or 5 s at the maximum temperature attained, and cooling rates of about 200 K/s. These elements of the time-temperature history pertain only to the parent sample since the volatiles, once formed, rapidly escape the sample and are quenched as mentioned above. Demineralized, calcite-pretreated, and CaO-pretreated samples were heated in 1 atm He to temperatures in the range 800 to 1400 K for both 0 and 5 s holding times. Other samples were pyrolyzed in helium at temperatures near 1300 K for 5 s holding times, and at temperatures near 1000 K for 0 s holding times. In hydrolysis runs, samples were heated in 69 atm H_2 to temperatures between 800 and 1400 K for the demineralized coal, and to one temperature, generally near 1100 K, for the pretreated samples. Only 0 s holding times were used in hydrolysis runs.

RESULTS

Pyrolysis in Helium

The total yield of volatiles and the yield of tar obtained from pyrolysis of the demineralized coal to different temperatures in 5 s holding time runs are shown in Fig. 1. Each data point represents the cumulative yield from one experimental run and is associated with a specific time-temperature history. The curves represent simple first-order reaction models fitted to the data, and are used to indicate trends in the data. The error bars represent ± 1 standard deviation from the yield calculated by the fitted model. Heating and cooling rates did not exactly reproduce from run to run, and thus the holding or peak temperature obtained is not necessarily a good representation of the entire time-temperature history of a run. Therefore the fitted models

were used to generate equivalent peak or holding temperatures for each run. The model parameters were used to determine a calculated yield of a given product for each actual time-temperature history. These yields were then compared with yields calculated using the same parameters and idealized (linear 1000 K/s heatup, 0 or 5 s hold time, linear 200 K/s cooldown) time-temperature histories. The peak or holding temperature of the idealized history having the same calculated yield as that of the actual history was picked as the temperature representative of the run. As a rule equivalent temperatures for different products were within 30 K of the corresponding observed peak or holding temperature.

Results for raw coal and for clay-, quartz-, and iron-pretreated samples are shown in Figs. 2-5. The curves and error bars plotted on all these graphs indicate demineralized coal yields, while each letter represents one run with a sample pretreated with a particular mineral or compound as specified in Table 2. Points labelled "W" represent runs with raw (undemineralized) coal.

There are in general few effects on pyrolysis due to any of these minerals. Figures 2 and 3 show that the total yield of volatiles and the yield of tar are unaffected by these additives. While there are no points in Fig. 3 for pyrite or FeSO_4 , other runs not plotted showed these additives to have no effect on tar yields. Data for most other products show similar trends. Methane yields (Fig. 4) are, however, significantly reduced by pyrite and FeSO_4 ("P" and "F" points). Kaolinite suppresses the yield of light liquid hydrocarbons (Fig. 5, "K" points), which consist mostly of BTX range compounds.

Results for calcium minerals have been reported previously (19). To summarize them, both CaO and CaCO_3 increase char yields, while strongly decreasing tar yields and slightly reducing yields of other hydrocarbon volatiles. Evolution of CO is enhanced by these additives by an amount approximately proportional to calcium loading. Comparison of CO_2 yields from CaCO_3 pretreated coal with those from demineralized coal and pure calcite indicates that calcite in the presence of coal decomposes yielding CO_2 at lower temperatures than it does when pyrolyzed alone.

Pyrolysis in Hydrogen

Effects of minerals in hydroxyrolysis were determined in a similar manner to that used for pyrolysis. Simple first-order models were fitted to hydroxyrolysis data from demineralized coal, and the resulting curves with error bars served as a basis of comparison for the data from hydroxyrolysis of mineral-treated coals.

Few of the minerals were found to influence hydroxyrolysis behavior to any significant extent. Total yield of volatiles (Fig. 6) is not affected by any of the additives tried, although tar yields are reduced slightly by addition of shale or calcite, and reduced strongly by addition of CaO , kaolinite, or acid-treated montmorillonite (17). Methane (Fig. 7) and ethane, the most important hydroxyrolysis products after tar, are suppressed by addition of calcite or shale. Carbon dioxide yields are strongly enhanced by the calcium minerals (Fig. 8). The calcite-pretreated sample in this case was different from the one used for pyrolysis in He , and contained only 14.55% by weight CaCO_3 .

DISCUSSION

The most striking point brought out in this study is the variation in catalytic activity exhibited by the different minerals present in coal. The clays, which might be expected to show hydrocarbon cracking activity due to their solid acidity, have virtually no effect on the pyrolysis yield structure. The reduction in liquid hydrocarbon yields by kaolinite (Fig. 5) might be attributable to secondary cracking of these compounds by this clay. The degree of reduction is, however, too small to determine the products of this postulated cracking. It is not immediately clear why kaolinite would crack light liquids and not crack tar (Fig. 3). One possible explanation is the relative ease of accessibility of the lighter liquids to the pore structure of the clay where most of its active surface area lies. The reduction in methane yields by shale in hydropyrolysis (Fig. 7) is not easily explained. Clays have been shown to retard the rate of CH_4 production in slow hydrogasification of chars (20). While the reactions in that system are substantially different from those of rapid hydropyrolysis, a common underlying mechanism for CH_4 yield suppression might be present. Kaolinite and acid-treated montmorillonite reduce tar yields in hydropyrolysis (17), while montmorillonite does not. The clays thus seem to show some hydrocracking activity, which is possibly dependent on their solid activity.

Iron-sulfur minerals, pyrite and FeSO_4 , also have little influence on pyrolysis behavior. Their only significant effect on pyrolysis in H_2 is to reduce CH_4 yields (Fig. 4). This phenomenon is difficult to explain as none of the other light hydrocarbon products are affected by iron-sulfur mineral addition. The lack of effects of iron-sulfur minerals on hydropyrolysis product yields is very surprising given the known activity of these minerals for hydroliquefaction. Weller *et al.* (21) did show that a pyrite sample that strongly enhanced liquefaction at 250 atm H_2 pressure had no effect on liquefaction at 69 atm H_2 , the pressure used in the present study. A pressure effect for iron-sulfur catalysis of coal hydrogenation might thus be indicated. The postulated active species for coal hydrogenation in the presence of iron-sulfur minerals is pyrrhotite. The precise stoichiometry of the pyrrhotite formed will be a function of the hydrogen pressure (22), and this stoichiometry will affect the subsequent activity of the pyrrhotite (23). Further study of pyrrhotite stoichiometry and activity as a function of hydrogen pressure is clearly needed.

The strong effects of calcium minerals on coal pyrolysis are in striking contrast to the comparative lack of activity of the other coal minerals. While the solid-acid clays show little cracking activity, calcium minerals reduce the yield of volatile hydrocarbon products (19). In addition, CaO and CaCO_3 are especially active in cracking oxygen functional groups to CO (19). A large portion of bituminous coal oxygen occurs in acidic functional groups such as phenols or carboxylic acids, and the strongly basic CaO might react with these groups. In addition, we have pointed out previously (19) that the reactions by which phenol decomposes homogeneously to CO would be catalyzed by a solid base. Non-acidic oxygen functional groups such as furans have also been shown to crack over CaO (24). Thus strong bases would seem to influence the decomposition of coal oxygen to a greater degree than would other additives. It also appears that solid bases, or at least CaO , are good catalysts for cracking aromatics or other coal hydrocarbon volatile products (19, 24). Since CaCO_3 , which decomposes to CaO during pyrolysis, is the only coal mineral which generates a solid base, it is the coal mineral with the strongest influence on coal pyrolytic behavior.

The effects of calcium minerals on hydrolysis are less easily explained. Calcite suppresses CH_4 yields (Fig. 7) in hydrolysis to about the same extent as do the clays. The same study (20) that showed clays to reduce char hydrogasification rates also showed calcite to reduce those rates. Why these two groups of minerals should have the same effects on coal hydrogen reactions is unclear. It is noteworthy that while calcite suppresses CH_4 yields, CaO does not. As discussed below, the CaCO_3 present in calcite-pretreated coal did not decompose to CaO under hydrolysis conditions, and its effects need not therefore parallel those of lime.

Carbon dioxide yields from CaO-pretreated coals hydrolyzed in 69 atm H_2 (Fig. 8) are almost identical to those from the same sample pyrolyzed in 1 atm He at similar time-temperature histories (17), and in both cases the CO_2 yields are considerably higher than those from demineralized coal. Since the carbonate content of the CaO-pretreated sample was small, this excess CO_2 probably results from accelerated decomposition of an as yet undetermined coal oxygen functional group. Carbon dioxide yields from calcite-pretreated coal under 69 atm H_2 are very similar to those from CaO-pretreated coal. This strongly contrasts with the pyrolysis behavior of this sample under 1 atm He (19) where, at similar time-temperature histories, the calcite itself had started to decompose. It is interesting to note that the calcite-pretreated sample gave CO_2 yields that were no larger than those from the CaO-pretreated sample, despite having 2.75 times as much Ca. A saturation effect is probably present.

There is no difference between pyrolysis yields of the raw coal and the demineralized coal. Since 90% of the native mineral matter of the coal used consisted of clays, pyrite, and quartz (Table 1) this result agrees with the other findings of this study as to the relative lack of activity of these minerals. It also implies, however, that the demineralization technique itself has no effect on the subsequent pyrolysis behavior of this bituminous coal.

CONCLUSIONS

Clays and iron-sulfur minerals have few effects on the pyrolytic behavior of this bituminous coal. Calcium minerals reduce yields of volatile hydrocarbon products, and enhance CO formation. Calcite and shale reduce yields of CH_4 in coal-hydrogen reactions, while acid-treated montmorillonite, kaolinite, and CaO reduce yields of tar under these conditions. Iron-sulfur minerals have few catalytic effects on coal hydrolysis at H_2 pressures of 69 atm.

ACKNOWLEDGEMENTS

Frank Cariello and Robert Steinberg obtained the data on mineral-treated coals. Financial support was provided by the United States Department of Energy, under Contract EX-76-A-01-2295, Task Order No. 26.

REFERENCES

1. Anthony D.B., Howard, J.B., *AIChE J* 22, 625 (1976).
2. Suuberg E.M., Peters W.A., Howard J.B., *Ind. and Eng. Chem. Proc. Des. and Dev.* 17, 37 (1978).
3. Suuberg E.M., Peters W.A., Howard J.B., Proc. 17th Symp. (International) on Combustion 1979 p. 117, The Combustion Institute, Pittsburgh, Pa.

4. Suuberg E.M., Peters W.A., Howard J.B., Amer. Chem. Soc. Adv. in Chem. Ser. 183, 239 (1979).
5. Suuberg E.M., Peters W.A., Howard J.B., Fuel 59, 405 (1980).
6. Howard H.C., Chemistry of Coal Utilization, Supplemental Volume, 1963, p.340 Wiley, New York.
7. Given P.H., EPRI Report No. 207-0-0, 1974 p. A-122.
8. Mukherjee D.K., Choudhury P.B., Fuel 55, 4 (1976).
9. Guin J.A., Tarrer A.P., Prather J.W., Johnson D.R., Lee J.M., Ind. and Eng. Chem. Proc. Des. and Dev. 17, 118 (1978).
10. Granoff B., Thomas M.G., Baca P.M., Noles G.T., Amer. Chem. Soc. Div. of Fuel Chem. Prepr. 23 (1), 23 (1978).
11. Gangwer J.E., Prasad H., Fuel 58, 577 (1979).
12. Feldmann H.F., Chauhan S.P., Longanbach J.R., Hissong D.W., Conkle H.N., Curran L.M., Jenkins D.M., Battelle Columbus Laboratories Report BMI-1986,1977.
13. Sears, J.T, Muralidhara H.S., Wen C.Y., Ind. and Eng. Chem. Proc. Des. and Dev., 19, 358 (1980).
14. Gray, D., Fuel 57, 213 (1978).
15. Painter P.C., Coleman M.M., Jenkins R.G., Whang P.W., Fuel 57, 337 (1978).
16. Padia A.S., ScD Thesis, MIT Dept. of Chem. Eng. 1976.
17. Franklin H.D. PhD Thesis, MIT Dept. of Chem. Eng. 1980.
18. Anthony D.B., Howard J.B., Meissner H.P., Hottel H.C., Rev. Sci. Instrum. 45, 992 (1974).
19. Franklin, H.D., Peters W.A., Howard J.B., Amer. Chem. Soc. Div. of Fuel Chem. Prepr. 26 (2), 121 (1981).
20. Tomita A., Mahajan O.P., Walker P.L., Amer. Chem. Soc. Div. of Fuel Chem. Prepr. 22 (1), 4 (1977).
21. Weller S., Pelipetz M.G., Friedman S., Storch H.H., Ind. and Eng. Chem. 43, 1243 (1950).
22. Richey W.D., 12th Central Regional Meeting Amer. Chem. Soc., Pittsburgh, Pa., Nov. 1980.
23. Montano P.A., Granoff B., Fuel 59, 214 (1980).
24. Mead D.W., M.S. Thesis, MIT Dept. of Chem. Eng. 1979.

TABLE 1

CHARACTERISTICS OF COAL EXAMINED

<u>Proximate Analysis</u>		<u>Ultimate Analysis</u>		
<u>Wt. % (as received)</u>		<u>Wt. % (dry)</u>	<u>Wt. % (dmmf)</u>	
Moisture	2.0	Carbon	71.74	82.91
Volatile Matter	36.2	Hydrogen	4.84	5.65
Fixed Carbon*	51.0	Oxygen*	6.22	7.19
Ash	<u>10.8</u>	Nitrogen	1.14	1.32
	100.0	Organic Sulfur**	2.54	2.94
		Mineral Matter	<u>13.47</u>	
			100.00	100.00
<u>Petrographic Analysis</u>		<u>Mineral Matter Analysis</u>		
<u>Wt. % mineral matter free</u>		<u>Wt. %</u>		
Vitrinite	81.5	Kaolinite	13	
Semi-Fusinite	6.0	Calcite	10	
Fusinite	2.5	Quartz	7	
Micrinite	3.0	Montmorillonite	14	
Macrinite	1.2	Illite	9	
Exinite	5.2	Pyrite*	<u>45</u>	
Resinite	<u>0.6</u>		100	
	100.0			

* by difference

**calculated from total sulfur (5.77% by weight dry coal) and measured pyrite content

TABLE 2

MINERAL MATTER ADDITIVES STUDIED

<u>MINERAL</u>	<u>PLOTTING SYMBOL</u>	<u>SOURCE</u>	<u>OBTAINED FROM</u>	<u>WT. % MINERAL IN PRE-TREATED SAMPLE*</u>
Kaolinite	K	Mesa Alta N.Mex. (API REF CLAY)	Ward's Natural Science Estab.	11.9
Montmorillonite	M	Belle Fourche N.D. (API REF CLAY)	Ward's Natural Science Estab.	8.8
Acid-Treated Montmorillonite	A	Made in house from above		10.2
Shale	S	Moundsville W. VA	U.S.G.S.	9.6
Pyrite	P	Moundsville W. VA	U.S.G.S.	17.1
Calcite	C	Sumterville FLA	Dixie Lime & Stone	20.2
Quartz	Q	not known	Harvard Mineralogy Museum	18.0
<u>CHEMICAL</u>			<u>OBTAINED FROM</u>	
CaO	L	-	Fisher Scientific	5.9**
FeSO ₄	F	-	Fisher Scientific	6.7

* Does not include 4.3% mineral matter content of demineralized coal

** Actual mineral in coal was mixture of 74% Ca(OH)₂ - 26% CaCO₃

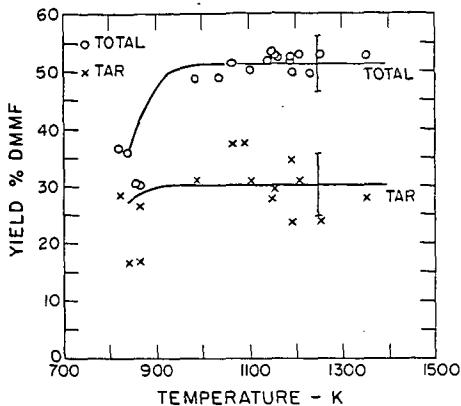


Figure 1 Total Yield of Volatiles and Yield of tar from Demineralized Coal Pyrolysis in 1 atm He, 5 s Holding-Time Runs.

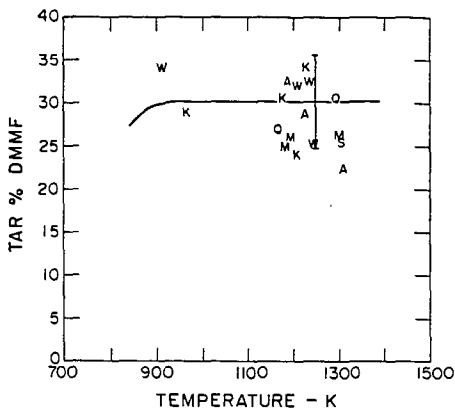


Figure 3 Yield of Tar from Pyrolysis of Pretreated Coal in 1 atm He, 5 s Holding-Time Runs.

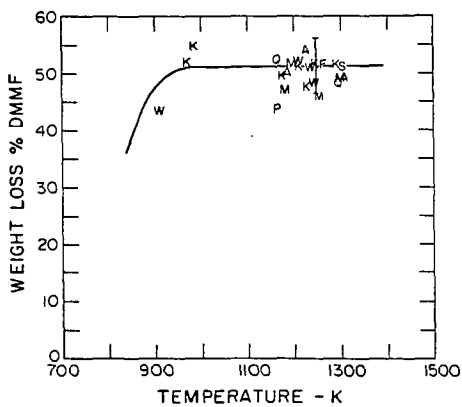


Figure 2 Total Yield of Volatiles from Pyrolysis of Pretreated Coal in 1 atm He, 5 s Holding-Time Runs.

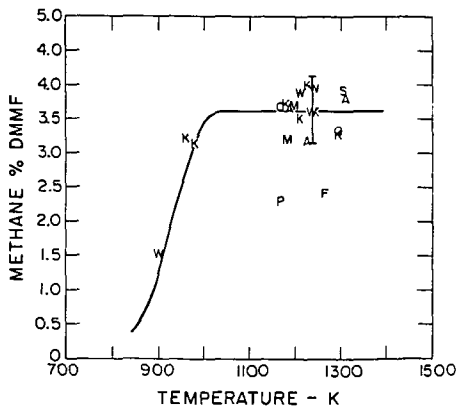


Figure 4 Yield of Methane from Pyrolysis of Pretreated Coal in 1 atm He, 5 s Holding-Time Runs.

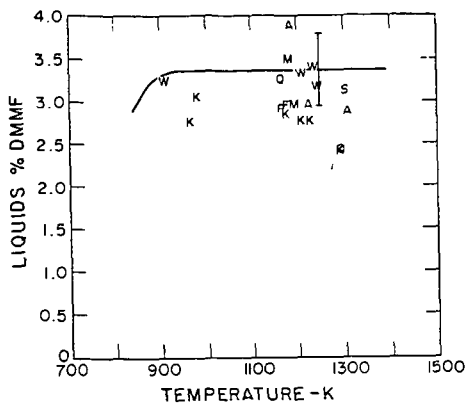


Figure 5 Yield of Light Liquid Hydrocarbons from Pyrolysis of Pretreated Coal in 1 atm He, 5 s Holding-Time Runs.

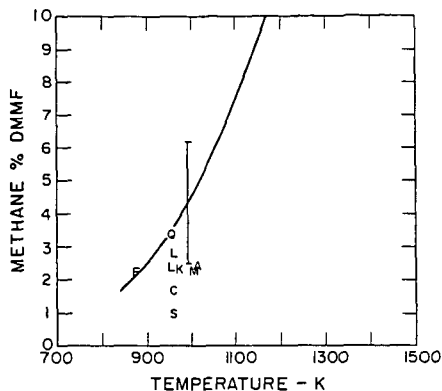


Figure 7 Yield of Methane from Pyrolysis of Pretreated Coal in 69 atm H₂, 0 s Holding-Time Runs.

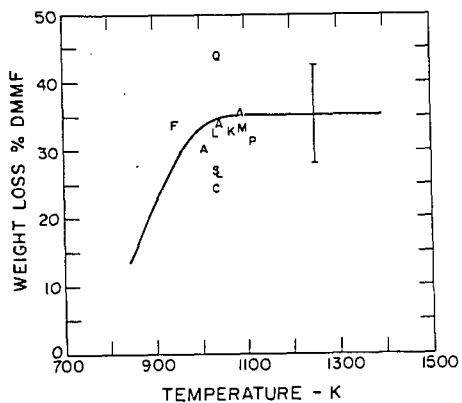


Figure 6 Total Yield of Volatiles from Pyrolysis of Pretreated Coal in 69 atm H₂, 0 s Holding-Time Runs.

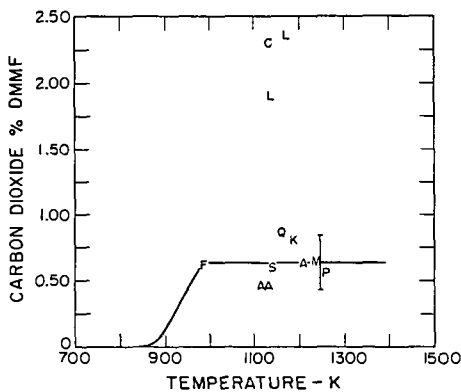


Figure 8 Yield of Carbon Dioxide from Pyrolysis of Pretreated Coal in 69 atm H₂, 0 s Holding-Time Runs.

HYDROGENOPYROLYSIS OF COAL AND COAL DERIVATIVES

R. Cyprès

Faculty of Applied Sciences
Department of General Chemistry
and Carbochemistry
Université Libre de Bruxelles
BELGIUM

1. INTRODUCTION

Coal hydrolysis is now developing as one of the third generation processes for coal gasification or partial liquefaction. The advantages of coal hydrolysis are : rapid primary devolatilisation of the coal, with production of more volatile matter than what is determined by standard methods; desulfurization of the char; simultaneous hydrocracking of the primary tar. General reviews on the subject have been published recently (1)(2)(3)(4) Present paper deals with three aspects of fixed bed hydrolysis : the increased formation of methane and light monocyclic aromatics and phenols; the desulfurization process and yield, with regard to the composition of the mineral constituents of the coal; the mechanism of thermal cracking of hydro- and perhydrocyclic hydrocarbons.

2. POSTCRACKING OF THE PRIMARY VOLATILE MATTER

During pyrolysis of coal under H_2 pressure, the primary volatile matter are submitted to hydrocracking. This postcracking is shown by the variation, compared to what happens in inert atmosphere, of the methane concentration in the gas and of the light aromatics (B.T.X. : benzene, toluene and xylene) and phenols (P.C.X. : phenol, cresols and xylenols) in the liquid phase.

Experiments have been made with a 32,8% V.M. coal from Beringen, sized $< 500 \mu m$, between 480 and 850°C at a fixed H_2 pressure of 30 bar. One run was made with 30 bar He pressure at 580°C. Residence time of carrier gas was about 60 s. Yields in gas, oil, water and char are given in table I.

T (°C)	H_2					He
	485	580	650	780	850	580
Char	75.7	70.9	66.7	61.6	60.6	75.0
Oil	9.5	9.2	8.8	6.4	5.5	6.4
Gas	9.1	10.2	15.1	24.2	28.3	7.9
Water	4.4	6.9	8.9	10.1	9.2	4.7

Table I : Yields (% maf) (30 bar H_2 pressure)

Above 700°C, coal devolatilisation is higher than the volatile matter content, determined following standard methods.

Hydrogen pressure influence at 580°C between 1 and 50 bar has been studied on the same coal. Yields obtained are given in table II.

H ₂ pressure-bar	H ₂					He
	0	10	20	30	50	30
Char	76.6	72.4	70.6	70.9	69.0	75.0
Oil	7.4	10.3	9.8	9.2	8.9	6.4
Gas	5.3	10.0	10.3	10.2	9.9	7.9
Water	5.3	6.0	7.0	6.9	6.1	4.7

Table II : Yields (% maf) at 580°C.

Fig. 1 gives the variation of CH₄ and C₂H₆ content in the gas at 30 bar H₂ pressure compared with conventional carbonisation, as a function of temperature. CH₄ content increases from 45% at 500°C to 80% at 850°C. Under conventional atmospheric carbonisation the known reverse evolution occurs. CH₄ formation is due to hydrodealkylation of higher hydrocarbons.

The change in composition of B.T.X., P.C.X. and naphthalenes is given on fig. 2 as a function of carbonisation temperature. Light aromatics are steadily increasing. Phenols, on the contrary, are at their highest concentration in the low temperature oil. Phenols dehydroxylation occurs only above 700°C. Water content shows an increase parallel to the decrease of P.C.X. (phenol, cresols, xylenols) content. The speed of cresols disappearance is equal to the speed of their formation by dealkylation of the xylenols. Phenol increase is a result of both processes. The optimal phenol production is at about 750°C. The dehydroxylation of P.C.X. contributes to the B.T.X. increase between 600 and 800°C.

Naphthalenes yields are increasing with temperature as a result of known formation of di- and polycyclic aromatics from cracking fragments. Under hydrogen pressure these reactions are markedly slowed down but nevertheless still present.

Fig. 3 shows that, for the light aromatics, hydrogen pressure influence at 580°C is important between 1 and 20 bar. This is not the case for the phenols. Naphthalenes increase with the pressure from 1,2% at 1 bar to 3,6% at 50 bar.

3. DESULFURIZATION OF THE COAL DURING HYDROGENOPYROLYSIS

It is known that high temperature hydrolysis leads to partially desulfurized char. In this paper, this hydrodesulfurization was considered regarding the nature of the sulfurous minerals present in the coal. As an example a high S containing Italian coal was submitted to a fixed bed hydrocarbonisation at 30 bar H₂ pressure. Experiments were performed at 580°C, 700° and 850°C. Pyrite is reduced by H₂ to an extent depending mainly upon pyrolysis temperature. The reduction of pure pyrite and mixtures of pyrite and pitch coke under hydrogen pressure has been studied by thermogravimetry between 1 and 50 bar up to 950°C. It can be seen on fig. 4 that the first loss of S, corresponding to the conversion of FeS₂ to FeS_x (pyrrhotite) is complete around 500°C.

The reduction to Fe is only complete at much higher temperature. At 950°C, under 50 bar, total reduction is achieved within 10 minutes, whereas at 1 bar, it needs 40 minutes. The same behaviour is observed for pyrite in the coal. The higher the pyrolysis temperature is, the more important is the pyritic sulfur elimination.

Scanning electron microscopy photographs show the distribution of S, Ca and Fe in the coal and in the char. The pyritic sulfur

is well localised in the coal, whereas the organic sulfur is uniformly distributed in the bulk of the sample. The calcium content of this Italian coal is high, mostly as CaCO_3 but also some CaSO_4 (Fig.5).

In the char, after hydrogen treatment, it can be observed on Fig.6 that FeS_2 has been reduced. At low temperature, reduction is limited to pyrrhotite (FeS_x), at high temperature, to iron. But where Ca is detected it is associated with S, probably in the form of CaS and some unreduced CaSO_4 . The experimental results are summarized in table III. They show in this case of a high calcium containing coal, that the higher the pyrolysis temperature is, the more sulfur remains in the char. It seems to be due to increased decomposition of CaCO_3 into CaO , which is more active to fix the volatile sulfur compounds. CaCO_3 from the ash would have the same effect under hydrocarbonisation conditions, as limestone or dolomite, added to coal, in combustion, as to reduce atmospheric SO_2 pollution. As a conclusion of this, it can be said that high calcium containing coals, will not be desulfurized in the same ratio as pyritic coals and that an increase of their hydrocarbonisation temperature will leave more sulfur in the char.

SULCIS COAL					
Proximate analysis		Ultimate analysis (Mf)			
Moisture	6,0	C	63,24	S, pyritic	0,83
Ash (Mf)	12,9	H	3,71	sulfate	0,05
Volatile Matter (% Maf)	56,4	O	14,11	organic	3,57
		N	1,77		
		S	4,45		
		Ash	12,9		
		Total	100,28	Total	4,45
HYDROGENOPYROLYSIS $p_{\text{H}_2} = 30$ bar					
T°C		580	700	850	
Devolatilisation (% Maf)		51,6	61,1	61,9	
Gas		19,2	36,2	39,7	
Oil		14,8	10,3	8,2	
Water		16,4	18,8	14,1	
Char		48,4	38,9	38,1	
S balance in					
Char		34,1	35,6	41,9	
Oil		7,0	6,0	4,7	
Gas		59,1	58,4	53,4	

Table III : Sulcis coal and chars.

THERMAL CRACKING OF DI- AND POLYHYDROAROMATICS AT ATMOSPHERIC PRESSURE OF INERT GAS

In connection with the high content of hydropolyaromatic compounds present in coal liquids produced by several industrial processes, due to partial hydrogenation, the thermal cracking in inert gas

at atmospheric pressure of di- and polycyclic compounds, partially and totally hydrogenated was studied in view of their conversion to monocyclic aromatic hydrocarbons.

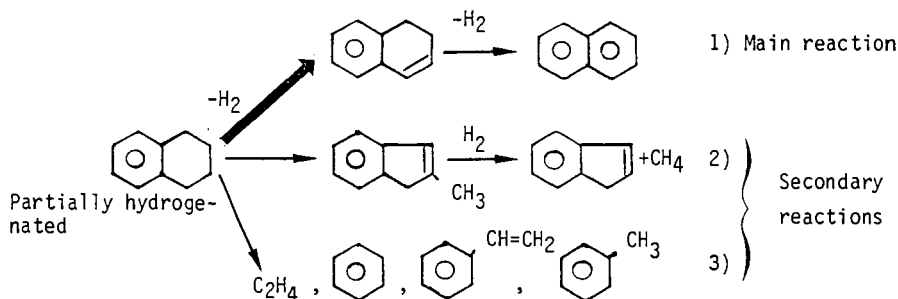
Korosi (5) has shown that steam cracking of decaline, with a steam to hydrocarbon ration of 16/1 at 854°C and nearly atmospheric pressure leads to 18 W% benzene and up to 19 W% C₂H₄ in the gas phase.

We made thermal cracking at atmospheric pressure in inert gas and without any catalyst of the following di- and polycyclic compounds:

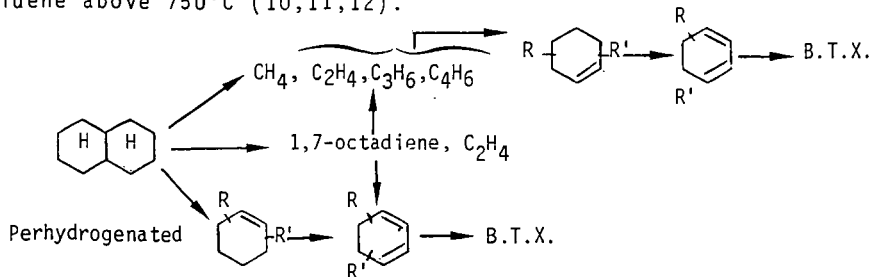
1,2-dihydronaphthalene, 1,2,3,4-tetrahydronaphthalene (tetraline), decahydronaphthalene (decaline), 1- and 2-naphtols, 1,2,3,4-tetrahydro-1-naphtol, 5,6,7,8-tetrahydro-1-naphtol, cisdecahydro-1-naphtol, perhydroindane, perhydrofluorene, perhydropyrene, 9,10-dihydrophenanthrene, 1,2,3,4,5,6,7,8-octahydrophenanthrene, perhydrophenanthrene and phenanthrene.

The experimental devices and results of some of those studies were already published (6,7,8,9).

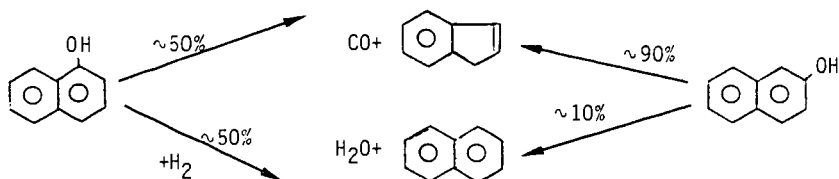
Comparison between B.T.X. and ethylene yields obtained by thermal cracking of tetraline and decaline is given in fig.7. It was demonstrated that cracking mechanism of partially hydrogenated naphthalene is completely different of what happens with decaline. In the first case the main cracking reaction is dehydrogenation leading back to naphthalene (Equation 1). Two other pathways, less important, occur at the same time. They can explain the formation of indene and of the small amounts of monocyclic aromatic (Eq. 2 and 3).



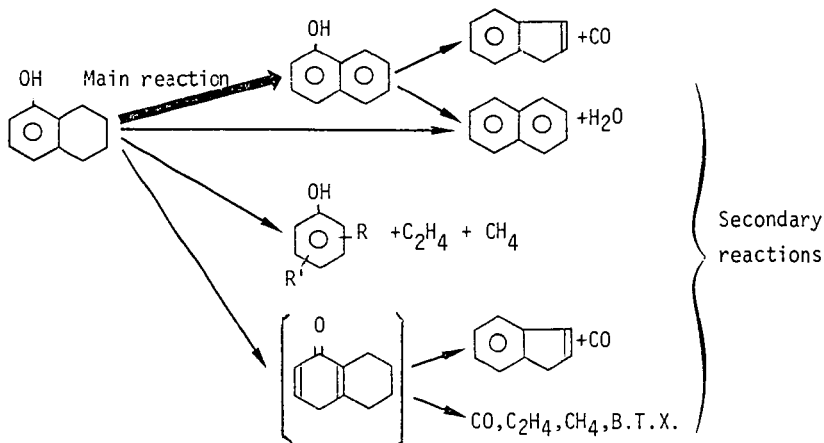
For the perhydrocompounds, on the contrary, the main reaction is the opening of one or two cycles with formation of alkylmonocyclic compounds whose subsequent dehydrogenation gives the corresponding aromatics. At the same time, C₂H₄ and H₂ are the major constituents of the gas phase. Smaller amounts of 1,3-C₄H₆, 1,7-octadiene, C₃H₆ and C₄H₈ are also observed. It was shown in previous work that the light olefines react to give benzene and toluene above 750°C (10,11,12).



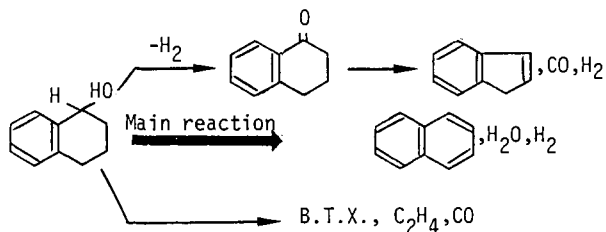
The influence of an hydroxyl group on thermal behaviour of dicyclic compounds was studied by cracking the naphthols, the tetrahydronaphthols and decahydro-1-naphthol. Results obtained show that two cracking mechanisms can be considered for naphthols. The first one is decarbonylation, similar to what was demonstrated to happen with phenol (13). Indene is formed. The second one is a dehydroxylation leading to naphthalene. The hydroxyl group position has a relative importance on the contribution of both of them.



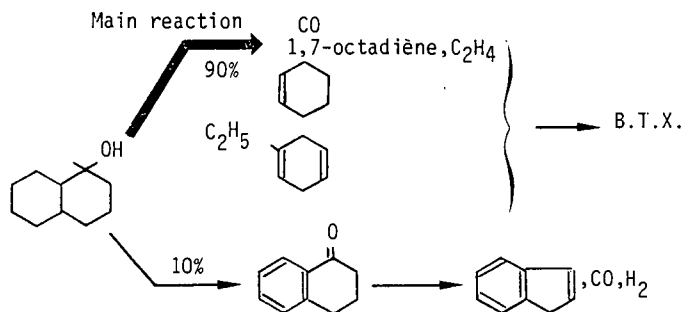
In the case of naphthol partially hydrogenated, the OH group can be located either on the aromatic ring or on the saturated one. Therefore, thermal cracking of 5,6,7,8-tetrahydro-1-naphthol and 1,2,3,4-tetrahydro-1-naphthol was performed. The main thermal degradation reaction was, in the first case, dehydrogenation into 1-naphthol, undergoing subsequently the above described reactions. B.T.X. and C_2H_4 production is low. Those different degradation pathways of 5,6,7,8-tetrahydro-1-naphthol can be summarized as follow :



Concerning 1,2,3,4-tetrahydro-1-naphthol, the main degradation reaction is a dehydroxylation with subsequent dehydrogenation into naphthalene. The presence of an hydroxyl group located on the saturated ring makes the rupture of the C-C bond easier, increasing the B.T.X. production. The different mechanisms are summarized as follow.



The main cracking reaction of decahydro-1-naphthol is similar to that of decahydro-naphthalene: C-C bond ruptures leading to olefines and cycloolefines, together, in this case, with CO elimination. The obtained olefines give easily B.T.X. A secondary reaction of partial dehydrogenation leading to indene formation occurs simultaneously and explains the lower B.T.X. yield compared with decahydronaphthalene.



Comparison between B.T.X. and ethylene yields obtained by thermal cracking of the hydrogenated naphthols is given in fig. 8.

It can be seen that the dicyclic perhydrocompounds lead to much higher B.T.X. yields than those of the partially hydrogenated products. The influence of the hydroxyl group is apparent when comparing tetrahydronaphthols and tetrahydronaphthalene. The B.T.X. yield of the two tetrahydronaphthols are higher than that of tetrahydronaphthalene. The hydroxyl position has also a marked effect. Located on the saturated ring, the B.T.X. yield is higher than when the OH group is on the aromatic ring.

Decahydronaphthol gives again higher B.T.X. yield but, due to a secondary dehydrodecarbonylation reaction, it reaches 24 W% against 34 W% for decahydronaphthalene.

As polycyclic model substances, phenanthrene and 3 hydrogenated derivatives (di-, octa- and perhydrophenanthrene), perhydrofluorene, perhydroindane and perhydropyrene have been cracked in the same conditions. Detailed results are available but not given in this paper for lack of time. The maximum yields of B.T.X. and ethylene are given for all of them in table IV.

It can be seen that all the perhydrocompounds give excellent yields of monocyclic aromatics and of ethylene, whereas the corresponding partially hydrogenated compounds show predominantly dehydrogenation, leading back to the aromatic starting hydrocarbon. The hydrogen saturation of all the polycyclic compounds mentioned, even in the case of pyrene with his 4 condensed aromatic rings, weakens the C-C bonds. It makes possible the rupture of the cycles, with light olefines production. Above 750°C, they contribute to an additional benzene formation as demonstrated in earlier work.

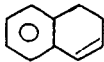
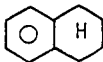
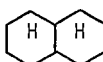
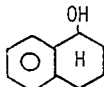
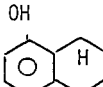
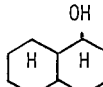
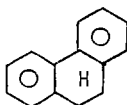
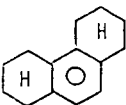
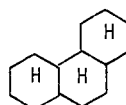
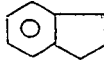
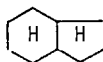
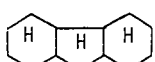
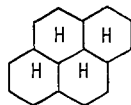
 B.T.X. 1,1 C ₂ H ₄ -	 3,8 2,9	 34,0 18,9
 B.T.X. 15,6 C ₂ H ₄ 2,6	 8,2 2,5	 23,9 17,6
 B.T.X. 1,3 C ₂ H ₄ 0,8	 1,3 3,6	 38,3 18
 B.T.X. - C ₂ H ₄ -	 33,6 ~ 15	 30,2 33
B.T.X. C ₂ H ₄	 27,3 17	

Table IV : Optimum B.T.X. and C₂H₄ yields (in W% of injected compounds) obtained by thermal cracking of di- and polyhydroaromatics.

As to show in which position of the starting molecule, cracking occurs first, polycyclic compounds labelled in specific position with ^{14}C and ^3H have been used. The radioactivity of the cracking products is measured by radiochromatography. Phenanthrene and perhydrophenanthrene are labelled in position 9 with ^3H , and in positions 9 and 10 with ^{14}C .

The radioactive ^3H or ^{14}C content in the cracking products is expressed as :

$$\frac{\text{molar specific activity of a given compound}}{\text{molar specific activity of the starting labelled compound}} \text{ in } \left(\frac{\text{mCi/mmole}}{\text{mCi/mmole}} \right)$$

Cracking of phenanthrene-9- ^3H and of phenanthrene-9,10- ^{14}C

Table V gives composition and tritium content of the cracking products.

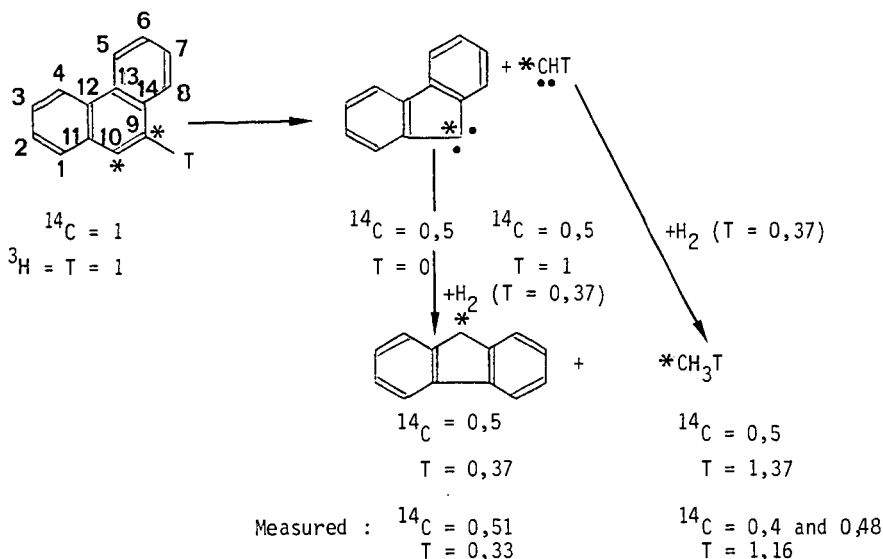
Gas phase	Composition (M %)			^3H content		
	875°C/2s	890°C/2s	900°C/2s	875°C/2s	890°C/2s	900°C/2s
Hydrogen	92,5	92,3	93,6	0,37	0,27	0,21
Methane	6,9	7,3	6,2	1,16	0,85	0,76
Ethylene	0,4	0,3	0,2	0,82	0,51	0,39
Ethane	0,05	0,07	0,03	1,36	0,66	0,57
Acetylene	Tr.	Tr.	Tr.			
Propene	-	Tr.	Tr.			
Liquid phase	850°C/2,5s		875°C/2s	850°C/2,5s		875°C/2s
Benzene	0,7		0,1	0,57		-
Indene	0,5		0,3	0,99		0,47
Naphthalene	3,6		1,6	0,77		0,90
Fluorene	0,5		0,5	0,39		0,32
Phenanthrene	91,6		95,0	1,02		1
Pyrene	0,3		0,4	-		1,70

Table V : Composition and tritium content of cracking of phenanthrene 9- ^3H

The tritium content in hydrogen is higher for low cracking yield. This means that there is preferential rupture of C-H bond in position 9. This is in agreement with what is admitted in literature where Beckwith and Thompson (14) give the following reactivity position sequence in phenanthrene : $9 > 1 > 3 = 2$. With increasing pyrolysis temperature the formation of 1-phenanthryl radical and even 2- and 3-phenanthryl radicals leads to a reduction of ^3H content in hydrogen. The ^3H content of methane is high, what demonstrates an important contribution of the ^3H located on C9.

Cracking of phenanthrene-9,10- ^{14}C at 885°C give ^{14}C content of 0,39 in CH_4 , 0,52 in naphthalene, 0,5 in fluorene and 1 for the uncracked phenanthrene.

The fluorene and methane formation, the only considered here, starts with the elimination of one C and two H in position 9. The hypothetical intermediate would be a fluorenyl biradical.



The intermediate fluorenyl biradical is hydrogenated by the hydrogen of the gas phase, whose tritium content is 0,37. Thus, the theoretical tritium content of the fluorene should be 0,37, as 1 mole H_2 is needed. The measured values are in very good agreement with this as ^3H content found was 0,33 and ^{14}C 0,51. For CH_4 , measured content was 1,16 for ^3H , and 0,4-0,48 for ^{14}C . The $::\text{CHT}$ biradical has taken one of the two radioactive carbon and all the tritium. His ^{14}C content is 0,5 and ^3H content 1. Hydrogenation of $::\text{CHT}$ to $::\text{CH}_3\text{T}$ needs one mole H_2 whose ^3H content is again 0,37. Thus, the total content is 1,37. This value is to compare with 1,16 measured. This lower value is due to the fact that not all the CH_4 is originated in this way.

Similar mechanisms were elaborated for some of the other minor constituents of the liquid phase : naphthalene and benzene. They will be available in more detailed publications.

- Cracking of perhydrophenanthrene -9,10 ^{14}C

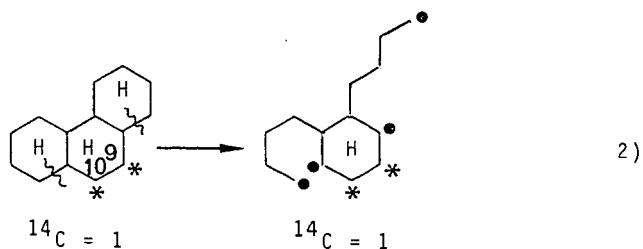
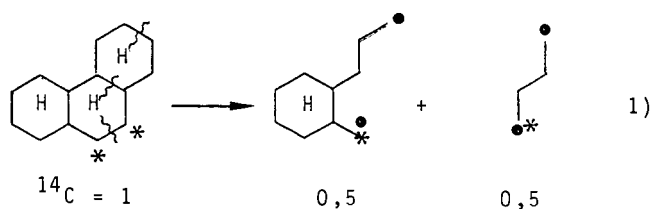
Table VI shows the composition, yields of cracking gaseous and liquid phases, and the respective ^{14}C content of the cracking compounds obtained at 750°C and 2s for perhydrophenanthrene -9,10 ^{14}C .

Experimental results show that no phenanthrene nor hydrophenanthrene are formed : there is no direct dehydrogenation of perhydrophenanthrene as is observed for the hydrophenanthrene. The C-C rupture happens before the C-H rupture. The H_2 production is due to subsequent dehydrogenation of the monocyclicperhydro-or hydrocaromatics.

	Composition(M%)	Yields	^{14}C content
	Gas phase	(M%)	$\frac{(\text{mCi/mM})}{(\text{mCi/mM})}$
H ₂	25,7	103,5	-
CH ₄	26,8	109,5	0,14
C ₂ H ₄	32,1	131,1	0,12
C ₂ H ₆	5,8	23,8	0,17
C ₃ H ₆	5,9	24,0	0,18
C ₃ H ₈	0,4	1,5	-
C ₄ H ₈	3,7	15,1	-
	Liquid phase	(M%)	$\frac{(\text{mCi/mM})}{(\text{mCi/mM})}$
Benzene	33,4	33,8	0,36
Toluene	18,3	18,4	0,60
Ethylbenzene	0,9	0,9	0,71
m,p-xylenes	2,8	2,8	0,74
o-xylene	0,6	0,6	0,74
Styrene	6,2	6,3	0,77
Naphthalene	9,6	9,7	0,87
Perhydrophenant.	-	-	1
Other compounds	28,2	28,6	

Table VI : Composition, yields and ^{14}C content obtained by cracking of perhydrophenanthrene -9,10 ^{14}C ($T^\circ 750^\circ\text{C}$, $t = 2\text{s}$)

Considering also that C₂ and C₃ olefins are detected in the gas phase as soon as the cracking begins two possible pathways can be considered.



The ^{14}C contents of the intermediate species are indicated. Let us consider benzene and toluene formation. Mechanism 1), followed by dealkylation and dehydrogenation of the remaining cycle, leads to inactive benzene and active CH_4 ($^{14}\text{C}=0,5$). Mechanism 2) leads to a benzene with a ^{14}C content of 1. The benzene ^{14}C content measured was 0,36. Thus pathways 1) and 2) contribute respectively for 2/3 and 1/3 to the benzene formation. This leads to the conclusion that in this perhydrocompound there is a preferential rupture between the carbons, in 9 and 10 position.

For toluene, the ^{14}C content measured was 0,6, twice that of benzene. This is in good agreement with what was said for the benzene formation. Pathway 1) is giving toluene with ^{14}C content of 0,5, after elimination of a C_3 radical from the intermediate. Pathway 2) gives as for benzene, toluene with ^{14}C content of 1, after a C_3 and a C_4 elimination and dehydrogenation of the cycle. Considering that as found for benzene, pathway 1) contributes for 2/3 and pathway 2) for 1/3 to the first step of the reaction, the theoretical activity of toluene should be a ^{14}C content of $(2/3 \times 0,5) + (1/3 \times 1) = 0,66$. as to compare with the measured content of 0,60.

Concerning the radioactivity in ethylene which is one of the major products in the gases, the measured ^{14}C content was 0,12. This demonstrates that ethylene is not formed by preferential elimination of the carbon atom in the 9 position.

5. CONCLUSIONS

During hydrocarbonisation of coal, the main reaction below 750°C is hydrodealkylation. This makes possible to optimize the B.T.X. and low boiling phenols formation. Dehydroxylation of the phenols is only important above 750°C giving an increase in water and additional light aromatics. The oxygen content of the coal, corresponding to the hydroxyl group is not hydrogen consuming below 750°C , as it is the case at high temperature where conversion to methane is the goal of the process. Dealkylation of alkylphenols and alkylaromatics explains the almost linear increase with temperature of methane. Hydrogen pressure prevents reassociation of free radicals, not only in the pyrolysis of coal itself, but also in the postcracking process. Due to this fact, naphthalene and other heavy polycyclicaromatics yields remain low, compared to what is found when carbonisation is performed under pressure of an inert gas.

The sulfur elimination in the char depends of the nature of the mineral constituents of the coal. CaCO_3 and MgCO_3 under hydrogen pressure react with sulfur compounds to form CaS . Calcium is not associated with sulfur in the coal, except for some CaSO_4 . But in the char, on the contrary, calcium is combined with the sulfur. The concentration of CaCO_3 is however not sufficient to fix all the sulfur. Pyritic sulfur is eliminated at high temperature. But it seems possible that this sulfur is trapped on CaCO_3 . High sulfur containing coals will only be well desulfurized under hydrolysis conditions if their ashes are poor in CaO and MgO .

Thermal pyrolysis at atmospheric pressure under inert gas demonstrates that all perhydrocyclic hydrocarbons are easily cracked into monocyclic aromatics and ethylene. The mechanism of the ring opening, in the case of perhydrophenanthrene, labelled with carbon 14 in 9 and 10 position, is a rupture of the C-C bond between 9 and 10. This conclusion is in good agreement with the perhydrocompounds cracking results. No formation of naphthalene was observed at low conversion yields of tricyclic perhydrocompounds, what would be the case if opening of the external ring would be the main reaction pathway. Hydrocyclic aromatics

undergo mainly dehydrogenation leading back to the corresponding aromatic starting compound.

The low stability of the perhydropolycyclic compound makes possible to convert industrially the hydropolycyclic compounds, abundant in coal liquid hydrogenates, into benzene and ethylene, two compounds of major importance in industrial organic chemistry. The polycyclic aromatics have to be saturated by additional hydrogenation to the corresponding perhydrocompounds, which can then be directly cracked at 800-850°C for 0,5s residence time, into benzene, ethylene, methane and hydrogen. The process is hydrogen self sufficient.

This work is part of the European Community Program on the "Chemical and Physical Valorisation of Coal".
Coworkers are B.BETTENS, C.BRAEKMAN-DANHEUX, P.BREDAEL, S.FURFARI, F.NINAUVE and TRAN HUU VINH.

REFERENCES

- 1) R.J. BELT, L.A. BISSETT, Report (1978)(DOE), MEJC/RI-79/2
- 2) H.D. COCHRAN, Jr
ACS Symp.Ser. (1979), 110, 37-54
- 3) G. FYNES, W.R. LADNER, J.O.H. NEWMAN
to be published in "Progress in Energy and Combustion Services"
- 4) R. CYPRES
Preprints of the Contribution to the Fifth International Conference on Coal Research, Vol.II, B-2, 23-40, Düsseldorf (1980)
- 5) A. KOROSI, H.N. WOEBCKE and P.S. VIRK
Am.Chem.Soc.div.Fuel Chem. (1976), 21 (6), 190-197
- 6) P. BREDAEL and D. RIETVELDE
Fuel (1979), 58, 215-218
- 7) P. BREDAEL and TRAN HUU VINH
Fuel (1979), 58, 211-214
- 8) C. DELAUNOIS
Ann.Mines de Belgique (1972), 2, 93-107
- 9) R. CYPRES and P. BREDAEL
Fuel Process.Techn. (1980), 3, 297-311
- 10) E. GIL-AV, J. SHABTAY and F. STECKEL
J.Chem.Eng.Data (1960), 5, 98-105
- 11) P. BREDAEL
Ann.Mines de Belgique (1974), 28, 1-6
- 12) R. CYPRES and C. BRAEKMAN-DANHEUX
Ann.Mines de Belgique (1974), 11, 1109-15
- 13) B. BETTENS and R. CYPRES
Tetrahedron (1974), 30, 1253-1260
- 14) A.L.J. BECKWITT and M.J. THOMPSON
J.Chem.Soc. (1961), 73

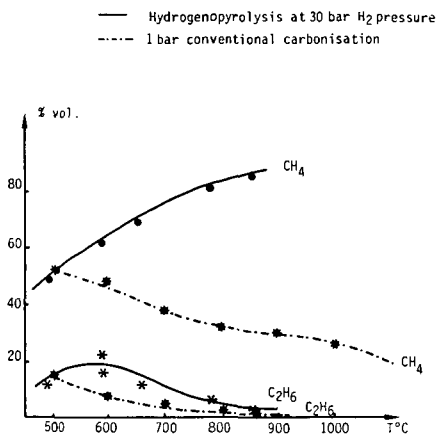


FIG. 1 : GAS COMPOSITION AS FUNCTION OF TEMPERATURE.

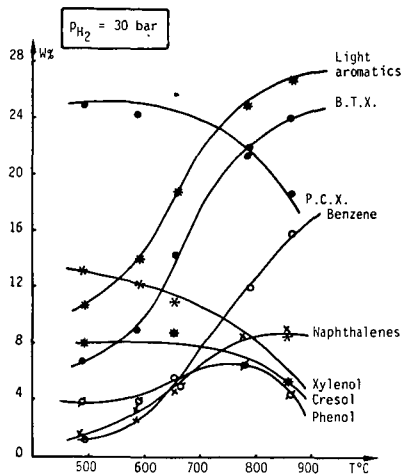


FIG. 2 : OIL COMPOSITION AS A FUNCTION OF TEMPERATURE.
 $\tau = 60s, < 500 \mu m$

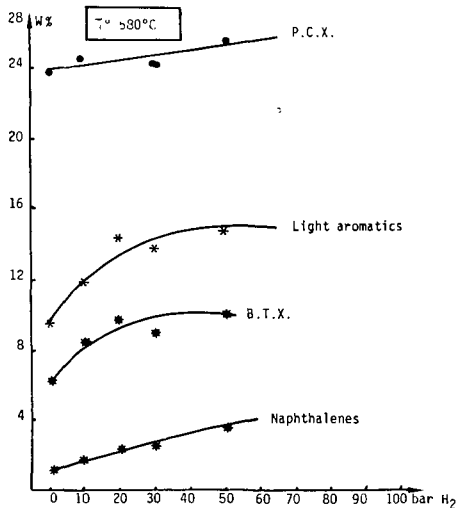


FIG. 3 : B.T.X. AND NAPHTHALENES YIELDS AS A FUNCTION OF H₂ PRESSURE (W% OF DIL)
 $\tau = 60s, < 500 \mu m$

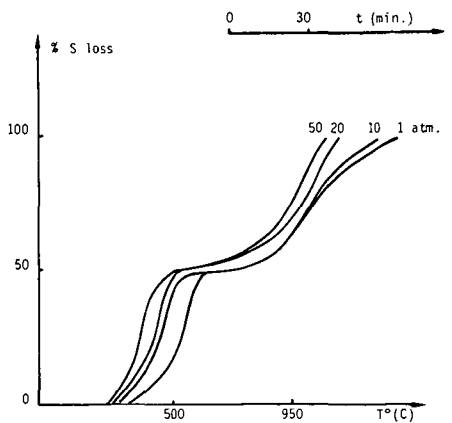


FIG. 4 : REDUCTION OF FeS₂ UNDER H₂ PRESSURE

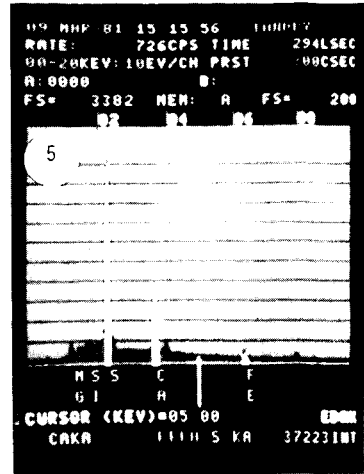
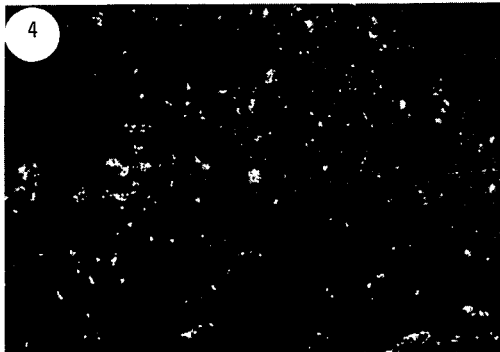
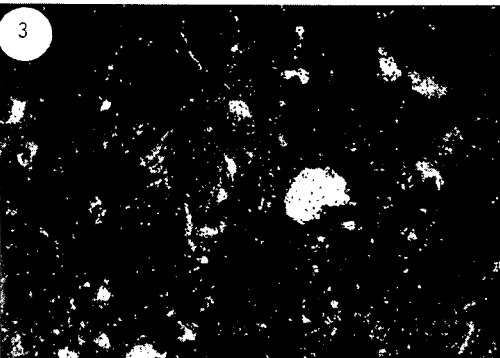
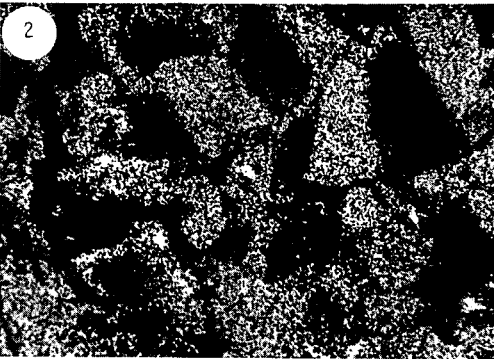


Fig.5 : SEM images

SULCIS COAL (56,4% VM, 12,9% ASH,
4,45% S_t)
before pyrolysis

1. Coal
2. S x-ray distribution image
3. Ca x-ray distribution image
4. Fe x-ray distribution image
5. x-ray spectrum

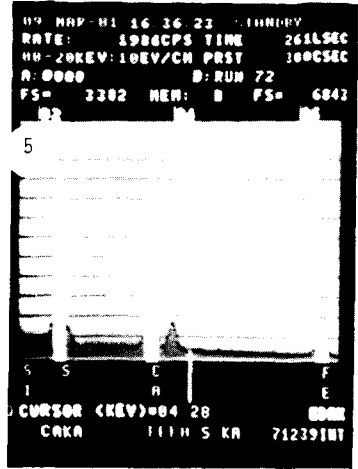
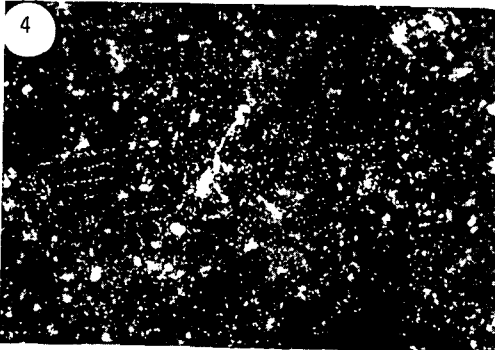
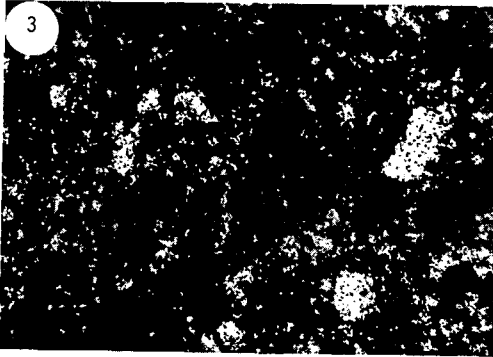
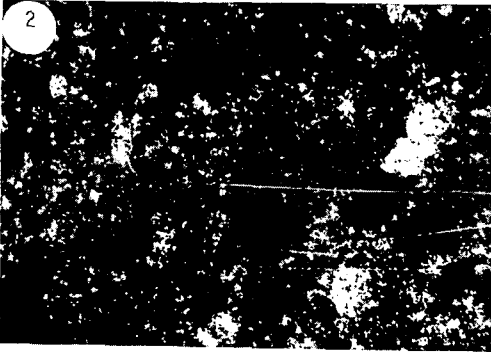
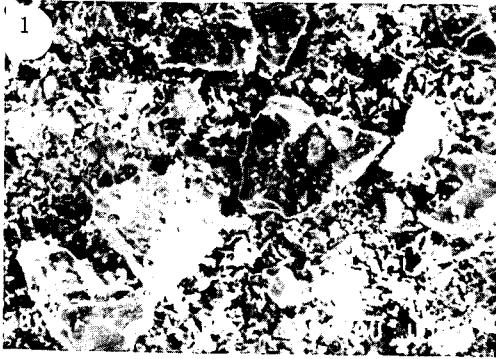


Fig. 6 : SEM images

SULCIS after Hydrogenopyrolysis
850°C - 30 bar H₂

1. Char
2. S x-ray distribution image
3. Ca x-ray distribution image
4. Fe x-ray distribution image
5. x-ray spectrum

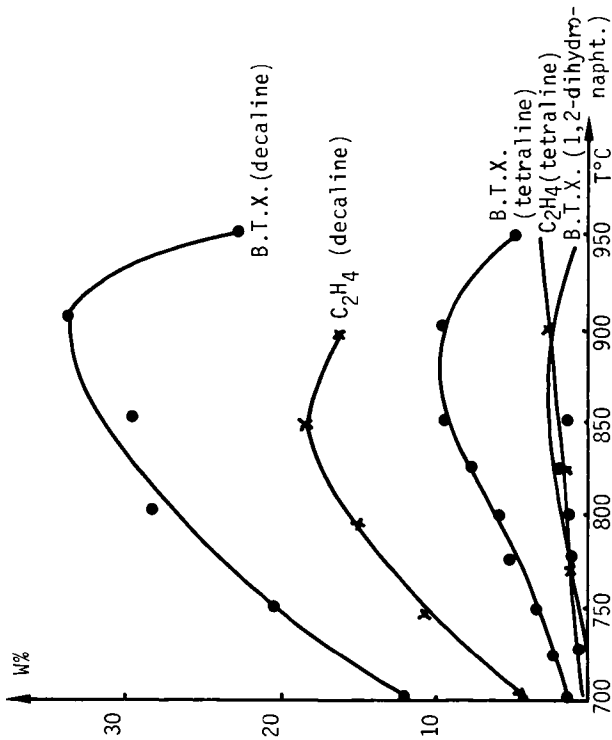


FIG. 7 : PYROLYSIS OF HYDRONAPHTHALENES
W% YIELDS IN B.T.X. AND ETHYLENE

1. B.T.X. (5,6,7,8 -tetrahydro-1-naphthol)
- 1'. C₂H₄ (5,6,7,8 -tetrahydro-1-naphthol)
2. B.T.X. (1,2,3,4 -tetrahydro-1-naphthol)
- 2'. C₂H₄ (1,2,3,4 -tetrahydro-1-naphthol)
3. B.T.X. (cis-1-decalol)
- 3'. C₂H₄ (cis-1-decalol)

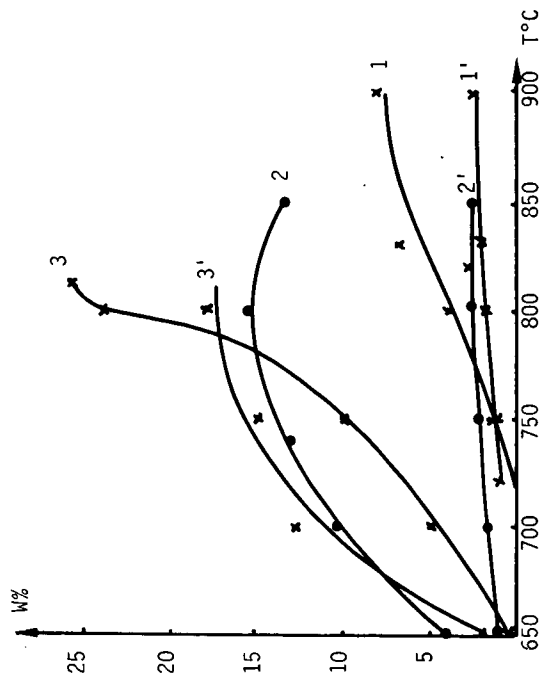


FIG. 8 : PYROLYSIS OF HYDRONAPHTOLS
B.T.X. AND ETHYLENE YIELDS (W%)

AN IN-SITU EXPERIMENTAL OBSERVATION AND
PREDICTIVE MODEL OF FREE RADICAL FORMATION
UNDER LIQUEFACTION REGIME CONDITIONS

By

L. Petrakis, D. W. Grandy and G. L. Jones
Gulf Research & Development Company
P. O. Drawer 2038
Pittsburgh, Pennsylvania 15230

Over the past 24 years, there have been many studies of free radicals in coal by electron spin resonance (ESR) techniques directed towards learning something about coal's chemical structure, petrography and geology (1). More recently, some of the more modern and potentially useful magnetic resonance techniques such as ENDOR have been used to probe the structure of coal (2). Beyond providing structural information and being a natural product of coal metamorphosis, the free radicals in coal, especially those formed during the heating of coal, are believed to play a key role in liquefaction and pyrolysis reactions (3). Our goal is to gain a more complete understanding of the effect of liquefaction process variables on the free radicals in coal and try to find what connection free radicals have with liquefaction, i.e. to answer the question: are free radicals the key to coal liquefaction? We have used ESR spectroscopy to study the free radicals in a variety of coals and vacuum pyrolyzed coals (4), free radicals in the various product components from the solvent refined coal (SRC-I) process (5), and the free radicals in a variety of coal solvent slurries reacted under a variety of conditions (6, 7). Coal macerals, or the various organic constituents of coal analogous to minerals in rocks have also been studied by ESR spectroscopy in our laboratory after a variety of pyrolysis (6) and liquefaction treatments (9). All of these experiments were performed as most have been done in the past, i.e. at room temperature after the reactions had taken place. Recently we have developed

a high temperature, high pressure ESR cavity to study the free radicals in coal during liquefaction (10, 11, 12).

We have used this high temperature, high pressure ESR cavity for detailed study of the effects of process variables on the free radicals in Powhatan #5 coal during liquefaction. The procedure used was a 2^5 factorial design involving two levels each of temperature (400 and 460°C), gas (H_2 and N_2), pressure (8.2 and 11 MPa), solvent (tetralin and SRC-II heavy distillate derived from Powhatan #5 coal) and heating time 3 and 15 minutes to reaction temperature. Free radical spectral parameters were monitored continually from about 2 minutes after reaction temperature was reached, up to one hour. After finding, from this work, that temperature and solvent were the two most important variables, we proceeded to study these variables in more detail, using 400, 425, 450, 460 and 480°C and tetralin, naphthalene and SRC-II as liquefaction solvents. The data from the study of process variables effects and the more detailed study of temperature and solvent effects were analyzed with the aid of a regression model.

Free radical measurements on the coal solvent slurries are done under liquefaction conditions, i.e. in-situ, using a high temperature, high pressure ESR cavity. The details of the cavity and its operation have been published previously (11, 12). The cavity system is basically a cylindrical brass TE₀₁₁ X-band cavity with internal modulation coils and internal axial heater inside a water-cooled beryllium copper pressure vessel. Samples are prepared in 4 mm OD, 2.5 mm ID quartz tubes by placing 0.5 g of Powhatan #5 coal in the bottom of the tube and injecting 0.5 g of tetralin or SRC-II heavy distillate (SHD). In the naphthalene experiments, the coal and naphthalene were premixed at 1:1 by weight and then poured into the sample tube. Temperature measurement is by a thermocouple imbedded in the sample. Typically, several spectra are recorded

before heating and then continuously from about 4 minutes after heating was begun up to one hour. Spin concentration measurements are made relative to the signal from a $\text{CuSO}_4 \cdot 5\text{H}_2\text{O}$ reference on the internal wall of the cavity. The calculations for spin concentration and its temperature correction are outlined in detail elsewhere (12, 13). Data are normally displayed as corrected (to 20°C) spin concentration versus time plots.

About 45 experiments were done using Powhatan #5 coal to screen the major process variables, such as solvent, temperature, gas type, pressure, and heating time. The data from these experiments were used to formulate a regression model to sort out the major effects and their interactions (13). Table I summarizes the results of this model. Reaction time alone was found to be insignificant. Temperature was found to be the most significant variable, accounting for about half of the effects present in the model. When solvent and solvent gas interactions are added in with temperature, almost 90% of the variation of the data is accounted for. Heating time, pressure and gas type alone or in combination with temperature have relatively minor effects on the data.

Based on these observations, it was decided that temperature and solvent type warranted further investigation. Experiments at 425, 440, 450 and 480°C were added as well as a complete series of experiments with Powhatan coal using naphthalene as the liquefaction solvent. Heating time was fixed at 3 minutes, pressure at 1600 psig and hydrogen was used in all of the additional experiments. Figure 1 shows the variation of spin concentration as a function of time for the three coal-solvent systems at 400°C . The points are experimental data and the solid lines are the spin concentrations predicted by the regression model. These are not fitted curves. At time 0,

the slurries are unheated. All points at $t > 0$ are at the desired experimental temperature. Note that the spin concentration in the tetralin solvent experiments is essentially the same as the unheated coal and that all the SHD and naphthalene experiments are somewhat higher. Figure 2 is a similar plot of the experimental data and predicted spin concentrations at 480°C . Here the spin concentration of all three Powhatan coal-solvent slurry systems is much higher than that of the unheated slurries. Again, the same ordering of spin concentration among the solvent systems is observed. The relative order of spin concentration in the solvents, tetralin < SHD < naphthalene, is believed to be due to the relative hydrogen donor capabilities of the three solvents. Naphthalene is a pure aromatic and should have no donatable hydrogens. Tetralin has four donatable hydrogens and SRC-II heavy distillate, although highly aromatic, would be expected to have some donatable hydrogen. Figures 3, 4 and 5 are spin concentration versus time plots displaying the data for all six temperatures used for each of the solvents. The naphthalene, Powhatan coal experimental data, shown in Figure 3, shows the general trend to higher spin concentration with increasing temperature. The data at 400 , 425 and 440° fall very close. There is a similar bunching at higher values for the 450 and 460° data. The spin concentration found at 480° is considerably higher than all the other data from the lower temperatures. The SHD Powhatan coal experiments, shown in Figure 4, show a similar ordering of spin concentration among the 6 temperatures, however, the values at the corresponding temperatures are lower than in the previous figure depicting the naphthalene experimental data. Figure 5, showing plots of spin concentration versus time for the tetralin solvent experiments, has a similar trend of increasing spin concentration with temperature, however, the order of the 460 and 480°C data are reversed compared to the other two solvents. From these data and a few data

taken under similar conditions at 470°C, there appears to be a maximum in spin concentration around 460°C in the Powhatan coal tetralin slurry system.

Discussion and Conclusions

1. In general, the coal free radicals are quenched in following the order of naphthalene<SHD<tetralin. This conclusion agrees with our expectations which are based upon the amount of donatable hydrogen present in the three solvents. The rate of free radical formation is assumed to be only temperature dependent. This is based on previous extensive pyrolysis experiments with coals and coal macerals. The observed free radical concentration depends on the competing effects of free radical formation and free radical quenching. The latter, unlike the former, is solvent dependent. The solvent dependency will be determined both by the amount of donatable hydrogen that is available as well as by the ease with which the free radical quenching hydrogen can be transferred to the coal free radicals.

2. The free radical concentration of the liquefaction slurry generally increases with increasing temperature. This is strictly true for the naphthalene and SHD experiments and is followed by the tetralin experiments up to 460°C where an apparent maximum is reached, with the spin concentration decreasing then at higher temperatures. The general increase in spin concentration with temperature is expected due to the greater thermal energy available for bond breaking. From the results of the correlative model, we find that about half of the variation in the spin concentration is due to temperature alone. Temperature and solvent interactions account for 70% of the observed effects.

3. The spin concentration is dependent upon reaction time and this dependence is also influenced by solvent and temperature. At 400°C, the relative slopes of the spin concentration versus time curves, from 0.1 to 1.0 hr., are 15, 5 and 0×10^{18} spins/g per hour for the naphthalene, SHD and tetralin experiments, respectively, demonstrating the solvent dependence. At 480°, the slopes have increased to 40, 35 and 20×10^{18} spins/g per hour for the same three solvents.

4. From the results of the full correlative model, we find that temperature, solvent and residence time and their interactions account for about 90% of the effects noted in the free radical concentration. Gas type has some minor significance as does pressure. Heating time has a negligible effect.

ACKNOWLEDGMENT

This work was performed under United States Department of Energy sponsorship, Contract No. DE-ACO-179ET14940. The authors wish to acknowledge the expert technical assistance of Mr. A. V. Fareri in the experimental aspects of this work.

References

1. H. T. Schamler and E. duRutter in "Chemistry of Coal Utilization", Supp. Vol. (H. H. Lowry Ed.) John Wiley and Sons, Inc. New York, 1963 pp 78-85.
2. H. L. Retcofsky, M. R. Hough and R. B. Clarkson, ACS Fuel Div. Preprints, Vol. 24, No. 1, 1979 p 83.
3. R. C. Neavel, Fuel 55, 237 (1976).
4. L. Petrakis and D. W. Grandy, Anal. Chem. 50, 303 (1978).
5. D. W. Grandy and L. Petrakis, Fuel, 58, 239 (1979).
6. L. Petrakis and D. W. Grandy, ACS Fuel Div. Preprints, Vol. 23, No. 4, 1978 p. 147.
7. L. Petrakis and D. W. Grandy, Fuel, 59, 227 (1980).
8. L. Petrakis and D. W. Grandy, Fuel, 60, 115 (1981).
9. L. Petrakis and D. W. Grandy, Fuel, 60, 120 (1981).
10. L. Petrakis and D. W. Grandy, Nature
11. D. W. Grandy and L. Petrakis, J. Mag. Res. 41, 367 (1980).
12. L. Petrakis, D. W. Grandy, R. G. Ruberto and N. L. Carr, "Fundamentals of Coal Depolymerization", Quarterly Report, DOE/ET/14940-2, NTIS, Springfield, VA 1980.
13. L. Petrakis and D. W. Grandy, submitted to Fuel.

TABLE I

GENERAL CORRELATION MODEL

<u>Variables Effects*</u>	<u>Sum of Square of Each Term</u>	<u>Fractional Contribution of Each Term</u>	<u>Fractional** Probability of Null Hypothesis (i.e., term not significant)</u>
C ₁ •time•temperature	119455	.480	.0001
C ₃ •time•temperature•solvent	51511	.207	.0001
C ₂ •time•temperature•solvent•gas	52284	.210	.0001
C ₄ •time•pressure	8025	.032	.0001
C ₅ •time•temperature•heating rate	6556	.026	.0001
C ₆ •time•temperature•gas	4739	.019	.0001
C ₇ •time•temperature•pressure•gas	4355	.017	.0001
C ₈ •time•pressure•heating rate	652	.003	.0129
C ₉ •time•temperature•pressure	565	.002	.0205
C ₁₀ •time•heating rate	358	.001	.0649
C ₁₁ •time	256	.001	.1184

Total Number of Points = 773; Total Data Sum of Squares = 328302; Total Model Sum of Squares = 248755; Error = 79548; R-Square (Model SOS/Total SOS) = 0.758

* Corrected Spin Concentration = Intercept + Sum of Terms.

** The lower the number, the higher the probability that the variable effects are real.

SPIN CONCENTRATION VS. ELAPSED TIME
POWHATAN #5 COAL, 1600 psig H₂, 400°C 3 min HT.

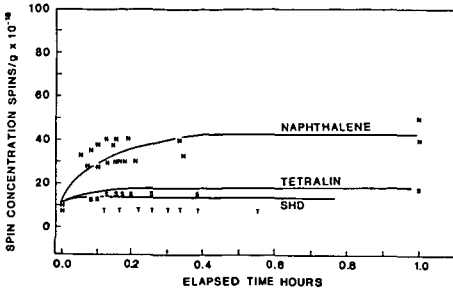


FIGURE 1

SPIN CONCENTRATION VS. ELAPSED TIME
POWHATAN #5 COAL, 1800 psig, 480°C 3 min HT.

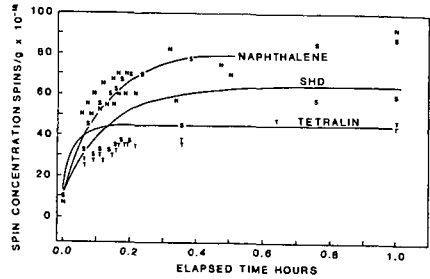


FIGURE 2

SPIN CONCENTRATION VERSUS ELAPSED TIME
POWHATAN #5 COAL AND NAPHTHALENE
1800 psig (11.0 MPa) H₂ 3 min HT
AVERAGE VALUES

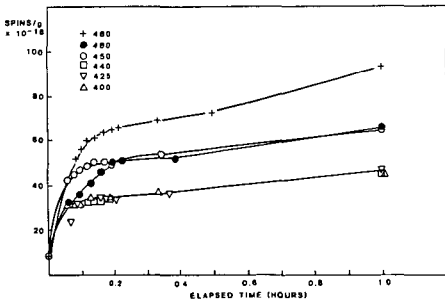


FIGURE 3

SPIN CONCENTRATION VERSUS ELAPSED TIME
POWHATAN #5 COAL AND SRC II HEAVY DISTILLATE
1800 psig (11.0 MPa) H₂ 3 min HT
AVERAGE VALUES

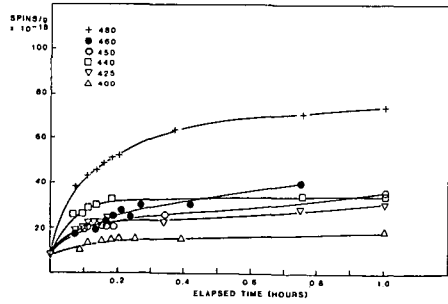


FIGURE 4

SPIN CONCENTRATION VERSUS ELAPSED TIME
POWHATAN #5 COAL AND TETRALIN
1800 psig (11.0 MPa) H₂ 3 min HT
AVERAGE VALUES

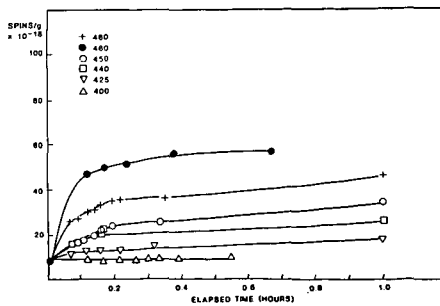


FIGURE 5

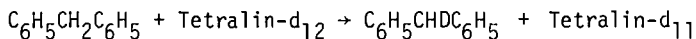
The Catalysis of the Exchange Reactions Between Tetralin- d_{12} and Diphenylmethane by Inorganic Compounds

C.B. Huang, H.-H. King and L.M. Stock

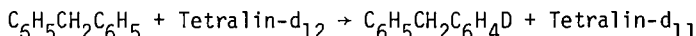
Department of Chemistry
University of Chicago
Chicago, Illinois 60637

Introduction

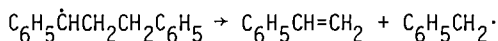
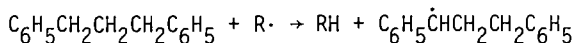
An array of inorganic compounds have been investigated as catalysts for coal gasification reactions (1,2). The pathways by which these compounds alter the rate and the product distributions in the gasification reaction have not been fully resolved. Whether the most effective catalysts promote the initiation reactions which occur at the threshold temperatures or the rapid gas forming reactions at the higher ultimate temperatures has not been established. We sought to resolve this point by an investigation of the influence of inorganic substances on the exchange reactions between the hydrogen atoms in the benzylic positions and the hydrogen atoms in the



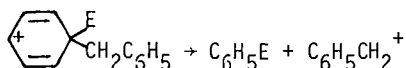
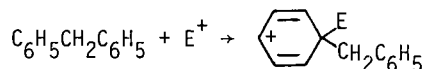
aromatic positions. These exchange reactions proceed slowly at 400°C in the



absence of catalysts (3). Both of these reactions may contribute in an important way to the breakup of the coal structure during the gasification reactions shown for the radical initiated decomposition of a 1,3-diphenylpropane:



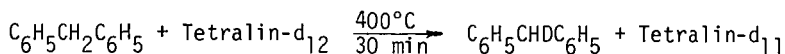
and the acid-catalyzed decomposition of a diphenylmethane with an electrophilic agent, E^+



In the absence of a catalyst at 400°C, the free radical exchange reaction between the hydrogen atoms in the benzylic positions occurs much more readily than the exchange reactions of the hydrogen atoms bonded to the aromatic ring (3). Accordingly, we sought evidence for the acceleration of either process in the presence of inorganic compounds.

Results and Discussion

In each experiment, diphenylmethane (0.377 mole) and tetralin-d₁₂ (0.377 mole) and a potential catalyst (0.045 mole) were sealed in a glass reactor at ambient temperature. The reactor was submerged in a fluid sand bath at 400°C for the desired reaction interval. After cooling, the organic contents of the reactor were separated from the inorganic reagents and analyzed by gas chromatography and nuclear magnetic resonance. The exchange reaction proceeds to give about 15% of the monodeuterio com-



15%

pound in 30 minutes in the absence of a catalyst. Lithium, sodium and potassium chloride are ineffectual as expected. Similarly, sodium fluoride, chloride, bromide and sulfate did not accelerate the exchange reactions. Sodium iodide enhanced the benzylic exchange reaction to a minor extent (22%). Iodine and hydrogen iodide accelerate the reaction to a much greater extent.

Lithium, sodium, and potassium carbonate and sodium and potassium bicarbonate do not enhance the exchange reactions. Thus, none of the alkali metal compounds exert any catalytic influence on this exchange reaction at the threshold temperature of 400°C.

Somewhat similar results were realized with the alkaline earth compounds. Neither calcium oxide or carbonate or barium carbonate or oxide enhance the exchange reaction. Calcium and magnesium chloride are also ineffectual catalysts for the exchange reaction after a 30 minute reaction. However, our preliminary results for reactions carried out for 120 minutes suggest that magnesium chloride enhances the rate of the exchange of the hydrogen atoms of the aromatic nucleus but not the benzylic exchange reaction.

Zinc halides also exert an accelerating influence on the rate of exchange of both the aliphatic and aromatic hydrogen atoms.

Compound	%D in Recovered Diphenylmethane		%D in Recovered Tetralin		
	Ar	α	Ar	α	β
ZnCl ₂	12	9	54	88	86
ZnI ₂	37	40	40	28	52

Whereas cadmium chloride is inactive, compounds such as stannous chloride and stannic chloride selectively enhance the rate of exchange of the aromatic hydrogen atoms of diphenylmethane and tetralin-d₁₂ at 400°C. Anhydrous vanadium trichloride and ferric chloride and hydrated chromous chloride and hydrated cupric chloride exert a similar effect on the reaction.

Compound	%D in Recovered Diphenylmethane		%D in Recovered Tetralin		
	Ar	α	Ar	α	β
SnCl ₂	19	0	28	91	91
CuCl ₂ ·2H ₂ O	24	5	44	92	92

Other highly reactive compounds such as aluminum chloride and molybdenum (V) chloride cause extensive reactions of the diphenylmethane and the tetralin. Moreover, oxidizing agents, for example, the oxides of lead and iron convert diphenylmethane to benzophenone.

The results obtained at the threshold temperature of 400°C strongly suggest that catalysts can selectively initiate free radical or electrophilic decomposition reactions of many coal molecules. The diverse character of the results will be emphasized in the presentation.

References

- (1) Johnson, J.L., "Kinetics of Coal Gasification," John Wiley and Sons, New York, New York (1979).

- (2) McKee, D.W., "Catalyzed Gasification Reactions of Carbon," in "Chemistry and Physics of Carbon" edited by P.L. Walker, Jr. and P.A. Thrower. Volume 16, p. 1 (1981).
- (3) H.-H. King and L.M. Stock, "Influence of Illinois No. 6 Coal and Coal-related Compounds on the Exchange Reaction Between Diphenylmethane and Perdeuteriotetralin," Fuel, 59, 447 (1980).

THE RATE AND THE MECHANISM OF CATALYTIC COAL LIQUEFACTION BY IRON SULFIDES: PART I.

THE SYSTEM $FeS_x : H_2 : H_2S$, RATES OF REACTION AND SURFACE CONVERSION

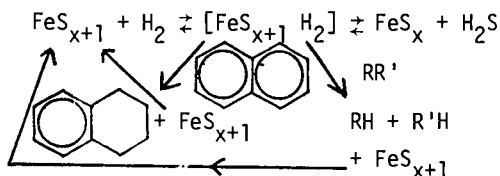
By: Attar, A. and Martin, J. B.

Dept. Chem., Eng., N.C.S.U., Raleigh, N.C. 27650

INTRODUCTION

The systems $FeS_2-H_2-H_2S$ and FeS_2 -hydrogen donor- H_2S play a critical role in the catalysis of coal liquefaction by naturally occurring minerals. Consequently, there is a tremendous incentive to understand the exact mechanism and rates of reaction which affect the catalysis of coal liquefaction by FeS_x .

Examination of the data available in the literature and studies from our own laboratory suggest that the dominant catalytic action is due to the formation of an intermediate compound, possibly $[FeS_{x+1}H_2]$ which can react according to the scheme:



The main function of the FeS_{x+1} is to permit conversion of molecular hydrogen to organically bound hydrogen, either in the form of donor molecules and/or coal derived molecules. The $[H_2S]/[H_2]$ plays a critical role in this system since its value determines the equilibrium distribution of the active catalytic intermediate, $FeS_{x+1}H_2$, and the less active species FeS_{x+1} and FeS_x .

This mechanism explains many of the observations in the system coal-solvent- FeS_2 . The most important facts are:

1. Catalytic action by Fe salts is observed only when H_2S is present in the reactor. The level of the catalysis depends on the ratio $[H_2S]/[H_2]$.
2. Regardless of the starting material, when the FeS_x is allowed to catalyze the reaction long enough, a fixed ratio of Fe to S is achieved, typically of the order of $Fe/S \approx 1/1.09$. Such a ratio could be the result of the thermodynamic equilibrium achieved for the coal at the prevailing $[H_2S]/[H_2]$.
3. The type of pyrite used to catalyze the reaction influences mainly the rate of the initial stages of the reaction but has little effect on the results of long time liquefaction.

Since the ratio $[H_2S]/[H_2]$ (gas) and the ratio Fe/S (solid) play such a critical role in the liquefaction, it appeared useful to quantitize the rate of the individual reactions involved. To achieve reasonable data, it appeared essential that the same sample of FeS_2 be tested so that it would be possible to avoid questions related to the conversion of the surface and so that small differences in reactivity could be determined. In this paper preliminary results are presented on the system $FeS_x-H_2-H_2S$.

EXPERIMENTAL

In order to have more or less the same surface area and the same surface conditions, a pulsed differential reactor (PDR) was used, similar to that described by Attar (1979). The only difference was that a S.S.

packed bed reactor 1/4" ID x 1 ft packed with -100+120 mesh FeS₂ particles was used as the reactor. Helium was used as the carrier gas and pulses of H₂, H₂S or CO were used to investigate the effect of the surface conversion of the pyrite on its reactivity, the activation energies for the reaction, etc. Figure 1 is a schematic diagram of the reaction system.

In a typical experiment, a pulse of H₂ was injected into the He carrier and the product pulse, which consists of unreacted H₂ and H₂S + S₂ was separated on a Chromosorb 105 column and the components were determined by a TC detector.

ANALYSIS OF THE DATA

The relative rate of reaction, r_j , in the j -th pulse was determined from the consumption of the hydrogen, i.e.,

$$r_j = \frac{W_{H_2}^0 - W_{H_2j}}{W_{H_2}^0} \quad (1)$$

where $W_{H_2}^0$ is the number of moles of H₂ injected and W_{H_2j} are the number of moles of incorporated H₂. The temperature was programmed during most of the experiments, in order to allow the determination of the variations of r_j with the temperature. To a first order approximation, since the surface was barely converted in each pulse, one may write, assuming Arrhenius dependence of the rate constant on the temperature:

$$r_j = k_0 \exp\left(-\frac{E}{RT}\right) [\overline{H_2}] \quad (2)$$

or roughly:

$$\log r_j = \log \left[1 - \frac{W_{H_2j}}{W_{H_2}^0}\right] = \log k_0 [\overline{H_2}] - \frac{E}{RT} \quad (3)$$

$[\overline{H_2}]$ is the average concentration of H₂ near the surface and E is the activation energy. Figure 2 shows some of the data obtained. Curves A, B and C were done on the same pyrite sample by successive injection of H₂ pulses in three cycles of heating and cooling of degassed FeS₂. The data indicate that as the surface is being converted, the activation energy rises slightly, from 26.4 to 27.4 kcal/mole for about 1% surface conversion and that the preexponential factor decreases. This is due to the accumulation of FeS_{2-y} near the surface which resists to the diffusion of S⁼ in the solid (see ref. 2).

Curve D was obtained using a different sample of iron pyrite while curve E was derived with a specially prepared sample of FeS₂. The last curve indicates that sample D is a much more reactive specimen, with an activation energy of 22.7 kcal/mole and a larger preexponential factor than the raw FeS₂.

SUMMARY

A new mechanism is proposed for catalytic coal liquefaction using FeS_x. The mechanism includes many of the observed facts on the role of Fe, S, H₂ and H₂S in such a system. Preliminary data are presented on one of the subsystems, i.e., FeS₂ + H₂ and the role of surface conversions in deactivation of the reaction of FeS₂ with pure H₂ is demonstrated. Specially prepared samples of FeS₂ appear to have a much larger activity toward H₂, and as will be shown in a future paper, much larger catalytic effect on the rate of coal liquefaction.

REFERENCES

1. Attar, A., Rev. Sci. Inst., 50 (1), 111 (1979).
2. Attar, A., Fuel, 58, 201 (1978).

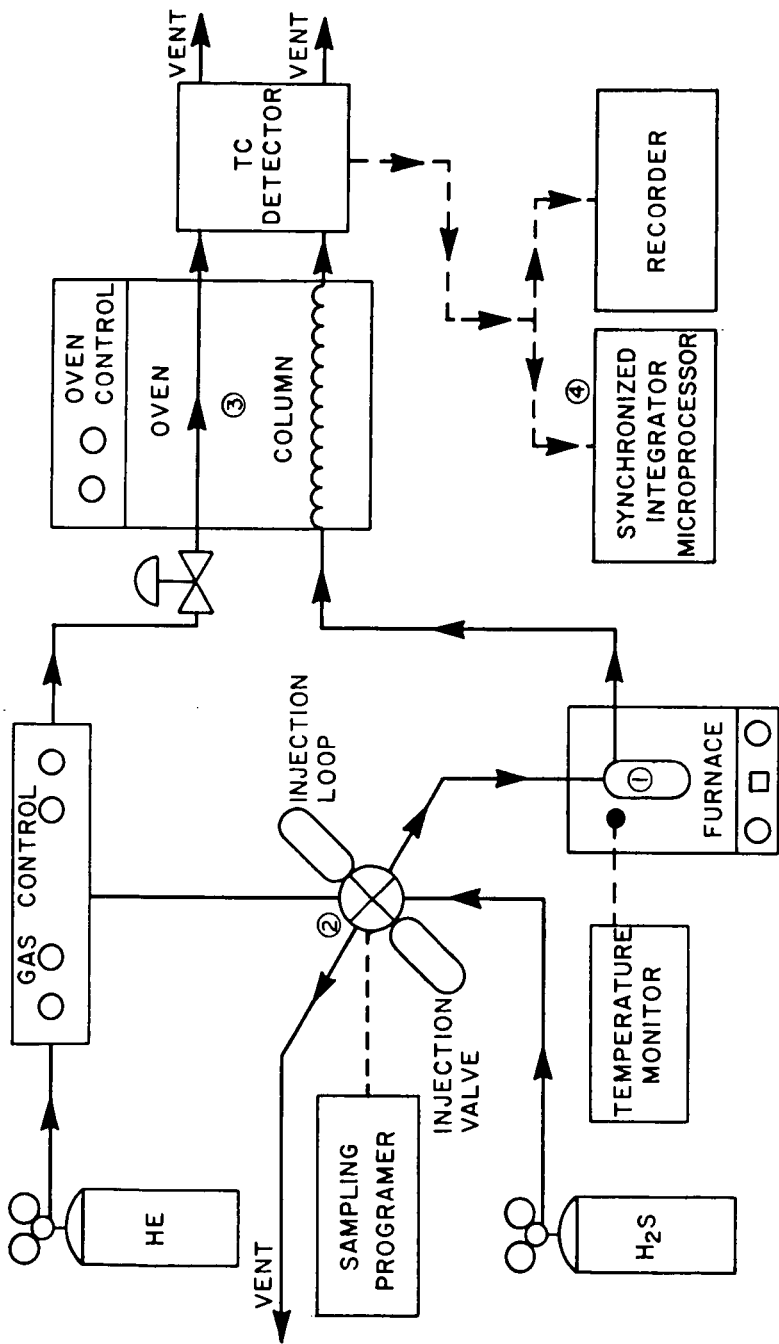


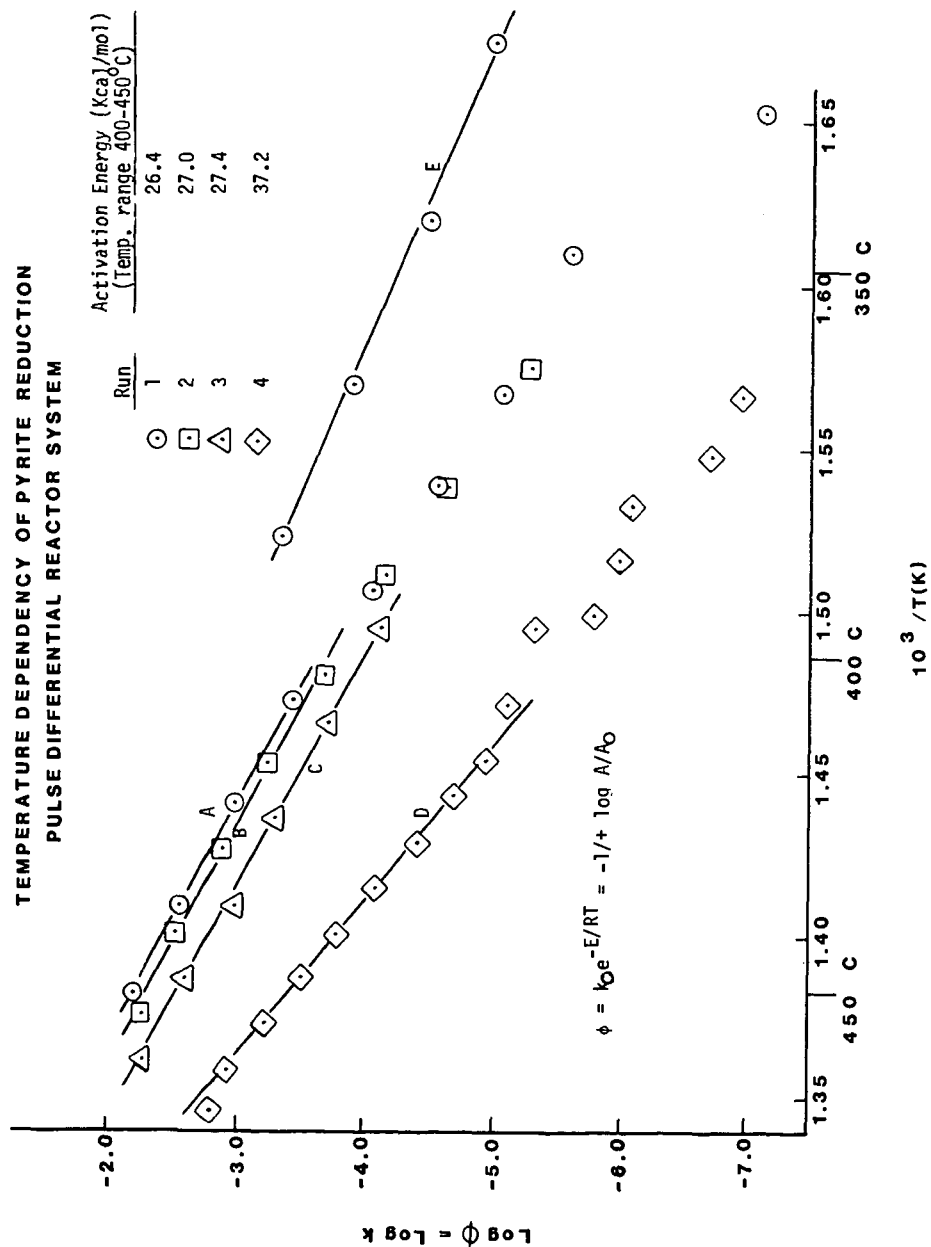
FIGURE 1

Figure 2

TEMPERATURE DEPENDENCY OF PYRITE REDUCTION
PULSE DIFFERENTIAL REACTOR SYSTEM

Activation Energy (kcal./mol)
(Temp. range 400-450°C)

Run	Activation Energy (kcal./mol)
1	26.4
2	27.0
3	27.4
4	37.2



MODELLING OF LIGNIN THERMOLYSIS [†]

M.T. Klein* and P.S. Virk

Department of Chemical Engineering
Massachusetts Institute of Technology, Cambridge, MA 02139

Introduction

The object of the present work was to attempt a fundamental description of lignin thermolysis. This was motivated by a recognition that the increased use of biomass and low-rank coal resources must be accompanied by an enhanced understanding of the factors which influence their thermal processing. Since lignin is a major component of biomass, and has a direct evolutionary linkage to peat and lignitic coals, insights into its thermolysis should prove relevant to the practical pyrolyses of both biomass and coal.

Our investigation comprised three major components. First, a critical examination of lignin structure and chemistry was undertaken to discern the most likely thermolysis reaction pathways. Second, based on the foregoing, model compounds mimicking the essential reactive moieties in the lignin substrate were selected and pyrolysed. Third, and finally, reaction pathways suggested by the model compound studies were coupled with a structural analysis of lignin to formulate a mathematical model which simulated the essential features of lignin thermolysis. The present paper will focus on the modelling of lignin thermolysis; a special effort is made to compare our model results with experimental data from lignin thermolyses previously reported in the literature.

In outline of what follows, our approach to the problem is described first. This includes an analysis of lignin structure; the choice of model compounds with a summary of their experimentally-ascertained pyrolysis pathways; and the logic and mathematics of the lignin thermolysis simulation. Representative results are presented next, the simulated lignin thermolyses being described by the time-evolution of products, including gases, aqueous liquids, phenolic tars, and residue (char). We conclude with a discussion wherein the results of our simulation are compared with experimental data reported in the literature for each of the foregoing product fractions.

Lignin Structure

Lignin is a natural phenolic polymer formed by an enzyme-initiated random free-radical co-polymerization of coniferyl, sinapyl and coumaryl alcohol monomers. The available information concerning lignin structure is best summarized in Freudenberg's (1) classic depiction of "a representative portion of spruce lignin", shown in Figure 1, which was the starting point for the present investigation. Freudenberg's formula should not be interpreted as a literal chemical structure for lignin but rather as a schematic depiction of the bond types and proportions found therein by experiments (1, 2, 3).

Analysis of Freudenberg's formula led to its characterization along the following lines. Each aromatic unit, arising from a monomer, possesses in general a set of propanoid (3-carbon-atom) and methoxy-phenol substituents. These aromatic units are connected by eight types of interunit linkages. The most prevalent linkage is the β -etherified guaiacyl glycerol moiety, as occurs between the methoxyphenol of

*Present Address: Department of Chemical Engineering
University of Delaware, Newark, DEL 19711

[†]This work was supported by seed funds from the MIT Energy Laboratory.

unit 6 in Figure 1. Other linkages found, in descending frequency of occurrence, are α -ether (units 3-4), diphenylmethane (units 2-3), diphenylether (units 6-7), biphenyl (units 9-10), pinoresinol (units 8-9), and phenylcoumaran (units 17-18). An essential feature of lignin structure is that the propanoid and methoxyphenol substituents on a given aromatic unit are essentially independent of one another since they are never involved in bonding with each other. Thus, the probability that an aromatic unit should contain a propanoid substituent of type k and a methoxyphenol of type j is the product of the individual probabilities of the occurrence of k and j, as given in Figure 1.

The foregoing probabilistic interpretation of Freudenberg's lignin formula is reduced to an aromatic unit matrix A in Figure 2. Each matrix element a_{jk} represents the number of aromatic units which possess type j methoxyphenol and type k propanoid substituents. Each row of the matrix represents a specific methoxyphenol found in lignin; these can originate from each of the three lignin monomers and within these the phenolic moiety may either be free or etherified in any of four forms, namely phenethylphenylether, benzylphenylether, phenylether and phenylcoumaran. Each column of the matrix represents a 3-carbon-atom propanoid side chain, respectively guaiacyl glycerol(β -ether, $\alpha\beta$ -ether, α -phenyl β -ether), phenyl hydroxy acetone, cinnamaldehyde, pinoresinol, conidendrinoidlactone, and phenylcoumaran.

The matrix A of Figure 2 serves three purposes. First, the chemical moieties contained in its rows and columns are the basis for selection of model compounds relevant to lignin thermolysis. Second, the numerical values of each element offer a concise probabilistic description of the lignin substrate. (Note, incidentally, that the present A-matrix refers to the prototypical spruce lignin described by Freudenberg's formula; in the more general case, A will be a function of lignin origin.) Third, as we shall shortly find, lignin thermolysis generally leaves aromatic units intact while altering the substituents; a natural extension of the A-matrix to account for all possible products from thermolysis of the moieties in its rows and columns can then be used to unambiguously chronicle lignin thermolysis in terms of the substituents associated at any time with each of the original (conserved) aromatic units of the lignin substrate.

Model Pathways

Model compounds selected to mimic the thermal reactions of lignin are listed in Table 1. For each entry, the table lists an abbreviated name, chemical structure, the aspect of lignin structure modelled, and experimental pyrolysis conditions of temperature, holding time, and initial concentration. It can be verified that the entries in Table 1 model most of the interunit linkages (IL), methoxyphenol substituents (MP), and propanoid chains (PC) which appear in Figure 1. Specifically, PPE models the β -ether linkage most prevalent in lignin; guaiacol models the methoxyphenol substituent associated with coniferyl alcohol which is the dominant monomer in spruce lignin; veratrole models an etherified methoxyphenol; cinnamyl alcohol models a propanoid chain substituent, as do cinnamaldehyde, iso-eugenol, and acetophenone. Note also that some of the compounds in Table 1 were chosen to model moieties which, while not originally present in lignin, arise during its thermolysis; for example, saligenol models a propanoid enol moiety resulting from the primary reversion of a guaiacyl-glycerol β -ether. Still other compounds in Table 1, such as anisole, served as controls in the mechanistic interpretation of the model pyrolyses.

Results of the model compound pyrolyses are summarized in Table 2. For each substrate, the table delineates the observed pyrolysis pathways, their associated products, and reaction kinetics. Primary pathways are designated with an R while secondary pathways, involving reactions of a primary product, are designated with an S. Reaction kinetics are described by Arrhenius parameters ($\log_{10}A(s^{-1})$, $E^*(kcal/mol)$) for pseudo-first order reaction; actual reaction orders, where experimentally ascertained, are quoted in the final column of the table. As an example, in entry 1, PPE decomposes by primary reaction R1 to phenol and styrene

products; the associated Arrhenius parameters are (11.1, 45.0) and the reaction was experimentally found to be first order in PPE; further, the styrene product of R1 undergoes secondary reaction S1 to form ethyl benzene, toluene, and benzene. The data presented in Table 2 now permit a quantitative description of reaction pathways and kinetics in lignin thermolysis.

Simulation of Lignin Thermolysis

The logic employed in our simulation of lignin thermolysis is depicted in Figure 3. Consider first some typical transformations experienced by a lignoid aromatic unit as shown in Figure 3a. Initially (time $t=0$), this unit I will be recognized as element a_{11} of the spruce lignin matrix A . During thermolysis, suppose the propanoid chain of I is sequentially subjected to β -ether reversion, pathway R1:PPE in Table 2, and enol product dehydration, by pathway R1:SAL in Table 2. At some time t_1 , then, the substrate I will, in part, be transformed to the intermediate product II with concurrent evolution of water. However, II can further react by parallel pathways R1:CAD and R1:GUA, respectively leading to propanoid chain decarbonylation and methoxyphenol demethanation; thus at some further time t_2 , II will, in part, be transformed to III, with concurrent evolution of carbon monoxide and methane. It should be noted that in Figure 3a, the original aromatic ring remains intact while its propanoid chain and methoxyphenol substituents are variously altered, chronicling the course of thermolysis. In mathematical terms, each substituent contained in the original A matrix gives rise to a new set of substituents that represent its thermolysis according to the pathways given in Table 2. At any time, the contents (aromatic units) of the original element a_{jk} of A are conserved while being redistributed into the elements p_{mn} of a new P (product)-matrix which represents all possible substituents that can arise from the original set. A little reflection will show that A is really a submatrix (the top left corner, say) of P . Some further detail into the nature of the P -matrix, and the methods for product accounting, is given in Figure 3b. Consider the coniferaldehyde unit II in lignin, undergoing thermolysis. In Figure 3a, for simplicity, this was shown to react by two parallel pathways; however, in practice, it will undergo all possible reactions accessible to its methoxyphenol and propanoid chain substituents. Since these substituents are independent, the products will be formed by a superposition of the type shown in Figure 3b. The methoxyphenol in II is modelled by guaiacol A, which can pyrolyse by pathways R1: GUA and R2: GUA of Table 2 to catechol B and phenol C. The propanoid chain in II is modelled by cinnamaldehyde D which can pyrolyse by R1: CAD to styrene E. Thermolysis of II will then form all of the products shown in Figure 3b (and their associated gases), in amounts commensurate with the kinetics of the pathways involved.

The foregoing chemical logic was employed to mathematically simulate a constant volume batch pyrolysis of lignin. In this simulation, a set of differential equations, which described the time-variation of aromatic unit substituents, were solved numerically from an initial condition representing Freudenberg's spruce lignin. The rate of change of a given substituent was, in general, proportional to all other substituents, so that:

$$\text{Differential Equations: } dX/dt = \underline{K}X; \quad dY/dt = \underline{L}Y \quad (1)$$

$$\text{Initial Condition: } X = X_0, Y = Y_0 \text{ at } t = 0 \quad (2)$$

In these the vector X represents all methoxyphenol-related substituents while vector Y represents propanoid chain-related substituents; these are, respectively, the rows and columns of the product matrix P . The matrices K and L , derived in large part from Table 2, respectively contain the kinetic rate constants of those chemical reactions producing the components of vectors X and Y . The initial values X_0, Y_0 coincide with the sums of each row and column in the matrix A , depicting the lignin substrate. Values of the vectors X and Y at any subsequent time t are a consequence of all possible chemical transformations embodied in the matrices K and L . The contents of an element p_{mn} of the product matrix P then show the number of aromatic

units with methoxy-phenol related substituent m and propanoid chain-related substituent n. The nature of substituents m and n further permits the classification of product p_{mn} as either tar (single-ring aromatic unit) or residue (multiple aromatic rings). Details of the simulation logic, mathematics, and numerical evaluation are available (4).

Results

Thermolysis of the prototypical spruce lignin of Figure 1 was simulated at temperatures of 300, 400, 500, and 600C to holding times of 10^4 , 10^4 , 10^2 , and 10^1 seconds, respectively. Representative results at 500C are presented in Figure 4, an arithmetic plot of product yield, expressed as weight percent of original lignin substrate, versus time. Four product fractions, namely, gas, aqueous liquids, phenolic liquids and carbonaceous residue, will be considered.

In regard to gas evolution, the simulation accounts for methane and carbon monoxide. In the uppermost section of Figure 4 it can be seen that both gases evolve fast initially and then more slowly, attaining asymptotic yields of circa 6 wt %, with methane slightly exceeding CO. The methane arises primarily from guaiacyl types of methoxyphenol moieties, both those which are initially present with a free hydroxyl and those which arise by reversion of etherified hydroxyls. The CO originates both from the decarbonylation of carbonyl-containing propanoid chains and, to a lesser extent, from the demethoxylation of methoxyphenols. An account of these dual sites for CO release possessing quite different activation energies relative to the sites for CH_4 release, the simulation predicts that the ratio of CO/ CH_4 should be >1 at low temperatures and conversions, <1 at moderate temperatures and conversions (as in Figure 4), and then again >1 at high temperatures.

Among aqueous liquids, the simulation accounts for water and methanol. As seen in the second (from top) section of Figure 4, the water yield increases monotonically, but with decreasing slope, to an ultimate value of ≈ 5 wt %. The water arises from two sources; predominantly it is formed from dehydration of enol units which result after β -ether reversion; minor amounts also arise from degradation of cinnamyl-alcohol types of propanoid chains. The ultimate methanol yield predicted is only about 0.1 wt %. This rather small value comes about because, in the simulation, methanol arises solely from cinnamyl alcohol moieties, which are relatively rare in lignin; further, the methanol-forming pathway is itself relatively minor amongst cinnamylalcohol pyrolysis pathways.

The phenolic liquids fraction of our simulated lignin thermolysis included some fifty individual phenolic compounds. The formation versus time for two sets of phenolic products is shown in the two lowest sections of Figure 4. In the upper of these two sections, it can be seen that the guaiacol production increases initially, reaches a maximum, and then decreases towards zero at long times; the catechol production increases slowly at low times but more strongly at longer times; phenol production increases monotonically with increasing time but always remains less than catechol. Qualitatively the same behavior is exhibited in the lowest section of Figure 4 by methylguaiacol, methylcatechol, and para-cresol products, each of which is the methyl-substituted analogue of the preceding products; note however that yields of the methyl-substituted phenols are almost an order of magnitude higher than those of their unsubstituted homologues. Phenolic product trends seen in Figure 4 arise from the following considerations. The guaiacyl moiety occurs directly in lignin, and further arises from reversion of etherified methoxy-phenols; associated with these guaiacyl units are various propanoid chains, also subject to degradation. Thus coniferaldehyde and guaiacyl vinyl ketone are the most nearly primary guaiacol products, degrading to vinyl guaiacol, and hence to ethyl-, methyl-, and unsubstituted guaiacol. Further, each guaiacyl moiety is capable of demethanation and demethoxylation, which respectively yield the corresponding catechol and phenol. Each guaiacol product thus possesses pathways for formation and destruction, resulting in the characteristic yield maxima seen in Figure 4. From the foregoing, catechols

are seen to be secondary products, arising from guaiacyl moiety demethanation; this causes their initial production to be slow but at long times they become the dominant phenolic products. Finally, phenols arise from two major sources, namely guaiacyl demethoxylation, noted above, and coumaryl alcohol monomer units directly incorporated in the lignin; the former source being of greater import. Phenol substitution patterns parallel those of guaiacol, with alkyl side-chains ranging from coumaraldehyde to vinyl-, ethyl-, and unsubstituted phenol. Yields of phenols relative to catechols increase somewhat with increasing temperature, since guaiacyl demethoxylation is more highly activated than guaiacyl demethanation; however the absolute yields of phenols always remained lower than those of catechols.

According to our simulation, the carbonaceous residue is comprised of all aromatic units involved in interunit bonding. If the gas, aqueous liquid, and phenolic product fractions are designated as volatile, and all multiple ring aromatics as non volatile, then the simulated carbonaceous residue fraction can be related to the weight loss that would be observed during lignin thermolysis. Such simulated weight-loss versus time curves are shown by the dashed lines in Figure 5, which will be more fully discussed in the next section.

Discussion

The discussion will be confined to comparisons between the present results and previous literature, as embodied in the matrix of Table 3. In the rows of this matrix, the four major product fractions have been delineated in terms of overall and constituent component yields. The matrix has six columns, representing our model predictions and five sets of literature references. The latter includes the collected reports of several authors as summarized in reference 4, the data of Iatridis and Gavalas (5), of Kirshbaum (6), and of Domburg (7, 8). In each matrix element, a numerical value or comment indicates that information relevant to that row was reported, whereas an 'X' implies that it was not. The present simulation column 1, provides entries for each row save CO₂ yield. The overall gas fraction is the sum of CO and CH₄; these are by far the prevalent constituents of the lignin off-gas. The aqueous distillate was composed of water and methanol only; acetone, acetic acid and other minor liquid products were not included in the simulation. The phenolic fraction comprised the sum of all single ring phenols; this overall yield should correspond best to the overall tar yield reported in pyrolysis experiments. Finally, the carbonaceous residue fraction is composed of all multiple ring aromatic units. The investigations of collected authors (4), column 2, provide detailed accounts of gas and aqueous distillate yields, and overall tar and char yields. Because detailed temperature-time information is lacking for many of these investigations, entries in this column are best considered the asymptotic 'ultimate' yields of destructive distillations. The data of Iatridis and Gavalas (5) were obtained in a reactor designed to emphasize primary reactions, providing detailed temperature-time information and entries for all save water and overall aqueous distillate yields. Kirshbaum (6) provided overall gas, phenolics, and carbonaceous residue yields; detailed phenolic product spectra were provided also. Detailed description of phenolic product spectra and DTA/DTG weight loss data were given by Domburg (7, 8). The discussion to follow considers each row of Table 3; note that all yields are in weight percent of original lignin substrate.

The simulated overall gas fraction rose with increasing time and temperature and ultimately achieved a value of about 15% at 600 C. This compares favorably with the data of collected authors (4) in Table 3, where gas yields ranged from about 10-20%. Iatridis and Gavalas report an overall yield as high as 23% at 650 C, but this included 7.2% CO₂. As discussed below, this rather high CO₂ content may be due to their use of a Kraft lignin. Omitting CO₂, their overall gas yield is 16%, in good agreement both with the simulation and earlier literature. Additionally, Kirshbaum reports total gas (and losses) yield of ~5% at 250 C and ~18% at 600 C. The simulated (CH₄, CO) yields are respectively (6.0, 5.0) % at (500 C, 100s) and

(6.1, 9.0) % at (600 C, 7s); both these CH₄ and CO yields are in substantial agreement with the collected literature (4) which provides ultimate (CH₄, CO) yields of (7.0, 7.0) %. Simulated methane and CO yields both somewhat exceed those of reference 5, but, interestingly, these authors report that the experimental CO/CH₄ ratio varied from about 2.3 at 400 C to 0.88 at 500 C and 1.8 at 600 C, which closely accords with the behavior of this ratio in our simulation. This was earlier interpreted in terms of dual sites for CO release from lignin.

The simulated overall yield of aqueous liquids, based on the sum of water and methanol yields, was about 6%, appreciably lower than the average yields of ~15% reported by the collected authors (4). Of the two individual components, the simulated water yields of 6% are about half of the values reported in the literature, although these latter are often unreliable on account of water being physically associated with the lignin or introduced during its isolation. Simulated methanol yields of 0.1% are also substantially lower than the yields of 0.28 to 1.5% reported by the collected authors (4). It would appear that further pathways for both water and methanol production need to be identified and incorporated into the present model of lignin thermolysis.

The simulated overall yield of phenolic liquids ranged from 7 to 80%. Experimental phenolic fraction yields typically range from 3 to 30% (4), although tar yields greater than 50% have been reported (9). The simulated phenolic fraction yields exceed experimental for two likely reasons. First, many complex phenols in the tar fraction are not experimentally identified and second, our simulation did not consider the condensation and polymerization reactions which might lower the yield of single ring phenols in practice. In regard to individual phenols, the present simulation predicts most of the thirty phenols which have been detected in the literature (6, 7, 8). In most cases, the simulated yields of individual phenols agree with experimental values to within a half an order of magnitude. It is particularly noteworthy that deviations between the present simulation and experiments are no greater than deviations between individual experiments.

The simulated carbonaceous residue yields of 91% at 300 C and 10⁴s and 40% at 600 C and 7s compare favorably with the literature. In Table 3, ultimate tar yields from destructive distillation (4) were 40 to 60%. Iatridis and Gavalas (5) report weight losses of 20% and 53% at 400 and 600 C, respectively, corresponding to char yields of 80% and 47%. Kirshbaum (6) reports a char yield of 91% at 250 C and only 26% at 600 C. The present definition of residue as multiple ring aromatics evidently provides simulated carbonaceous residue yields that are in good accord with the experimental literature.

Finally, simulated weight-loss kinetics, derived from the carbonaceous residue yields as noted earlier, are compared with the experimental data reported by Iatridis and Gavalas (5) in Figure 5. It can be seen that the simulated weight loss curves (dashed), accord well with the experimental weight loss curves (solid), both in regard to shape and absolute magnitudes. The observed agreement is noteworthy in that the simulation was based entirely on our *a priori* description of lignin structure, reaction pathways, and kinetics, and incorporated no information derived from actual lignin thermolyses. Furthermore, the modest deviations between simulated and experimental weight loss curves in Figure 5 can reasonably be attributed to differences between the respective lignin substrates. The authors (5) used a Douglas fir precipitated Kraft lignin, whereas the present simulation was based on Freudenberg's unperturbed "protolignin." Kraft pulping alters the chemical nature of lignin, resulting in increased internal condensations, with the original reactive α - and β -ether linkages transformed into less reactive diphenyl-methane, ethane, and ethylene linkages; it also introduces carboxylic acid units into the lignin macromolecule. The low temperature reactivity of a Kraft lignin might be expected to be greater than its protolignin counterpart because of facile CO₂ evolution from the carboxylic acid units. At higher temperatures and conversions, the reactivity of a Kraft lignin may well be lower than that of the protolignin since relatively re-

fractory diphenylmethane, ethane and ethylene units have replaced the original reactive α - and β -ethers. In the light of these assertions, it is interesting that Iatridis and Gavalas report CO_2 yields of 5.9% at 400 C and 120s, and 4.1% at 600 C and 10s. These suggest a constant number of easily decarboxylated acid sites in their substrate. Further, the authors' reported weight loss of 20% at 400 C and 120s exceeds our simulated weight loss of 13% by an amount substantially equal to their CO_2 yield. At 600 C and 10s the experimental weight loss corrected for CO_2 is $\sim 50\%$, somewhat lower than our simulated value of 60% on account of the reduced reactivity of their Kraft lignin.

Summary and Conclusions

Mathematical simulation of whole-lignin pyrolyses, at 300 to 600 C with holding times of 1 to 10^4 s, was achieved by combining a statistical interpretation of lignin structure with experimental results of model compound pyrolyses. The outcome of these simulations, expressed in terms of product fractions as a percent of initial lignin was:

(i) Gas Fraction: Simulated overall gas, methane, and CO yields accorded with previous experimental lignin pyrolyses; respective ultimate yields typically 15%, 6%, and 9% were in quantitative agreement with the literature. The simulated variation of (CH_4/CO) ratio with time and temperature further agreed with that recently reported by Iatridis and Gavalas (5).

(ii) Aqueous Fraction: Simulated water yields were typically about half the reported experimental yields of 12%. Simulated methanol yields were half an order of magnitude lower than the literature yields of 0.3-1.5%.

(iii) Phenolic Fraction: Simulated overall phenolic liquids yields were generally higher than experimentally observed. The simulation accounted for more than thirty individual phenols reported in the literature. Simulated yields of simple individual guaiacols, catechols, syringols, and phenols, each nominally 2%, were within the band of values reported in the literature.

(iv) Carbonaceous Residue: Simulated curves of weight loss versus time at 400, 500, and 600 C were nearly coincident with the experimental curves reported by Iatridis and Gavalas (5) for pyrolysis of a Kraft lignin. Also, the modest disagreements between these curves, at both low and high temperatures, were traced to structural differences between the respective lignin substrates.

References

1. Freudenberg, K., Neish, A.C., Constitution and Biosynthesis of Lignin, Springer-Verlag, New York (1968).
2. Harkin, J.M., in Battersby and Taylor, Oxidative Coupling of Phenols, Marcel-Dekker (1967).
3. Sarkanen, K.V., in Sarkanen, K.V., and Ludwig, C.H., eds., Lignins: Occurrence, Formation, Structure and Reactions, Wiley Interscience, New York, (1971).
4. Klein, M.T., Model Pathways in Lignin Thermolysis, Sc.D. Thesis, Department of Chemical Engineering, M.I.T., Cambridge, Mass. (1981).
5. Iatridis, B. and Gavalas, G.R., *I & EC Prod. Res. Dev.*, **18** (2), 127 (1979).
6. Kirshbaum, I.Z., Domburg, G.E., Sergeeva, V.N., *Khim. Dev.* No. 4, 96 (1976).
7. Domburg, G.E., Sergeeva, V.N., Kalnish, A.I., Thermal Analysis, Vol.3 (Proc. 3rd ICTA Davos (1971)) pp. 327-40, Burkhäuser, Basel, (1972).
8. Domburg, G.E., Sergeeva, V.N., *J. Thermal. Anal.*, **1**, 53 (1969).
9. Domburg, G.E., Kirshbaum, I., Sergeeva, V.N., *Khim. Dev.* **7**, 51 (1971).

TABLE 1. MODEL COMPOUNDS FOR LIGNIN THERMOLYSIS

Compound	Abbr.	Structure	Model of	Pyrolysis T/C	Conditions t/s	C ₀ mo/l ^{1/2}	Substrate	Pathway	Products	log ₁₀ A(s ⁻¹)	E* (kcal/mol)	Order
1 Phenethyl-phenyl ether	PPE		IL	300-550	30-14400	0.083-1.68	PPE	R1:		11.1	45.0	1
2 Guaiacol	GUA		MP	250-535	110-6000	0.46-3.07	GUA	R1:		5	22	(>1)
3 Veratrole	VER		MP	350-550	60-1500	0.33	VER	R2:		11.5	47.4	1
4 Cinnamylaldehyde	CAD		PC	250-400	120-1500	0.38-1.3	VER	R1:		13.9	55.9	1
5 Salligenol	SAL		PC	175-350	60-1500	0.37	VER	R1:		14.1	58.4	1
6 Cinnamyl-siliconol	CAL		PC	300-500	50-1500	0.37-1.1	CAD	R2:		14.8	60.1	1
7 2,6-Dimethoxypropane	DMP		NP	300-500	120-1600	0.32	SAL	R3:		11.2	49.2	1
8 Isoeugenol	IEG		NP,PC	300-500	60-1560	0.33	SAL	R1:		12.1	48.2	1
9 Vanillin	VAN		NP	300-500	120-1500	0.85	CAL	R2:		8.6	33.7	(2)
10 Acetophenone	APH		PC	350-550	120-5000	0.14-1.4	CAL	R1:		13.4	33.4	(1)
11 o-Hydroxy-diphenylmethane	DHD		IL	400-550	120-6000	0.27	DMP	R1:		4.2	21.8	1
12 Phenylether	PET		IL	500-587	240-9000	0.30	IEG	R2:		10.4	42.2	1
13 Cinnamic Acid	CIA		PC	250-400	120-1500	0.20	IEG	R1:		11.1	45.5	1
14 Ferulic Acid	FEA		PC,MP	200-350	120-1500	0.50	VAN	R2:		10.8	42.9	1
15 Anisole	ANI		CON	344-550	180-1500	0.46-3.07	VAN	R1:		11.3	46.2	1
16 Benzaldehyde	BZO		CON	300-500	120-3600	0.16-3.3	APH	R2:		12.2	47.3	1
							APH	R1:		10.9	38.5	1
							OHG	R2:		9.6	50.5	(1.5)
							PE	R1:		9.6	43.4	1
							CAA	R1:		14.8	72.1	1
							FEA	R1:		8.0	31.0	(1)
							ANI	R1:		5.2	19.8	1
							ANI	R1:		13.0	54.7	1
							BZO	R2:		14.5	61.0	1
							BZO	R3:		7.9	40.5	(1)
							BAD	R1:		9.5	41.5	1

Note: Model codes are: IL - Interunit link, MP - Methoxyphenol, PC - Propanoid chain, CON - Control.

Item Model Prediction

Gas

Fraction

Overall

yields

CH₄

CO

CO₂

Aqueous

Fraction

Overall

H₂O

HCOH

Phenolic

Fraction

Overall

Individual

Phenols

Carbonaceous

Residue

Overall

Kinetics

23% max including CO₂

4.8% @ 650C

9.2% @ 650C

near 6%, all temperatures

1.5%

X not included
in simulation

overall mean 15%

12-15%

0.2-1.0%

3-30%

Sum of single ring
phenols as function
of time 7-80%,
include complex
phenols

Detailed yields
of individual
phenols as a
function of time
and temperature

40-60% yield of char

weight loss of
400-600C as in
function of time

weight loss for
400-600C as in
function of time

5% @ 250C, 15% @
600C gases and losses

X

X

X

X

X

X

X

0.2% @ 250C, 74%
@ 500C

3.3-14.5% @ 75C

detailed yields of
20+ different
phenols

detailed yields of
20+ different
phenols

X

DTA/DTG experiments
yield E
26-30
kcal/m²h

TABLE 3. COMPARISON BETWEEN LIGNIN THERMOLYSIS SIMULATION AND EXPERIMENTS.

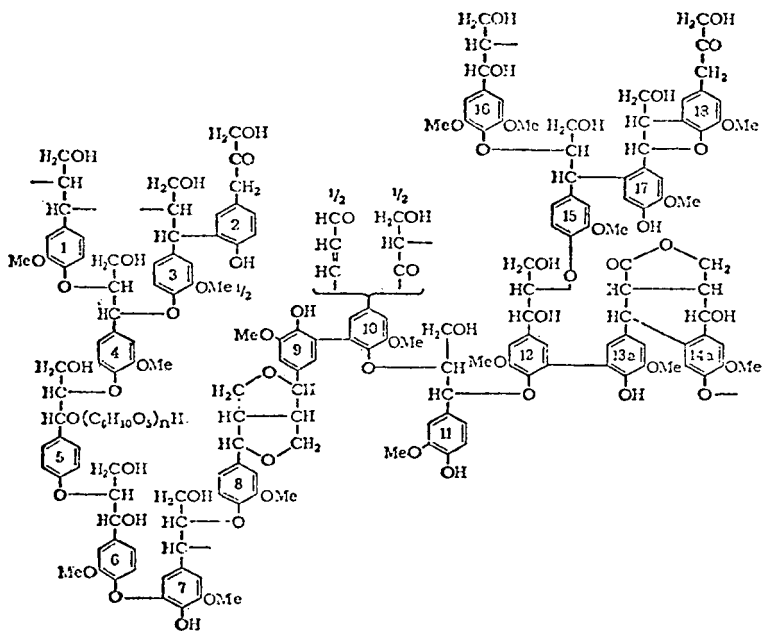


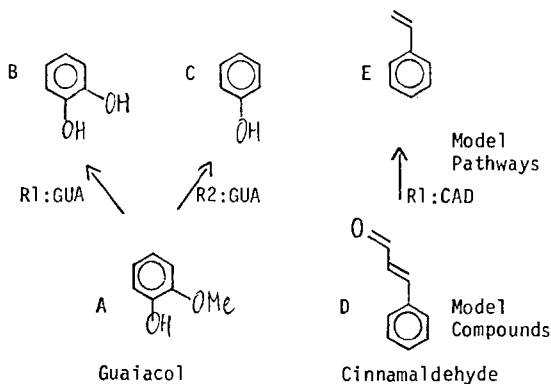
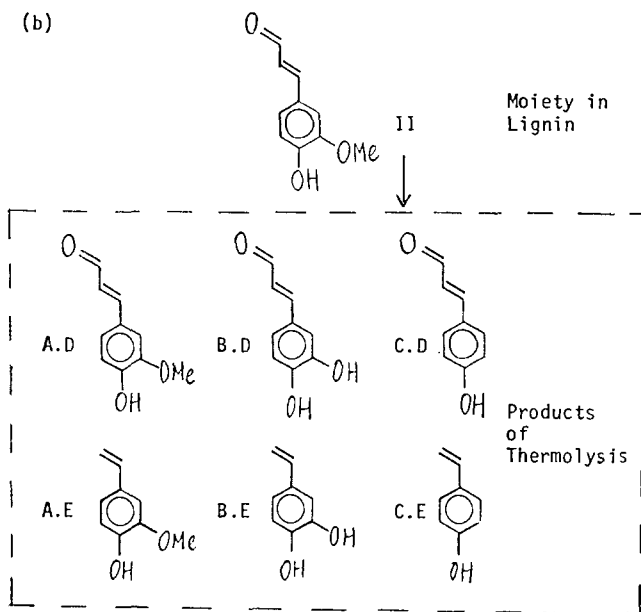
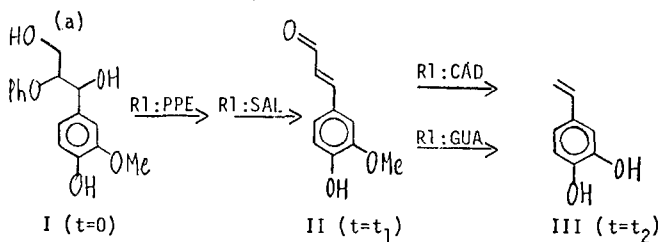
FIGURE 1. MODEL OF SPRUCE LIGNIN STRUCTURE (Freudenberg, 1)

MP / PC									$\sum MP$	
	(.33)	(.11)	(.11)	(.11)	(.06)	(.11)	(.11)	(.06)		
NONALIZED DISTRIBUTION	(.33)	(.11)	(.11)	(.11)	(.06)	(.11)	(.11)	(.06)	(1)	
CONFERYL ALCOHOL										
FREE (.28)	1.66	.55	.55	.55	.30	.55	.55	.30	5	
ETHERIFIED (.56)	3.33	1.11	1.11	1.11	.60	1.11	1.11	.60	10	
CONARYL ALCOHOL										
FREE (.055)	.327	.11	.11	.11	.060	.11	.11	.060	1	
ETHERIFIED (.055)	.327	.11	.11	.11	.060	.11	.11	.060	1	
SINAPYL ALCOHOL										
FREE (0)	0	0	0	0	0	0	0	0	0	
ETHERIFIED (.055)	.327	.11	.11	.11	.060	.11	.11	.060	1	
$\sum PC$	(1)	6	2	2	2	1	2	2	1	18

FIGURE 2. AROMATIC UNIT MATRIX A FOR SPRUCE LIGNIN

FIGURE 3. LOGIC OF LIGNIN THERMOLYSIS SIMULATION.

- (a) Thermal Transformation of Lignin Moiety.
 (b) Superposition of Model Pathways.



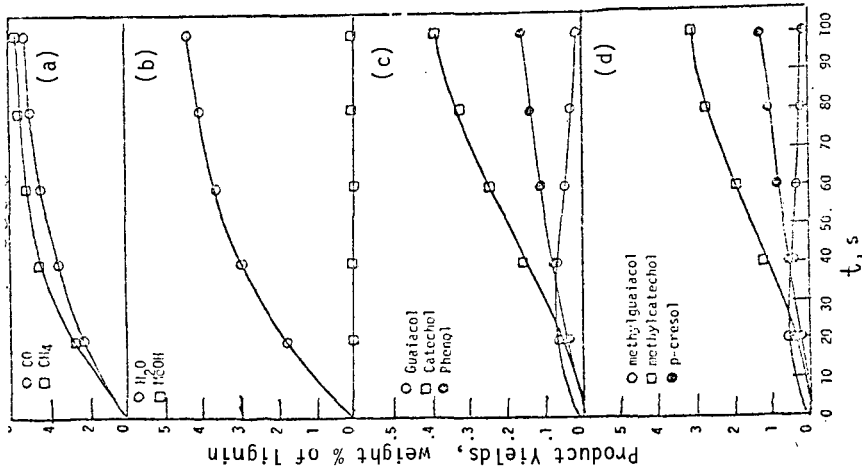


FIGURE 4. RESULTS OF LIGNIN THERMOLYSIS SIMULATION AT T = 500 C.

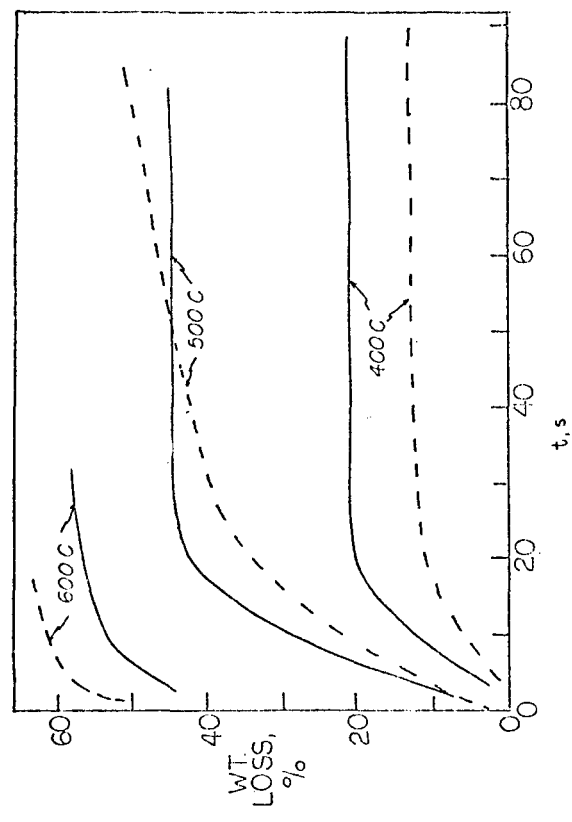


FIGURE 5. WEIGHT-LOSS KINETICS IN LIGNIN THERMOLYSIS. — Experimental (5) --- Present Simulation.

ENHANCED COAL LIQUEFACTION WITH HIGH BOILING SOLVENTS. D. D. Whitehurst. Mobil Research & Development Corp., P.O. Box 1025, Princeton NJ 08540

In the accelerated development of coal liquefaction since 1973, it has been the general practice to use distillates as recycle solvents. This stems from the earlier German experience where recycling asphaltenic products required more severe processing. Recently, it has been demonstrated that the inclusion of vacuum tower bottoms or of solvent fractionated heavy products in a recycle loop can produce dramatic process improvements.

An investigation of the mechanisms of coal conversion in high boiling solvents has been conducted using both model compounds, process derived materials, and fractions thereof. These studies identified polycondensed aromatics as effective solvent components. Due to their relative ease of hydrogenation and dehydrogenation they can effectively interact with hydroaromatic species in the coal (H-shuttling), with less active H donors or with hydrogen gas (H-transfer). Mineral matter catalysis can play an important role in these reactions.

Polyfunctional components have a propensity for promoting char formation and can produce adverse reactants. Information of this type can lead to identification and generation of optimal recycle solvent composition.

These studies show that the mechanistic pathways discernible from the model compound studies and the behavior of different chemical classes in heavy process solvents can lead to improvements in coal liquefaction processes.

H-COAL SLURRY OIL COMPOSITION AND PROCESS PERFORMANCE

F. P. Burke and R. A. Winschel

Conoco Coal Development Company, Research Division, Library, PA 15129

INTRODUCTION

The H-Coal process, developed by Hydrocarbon Research, Inc., is a catalytic coal hydrogenation in which the coal is contacted with, usually, an alumina supported Co/Mo, or similar catalyst in an upflowing fluidized bed. The distinguishing features of the process are the reactor internals, which allow for fluidization of the catalyst bed, and catalyst addition and withdrawal systems to allow maintenance of the catalyst activity. The 3 TPD process development unit (PDU), operated by HRI at Trenton, NJ, has been used to study feed coal and space velocity effects, and to provide design data for scale-up of the process. A schematic of the unit (Figure 1) shows that the coal is fed to the reactor as a slurry with two recycle components. The hydroclone overflow (HO) contains distillate, non-distillate oils (resid), and solids. The clean oil tank (COT) is a surge vessel containing atmospheric still bottoms and vacuum still overhead. The amounts of these distillates in the clean oil tank can be independently varied.

An interest in the composition of these recycle oils, and how their composition is related to process performance, was the motivation for a recently completed program to analyze daily samples of recycle slurry oils from H-Coal PDU Runs 5, 8 and 9 by a variety of analytical techniques, and to relate the composition data to process performance in those PDU runs. PDU Runs 5 and 8 were made with Illinois 6 coal while PDU 9 used Kentucky 11 coal^(1,2,3). PDU Runs 5 and 9 were made in the Syncrude mode (space velocity = 31) while PDU Run 8 consisted of operations in both the Fuel Oil and Intermediate modes (Table 1). Daily samples of the clean oil tank and the hydroclone overflow were taken by HRI and shipped to CCDC for analysis. The analytical techniques used and the information desired from each are given in Table 2. The object of the study was to determine the relationship between slurry oil composition and process performance in eight specific areas:

1. Changes in the slurry recycle stream composition during startup.
2. The manner in which the process reaches steady state operation during startup.
3. The composition of the recycle stream during stable operation.
4. The changes in recycle composition in response to planned variations in process variables.
5. Changes in the recycle composition which cause or result from unplanned upsets in the process operation.
6. Changes in the recycle composition as evidence of changes in catalyst activity.
7. Differences in recycle composition as a function of space velocity (mode).
8. Differences in recycle composition as a function of feed coal (same space velocity).

In making interpretations of these data it is important to recognize that there are two ways in which the data can be expressed. The recycle slurry oil characterizations can be given as compositions, or intensive variables. For example, the weight percent

of benzene solubles in the recycle resid represents the nature of the material that is being recycled, without reference to the amount. Alternatively, the data can be expressed on a recycle rate, or extensive variable basis. Thus, the pounds of benzene insolubles recycled per pound of coal fed reflects both the composition of the recycle resid, and the total recycle rate of that resid. Both the composition and recycle rate data can be used to draw conclusions regarding steady state performance. In the work described here, all conclusions concerning steady state performance are based on a statistical treatment of the data which compares variations in the data with the experimental uncertainty of the measured variables. The mathematical basis of this treatment is described in the first topical report prepared under this contract⁽⁴⁾. The results presented below are abstracted from the much more extensive body of data included in the two topical reports and final report prepared under this contract^(4,5,6).

The purpose of this paper is to illustrate the major conclusions reached in this study. Therefore, confirming results of other analyses are not generally presented.

COMPARISONS OF RECYCLE COMPOSITIONS

Because H-Coal is a hydrogenation process, ¹H-NMR was expected to provide a useful measure of recycle oil composition. Table 3 presents average ¹H-NMR distributions for PDU Runs 5 and 9 and for the two space velocity periods of PDU Run 8. The periods of Runs 5 and 9 used for averaging were chosen to represent the best approach to steady state in those runs. Because of a number of upsets over the first 16 days, we could not identify steady state periods for PDU Run 8, and all the data were used to calculate averages. Comparing first the results from Runs 5 and 8 (both Illinois 6 coal) we see that the higher space velocities produce a less aromatic recycle distillate. Since hydrogenation severity decreases with space velocity this was unexpected. The gain in aliphatics between the Syncrude, Fuel Oil and Intermediate space velocities is seen in the alkyl alpha and gamma protons, which measure long chain aliphatics, such as paraffins. These differences in distillate composition may reflect the fact that lower distillate yields at the higher space velocity mean that the recycle distillate will see more passes through the unit. Of course, the operability difficulties encountered in PDU Run 8, and the intentionally divided nature of that run, make firm conclusions unlikely.

PDU Run 9 (Kentucky 11 coal, Syncrude mode) gives a less aromatic recycle distillate than PDU Run 5 (Illinois 6 coal, Syncrude mode), though the difference is not as great as between PDU Run 5 and the Intermediate mode of PDU Run 8. Apparently, space velocity has more effect on recycle distillate composition than feed coal.

Selected samples of the recycle distillates from the three runs were used to extract Indiana V coal in a microautoclave at two standard conditions. The results (Table 4) show that all of the recycle distillates are good liquefaction solvents. The conversions to THF solubles are generally in the 70-80% range, and these results are indicative of good liquefaction solvents⁽⁷⁾. Differences which occur in a given run, and among the different runs, indicate that recycle distillates produced in the Syncrude mode are better liquefaction solvents than those from either the Intermediate or Fuel Oil modes. In PDU Run 5 there was a general tendency toward improved solvent quality as the run progressed. In PDU Run 9 the trend is reversed, although the conversions obtained with the PDU Run 9 distillates are equivalent to or better than those from PDU Run 5. For PDU Run 8 the two days shown compare conversions for distillates produced in the Fuel Oil mode with distillates produced in the Intermediate mode operation. The distillates from the Intermediate mode are consistently poorer, and in some cases by a large margin, than those from the Fuel Oil mode. This is consistent with data shown in Table 3 giving the average NMR distributions of these distillates, which show a surprisingly high concentration of alkyl beta and gamma protons for distillates produced at the Intermediate space velocity.

While the recycle distillates were qualitatively similar, the recycle resids (975°F⁺, THF soluble) showed a much greater variation in composition, primarily as a function of

space velocity. Table 5 shows that the recycle resid from PDU Runs 5 and 9 (Syncrude) averaged around 49% oils (hexane solubles). The recycle resid in PDU Run 9 had a somewhat higher preasphaltene and lower asphaltene content than the recycle resid from PDU Run 5. However, the recycle resid in PDU Run 8 showed much lower oils content and much higher preasphaltenes content than for either of the Syncrude runs. This lower quality recycle resid in PDU Run 8 may have been related to (either as cause or effect) the operability problems which occurred in that run.

APPROACH TO STEADY STATE RECYCLE COMPOSITION

The data from PDU Runs 5 and 9 allow us to draw several conclusions concerning the approach to a steady state recycle slurry oil during those two runs. Because of the fragmented nature of PDU Run 8 we are not able to draw any conclusions concerning steady state operation from the data for that run. The majority of the data from PDU Runs 5 and 9 indicates that the recycle resid composition, but not the recycle rate, reached steady state between days 10 and 15. The recycle resid composition in PDU Run 5 does show some variation after day 20 of that run, when the hydrogen partial pressure was increased from an average of 1600 psig for the first 20 days of the run to an average of 1860 psig during the last 10 days. However, this appears to be an adjustment to a new equilibrium composition as opposed to a long term variation in the recycle resid composition. The plot of the ratio of benzene solubles to insolubles in the THF soluble recycle resid during PDU Runs 5, 8 and 9 (Figure 2) demonstrates this conclusion.

In contrast to the behavior of the recycle resid composition, the recycle rate of the resid did not reach steady state in PDU Run 9. This is illustrated in Figure 3, which shows the recycle rates of oils, asphaltenes and preasphaltenes on a lb/lb coal fed basis. Because the composition of the recycle resid reached steady state by about day 12, the plots are nearly parallel after that point. However, all three show steady increases throughout the 30-day run. A more rigorous treatment of the data⁽⁶⁾ shows that the preasphaltene recycle rate reached an apparent steady state by about day 25. These results are important since a steadily increasing resid recycle rate tends to reduce the apparent resid yield from the unit. Therefore, the recycle composition can have a direct and immediate impact on the perceived unit performance.

Two measures of the recycle distillate composition, the ratio of aromatic to aliphatic protons, and the concentration of phenolic-OH in the clean oil tank, are shown in Figures 4 and 5, respectively. These data demonstrate that the recycle distillate composition did not reach steady state in PDU Run 9. The data on samples from PDU Run 5 indicate a steady state recycle distillate composition sometime near the midpoint of that run. However, the data from PDU Runs 5 and 9 are very similar up to about day 20 of those runs, and the behavior of the samples from PDU Run 5 after day 20 may have been influenced by increased hydrogen partial pressure, as discussed above. Note that an increase in hydrogen partial pressure would tend to decrease both the aromatic-to-aliphatic ratio and the concentration of phenolic-OH. This could compensate for declining catalyst activity at the end of PDU Run 5.

These data and others concerning the approach of the recycle resid and distillate compositions to steady state indicate that the rate of catalyst deactivation for the larger resid molecules is more rapid than the rate of catalyst deactivation for the smaller distillate molecules. In other words the catalyst has reached a steady state with respect to conversion of the resid to distillate range material by day 10-15 of both PDU Runs 5 and 9. However, the catalyst activity with respect to hydrogenation of the distillate is still declining at the end of the 30 day run.

CONCLUSIONS

The major conclusions drawn from this work are:

- Startup solvent is rapidly replaced in PDU operation. Any aromatic startup solvent of the appropriate boiling range should suffice if it is physically compatible.

- Aromaticity of recycle oil increases during run with declining catalyst activity. Distillate aromaticity reached steady state in PDU 5 but not in PDU 9, perhaps because of increased P_{H_2} after day 20 of PDU 5. Same is true for hydroxyl contents of recycle distillates.
- Composition of recycle resid reached steady state in PDU Runs 5 and 9, by about day 12, but changed in Run 5 coincident with increased P_{H_2} .
- Recycle rate of resid did not reach steady state in PDU 9, although composition did. Situation in PDU 5 was complicated by increased P_{H_2} .
- Recycle resid in PDU 8 was much higher in preasphaltenes than PDU 5 or 9, probably related to operability problems.
- Recycle distillates were qualitatively similar regardless of mode or coal. All are good liquefaction media.
- PDU 5 and 9 data indicate a fast catalyst deactivation for resid hydrogenation (10-15 days) and a slower catalyst deactivation for distillate hydrogenation (> 30 days).
- Kentucky 9 and Illinois 6 coals give similar slurry recycle oils at the Syncrude mode. Differences among Fuel Oil, Intermediate and Syncrude space velocities, with same coal, are greater.

This work was supported by U.S. DOE Contract DE-AC05-79ET14503.

REFERENCES

- (1) Johanson, E. S. and Comolli, A. G., "PDU Run 9, Syncrude Mode Operation With Catalyst Addition and Withdrawal, Kentucky 11 Coal," U.S. DOE Contract EX-77-C-01-1547, Milestone Report (Draft), FE/2547-50, March 1990.
- (2) Johanson, E. S. and Comolli, A. G., "PDU Run 5, Syncrude Mode Operation With Catalyst Addition and Withdrawal," U.S. DOE Contract EX-77-C-01-2547, Milestone Report, FE-2547-19, June 1978.
- (3) Johanson, E. S. and Comolli, A. G., "PDU Run 8, Fuel Oil and Intermediate Mode Operation With Catalyst Replacement," U.S. DOE Contract EX-77-C-01-2547, Milestone Report, FE-2547-46, December 1979.
- (4) Burke, F. P., Winschel, R. A. and Pochapsky, T. C., "Development of a Correlation Between Slurry Oil Composition and Process Performance," U.S. DOE Contract DE-AC05-79ET-14503, Topical Report No. 1, DOE/ET-14503-1, April 1980.
- (5) Burke, F. P., Winschel, R. A. and Pochapsky, T. C., "Development of a Correlation Between Slurry Oil Composition and Process Performance," U.S. DOE Contract DE-AC05-79ET-14503, Topical Report No. 2, DOE/ET-14503-2, August 1980.
- (6) Burke, F. P., Winschel, R. A. and Pochapsky, T. C., "Development of a Correlation Between Slurry Oil Composition and Process Performance," U.S. DOE Contract DE-AC05-79ET-14503-3, Final Report, DOE/ET-14503-3, January 1981.
- (7) Kleinpeter, J. A., Burke, F. P., Dudt, P. J. and Jones, D. C., "Process Development for Improved SRC Options: Short Residence Time Studies," EPRI Project 1134-1, Final Report, EPRI AP-1425, June 1980.

Table 1
H-Coal PDU Runs Studied

<u>PDU Run</u>	<u>Coal</u>	<u>Space Velocity (lb/hr-ft³) Mode</u>	<u>Operations Note</u>
5	Illinois 6	31 (Syncrude)	Increased P _{H₂} after day 20.
8	Illinois 6	78 (Fuel Oil) 50-65 (Intermediate)	Operating problems caused by plugging.
9	Kentucky 11	31 (Syncrude)	Uneventful.

Table 2
Analytical Techniques

- ¹H-NMR (COT, HO Distillate, HO Resid)
 - Hydrogen Distributions
 - Donatable Hydrogen
- LIQUID CHROMATOGRAPHY (HO Resid)
 - Solvent Fractionation (Oils, Asphaltenes, Preasphaltenes)
 - Chemical Functionalities
 - Molecular Size Distribution
- GC/MS AND REVERSE PHASE LIQUID CHROMATOGRAPHY (COT and HO Distillates)
 - Detailed Compositional Analysis
 - Characteristic Parameters
- ¹⁹F-DERIVATIZATION AND ¹⁹F-NMR
 - Hydroxyl (OH) Content
- MICROAUTOCLAVE
 - Empirical Measure of Solvent Quality

Table 3
Average ¹H-NMR Distributions
of Hydroclone Overflow Distillates

PDU Run	Period	Mode	Average ¹ H-NMR Distributions, Hydroclone Overflow Distillates						
			Cond.	Uncond.	Cyclic	Alkyl	Cyclic	Alkyl	γ
			Ar	Ar	α	α	β	β	
5	12-30	Syncrude	26.7	11.1	17.3	12.2	11.9	13.5	7.3
8	3-15	Fuel Oil	26.6	9.2	17.5	11.9	12.2	15.3	7.3
8	17-21	Intermediate	21.6	8.6	16.5	11.8	12.5	19.4	9.5
9	10-26	Syncrude	22.4	9.7	17.5	12.2	13.6	16.2	8.4

Table 4

Microautoclave Extractions of Indiana V Coal With H-Coal
Recycle Distillates - Conversion to THF Solubles, Wt % MAF Coal

PDU RUN Sample	5		8			9			
	HO	COT	HO	COT		HO	COT		
	Day		Day			Day			
EQ Conditions	3	80.6	69.8	--	--	--	3	85.7	81.0
	12	79.6	76.5	13	73.8	72.3	19	79.9	76.8
	25	77.9	77.3	20	72.9	62.3	26	77.6	75.9
	Avg	79.4	74.5		73.4	67.3		81.1	77.9
KIN Conditions	3	76.3	74.8	--	--	--	2	78.2	75.3
	12	80.8	74.3	13	82.7	73.6	19	78.7	72.7
	25	83.3	75.0	20	70.4	68.9	26	79.8	73.9
	Avg	80.1	74.7		75.6	71.2		78.9	74.0

EQ - 750°F, 30 min, 2/1 solvent/coal
KIN - 750°F, 10 min, 8/1 solvent/coal

Table 5

Solubility Fractionation of Hydroclone Overflow THF Soluble Resids

PDU Run	Period	Mode	Average, wt % THF Soluble Resid		
			Oils	Asphaltenes	Preasphaltenes
5	12-30	Syncrude	49.0	32.9	18.1
8	11-15	Fuel Oil	28.4	32.8	38.8
8	17-23	Intermediate	33.7	33.6	32.7
9	10-30	Syncrude	48.5	27.4	24.1

Figure 1
H-Coal Process Simplified Flow Diagram

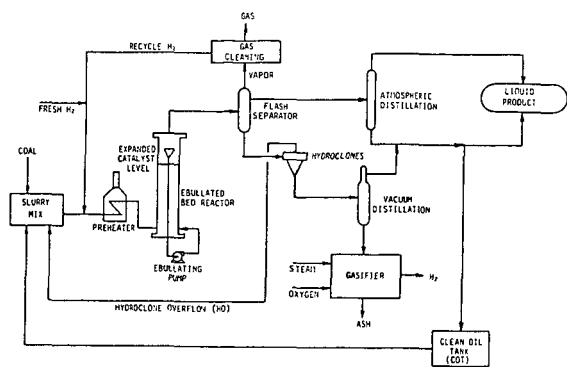


Figure 2
Comparison of Benzene Soluble/Insoluble Ratios
Recycle Resid - PDU Runs 5, 8 and 9

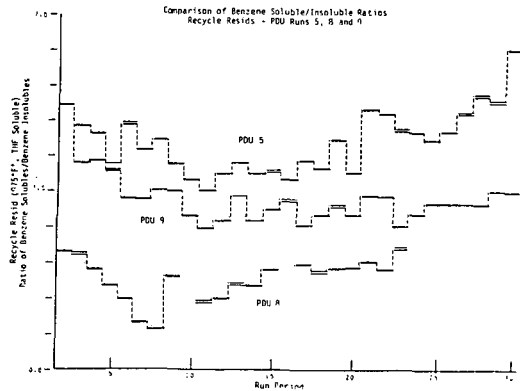


Figure 3
LCF Separation of HO THF Soluble Resid
H-Coal PDU Run 9

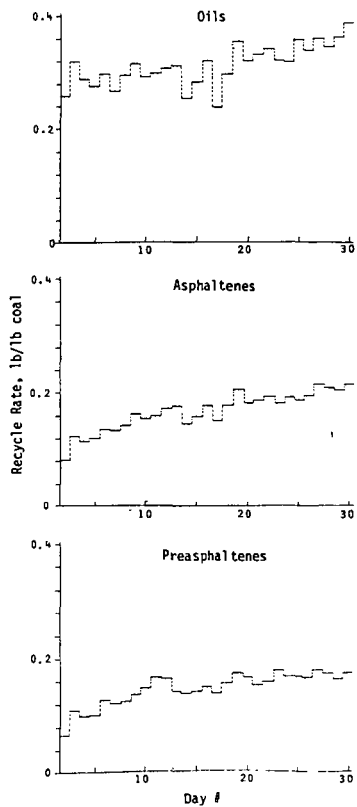


Figure 4
 Ratio of Aromatic/Aliphatic Protons,
 Total Recycle Distillate
 H-Coal PDU Run 5 and 9

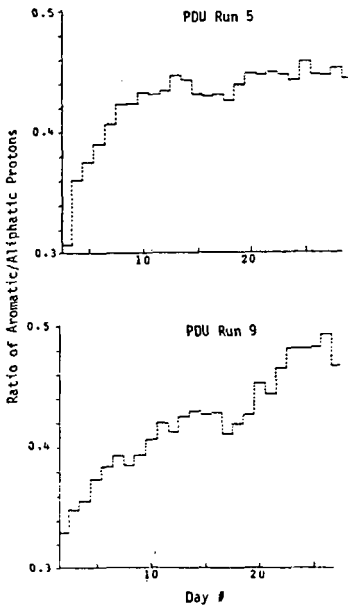
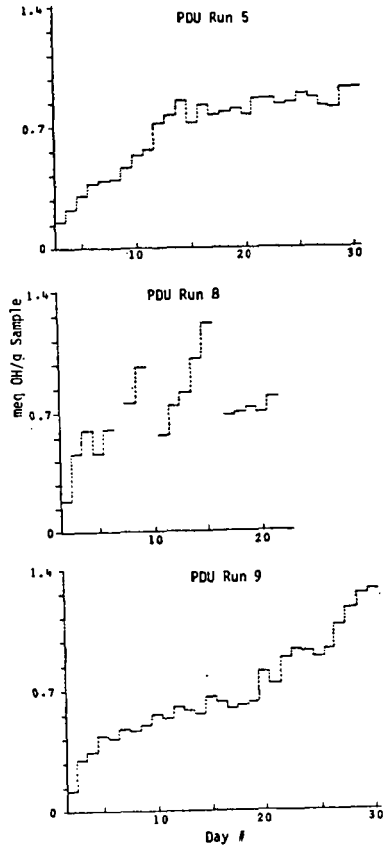


Figure 5
 Concentration of Phenolic -OH by $^1\text{F-NMR}$
 COT Samples
 H-Coal PDU Runs 5, 8 and 9



THE OCCURANCE OF AUTOGENIOUS WATER-GAS SHIFT REACTION ON HYDROGENATION OF SUB-BITUMINOUS COALS. M. Gawlak, D. Carson, H. Wasylyk, B. Ignasiak, Alberta Research Council 11315 - 87 Avenue, Edmonton, Alberta, Canada, T5G 2C2.

Two subbituminous Alberta Coals (21-22% O, on daf matter) were liquefied in a continuous unit, in a recycle mode, with hydrogen. Independently, autoclave liquefaction tests were carried out in hydrogen using recycle solvent from continuous liquefaction as a medium. The results revealed that in both cases from 10-30% of the hydrogen consumed on liquefaction (4-6% by weight of daf coal) was used up for generation of water. However, when the same coals were liquefied in autoclave under similar conditions but in anthracene oil, a water-gas shift reaction occurred which resulted in net consumption of water introduced with coal into autoclave. The results are tentatively interpreted in terms of different acidity of solvents in relation to metals contents of the treated coals.

SOLVENT EFFECTS IN EXXON DONOR SOLVENT COAL LIQUEFACTION. P. Maa, K. L. Trachte, and R. Williams. Exxon Research & Engineering Co., P.O. Box 45, Linden NJ 07036. Exxon Research & Engineering Co., P.O. Box 4265, Baytown TX 77520.

The Exxon Donor Solvent (EDS) coal liquefaction process utilizes a wide range of coal ranks, from lignitic to bituminous, and produces a variety of liquid product slates under moderate processing conditions. The recycle of hydrogenated, coal derived solvent is a key to the performance of the EDS Process.

The role of the recycle solvent in EDS is to provide a convenient vehicle for transporting coal into the process, to disperse the coal, and to donate hydrogen to free radicals produced by the thermal rupture of chemical bonds. The hydrogen donating capability of the recycle solvent allows a balanced utilization of both donor as well as molecular hydrogen under moderate processing conditions. In addition, through solvent conversion in the liquefaction reactor, product selectivity can be controlled to provide either predominantly naphtha or distillate product slates.

Liquefaction studies have been conducted in small batch autoclaves and integrated pilot units in order to better understand solvent-coal interactions in the EDS Process. Results of these studies will be discussed in this paper.

UPGRADING COAL LIQUEFACTION RECYCLE BOTTOMS

H. F. Silver, R. L. Miller and R. G. Corry
Chemical Engineering Department

R. J. Hurtubise
Chemistry Department

University of Wyoming, Laramie, Wyoming 82071

INTRODUCTION

In both the EDS and the SRC-II direct coal liquefaction processes, distillate yields have been increased significantly by including vacuum column bottoms product in the recycle solvent. While the distillable portion of the recycle solvent is upgraded in the EDS process, no specific effort is made to upgrade the non-distillable portion of the recycle solvent in either the EDS nor the SRC II processes. A study was therefore initiated at the University of Wyoming to determine the effect of upgrading coal liquefaction recycle bottoms.

EXPERIMENTAL PROCEDURE

Liquefaction of both subbituminous Wyodak and bituminous Kentucky coals has been studied in a two-liter Autoclave Magnedrive-II batch reactor. Samples of Wyodak coal, Wyodak coal derived recycle solvent, and solvent refined coal, SRC, were supplied by Catalytic, Inc. from the Southern Services Inc. pilot plant at Wilsonville, Alabama. Samples of Kentucky coal, Kentucky coal derived recycle solvent and SRC were supplied by the Pittsburg & Midway Coal Mining Co. from their pilot plant near Tacoma, Washington.

Portions of the recycle solvents boiling above 533K were used as received while other portions were mildly hydrogenated over a Co-Mo on Al_2O_3 catalyst (Nalcom 477) for 60 minutes at 644K using an initial cold reactor hydrogen pressure of 13.8 MPa. Portions of the SRC were used as received while other portions were upgraded by solvent fractionation and by hydrogenation. The SRCs were solvent fractionated into cyclohexane soluble oils, cyclohexane insoluble - benzene soluble asphaltenes, benzene soluble oils plus asphaltenes and benzene insoluble-pyridine soluble preasphaltenes. Portions of the SRCs and their oil plus asphaltene fractions were mildly hydrogenated over catalyst at 644K for 60 minutes using an initial cold reactor hydrogen pressure of 13.8 MPa. Other portions were severely hydrogenated over catalyst at 700K for 60 minutes using an initial cold reactor hydrogen pressure of 20.7 MPa.

Coal liquefaction experiments were then conducted by charging the reactor with recycle solvent, SRC or SRC fraction and coal in a 1:1:1 weight ratio. The reaction was carried out at 714K for 60 minutes using an initial cold reactor hydrogen pressure of 13.8 MPa. Gaseous products were analyzed using an HP 5840 gas chromatograph. Liquid products were distilled using a modified ASTM-D 1160 apparatus. Unreacted coal and mineral matter were determined by soxhlet extractions using pyridine. All runs were duplicated.

DISCUSSION OF RESULTS

The extent of coal liquefaction in this work was measured using percent 700K+ conversion, X_{700} , defined by the relationship

$$X_{700} = \frac{W_{IN} - W_{OUT}}{W_{IN}} \times 100$$

where W_{IN} = grams of MAF coal plus grams of SRC or SRC fraction plus grams of 700K+ distillate charged to the reactor.

and W_{OUT} = grams of MAF 700K+ product recovered from the reactor.

A summary of the conversions obtained using different solvents is presented in Table I. The average reproducibility of conversions for duplicated runs was within $\pm 1.0\%$ of the mean values reported in this table.

Examination of the results for solvents 1-6, containing Wyodak coal derived SRC, and solvents 12-16, containing Kentucky coal derived SRC, suggest that maximum conversions are obtained if the SRC is mildly hydrogenated. The data obtained from Wyodak solvents 4, 5 and 6, and for Kentucky solvents 13, 14 and 16 suggest that SRC component effectiveness may pass through a maximum as hydrogenation severity is increased. Comparison of solvent 3 with solvent 5 and solvent 15 with solvent 16 suggests that the observed increases in conversion relative to solvents 1 and 12 are due more to mildly hydrogenated SRC than mildly hydrogenated distillate.

While the relatively high conversion obtained from solvent 2 could be attributed to the catalytic activity of the ash in this sample of unfiltered SRC, ash found in Wyodak coal is generally not considered to be a catalyst for the coal liquefaction reaction. A more reasonable explanation for the high conversion observed when using solvent 2 is the lower initial boiling point of the high ash SRC as compared to the filtered SRCs. In the pilot plant, ash increases the viscosity of SRC. In order to reduce this viscosity, some of the normally distillable liquids were not removed from the high ash SRC during distillation.

The results shown in Table I also suggest that solvent fractionation may also improve the liquefaction effectiveness of SRCs. Results obtained using solvents 17-19 suggest that little, if any, improvement in Kentucky coal solvent effectiveness can be obtained by hydrogenating the benzene soluble oils plus asphaltenes obtained from Kentucky SRC.

Liquid yields and hydrogen consumption depend upon the extent of coal conversion. Net liquid yields of C₄-533K and 533-700K from Wyodak coal as a percent of the MF coal are presented in Figures 1 and 2 as a function of X_{700} . Points presented on these and the following figures are identified by the number in Table I identifying the solvent used in the experiment. As would be expected, liquid yields increase with increasing X_{700} . Similar plots of liquid yields for Kentucky coal are presented in Figures 3 and 4. For comparison purposes, the solid lines in Figures 1 and 2 have been reproduced as dashed lines in Figures 3 and 4, respectively, so that direct comparisons can be made between Wyodak and Kentucky coal yields. As can be seen in Figures 3 and 4, Kentucky coal produced greater liquid yields than Wyodak coal at low conversions. However, at high conversions, the liquid yields from the two coals are quite comparable.

Hydrogen consumptions for both Wyodak and Kentucky coal experiments are presented in Figures 5 and 6. The consumptions shown in these figures do not include the hydrogen consumed in upgrading either the distillable solvent nor the SRC or SRC fractions. It has been estimated that hydrogen consumed in this manner would be in the order of 1.0 to 2.0 wt% of the MAF coal charged to the reactor.

CONCLUSIONS

Results obtained from this work indicate the importance of solvent composition on the coal liquefaction reaction. Through the addition of mildly hydrogenated SRC to a recycle solvent, for example, net C₄-700K liquid yields approaching 60 wt% of the MF coal charged to a batch reactor were obtained from both Wyodak and Kentucky coals used in this study.

A certain amount of bottoms recycle upgrading may occur indirectly in processes such as the EDS process with bottoms recycle or the SRC-II process. However, it may be possible to obtain even further increases in distillate yields by direct upgrading of a bottoms recycle, either by hydrogenation or by solvent fractionation. It should be pointed out that these hypotheses are based on batch reactor runs, simulating continuous coal liquefaction operation. Deleterious compounds could build up in recycle streams in continuous plants that were not observed in this study. Further work in this area appears to be warranted.

ACKNOWLEDGEMENTS

Mr. Ronald Borgianni and Mrs. Jane Thomas have made substantial contributions to this program. The work has been carried out under DOE Contract No. DE-AC01-79ET14874.

TABLE I
X₇₀₀ CONVERSION RELATED TO THE DEGREE OF SOLVENT HYDROGENATION

COAL	SOLVENT NO.	DISTILLABLE PORTION	SOLVENT	
			NONDISTILLABLE PORTION	X ₇₀₀ (%)
WYODAK	1	UH ⁽¹⁾	SRC, UH	23.8
	2	UH	(SRC+Ash), UH	36.5
	3	UH	SRC, MH ⁽²⁾	42.5
	4	MH	SRC, MH	35.8
	5	MH	SRC, UH	32.0
	6	MH	SRC, SH ⁽³⁾	27.2
	7	UH	(O+A) ⁽⁴⁾ , UH	28.4
	8	MH	(O+A), MH	37.4
	9	MH	(O+A), SH	29.0
	10	UH	A ⁽⁵⁾ , UH	34.6
	11	UH	O ⁽⁶⁾ , UH	35.9
KENTUCKY	12	UH	SRC, UH	28.5
	13	MH	SRC, MH	39.9
	14	MH	SRC, SH	36.4
	15	UH	SRC, MH	38.8
	16	MH	SRC, UH	30.5
	17	UH	(O+A), UH	35.5
	18	MH	(O+A), MH	37.0
	19	MH	(O+A), SH	37.0

- NOTES: (1) UH = Unhydrogenated
 (2) MH = Mildly Hydrogenated
 (3) SH = Severely Hydrogenated
 (4) O+A= Oils plus Asphaltenes
 (5) A = Asphaltenes
 (6) O = Oils

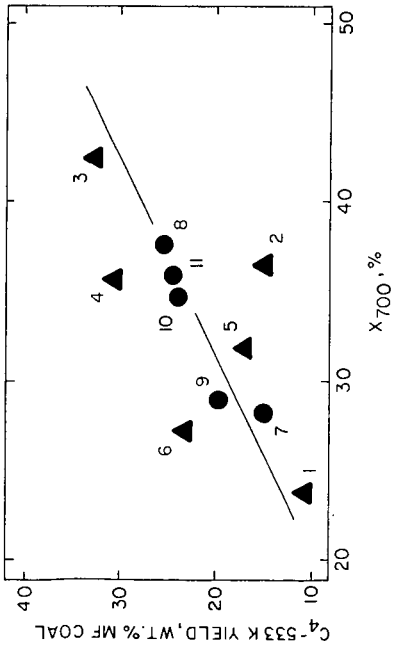


Figure 1. C_4 -533K Wyodak Coal Liquid Yields as a Function of X_{700}

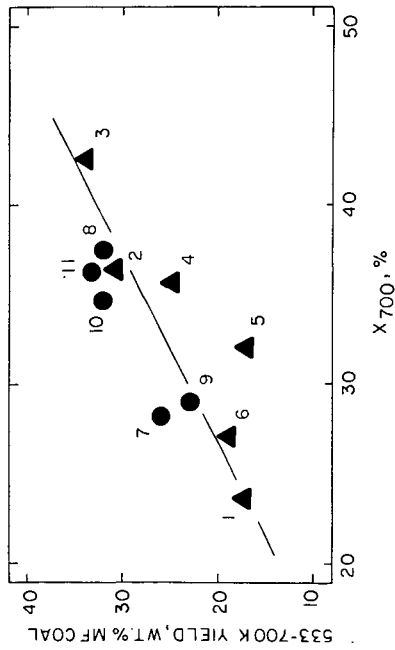


Figure 2. 533-700K Wyodak Coal Liquid Yields as a Function of X_{700}

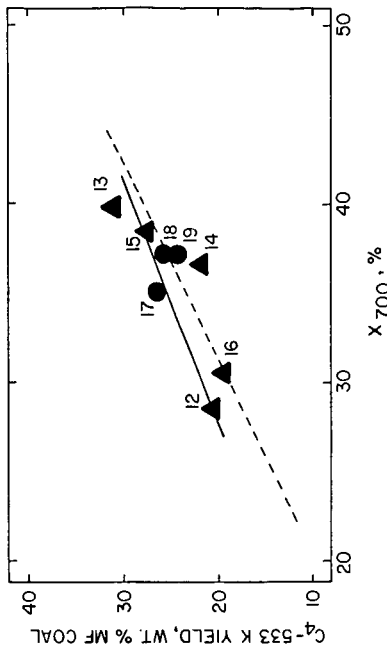


Figure 3. C_4 -533K Kentucky Coal Liquid Yields as a Function of X_{700}

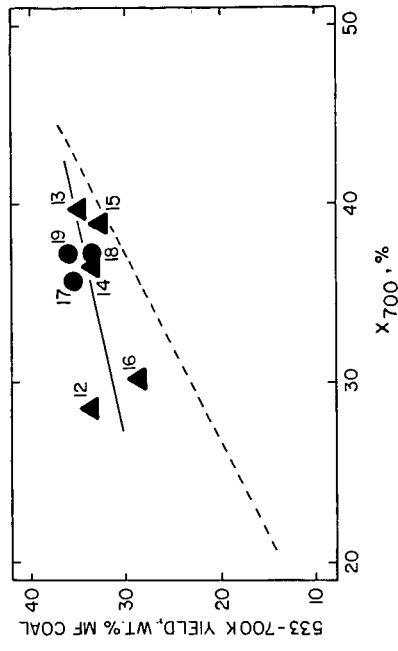


Figure 4. 533-700K Kentucky Coal Liquid Yields as a Function of X_{700}

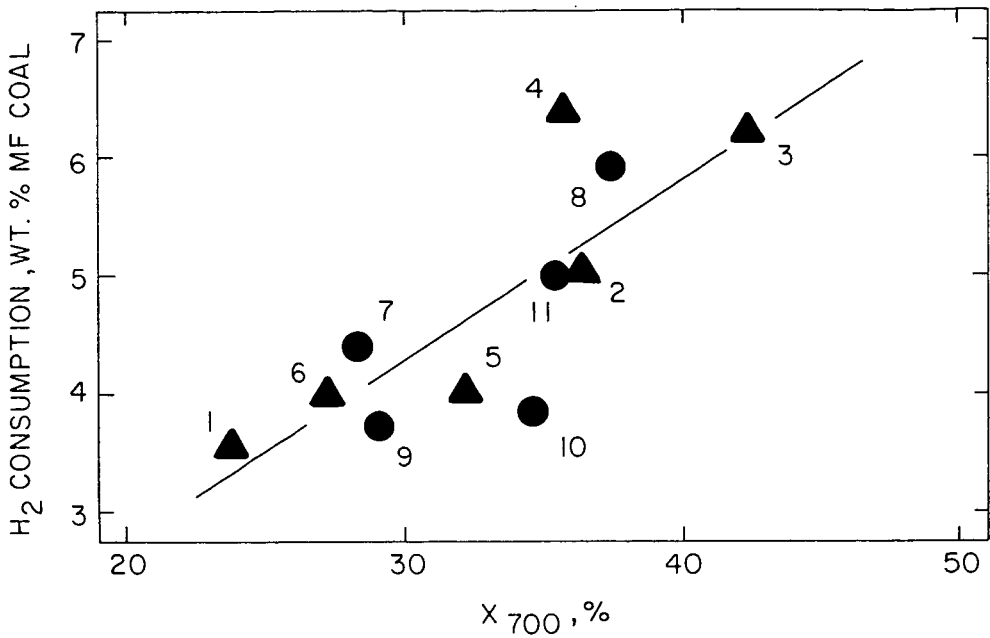


Figure 5. Hydrogen Consumption for Wyodak Coal as a Function of X_{700}

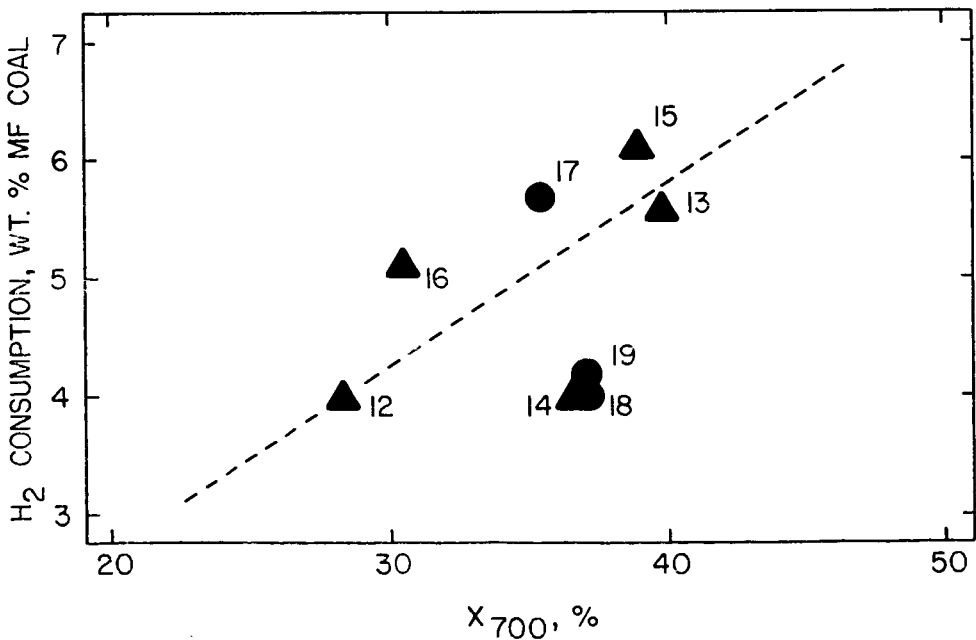


Figure 6. Hydrogen Consumption for Kentucky Coal as a Function of X_{700}

COAL LIQUEFACTION WITH SELECTIVE HEAVY RECYCLE. C. J. Kulik, H. E. Lebowitz, and W. Weber. Electric Power Research Institute, 3412 Hillview Avenue, P.O. Box 10412, Palo Alto CA 94303.

Earlier EPRI programs have shown the effects of recycling a light vacuum bottoms (so called "Light SRC") stream as part of the solvent for coal liquefaction. The previous work showed that the Light SRC recycle resulted in improved performance, particularly at relatively low temperatures, below 800°F. The previous work consisted of comparatively short runs in which the recycle streams were not equilibrated; the ash separation and vacuum bottoms fractionation were not integrated with the coal liquefaction. The results were thus somewhat tentative.

Several runs have now been completed at the Wilsonville 6 ton per day coal liquefaction pilot plant which substantially confirm the previous findings, and add interesting data regarding the scale-up from semi-continuous to continuous operation. This paper will discuss the pilot plant results and relationship between the two scales of operation.

ROLE OF THE AROMATIC OXIDATIVE COUPLING
REACTION IN FUEL CHEMISTRY

J. B. Pierce *

Department of Chemistry
University of Lowell
Lowell, Massachusetts 01854

In the temperature range of 300° to 500°C bituminous coals pass through one or more plastic stages, but after each occurrence continued heating causes solidification (1). In the direct liquefaction of coals or processing of coal-derived liquids at pyrolytic temperatures catalytic surfaces become fouled with carbonaceous deposits (2,3,4). In jet fuels the presence of heterocyclic aromatic compounds containing nitrogen in the rings causes sludge to form (5). Carbazoles and related compounds tend to form carbonaceous electrode deposits at anodes in electrochemical cells.

Each of these effects is caused by an increase in molecular weight which might arise from a number of different chemical reactions. However, in these specific oxidation-reduction reactions a favored oxidation half reaction is the oxidative coupling of aromatic ring structures. The first clue to the operation of aromatic oxidative coupling as a route to products of higher molecular weight and lower solubility resulted from the observation of electrode film formation on anodes when coal-derived liquids were being examined electrochemically (6).

EXPERIMENTAL

The electrode films formed by anthracene oil and SRC-II type product oils derived from Blacksville No. 9 coal were studied by means of cyclic voltammetry and double potential step chronoamperometry. A Princeton Applied Research Model 170 Electrochemistry System was employed. The electrolyte was tetrabutyl ammonium fluoroborate, and solvents were acetonitrile for the anthracene oil and tetrahydrofuran for SRC-II type product oils.

DISCUSSION

Anthracene oil and many samples of SRC-II type product oil from the 1000 pound per day pilot plant at Pittsburgh Energy Technology Center (PETC) were examined electrochemically and found to form electrode deposits under oxidizing conditions. Successive voltammetric traces show the insulating effect of the film deposited by anthracene oil (Figure 1a). Progressive changing of the switching potential toward more cathodic potentials shows a decrease (Figure 1b) and elimination (Figure 1c) of the film-forming tendency.

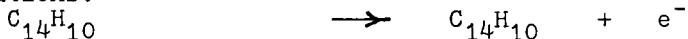
*Work done at Pittsburgh Energy Technology Center, P.O. Box 10940, Pittsburgh, Pennsylvania 15236.

In a different experiment the initial potential of an SRC-II type solute was held at +1.000 volt for different lengths of time, and the resulting films were reduced in the voltammetric scan toward more cathodic potentials. The peak heights reflect the currents used to reduce the films formed by oxidation at +1.000 volt. A linear variation in peak height with time is shown (Figure 2). In these samples the films are much more reactive than those formed from anthracene oil.

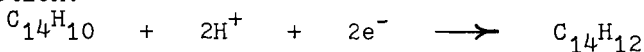
The films formed on anodes proves the reaction to be an oxidation. The formation of electrode films, which, depending on conditions, varied from soft, brown, and soluble to hard, glossy, black, and insoluble in pyridine, proves an increase in molecular weight. The presence of reactive aromatic structures in coals and coal-derived liquids (7) suggests the operation of the aromatic oxidative coupling reaction. Table I comprises a list of selected compounds that undergo oxidative coupling.

As reported by Dworkin and others(8) and illustrated with anthracene, $C_{14}H_{10}$, aromatic oxidative coupling proceeds by way of a radical cation intermediate.

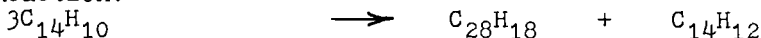
Oxidations:



Reduction:



Net Reaction:



Many common reagents and catalysts cause radical cation formation which initiate aromatic oxidative coupling. These include H_2SO_4 (9,10), oxidizing agents in acidic media (9,11,12,13), Lewis acids (14-26), halogens (27), $Ag(ClO_4)$ and iodine (28,29), and metal salts (30,31). Free radical cations are also formed by such solid catalytic surfaces as gamma-alumina (32), silica alumina (33), and zeolites (34). They may also be generated by photoionization (35,36,37) and electrochemical oxidation(38). Both radical cations and radical anions were generated at PETC by electrolysis of SRC-II type solutes in an ESR cavity (39).

In support of this information Ross and Blessing report, "In the absence of an H-donor, then, oxidative crosslinking takes place within the coal upon heating, yielding a product even less soluble in solvents such as pyridine than was the starting coal" (40). Others have reported the same behavior (41,42). Thus, one may conclude that Lewis acids cause oxidative hydrogen transfer from hydrogen donors or oxidative polymerization through a sequence of coupling reactions. Other radical cation forming catalysts and reagents may be expected to behave similarly.

CONCLUSIONS

Aromatic structures may polymerize by a stepwise, oxidative coupling reaction, initiated by formation of radical cations. Common reagents and catalysts cause radical cations to form.

REFERENCES

1. Davis, J.D., Reynolds, D.A., Naugle, B.W., Wolfson, D.E., and Birge, G.W., Technical Paper 726, U.S. Department of the Interior, U.S. Government Printing Office, 1949.
2. Kriz, J.F., and Ternan, M. A.C.S. Div. Fuel Chem. Preprints, Vol. 25, No. 2, p 146, March 24-28, 1980.
3. Sivasubramanian, R., Olson, J.H., and Klatzer, J.R., A.C.S. Div. Fuel Chem. Preprints, Vol. 25, No. 1, p 86, March 24-28, 1980; ibid. p 149.
4. Shih, S.S., Angevine, P.J., Heck, R.H., and Sawruk, S., A.C.S. Div. Fuel Chem. Preprints, Vol. 25, No. 1, p 154, March 24-28, 1980.
5. Frankenheld, J.W., and Taylor, W.F., A.C.S. Div. Fuel Chem. Preprints, Vol. 23, No. 4, p 205, September 10-15, 1978.
6. Pierce, J.B., "New Approches in Coal Chemistry", A.C.S. Symposium Series, Ed. by Blaustein, B.D., Bockrath, B.C., Friedman, S., and Retcofsky, H.L. (in press).
7. Philip, C.V., and Anthony, R.G., A.C.S. Div. Fuel Chem. Preprints, Vol. 24, No. 3, p 204-14, September 10-14, 1979.
8. Dworkin, A.S., Poutsma, M.L., Brynstad, J., Brown, L.L., Gilpatric, L.O., and Smith, G.P., J. Am. Chem. Soc. 1979, 101, 5299.
9. Hoijtink, G.J., and Weijland, W.P., Rec. Trav. Chim., 1957, 76, 836.
10. Carrington, A., Dravnieks, F., and Symons, M.C.R., J. Chem. Soc., 1961, 905.
11. MacLean, C., and Van der Waals, J.H., J. Chem. Phys., 1957 27, 287.
12. Aalbersberg, W.I., Gaaf, J., and Mackor, E.L., J. Chem. Soc. 1961, 905.
13. Dallinga, G., Mackor, E.L., and Verrijn Stuart, A.A., Mol. Phys., 1958, 1, 123.
14. Weissman, S.I., de Boer, E., and Conradi, J.J., J. Chem. Phys. 1957, 26, 963.
15. Lewis, I.C., and Singer, L.S., J. Chem. Phys., 1965, 43, 2712.
16. Lewis, I.C., and Singer, L.S., J. Chem. Phys. 1966, 44, 2082.
17. Forbes, W.F., and Sullivan, P.D., J. Am. Chem. Soc., 1966, 88, 2862.
18. Shine, H.J., and Sullivan, P.D., J. Phys. Chem., 1968, 72, 1390.
19. Sullivan, P.D., J. Am. Chem. Soc., 1968, 90, 3628.
20. Buck, H.M., Bloemhoff, W., and Oosterhoff, L.J., Tetrahedron Lett. 1960, 5.

21. Rooney, J.J., and Pink, R.C., Proc. Chem. Soc., 1961, 142.
22. Sato, H., and Aoyama, Y., Bull. Chem. Soc. Japan, 1973, 46, 631.
23. Forbes, W.F., and Sullivan, P.D., J. Am. Chem. Soc., 1966, 88, 2862.
24. Bell, F.A., Ledwith, A., and Sherrington, D.C., J. Chem. Soc. (B), 1969, 2719.
25. Aalbersberg, W.I., Hoiijtink, G.J., Mackor, E.L., Weijland, W.P., J. Chem. Soc., 1959, 3055.
- 26 Buchanan, III, A.C., Dworkin, A.S., Brynstad, J., Gilpatrick, L.O., and Smith, G.P., J. Am. Chem. Soc. 1979, 101, 5430.
27. Fitzgerald, Jr., E.A., Wuefling, Jr., P., and Richtol, H.H. J. Phys. Chem., 1971, 75, 2737.
28. Sata, Y., Kinoshita, M. Sano, M., and Akamatu, H., Bull. Chem. Soc. Japan, 1969, 42, 548, 3051.
29. Ristagno, C.V., and Shine, H.J., J. Org. Chem., 1971, 36, 4050.
30. Heiba, E.I., Dessau, R.M., and Koehl, Jr., W.J., J. Am. Chem. Soc. 1969, 91, 6830.
31. Dessau, R.M., Shih, S., and Heiba, E.I., J. Am. Chem. Soc., 1970, 92, 412.
32. Flockhart, B.D., Scott, J.A.N., and Pink, R.C., Trans. Faraday Soc., 1966, 62, 730.
33. Rooney, and Pink, R.C., Trans. Faraday Soc. 1962, 58, 1632.
34. Kurita, Y., Sonoda, T., and Sata, M. J. Catalysis, 1970, 19, 82.
35. Lewis, G.N., and Lipkin, D., J. Am. Chem. Soc., 1942, 64, 2801.
36. Lewis, G.N., and Bigeleisen, J., J. Am. Chem. Soc. 1943, 65, 2419.
37. Land, E.J., and Porter, G., Trans. Faraday Soc., 1963, 59, 2016, 2027.
38. Bard, A.J., Ledwith, A., and Shine, H.J., "Advances in Physical Organic Chemistry", Vol. 13, Ed. bt V. Gold and D. Bethell, Academic Press, 1976, pp. 156-278.
39. Sprecher, R.S., and Pierce, J.B., Unpublished Work, 1980.
40. Ross, D.S., and Blessing, J.E., A.C.S., Div. Fuel Chem. Preprints, Vol. 24, No.2, p 130, April 2-6, 1979.
41. Low, J.Y., and Ross, D.S., A.C.S., Div. Fuel Chem. Preprints, Vol. 22, No. 7, p 121, August 29-September 2, 1977.
42. Mobley, D.P., Salim, S., Tanner, K.I., Taylor, N.D., and Bell, A.T., A.C.S., Div. Fuel Chem. Preprints, Vol. 23, No. 4, p 138, September 10-15, 1978.

43. Osa, T., Yildiz, A., and Kuwana, T., J. Am. Chem. Soc., 1969, 91, 3994.
44. Nyberg, K., Acta Chemica Scandinavica 1970, 24, 1609.
45. Bobbitt, J.M., Weisgraber, K.H., Steinfeld, A.S., and Weiss, S.G., J. Org. Chem., 1970, 35, 2884.
46. Bobbitt, J.M., Yagi, H., Shibuya, S., and Stock, J.T., J. Org. Chem., 1971, 36, 3006.
47. Bobbitt, J.M., Noguchi, I., Yagi, H., and Weissgraber, K.H., J. Am. Chem. Soc., 1971, 93, 3551.
48. Bechgaard, K., and Parker, V.D., J. Am. Chem. Soc., 1972, 94, 4749.
49. Nelson, R.F., and Adams, R.N., J. Am. Chem. Soc., 1968, 90, 3925.
50. Marcoux, L.S., Adams, R.N., and Feldberg, S.N., J. Phys. Chem. 1969, 73, 2611.
51. Nelson, R.F., and Feldberg, S.W., J. Phys. Chem., 1969, 73, 2623.
52. Bacon, J. and Adams, R.N., J. Am. Chem. Soc. 1968, 90, 6596.
53. Ambrose, J.F., Carpenter, L.L., and Nelson, R.F., J. Electrochem. Soc., 1975, 122, 876.
54. Ambrose, J.F., and Nelson, R.F., J. Electrochem. Soc., 1968, 115, 1159.
55. Frank, S.N., Bard, A.J., and Ledwith, A., J. Electrochem. Soc. 1975, 122, 898.
56. Solis, V., Iwasita, T., and Giordano, M.C., J. Electroanal. Chem., 1975, 105, 169.
57. Jordan, J., Ankabrandt, S.J., Robot, A., and Stutts, J.D., Abstract No. 133, 12th Central Regional Meeting, Am. Chem. Soc., Pittsburgh, Pa., November 12-14, 1980.

Table I

Compounds Susceptible to Oxidative Coupling

<u>Compounds</u>	<u>References</u>	<u>Compounds</u>	
Benzene	43	Triphenylamines	49,50,51
p-Xylene	44	Anilines	52
Mesitylene	44	Carbazoles	53,54
Durene	44	Iminobibenzyls	55
Phenolic Tetrahydro- isoquinolines	45,46,47	o-Phenylenedianine	56
Catechol Ethers	48	Dibenzothiophene	57

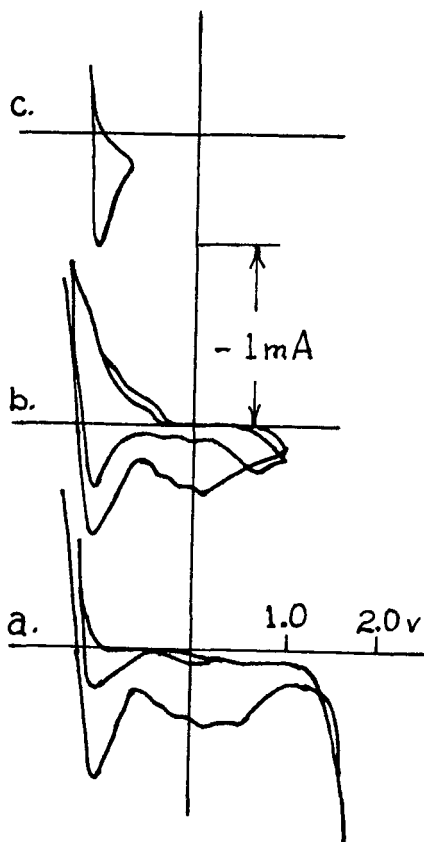


Figure 1. Effect of Film Formation on Voltammograms of Anthracene Oil.

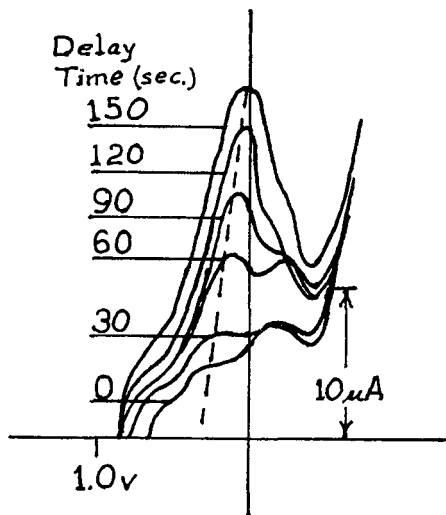


Figure 2. Effect of Film Formation on Voltammogram of SRC-II Type Liquids.

Low Temperature Hydrogenation of Polycyclic Aromatic Hydrocarbons (PAH's)
by Tetralin in a Molten Salt Catalyst*

A. C. Buchanan, III, A. S. Dworkin, L. L. Brown, and G. P. Smith

Chemistry Division, Oak Ridge National Laboratory
P. O. Box X, Oak Ridge, Tennessee 37830

Molten SbCl_3 has been shown to be an effective catalyst for the hydrocracking of coal with a high selectivity for the production of distillate hydrocarbons (1), analogous to the more extensively studied molten salt hydrocracking catalysts based on ZnCl_2 (2,3). Our research is aimed at a basic study of molten salt catalysis with recent studies examining the chemical behavior of PAH's (model compounds for some of the structural units of coal) in molten salts in which SbCl_3 is the primary constituent (4-7). We have observed reactions for PAH's in SbCl_3 based melts in which the anhydrous SbCl_3 solvent is involved catalytically (4) and stoichiometrically (5,6). Both types of chemistry have been explained by redox driven reactions in the melt in which Sb^{3+} is an oxidant.

Tetralin is often used as a hydrogen donor solvent for thermally generated neutral radicals in coal liquefaction and model compound studies. In the present work, we investigate the possibility that tetralin may act as a hydrogen donor to some PAH's under extremely mild (80°C , no H_2) molten salt catalytic conditions in which PAH radical cations are believed to be present as reactive intermediates.

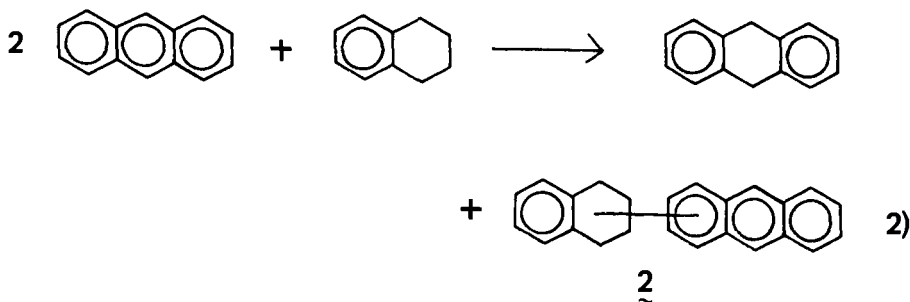
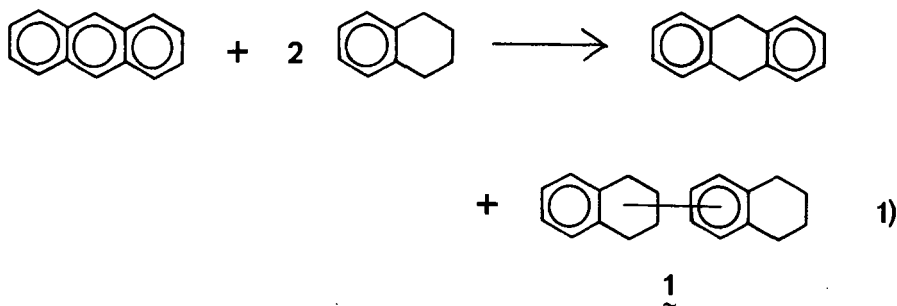
We have studied the reaction behavior of phenanthrene, pyrene, anthracene, and naphthacene (tetracene) with tetralin at 80°C in neat aprotic SbCl_3 by in situ ^1H NMR, and by determining the reaction stoichiometry via product analysis following quench and separation procedures. All reagents were carefully purified (4,5), and material transfers were carried out in a controlled argon atmosphere dry box. ^1H NMR experiments (at 200 MHz) were performed under argon in sealed 5mm OD tubes while larger scale reactions were performed under argon in Schlenk glassware. Following a 30 min reaction period, the reaction mixture was hydrolyzed with 6 M HCl and the organic products were extracted into CH_2Cl_2 . SbCl_3 is a catalyst in these reactions, and no antimony metal was ever observed. The organic products from the reaction of anthracene with tetralin in SbCl_3 were analyzed by GC-MS using a 30 m x 0.25 mm ID glass capillary column with an OV-101 liquid phase. Quantitative results were obtained by GC using a 10' x 1/8" column packed with 3% Dexsil 300 and flame ionization detection. Hexamethylbenzene was used as an internal standard, and the results were corrected for differences in detector response.

Solutions of pyrene and phenanthrene with tetralin do not react in neat SbCl_3 at 80°C . Only the NMR spectra of the parent PAH and tetralin are observed even at temperatures up to 130°C . However, anthracene and naphthacene react rapidly with tetralin at 80°C , and are selectively hydrogenated to 9,10-dihydroanthracene (DHA) and 5,12-dihydronaphthacene (DHN) respectively. DHA and DHN were identified from a comparison of their ^1H NMR spectra with those of authentic samples (4).

* Research sponsored by the Division of Chemical Sciences, Office of Basic Energy Sciences, U. S. Department of Energy under contract W-7405-eng-26 with the Union Carbide Corporation.

The reaction of anthracene with tetralin in SbCl_3 is currently the most extensively studied. Tetralin itself is unreactive in SbCl_3 ($80\text{--}130^\circ\text{C}$), and anthracene also does not show any reaction in SbCl_3 at 80°C for the 30 min reaction period. At longer reaction periods, anthracene slowly undergoes Scholl condensation reactions that we have previously reported (4). This Scholl reaction is believed to proceed through the anthracene radical cation. In the presence of tetralin, however, anthracene does not undergo Scholl condensation but instead is rapidly hydrogenated by tetralin. ^1H NMR experiments using fully deuterated anthracene demonstrate that the hydrogens added at the 9 and 10 positions of anthracene ($\delta 3.99$) are from the tetralin. This observation is supported by the quantitative analysis of tetralin, anthracene, and DHA in the organic products from larger scale reactions.

The product distribution and reaction stoichiometry are found to depend on the amount of tetralin initially present. We find that the yield of DHA increases with increasing amounts of tetralin and reaches a maximum of 39% at a 2:1 tetralin:anthracene mole ratio (Table 1). Furthermore, we find from GC-MS that the dehydrogenated tetralin does not produce naphthalene. Instead it forms principally two condensed products 1 (MW = 262) and 2 (MW = 308) whose relative amounts also depend on the initial amount of tetralin present as shown in Table 1. The overall reaction stoichiometry can be described as the sum of two limiting equations with Equation 1 predominating at high tetralin/anthracene mole ratios and Equation 2 predominating at low tetralin/anthracene mole ratios.



We are in the process of determining the structures of λ and λ' , and these results should provide useful clues towards understanding the reaction mechanism.

Although anthracene and naphthacene are hydrogenated by tetralin in $SbCl_3$, phenanthrene and pyrene are unreactive. From a previous ESR study (7) we know that phenanthrene and pyrene are not oxidized by $SbCl_3$ to radical cations, whereas the more easily oxidized PAH's, anthracene and naphthacene, do form radical cations in $SbCl_3$. These results, along with our previous observations of redox driven reactions in $SbCl_3$ in which Sb^{3+} acts as an oxidant (4-6), suggest that the unusual low temperature hydrogenation reactions reported here proceed via reaction of the PAH radical cation with tetralin. Research in this area is continuing in an effort to further elucidate the reaction mechanism.

REFERENCES

1. Wald, M. M.; U.S. Patent 3 542 665, 1970.
2. Zielke, C. W.; Struck, R. T.; Evans, J. M.; Costanza, C. P.; Gorin, E. Ind. Eng. Chem. Process. Des. Dev. 1966, 5, 151, 158; Zielke, C. W.; Klunder, E. B.; Maskew, J. T.; Struck, R. T. ibid. 1980, 19, 85.
3. Ida, T.; Nomura, M.; Nakatsuji, Y; Kikkawa, S. Fuel 1979, 58, 361.
4. Dworkin, A. S.; Poutsma, M. L.; Brynestad, J.; Brown, L. L.; Gilpatrick, L. O.; Smith, G. P. J. Am. Chem. Soc. 1979, 101, 5299.
5. Buchanan, A. C., III; Dworkin, A. S.; Smith, G. P. J. Am. Chem. Soc. 1980, 102, 5262.
6. Buchanan, A. C., III; Dworkin, A. S.; Smith, G. P. J. Org. Chem. 1981, 46, 471.
7. Buchanan, A. C., III; Livingston, R.; Dworkin, A. S.; Smith, G. P. J. Phys. Chem. 1980, 84, 423.

Table 1. Influence of Tetralin Concentration on the Anthracene-Tetralin- $SbCl_3$ Reaction^a

Tetralin (mmol)	Anthracene (mmol)	DHA yield (%) ^b	λ/λ' mole ratio ^c
0	1.40	0	—
0.70	1.40	20	.15
1.40	1.40	30	.50
2.80	1.40	39	1.5
5.60	1.40	38	3.5

^aReactions were run in 34.2 mmol $SbCl_3$ at 80°C for 30 min.

^bBased on original anthracene ($\pm 2\%$).

^cBased only on gc area ratios.

Copper Catalyzed Aging Reactions of a SRC II Middle Distillate

Laudie Jones and Norman C. Li

Duquesne University, Pittsburgh, PA 15282

INTRODUCTION

Stability of synfuels is an important consideration in direct utilization or upgrading processes. The tendency of synfuels to form gums and sediments and to increase in viscosity poses a serious detriment in handling procedures and burning efficiency. Recently, investigators have studied the aging characteristics of shale (1) and coal-derived liquids (2-5) in an attempt to identify the reactive components and to postulate mechanisms. In aging studies of a Synthoil product in an oxygen atmosphere, the viscosity increase was accompanied by a decrease in the content of oil components and in increase in the content of benzene-insoluble components (4). Similar results were observed in a study of a SRC I/SRC II blend aged by bubbling oxygen directly into the sample (6). These studies indicate that during oxidative degradation, the oil components 'react' to form benzene-insoluble components which are primarily responsible for the increased viscosity.

The oxidative degradation of a SRC-II middle distillate, which is an oil free of asphaltenes and benzene-insolubles was investigated in this study. The objective was to determine the molecular types of compounds responsible for the viscosity change and postulate mechanisms. Since the middle distillate is relatively stable to oxidative degradation, copper shavings were added to accelerate the process.

EXPERIMENTAL

SRC II middle distillate (b.p. range, 170-276°C) from Illinois no. 6 coal was obtained from Gulf R&D Co., and from a process run operated at 2000 psi hydrogen pressure at 454°C for 1 hr residence time. The coal liquid was placed in a 3-necked flask, equipped with a gas bubbling inlet and a condenser to minimize the loss of volatiles. Oxygen was bubbled through the sample (1-2 ml/min) and copper shavings, 2 wt %, were added to accelerate the degradation. The flask was immersed in a thermostat bath at 62°C, and samples were withdrawn at time intervals, for viscosity and other measurements.

Separation of Aged Coal Liquid into Pentane-Soluble and Pentane-Insoluble Components:

Pentane, 20-fold by volume, was added to the aged coal liquid, mixed (magnetic stirring bar) for 1 hr at room temperature and then filtered through a 0.5 micron millipore styrene membrane. The precipitate was dried in a vacuum oven at 80° for 12 hr to remove pentane (94% of the precipitate is soluble in benzene). Pentane from the pentane-soluble fraction was removed by distillation at 40°C. The sample was then subjected to rotary evaporation at 70° for 5 min to insure complete removal of pentane.

INSTRUMENTATION

Viscosity data were obtained at 30° using a Brookfield Synchroelectric

viscometer with a small sample adaptor. Infrared spectra of CS₂ solutions (5g/L) in a 5 mm KBr liquid cell were obtained with a Beckman IR-20 spectrometer. NMR spectra were obtained with a 60-MHz or 600-MHz spectrometer as CDCl₃ solutions with TMS as internal reference. Gel permeation chromatograms were obtained with a Waters HPLC and three μ -styragel columns in series: 10³, 500, and 100 A using THF as solvent at a flow rate of 1 ml/min.

RESULTS AND DISCUSSION

Viscosity of the coal liquid increased exponentially with time when aged at 62°C with oxygen and copper. Aging with copper or oxygen alone at 62°C does not affect the viscosity in a 5-day period. Thus, the loss of volatiles which undoubtedly occurs with oxygen bubbling through the sample does not contribute to the observed viscosity change.

Infrared spectra of dilute solutions of the coal liquid before and after aging 5 days at 62°C were obtained. The unaged coal liquid shows a prominent free hydroxyl stretching band at 3600 cm⁻¹. The intensity of this band is not significantly affected by aging with copper or oxygen alone. Aging with both copper and oxygen, however, reduces the intensity of this band. This indicates that the hydroxyl group is modified during aging.

The unaged coal liquid is completely soluble in pentane. After aging 5 days, 30% of the aged coal liquid becomes insoluble in pentane. Therefore, pentane was used to separate the aged material into two fractions: the pentane-soluble and pentane-insoluble fractions.

Comparison of the 60 MHz NMR spectra of the coal liquid before and after aging 4 days shows that for the aged pentane-soluble fraction: (a) there is a decrease in the intensity of the signal at 2.3 ppm attributed to the methyl protons attached to benzylic groups, (b) the hydroxyl signal at 5 ppm is absent, and (c) the higher-field aromatic signals from 6.3 to 6.8 ppm are also absent. The 600-MHz spectra of the unaged coal liquid and its acid-free fraction (obtained by ion exchange chromatography) are presented in Fig. 1. The acid-free spectrum is identical to that of the aged pentane-soluble fraction (not shown). Obviously, during aging, acidic methyl substituted phenols are modified and are no longer soluble in pentane.

The gel permeation chromatography of the unaged coal liquid shows three peaks (retention times of ~28, 29 and 30 min.) After aging for three days, profiles of the pentane-separated fractions (Fig. 2) show that the aged pentane-soluble fraction (top), which constitutes 70 wt % of the aged coal liquid, contains components which elute at 29 and 30 min. Components of the unaged coal liquid which elute at 28 min are no longer present after aging. As comparison, the acidic and basic components of the unaged coal liquid (isolated by ion-exchange chromatography) also elute at 28 min. The profile of the pentane-insoluble fraction (Fig. 2 bottom) shows that this fraction is composed of large molecular size components. These results suggest that the polar constituents of the coal liquid are reacting during aging to form large molecular aggregates which are pentane-insoluble.

The coal liquid was also enriched 10 wt % with acidic and basic fractions which were isolated by ion-exchange chromatography. The effect of these additives on the formation of pentane-insoluble material is shown in Table 1. The enriched coal liquids were aged at 62°C for 1 day with oxygen and 1% copper. Clearly, enrichment with the acid II fraction

yields the largest amount of pentane-insoluble material (46 wt %). The acid-II fraction consists of alkyl substituted phenols, the base II fraction contains quinoline type compounds and the acid I fraction contains carbazoles, indoles, anilines and xylenols (5).

The elemental composition of the coal-liquid before and after aging 4 days is presented in Table 2. The aged pentane-soluble fraction contains 23% less oxygen and 50% less nitrogen than the unaged coal liquid. The decrease in oxygen content is consistent with IR, NMR, and GPC results showing a reduction in the amount of phenolic compounds during aging. The large amount of oxygen contained in the pentane-insoluble fraction indicates: (a) oxygen containing compounds of the coal liquid have been concentrated in this fraction and (b) the oxygen bubbled into the coal liquid has been incorporated into the structure of this fraction. This is confirmed in FTIR spectra (not shown). The increased nitrogen content of the pentane-insoluble fraction indicates that nitrogen containing compounds are involved in the aging reaction.

Significant characteristics of the aged pentane-soluble fraction are that the viscosity and the atomic H/C ratio are similar to those of the unaged coal liquid, but the oxygen and nitrogen contents are less (Table 2). A low heteroatom content is required in syncrude upgrading procedures to prevent fouling of the catalyst. Our experiments have shown that a reduction in heteroatom content can be achieved with metallic copper under mild conditions.

The results of this study suggest that at least one of the aging reactions is the selective polymerization of phenolic compounds. Incorporation of oxygen and polymerization of nitrogen compounds also occur. In oxidative coupling of phenols, -OH groups give way to ether linkages, in the formation of polymers. The distinctly smaller retention time of the pentane-insolubles in the GPC profiles and the increased VPO molecular weight of the pentane-insolubles are consistent with the formation of polymers.

ACKNOWLEDGEMENTS

We acknowledge support of the U.S. Department of Energy under Contract No. DE-AC22-80 PC 30252. The 600 MHz NMR spectrometer at Carnegie-Mellon University, supported by PHS Grant No. RR-00292, was used, and we thank K.S. Lee and J. Dadok for expert advice in carrying out the ¹H NMR measurements.

REFERENCES

- (1) C.J. Nowack, R.J. Del Fosse, G. Speck, J. Solash and R.N. Hazlett, Preprint, Div. Fuel Chem., Am. Chem. Soc., 25 (3), 40 (1980).
- (2) Y.Y. Lin, L.L. Anderson, and W.H. Wiser, Preprint, Div. Fuel Chem., Am. Chem. Soc., 19 (5), 2 (1974).
- (3) D. Finseth, M. Hough, J.A. Queiser, and H.L. Retcofsky, Preprint, Div. Petrol. Chem. Am. Chem. Soc., 24 (4), 979 (1979).
- (4) F.R. Brown and F.S. Karn, Fuel, 59, 431 (1980).
- (5) D.W. Brinkman, J.N. Bowden, J.W. Frankenfeld, and W.F. Taylor, Preprint, Div. Fuel Chem., Am. Chem. Soc., 25 (3), 110 (1980).
- (6) T. Hara, L. Jones, N.C. Li, and K.C. Tewari, unpublished results.

Table 1. Aging of Enriched Coal Liquids

(62°C, 1% Cu, O₂, 1 Day)

Pentane Insolubles	
Ill #6	14%
10% Acid-Free Enriched	10
10 Acid I Enriched	11
10% Acid II Enriched	46
10% Base II Enriched	12

Table 2. Elemental Composition and Characterization of SRC II Middle Distillate, Before and After Aging 4 days, 2 wt % Copper and Oxygen at 62°C

	Unaged	Aged Pentane-Soluble	Aged Pentane-Insolubles
C	85.58	86.67	75.48
H	9.12	9.33	6.00
N	0.85	0.43	1.80
O	4.29	3.31	12.78
S	<u>0.19</u>	<u>0.27</u>	<u>0.27</u>
	100.03	100.00	96.29
Copper			3.7
MW	172*	170**	570***
Viscosity [†]	4.3	3.6	
Atomic H/C	1.28	1.28	0.96

*VPO method, toluene, 37°C 2-15 g/l

**VPO method, methylene chloride, 28°C, 4-7 g/l

***VPO method, pyridine, 86°C, 4-7 g/l

†Centipoise at 30°C

FIG. 1
600 MHZ ^1H NMR SPECTRA
ILL NO. 6

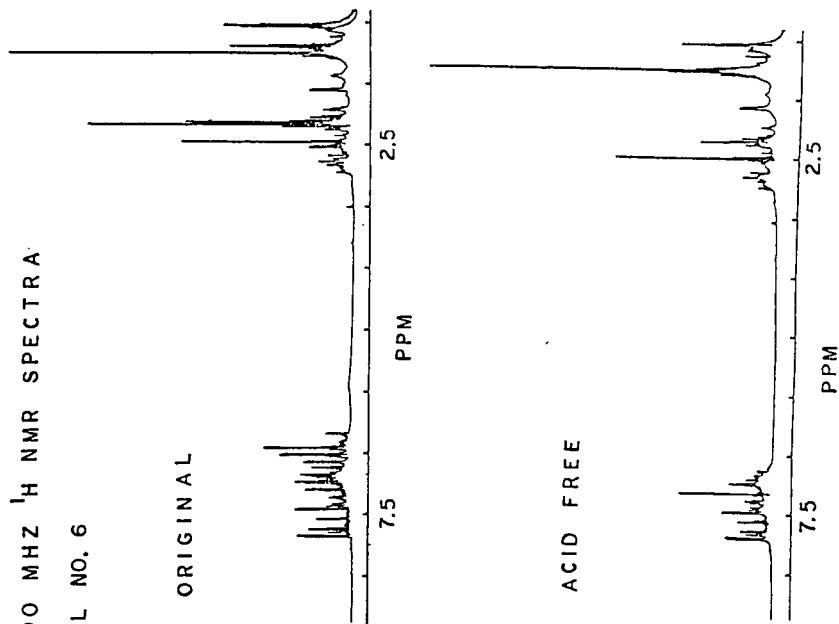
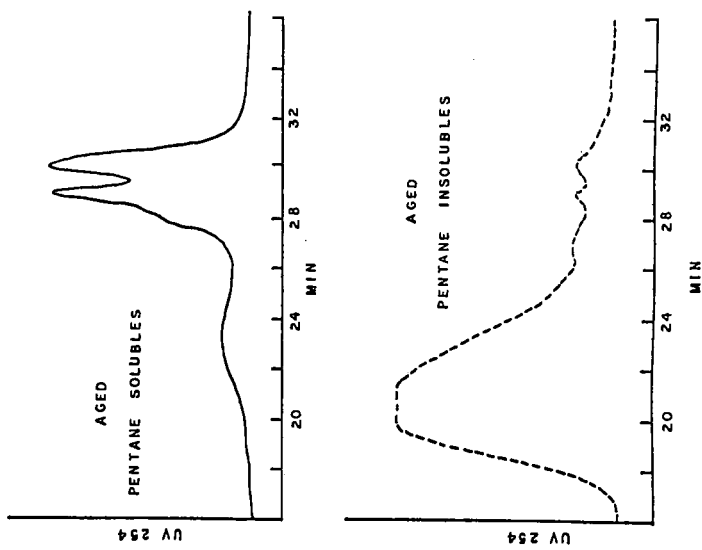


FIG. 2
GPC PROFILES AGED ILL NO. 6



THE OXIDATION OF FUEL OIL #6 STUDIED BY
DIFFERENTIAL SCANNING CALORIMETRY

By

J.A. Ayala and M.E. Rincón
Instituto de Investigaciones Eléctricas,
Departamento de Combustibles Fósiles,
Apdo. Postal 475, Cuernavaca, Mor.,
México.

INTRODUCTION

The studies on combustion of heavy fuel oil are important because of the extended use of this fuel as an energy source for the production of electricity. With the continuous increase in the extraction of products from crude oil, there exists a continuous degradation in the quality of the residue that is to be burned in a utility boiler. The degradation of the quality in the residual oil, means a higher sulfur content in the fuel, higher aromaticity, and higher asphaltene and metallic content. Some of these species, yield products of combustion which are aggressive to both the environment, and some of the components within the boiler. It is believed (1) that an understanding of why and how pollutants form, must come from an understanding of the chemical kinetics in the flame. That is, in order to protect the environment, and increase the availability of a large boiler more research is needed to understand the chemistry of oxidation of complex fuel mixtures.

Various authors (2-6) have pointed out the potentiality of the different techniques in thermal analysis for the characterization of petroleum products and coal. However, very little kinetic information has been extracted from the studies which involve the use of thermoanalytical techniques. The chemical kinetics of thermo-oxidative processes in fuels, may contribute to a large extent to the understanding of the chemistry

of oxidation of such mixtures. Weber (2), has reported the potential utilization of differential thermal analysis (DTA) to obtain kinetic parameters for the oxidation of hydrocarbons. He concluded, though, that for the kinetics of oxidation of heavy fuel oil no theory for DTA could yet be used, because of the complexity of the thermograms. Adonyi (3), has shown that kinetics may be obtained for petroleum products by means of DTA, and thermogravimetric techniques (TG). More recently, Noel and Cranton (4), have measured the activation energy, E_a , for the oxidation of lube oil by differential scanning calorimetry (DSC). These authors make the observation that more research is necessary in order to have a better understanding of the results observed by DSC. Smith et al. (7), have used TG to measure the rate, and the E_a for the oxidation of sixty-six coal samples. Valayavin et al. (8), utilized TG to study the thermolysis of high molecular weight petroleum residues, and established a reaction rate law as a function of the viscosity of the medium and a diffusion parameter.

In the present work, we have utilized DSC to study the thermal oxidation of four samples of mexican fuel oil. We have also obtained kinetic parameters such as the overall activation energy for the oxidation of the fuel at low temperature (200 - 550°C).

EXPERIMENTAL

The experimentation was carried out by means of a DuPont Thermal Analyzer Model 990 with its standard DSC attachment. The instrument was calibrated with Indium. The temperature was varied from 20 to 550°C with a scanning rate of 10°C/min. The sensitivities used were 20 and 50 mV/cm. The sample and reference pans were made of aluminum, and the sample weight was kept at around 2 mg. Four different samples of mexican fuel oil # 6 were analyzed, and the experiments were performed with a constant flow of nitrogen, oxygen or a mixture of both. The flow rates, and the O_2/N_2 ratios utilized

throughout the experiments are shown in Table 1.

RESULTS AND DISCUSSION

Experiments with pure nitrogen flow did not show any endothermic reaction, but a gradual displacement from the baseline, especially above 300°C. This displacement indicates that the evaporation of some compounds in the fuel has occurred. A residue was observed in the sample pan after the run was completed. Figure 1 shows a typical thermogram obtained with pure oxygen flow. This thermogram is very similar to those shown in the literature for tar sands (2), or high asphaltene crude oil (9), which may show the quality or the characteristics of the fuel. Indeed, the fuel studied here has a > 10% asphaltene content, and > 3% sulfur. In figure 1, it is observed a small exothermic reaction zone (zone 1) at ~ 300°C, and a larger zone (zone 2), also exothermic, which starts at ~ 400°C. Several small peaks are shown at the low temperature side of the second zone. It is also observed a rapid fall-off of the signal after the maximum has been reached. All the sample was consumed during the experiments with high oxygen concentration in the gas flow. Figure 2, presents a thermogram obtained with a low oxygen concentration in the gas flow. It is observed that the reaction zone is shifted towards higher temperatures.

From the calibration of the instrument with In, it was calculated that the sensitivity of 20 mV/cm corresponded to 43.5 mcal/min-cm. Table 2 shows the results for the heat of reaction measured for both exothermic zones in the thermograms. The values in Table 2 range from as high as 3.3 Kcal/g for the experiments with pure O₂, to as low as 1.4 Kcal/g for the experiments with a 1:9 O₂/N₂ ratio. These values for the heat of reaction, are low if they are compared with the usual heat content of these fuels, which is ~ 10 Kcal/g. Other reports (4), have also measured similar heats of reaction to those reported here, and utilizing a similar

technique. The difference between our values, and the value of 10 Kcal/g for the heat content of the fuel are explained as follows: 1) First, we have a flow system in which we are continuously carrying away heat from the reaction envelope. 2) Second, most probably, we do not have a complete oxidation of the fuel. That is, we do not have a complete adiabatic combustion-type of experiment from which the heat content of the fuel is normally evaluated. It must be observed, that the extreme values for the heat of reaction in table 2 were obtained for experiments with approximately the same total flow. The only difference among both experiments is the oxygen concentration. Similar features were observed in other investigations where TG and DTA were used (2,9), and in which the pressure of air inside the reaction device was varied. That is, the actual oxygen concentration, and availability for the fuel was varied. We may conclude that different reaction channels are being followed according to the oxygen concentration. Hence, different heats of reaction are measured for the experiments with pure O₂, and for experiments with a 1:9 O₂/N₂ ratio.

In order to obtain kinetics parameters from the thermograms, we utilized the theory of Borchardt and Daniels (10). The zones I and II in the thermograms were treated independently, and it was assumed a reaction of pseudo-first order. A pseudo-first order kinetics implies a first order reaction with respect to the fuel, and a constant oxygen concentration. The latter assumption is clearly justified for the experiments with a high oxygen content in the gas flow. A first order reaction with respect to the fuel may be justified through the results. Figure 3 and 4 show the Arrhenius plot for the zone I of the thermograms. The results in figure 3 are for the experiments with pure oxygen; whereas those in figure 4 present the experiments with low concentrations of O₂ in the gas flow. For the data in figure 3 it is possible to draw two different straight lines. Thus, two different activation energies are obtained, one of 12_±1 Kcal/mol, and a higher one of 22_±1 Kcal/mol. From the data

in figure 4, only one activation energy has been obtained with a value of 16 ± 1 Kcal/mol. The lower value for E_a in the experiments with pure O_2 occurs at the higher temperatures of zone I in the thermograms. Thus, it is possible that diffusion controlled reactions occur at these temperatures. In fact, it has been found (8) that, the thermolysis of petroleum residues in a TG experiment is highly influenced by diffusion processes. The results in figure 4, along with the results of the heat of reaction for the experiments with a poor oxygen concentration, indicate that a different reaction scheme is being followed. This last statement should be supported by the identification of the reaction products.

Figures 5 and 6 show the results for zone II in the thermograms. Figure 5 presents the results for the pure O_2 experiments, and figure 6 presents the data for the experiments with a low oxygen concentration. In this case, we only obtain one activation energy for the pure oxygen data (figure 5) $E_a = 36 \pm 1$ Kcal/mol. In figure 6 we observe a straight line only for the experiments with a 1:3 O_2/N_2 ratio, and gas flows of 41 ml/min and 87 ml/min. The rest of the data points in figure 6 show large deviations from a straight line. These deviations in the experiments, with the lowest oxygen concentration in the gas flow, seem to indicate that we may no longer assume a pseudo-first order kinetics.

The various techniques in thermal analysis, may be very useful to obtain an overall view of the oxidation reactions for mixtures as complex as the heavy fuel oil. This overall picture, may include quantitative information such as activation energies. In general, we believe that these studies may serve as a basis to understand more complex oxidation reactions such as those occurring within a flame.

ACKNOWLEDGMENTS

This work is a result of the projet FE-F-14/N of the Instituto de Investigaciones Eléctricas.

REFERENCES

- 1) I. Glassman, "The Homogeneous Oxidation Kinetics of Hydrocarbons: Concisely and With Application", Annual Meeting of The Combustion Institute. Sezione Italiana, Torino, June 1979.
- 2) L. Weber, "Application of DTA to Petroleum Chemistry", Chem. Inst. Can., Proc. 1st. Toronto Symp. on Thermal Analysis, Feb. 8 1965, p.141-62.
- 3) Z. Adonyi, "Thermoanalysis of Petroleum products criticism to the Conradson number and a possibility to determine the flash point", Period Polytech, Chem. Eng. v 16 n 3, 1972, p.285-298.
- 4) F. Noel and G.E. Cranton, Anal. Calorimetry, 3, 305 (1974).
- 5) R.L. Blaine, American Laboratory, January 1974, 18.
- 6) E.J. Gallegos, "Analysis of Five U.S. Coals", Adv. in Chem. Ser., No. 170, p. 13 (1979).
- 7) S.E. Smith, R.C. Neavel, R.N. Miller and E.J. Hippo, "DTGA Combustion of Coals in the Exxon Coal Library", The Combustion Institute, Spring Meeting, Central States Section, Baton Rouge, March 1980.
- 8) G.G. Valayavin. V.V. Fryazinov, M. Yu. Dolomatov, and E.V. Artamonova, Khim. Tekh. Toplivi Masel, March 1980, p. 54.
- 9) J.H. Bae, Soc. Petr. Eng. J., June 1977, p.211.
- 10) H.J. Borchardt and F. Daniels, J.Phys.Chem., 61, 917(1957).

TABLE 2
HEAT OF REACTION

SAMPLE	FLOW (ml/min)	RATIO O ₂ :N ₂	ZONE I (Kcal/g)	ZONE II (Kcal/g)
#1	90	1:0	0.4	1.9
#2	90	1:0	0.6	2.5
#3	90	1:0	0.5	2.5
#4	98	1:0	0.5	2.7
#4	89	1:1	0.3	1.8
#4	87	1:3	0.2	1.6
#4	91	1:9	0.2	1.2
#4	41	1:3	0.3	1.6
#4	24	1:3	0.2	1.4

TABLE 1
EXPERIMENTAL FLOW CONDITIONS

FLOW (ML /MIN)	GAS	RATIO O ₂ :N ₂
90-100	N ₂	0:1
90-100	O ₂	1:0
85-90	O ₂ /N ₂	1:1
85-90	O ₂ /N ₂	1:3
40	O ₂ /N ₂	1:3
24	O ₂ /N ₂	1:3
11	O ₂ /N ₂	1:3
90	O ₂ /N ₂	1:9

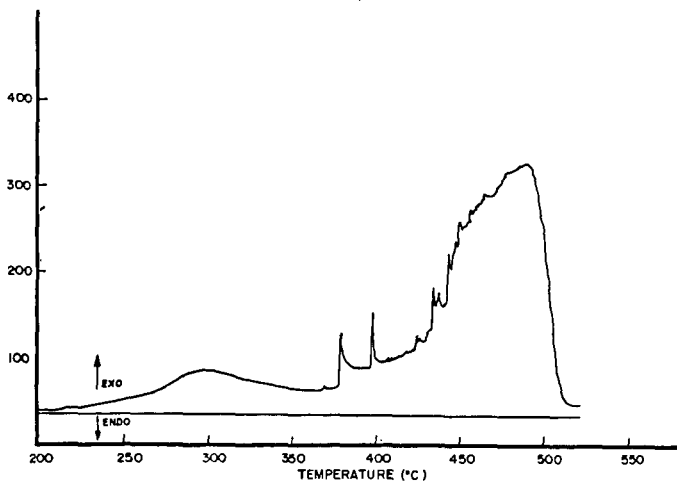


Figure 1. Sample #4. Atmosphere: pure oxygen.
Total flux: 98 ml/min.

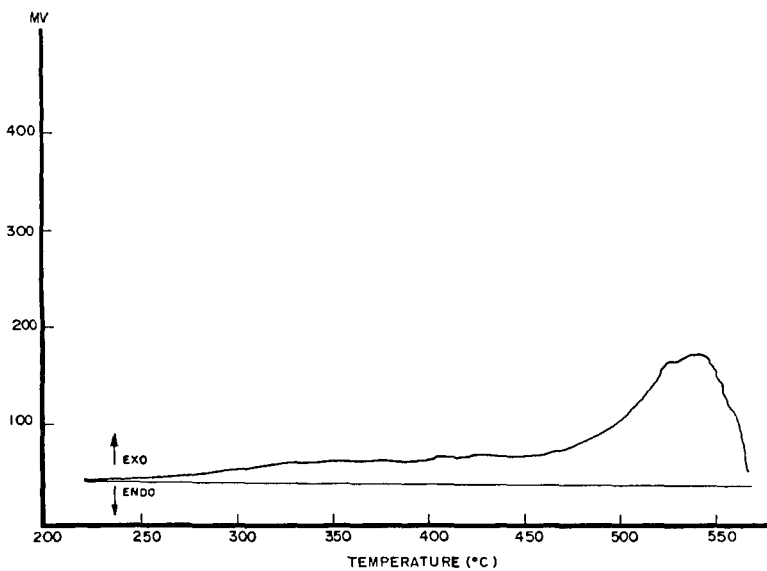


Figure 2. Sample #4. Atmosphere: O₂/N₂ (1:9).
Total flux: 91 ml/min.

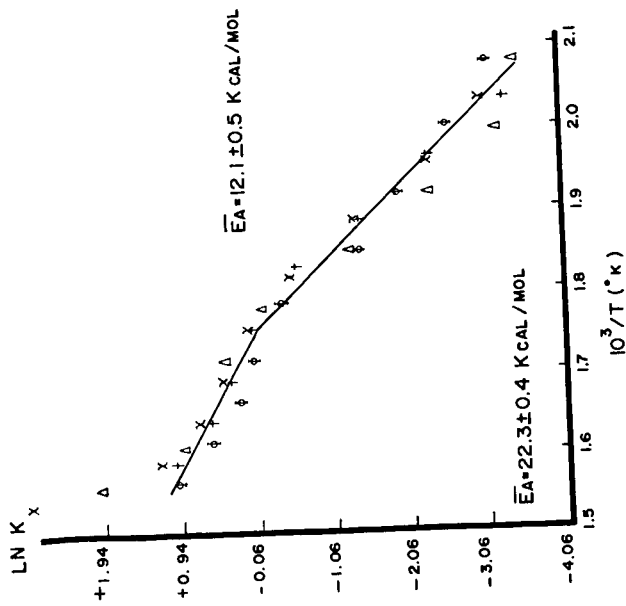


Figure 3. Arrhenius plot for experiments with pure oxygen. Zone I.
 Δ Sample #1 (O₂ = 90 ml/min)
 φ Sample #2 (O₂ = 90 ml/min)
 † Sample #3 (O₂ = 90 ml/min)
 x Sample #4 (O₂ = 98 ml/min)

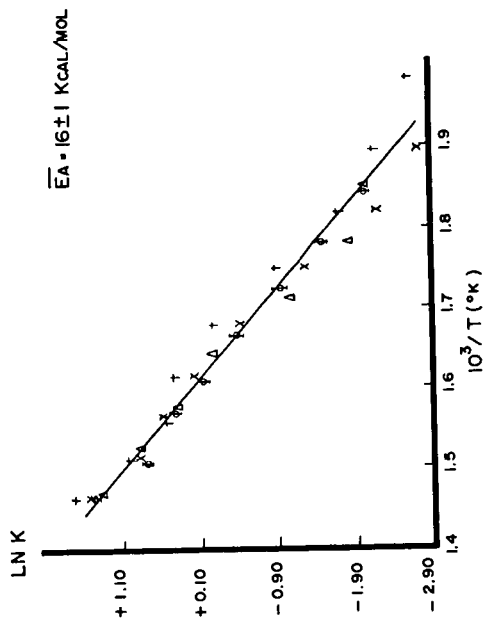


Figure 4. Arrhenius plot for experiment with low oxygen concentration
 Zona I. Sample #4.
 x 1:3 O₂/N₂ (87 ml/min)
 † 1:3 O₂/N₂ (41 ml/min)
 φ 1:3 O₂/N₂ (24 ml/min)
 Δ 1:9 O₂/N₂ (91 ml/min)

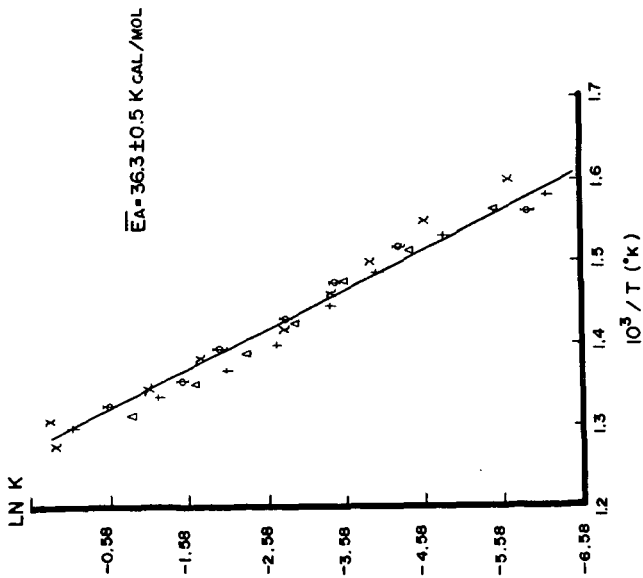


Figure 5. Arrhenius plot for experiments with pure oxygen, zone II.
 Δ Sample #1 ($O_2 = 90 \text{ ml/min}$)
 ϕ Sample #2 ($O_2 = 90 \text{ ml/min}$)
 $+$ Sample #3 ($O_2 = 90 \text{ ml/min}$)
 \times Sample #4 ($O_2 = 98 \text{ ml/min}$)

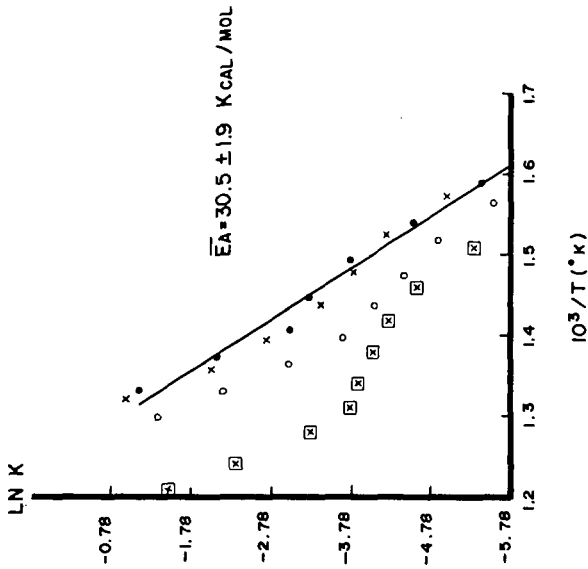


Figure 6. Arrhenius plot for experiments with low oxygen concentration, zone II, sample #4.
 \times 1:3 O_2/N_2 (87 ml/min)
 \bullet 1:3 O_2/N_2 (41 ml/min)
 \square 1:3 O_2/N_2 (24 ml/min)
 \circ 1:9 O_2/N_2 (91 ml/min)

INVESTIGATION IN THE USE OF HEAVY OILS
(AND DERIVATIVES) TO PROCESS COAL

SPEROS E. MOSCHOPEDIS¹, RANDALL W. HAWKINS¹ and
JAMES G. SPEIGHT²

1. Coal Research Department
Alberta Research Council
11315 - 87th Avenue
Edmonton, Alberta, Canada
T5G 2C2
2. Corporate Research Science Laboratories
Exxon Research and Engineering Company
P.O. Box 45, Linden, N.S. 07036

INTRODUCTION

The use of oil as an energy source started from the beginning of this century, and for many years has been regarded as the cheapest source of liquid fuels. However, the recent dramatic escalation in work oil consumption and price, and the concern over future supplies, which are expected to fall short of demand by the end of this century, have forced the energy industry to consider other sources for the production of liquid fuels. The sources which can provide liquid fuels are coal and lignite, oil sands, oil shales, peat, and biomass.

Coal is the largest source of hydrocarbons in the world which can be converted to liquid fuels, but requires enormous amounts of expensive hydrogen. In an attempt to reduce the cost of hydrogen required to convert coal to liquid fuels, the use of oil sands bitumens, Lloydminster heavy oil, and other liquids derived therefrom, have been reported (1,2) as potential low cost hydrogen donor solvents. The present study is a continuation of the work reported elsewhere (1,2) and reports the effect of process parameters (i.e. temperature, pressure and time) on the extent of the coal conversion and on product distribution.

EXPERIMENTAL

Oil sands bitumen (dry) and coker gas oil were obtained from Great Canadian Oil Sands Ltd. (GCOS)*. Cold Lake bitumen and Lloydminster heavy oil were obtained from the Alberta Research Council sample bank. All samples were used as received.

The experimental conditions for the solvation and catalytic hydrogenation of coal, and the procedure for the fractionation of the bitumen and various liquid derivatives are described elsewhere (2,3).

Elemental compositions were determined by the micro-analysis laboratories of the Alberta Research Council and the University of Alberta. Molecular weights were measured osmotically in pyridine, and the nmr spectra were recorded (carbon tetrachloride solutions) by means of a Varian E-60B spectrometer. Gas analysis were obtained by means of a Hewlett Packard gas chromatograph fitted with a Poropak N column and a molecular sieve.

* Now Suncor, Oil Sands Division.

The aromatics content, f_a , of the bitumen and derived liquids has been defined elsewhere (2).

RESULTS AND DISCUSSION

The current communication is a continuation of the previous investigations (1,2) whereby coal can be converted to soluble products using oil sands bitumen, Lloydminster heavy oil and liquids derived therefrom as solvents.

The data (Figure 1) indicate that it is, indeed, possible to solubilize part of the coal by using the Athabasca bitumen, and related liquids as solvents, and as previously reported (1,2) the extent of solubilization varies depending upon the type of solvent used. Nevertheless conversion yields using these solvents compared favorably to the results obtained when tetralin (a well-known hydrogen donor for coal liquefaction) was used as a solvent, particularly in the presence of hydrogen. It is note worthy that when tetralin was used as solvent, coal conversion yields from the solvation and noncatalytic and catalytic hydrogenation show little variation (i.e. from 47-50%) and practically remain constant. On the other hand, the percent conversion yields of the other solvents have shown a substantial increase in the presence of hydrogen, for example, from 10 to 24% in coal solvation to 30 to 40% in the catalytic hydrogenation (Figure 1).

CONTROL EXPERIMENTS

Control experiments were performed in the manner described elsewhere (2), in order to determine the degree of coke (toluene insolubles) formation during the thermal treatment of the solvents. Briefly, when these liquids are heated with or without hydrogen (in the absence of catalyst) for 60 minutes at 400°C, an overall increase in the aromatic contents is evident as their H/C atomic ratios decrease and their f_a values increase when compared with the parent solvents (Table 1). In contrast, when the solvents are heated in the presences of hydrogen and catalyst, an overall increase in the aliphatic content is evident. The API gravities of the solvents are generally increased by the heat treatment but surprisingly the API gravities of CGOS bitumen and coker gas oil are drastically reduced (Table 2) when these solvents are heated at 450°C, although liquid products of high fluidity were obtained. In addition, changes in the hetero-atom contents in these solvents (Table 1). For example oxygen and sulphur contents are decreased, particularly during the catalytic hydrogenation of the solvent, while nitrogen contents in general remained unchanged or increased supporting the concept of thermal stability due to its inclusion in hetero-aromatic systems (4). Compositional differences of the solvents as a result of heat treatment also occur (Table 2) and there are variations in the distribution of products--coke (toluene insolubles), liquids (toluene solubles), and gases (Table 3). Coke formation under these conditions (temperature 400°C and 450°C) was anticipated since oil sands bitumen and heavy oil are susceptible to heat (5,6). Composition of gases from the thermal treatment of solvents (Table 4) shows that the gas products mainly consist of hydrocarbons and hydrogen sulfide.

PROCESS CONDITIONS

EFFECT OF TEMPERATURE

a) Coal Solvation

Comparison of the conversion yields of coal solvation, using GCOS bitumen and coker gas oil as solvents (Table 5), shows that the conversion yield is constantly increased with increasing temperature for coal/bitumen processing whilst the conversion yield reaches a maximum value at 400°C, and then drastically drops to almost zero for coal/coker gas oil processing. Trends in the distribution of the reaction products (solids, liquids, and volatiles, (Table 5) using these two solvents were similar.

The toluene insoluble products (solids, undissolved coal plus coke) has a minimum value at 400°C, which coincides with the optimum conditions for the liquid and volatile products, and then drastically increases at 450°C due to coke formation as determined from blank experiments (Table 3). Because coke formation occurs simultaneously while coal is converted to liquid and gaseous products, greater amounts of toluene insolubles are obtained than the initial coal charge at 450°C. Furthermore, the liquid (toluene solubles) and volatile products follow opposite paths; as the reaction temperature increases, the maximum yield of volatiles (at 450°C) correspond to the lowest yield of liquids, suggesting that solids and volatiles are produced at the expense of liquid products.

b) Catalytic Hydrogenation

It is apparent from the data (Table 5) presented that the trends due to increase of reaction temperatures are similar for both solvents with the only difference in the yields of solid products. Thus, the conversion yields for both solvents are increased with temperature but when bitumen is used as solvent coal conversion yields reaches a maximum (at about 400-450°C) while coal conversion yields with coker gas oil continue to increase with temperature.

The percent distribution of the various products derived by processing coal with the two types of solvents show (Table 5) that the yields of liquids are high at lower temperatures (i.e., decrease with increasing temperature) while the yields of volatiles increase with increasing temperature indicating again, that the volatiles are produced at the expense of liquid products. On the other hand, the yield of solids produced using coker gas oil as solvent continuously decreases as temperature increases; the solids decrease and then appear to increase as the temperature exceed 400°C.

EFFECT OF TIME

a) Coal Solvation

The data demonstrate (Table 6) that coal solvation yield with both solvents reaches a maximum value after 60 minutes at 400°C, and then drastically drops. The product distribution (solids, liquids, and volatiles) is similar for both the coker gas oil and bitumen and resembles the product distribution for coal solvation with both solvents (Table 6). It is apparent that a reaction time of 60 minutes at 400°C coincides with the optimum conditions for the most efficient production of liquid products.

b) Catalytic Hydrogenation

Conversion yields using bitumen as solvent reach a maximum after 60 minutes reaction time, and then levels off, while with coker gas oil continues to increase linearly (Table 6). The relationship between time and product distribution by processing coal with bitumen show that there is not a drastic effect as the time exceeds 60 minutes. However, when coker gas oil is used as solvent, the liquid products are steadily increased and solids decrease without a substantial increase of gases indicating that under these conditions, longer periods are beneficial.

EFFECT OF PRESSURE

The limited data available (Table 7) show that conversion yields reach a maximum at a pressure of approximately 1000 psig. There is a pronounced effect on the yields of liquid products which are constantly increased with increasing pressure; volatiles decrease with increasing reaction pressure, while there is a small variation of the solids at pressure over 1000 psig.

Tables 8, 9, and 10 show the relative composition of gases derived from processing coal under various conditions using bitumen and coker gas oil as solvents. As previously discussed, the evolution of oxygen and sulphur from coal as carbon monoxide and dioxide, and as hydrogen sulphide particularly in the catalytic hydrogenation of coal are the most noticeable features.

ACKNOWLEDGEMENT

We thank Dr. M. P. du Plessis for encouragement throughout this work.

REFERENCES

1. Moschopedis, S.E.: "The use of oil sands bitumen and its derivatives as hydrogen donors to coal", *Fuel*, 59, 67, 1980.
2. Moschopedis, S.E., Hawkins, R.W., Fryer, J.F., and Speight, J.G.: "The use of heavy oils (and derivatives) to process coal". *Fuel*, 59, 647, 1980.
3. Moschopedis, S.E., Fryer, J.F., and Speight, J.G.: "Investigation of the carbonyl functions in a resin fraction". *Fuel*, 55, 187, 1976.
4. Moschopedis, S.E. and Speight, J.G. "Investigation of nitrogen types in Athabasca bitumen". Preprints, Am. Chem. Soc., Div. Fuel Chem., 24, (4), 1007, 1979.
5. Speight, J.G. "Thermal cracking of Athabasca bitumen, Athabasca asphaltenes, and Athabasca deasphalted heavy oil", *Fuel*, 40, 134, 1970.
6. Speight, J.G., and Moschopedis, S.E., "The production of low-sulfur liquids and coke from Athabasca bitumen", *Fuel Processing Technology* 2, 295, 1979.

Table 1 Analyses of bitumens and derived liquids

Material description	2 Composition										N/C	H/C	N _{atom} %	S _{atom} %	
	C	H	N	O	S	Mt	Mt	Mt	Mt	Mt					
a) <u>Parent material</u>															
GCOS bitumen Athabasca deposit	84.18	10.31	0.40	0.78	4.33	532	1.47	5.8	29.9						
GCOS coker gas oil	84.65	10.95	0.40	0.64	3.34	296	1.55	8.2	28.7						
Lloydminster heavy oil	83.75	10.94	0.27	1.47	3.55	410	1.57	7.0	27.1						
Cold Lake bitumen	83.68	10.66	0.39	1.13	4.13	508	1.53	7.3	29.1						
b) Heated for 60 min at 400°C															
GCOS bitumen Athabasca deposit	84.96	9.98	0.67	0.68	3.41	394	1.41	6.8	34.3						
GCOS coker gas oil	85.61	10.73	0.30	0.60	3.32	311	1.50	9.4	31.8						
Lloydminster heavy oil	84.77	10.80	0.30	0.81	3.04	335	1.52	9.7	31.0						
Cold Lake bitumen	84.34	10.67	0.41	0.80	3.58	668	1.51	9.5	31.5						
c) Heated for 60 min at 400°C, H ₂ - 1000 psig															
GCOS bitumen Athabasca deposit	85.64	9.90	0.45	0.85	3.13	420	1.39	11.5	38.6						
GCOS coker gas oil	84.74	10.52	0.28	0.80	3.65	350	1.49	10.9	33.6						
Lloydminster heavy oil	86.08	10.25	0.26	0.83	2.56	410	1.43	12.0	37.1						
Cold Lake bitumen	84.84	9.78	0.42	1.24	3.69	374	1.38	9.5	37.4						
d) Heated for 60 min at 400°C, H ₂ - 1000 psig + catalyst															
GCOS bitumen Athabasca deposit	84.88	10.93	0.33	0.69	3.16	551	1.54	4.7	32.8						
GCOS coker gas oil	87.81	11.26	0.15	0.11	0.67	341	1.54	5.4	27.1						
Lloydminster heavy oil	85.52	11.86	0.19	0.40	2.01	425	1.66	5.0	20.9						
Cold Lake bitumen	85.61	11.63	0.30	0.63	1.81	440	1.63	8.8	25.6						

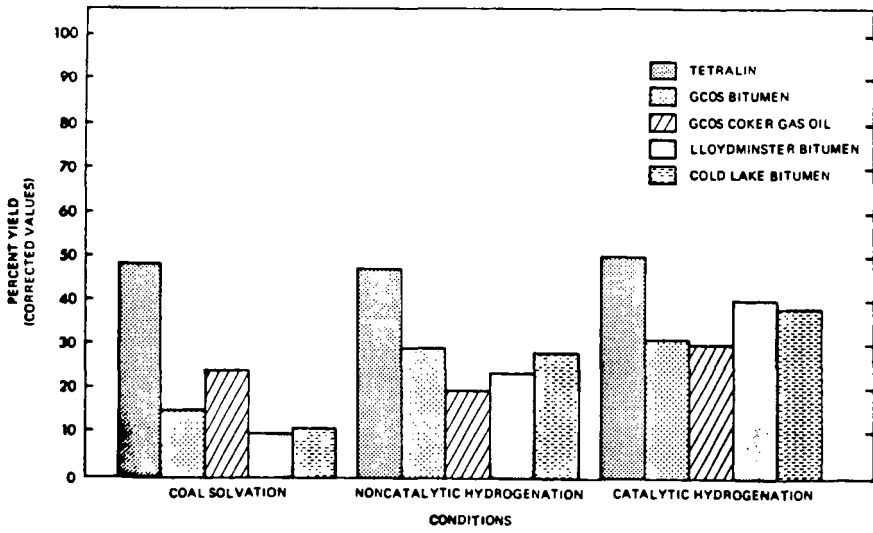


FIGURE 1.

Table 2. Composition and properties of bitumens and liquids derived from bitumen heated under various conditions

Material description	% Asphaltenes	% Resins	% Oils	API gravity
a) <u>Parent material</u>				
GCOS bitumen Athabasca deposit	15.4	22.3	62.3	7.5
GCOS coker gas oil	0.5	5.6	93.9	17.3
Lloydminster heavy oil	11.9	20.5	67.6	14.6
Cold Lake bitumen	16.1	16.9	64.9	7.5
b) <u>Heated for 60 min at 400° C</u>				
GCOS bitumen Athabasca deposit	15.0	20.1	64.9	9.6
GCOS coker gas oil	0.2	10.2	89.6	16.0
Lloydminster heavy oil	12.5	13.5	74.0	14.3
Cold Lake bitumen	14.5	12.0	73.5	11.4
c) <u>Heated for 60 min at 450° C</u>				
GCOS bitumen Athabasca deposit	7.8	11.4	80.8	3.8*
GCOS coker gas oil	11.2	17.9	70.9	3.6*
d) <u>Heated for 60 min at 400° C, H₂ - 1000 psig</u>				
GCOS bitumen Athabasca deposit	8.7	16.5	74.8	17.7
GCOS coker gas oil	0.2	10.3	89.5	21.9
Lloydminster heavy oil	6.3	27.0	66.7	16.8
Cold Lake bitumen	11.2	12.2	76.6	12.9
e) <u>Heated for 60 min at 400° C, H₂ - 1000 psig + catalyst</u>				
GCOS bitumen Athabasca deposit	8.4	12.1	79.5	12.5
GCOS coker gas oil	0	7.9	92.1	23.7
Lloydminster heavy oil	7.3	15.5	77.2	18.4
Cold Lake bitumen	7.4	13.3	79.3	17.4
f) <u>Heated for 60 min at 400° C, H₂ - 2000 psig + catalyst</u>				
GCOS bitumen Athabasca deposit	8.4	-	91.6	13.7
GCOS coker gas oil	0.3	-	97.7	16.2
g) <u>Heated for 60 min at 450° C, H₂ - 1000 psig + catalyst</u>				
GCOS bitumen Athabasca deposit	4.7	10.1	85.2	10.3
GCOS coker gas oil	0	7.0	93.0	20.6

Table 3. Product distribution of bitumen and liquids derived from bitumen heated under various conditions.

Material description	Toluene insoluble residue 1	Toluene insoluble residue 2	Relative yield, %
a) Heated for 60 min. at 150°C			
GCOS bitumen Athabasca deposit	90.2	7.2	
GCOS cohar gas oil	90.7	7.9	
Lloydminster heavy oil	92.0	7.8	
Cold Lake bitumen	89.8	8.2	
b) Heated for 60 min. at 450°C			
GCOS bitumen Athabasca deposit	28.7	45.1	
GCOS cohar gas oil	47.6	40.8	
c) Heated for 60 min. at 400°C, $P_2 = 1000$ psig			
GCOS bitumen Athabasca deposit	91.2	7.7	
GCOS cohar gas oil	97.0	3.0	
Lloydminster heavy oil	86.6	11.9	
Cold Lake bitumen	90.6	7.7	
d) Heated for 60 min. at 400°C, $P_2 = 1000$ psig - stabilizer			
GCOS bitumen Athabasca deposit	91.7	7.1	
GCOS cohar gas oil	94.0	6.0	
Lloydminster heavy oil	95.9	3.3	
Cold Lake bitumen	94.4	4.5	
e) Heated for 60 min. at 400°C, $P_2 = 2000$ psig - stabilizer			
GCOS bitumen Athabasca deposit	89.6	8.4	
GCOS cohar gas oil	96.4	3.6	
f) Heated for 60 min. at 450°C, $P_2 = 1000$ psig - stabilizer			
GCOS bitumen Athabasca deposit	34.7	59.0	
GCOS cohar gas oil	48.5	50.0	

Table 4. Gas product distribution derived from bitumen and liquids derived from bitumen heated under various conditions.

Material description	CO	CO ₂	H ₂	CH ₄	C ₂ H ₆	C ₃ H ₈	C ₄ H ₁₀	C ₅ H ₁₂	C ₆ H ₁₄	C ₇ H ₁₆	C ₈ H ₁₈	C ₉ H ₂₀	C ₁₀ H ₂₂	C ₁₁ H ₂₄	C ₁₂ H ₂₆	C ₁₃ H ₂₈	C ₁₄ H ₃₀	C ₁₅ H ₃₂	C ₁₆ H ₃₄	C ₁₇ H ₃₆	C ₁₈ H ₃₈	C ₁₉ H ₄₀	C ₂₀ H ₄₂	C ₂₁ H ₄₄	C ₂₂ H ₄₆	C ₂₃ H ₄₈	C ₂₄ H ₅₀	C ₂₅ H ₅₂	C ₂₆ H ₅₄	C ₂₇ H ₅₆	C ₂₈ H ₅₈	C ₂₉ H ₆₀	C ₃₀ H ₆₂	C ₃₁ H ₆₄	C ₃₂ H ₆₆	C ₃₃ H ₆₈	C ₃₄ H ₇₀	C ₃₅ H ₇₂	C ₃₆ H ₇₄	C ₃₇ H ₇₆	C ₃₈ H ₇₈	C ₃₉ H ₈₀	C ₄₀ H ₈₂	C ₄₁ H ₈₄	C ₄₂ H ₈₆	C ₄₃ H ₈₈	C ₄₄ H ₉₀	C ₄₅ H ₉₂	C ₄₆ H ₉₄	C ₄₇ H ₉₆	C ₄₈ H ₉₈	C ₄₉ H ₁₀₀	C ₅₀ H ₁₀₂	C ₅₁ H ₁₀₄	C ₅₂ H ₁₀₆	C ₅₃ H ₁₀₈	C ₅₄ H ₁₁₀	C ₅₅ H ₁₁₂	C ₅₆ H ₁₁₄	C ₅₇ H ₁₁₆	C ₅₈ H ₁₁₈	C ₅₉ H ₁₂₀	C ₆₀ H ₁₂₂	C ₆₁ H ₁₂₄	C ₆₂ H ₁₂₆	C ₆₃ H ₁₂₈	C ₆₄ H ₁₃₀	C ₆₅ H ₁₃₂	C ₆₆ H ₁₃₄	C ₆₇ H ₁₃₆	C ₆₈ H ₁₃₈	C ₆₉ H ₁₄₀	C ₇₀ H ₁₄₂	C ₇₁ H ₁₄₄	C ₇₂ H ₁₄₆	C ₇₃ H ₁₄₈	C ₇₄ H ₁₅₀	C ₇₅ H ₁₅₂	C ₇₆ H ₁₅₄	C ₇₇ H ₁₅₆	C ₇₈ H ₁₅₈	C ₇₉ H ₁₆₀	C ₈₀ H ₁₆₂	C ₈₁ H ₁₆₄	C ₈₂ H ₁₆₆	C ₈₃ H ₁₆₈	C ₈₄ H ₁₇₀	C ₈₅ H ₁₇₂	C ₈₆ H ₁₇₄	C ₈₇ H ₁₇₆	C ₈₈ H ₁₇₈	C ₈₉ H ₁₈₀	C ₉₀ H ₁₈₂	C ₉₁ H ₁₈₄	C ₉₂ H ₁₈₆	C ₉₃ H ₁₈₈	C ₉₄ H ₁₉₀	C ₉₅ H ₁₉₂	C ₉₆ H ₁₉₄	C ₉₇ H ₁₉₆	C ₉₈ H ₁₉₈	C ₉₉ H ₂₀₀	C ₁₀₀ H ₂₀₂	C ₁₀₁ H ₂₀₄	C ₁₀₂ H ₂₀₆	C ₁₀₃ H ₂₀₈	C ₁₀₄ H ₂₁₀	C ₁₀₅ H ₂₁₂	C ₁₀₆ H ₂₁₄	C ₁₀₇ H ₂₁₆	C ₁₀₈ H ₂₁₈	C ₁₀₉ H ₂₂₀	C ₁₁₀ H ₂₂₂	C ₁₁₁ H ₂₂₄	C ₁₁₂ H ₂₂₆	C ₁₁₃ H ₂₂₈	C ₁₁₄ H ₂₃₀	C ₁₁₅ H ₂₃₂	C ₁₁₆ H ₂₃₄	C ₁₁₇ H ₂₃₆	C ₁₁₈ H ₂₃₈	C ₁₁₉ H ₂₄₀	C ₁₂₀ H ₂₄₂	C ₁₂₁ H ₂₄₄	C ₁₂₂ H ₂₄₆	C ₁₂₃ H ₂₄₈	C ₁₂₄ H ₂₅₀	C ₁₂₅ H ₂₅₂	C ₁₂₆ H ₂₅₄	C ₁₂₇ H ₂₅₆	C ₁₂₈ H ₂₅₈	C ₁₂₉ H ₂₆₀	C ₁₃₀ H ₂₆₂	C ₁₃₁ H ₂₆₄	C ₁₃₂ H ₂₆₆	C ₁₃₃ H ₂₆₈	C ₁₃₄ H ₂₇₀	C ₁₃₅ H ₂₇₂	C ₁₃₆ H ₂₇₄	C ₁₃₇ H ₂₇₆	C ₁₃₈ H ₂₇₈	C ₁₃₉ H ₂₈₀	C ₁₄₀ H ₂₈₂	C ₁₄₁ H ₂₈₄	C ₁₄₂ H ₂₈₆	C ₁₄₃ H ₂₈₈	C ₁₄₄ H ₂₉₀	C ₁₄₅ H ₂₉₂	C ₁₄₆ H ₂₉₄	C ₁₄₇ H ₂₉₆	C ₁₄₈ H ₂₉₈	C ₁₄₉ H ₃₀₀	C ₁₅₀ H ₃₀₂	C ₁₅₁ H ₃₀₄	C ₁₅₂ H ₃₀₆	C ₁₅₃ H ₃₀₈	C ₁₅₄ H ₃₁₀	C ₁₅₅ H ₃₁₂	C ₁₅₆ H ₃₁₄	C ₁₅₇ H ₃₁₆	C ₁₅₈ H ₃₁₈	C ₁₅₉ H ₃₂₀	C ₁₆₀ H ₃₂₂	C ₁₆₁ H ₃₂₄	C ₁₆₂ H ₃₂₆	C ₁₆₃ H ₃₂₈	C ₁₆₄ H ₃₃₀	C ₁₆₅ H ₃₃₂	C ₁₆₆ H ₃₃₄	C ₁₆₇ H ₃₃₆	C ₁₆₈ H ₃₃₈	C ₁₆₉ H ₃₄₀	C ₁₇₀ H ₃₄₂	C ₁₇₁ H ₃₄₄	C ₁₇₂ H ₃₄₆	C ₁₇₃ H ₃₄₈	C ₁₇₄ H ₃₅₀	C ₁₇₅ H ₃₅₂	C ₁₇₆ H ₃₅₄	C ₁₇₇ H ₃₅₆	C ₁₇₈ H ₃₅₈	C ₁₇₉ H ₃₆₀	C ₁₈₀ H ₃₆₂	C ₁₈₁ H ₃₆₄	C ₁₈₂ H ₃₆₆	C ₁₈₃ H ₃₆₈	C ₁₈₄ H ₃₇₀	C ₁₈₅ H ₃₇₂	C ₁₈₆ H ₃₇₄	C ₁₈₇ H ₃₇₆	C ₁₈₈ H ₃₇₈	C ₁₈₉ H ₃₈₀	C ₁₉₀ H ₃₈₂	C ₁₉₁ H ₃₈₄	C ₁₉₂ H ₃₈₆	C ₁₉₃ H ₃₈₈	C ₁₉₄ H ₃₉₀	C ₁₉₅ H ₃₉₂	C ₁₉₆ H ₃₉₄	C ₁₉₇ H ₃₉₆	C ₁₉₈ H ₃₉₈	C ₁₉₉ H ₄₀₀	C ₂₀₀ H ₄₀₂	C ₂₀₁ H ₄₀₄	C ₂₀₂ H ₄₀₆	C ₂₀₃ H ₄₀₈	C ₂₀₄ H ₄₁₀	C ₂₀₅ H ₄₁₂	C ₂₀₆ H ₄₁₄	C ₂₀₇ H ₄₁₆	C ₂₀₈ H ₄₁₈	C ₂₀₉ H ₄₂₀	C ₂₁₀ H ₄₂₂	C ₂₁₁ H ₄₂₄	C ₂₁₂ H ₄₂₆	C ₂₁₃ H ₄₂₈	C ₂₁₄ H ₄₃₀	C ₂₁₅ H ₄₃₂	C ₂₁₆ H ₄₃₄	C ₂₁₇ H ₄₃₆	C ₂₁₈ H ₄₃₈	C ₂₁₉ H ₄₄₀	C ₂₂₀ H ₄₄₂	C ₂₂₁ H ₄₄₄	C ₂₂₂ H ₄₄₆	C ₂₂₃ H ₄₄₈	C ₂₂₄ H ₄₅₀	C ₂₂₅ H ₄₅₂	C ₂₂₆ H ₄₅₄	C ₂₂₇ H ₄₅₆	C ₂₂₈ H ₄₅₈	C ₂₂₉ H ₄₆₀	C ₂₃₀ H ₄₆₂	C ₂₃₁ H ₄₆₄	C ₂₃₂ H ₄₆₆	C ₂₃₃ H ₄₆₈	C ₂₃₄ H ₄₇₀	C ₂₃₅ H ₄₇₂	C ₂₃₆ H ₄₇₄	C ₂₃₇ H ₄₇₆	C ₂₃₈ H ₄₇₈	C ₂₃₉ H ₄₈₀	C ₂₄₀ H ₄₈₂	C ₂₄₁ H ₄₈₄	C ₂₄₂ H ₄₈₆	C ₂₄₃ H ₄₈₈	C ₂₄₄ H ₄₉₀	C ₂₄₅ H ₄₉₂	C ₂₄₆ H ₄₉₄	C ₂₄₇ H ₄₉₆	C ₂₄₈ H ₄₉₈	C ₂₄₉ H ₅₀₀	C ₂₅₀ H ₅₀₂	C ₂₅₁ H ₅₀₄	C ₂₅₂ H ₅₀₆	C ₂₅₃ H ₅₀₈	C ₂₅₄ H ₅₁₀	C ₂₅₅ H ₅₁₂	C ₂₅₆ H ₅₁₄	C ₂₅₇ H ₅₁₆	C ₂₅₈ H ₅₁₈	C ₂₅₉ H ₅₂₀	C ₂₆₀ H ₅₂₂	C ₂₆₁ H ₅₂₄	C ₂₆₂ H ₅₂₆	C ₂₆₃ H ₅₂₈	C ₂₆₄ H ₅₃₀	C ₂₆₅ H ₅₃₂	C ₂₆₆ H ₅₃₄	C ₂₆₇ H ₅₃₆	C ₂₆₈ H ₅₃₈	C ₂₆₉ H ₅₄₀	C ₂₇₀ H ₅₄₂	C ₂₇₁ H ₅₄₄	C ₂₇₂ H ₅₄₆	C ₂₇₃ H ₅₄₈	C ₂₇₄ H ₅₅₀	C ₂₇₅ H ₅₅₂	C ₂₇₆ H ₅₅₄	C ₂₇₇ H ₅₅₆	C ₂₇₈ H ₅₅₈	C ₂₇₉ H ₅₆₀	C ₂₈₀ H ₅₆₂	C ₂₈₁ H ₅₆₄	C ₂₈₂ H ₅₆₆	C ₂₈₃ H ₅₆₈	C ₂₈₄ H ₅₇₀	C ₂₈₅ H ₅₇₂	C ₂₈₆ H ₅₇₄	C ₂₈₇ H ₅₇₆	C ₂₈₈ H ₅₇₈	C ₂₈₉ H ₅₈₀	C ₂₉₀ H ₅₈₂	C ₂₉₁ H ₅₈₄	C ₂₉₂ H ₅₈₆	C ₂₉₃ H ₅₈₈	C ₂₉₄ H ₅₉₀	C ₂₉₅ H ₅₉₂	C ₂₉₆ H ₅₉₄	C ₂₉₇ H ₅₉₆	C ₂₉₈ H ₅₉₈	C ₂₉₉ H ₆₀₀	C ₃₀₀ H ₆₀₂	C ₃₀₁ H ₆₀₄	C ₃₀₂ H ₆₀₆	C ₃₀₃ H ₆₀₈	C ₃₀₄ H ₆₁₀	C ₃₀₅ H ₆₁₂	C ₃₀₆ H ₆₁₄	C ₃₀₇ H ₆₁₆	C ₃₀₈ H ₆₁₈	C ₃₀₉ H ₆₂₀	C ₃₁₀ H ₆₂₂	C ₃₁₁ H ₆₂₄	C ₃₁₂ H ₆₂₆	C ₃₁₃ H ₆₂₈	C ₃₁₄ H ₆₃₀	C ₃₁₅ H ₆₃₂	C ₃₁₆ H ₆₃₄	C ₃₁₇ H ₆₃₆	C ₃₁₈ H ₆₃₈	C ₃₁₉ H ₆₄₀	C ₃₂₀ H ₆₄₂	C ₃₂₁ H ₆₄₄	C ₃₂₂ H ₆₄₆	C ₃₂₃ H ₆₄₈	C ₃₂₄ H ₆₅₀	C ₃₂₅ H ₆₅₂	C ₃₂₆ H ₆₅₄	C ₃₂₇ H ₆₅₆	C ₃₂₈ H ₆₅₈	C ₃₂₉ H ₆₆₀	C ₃₃₀ H ₆₆₂	C ₃₃₁ H ₆₆₄	C ₃₃₂ H ₆₆₆	C ₃₃₃ H ₆₆₈	C ₃₃₄ H ₆₇₀	C ₃₃₅ H ₆₇₂	C ₃₃₆ H ₆₇₄	C ₃₃₇ H ₆₇₆	C ₃₃₈ H ₆₇₈	C ₃₃₉ H ₆₈₀	C ₃₄₀ H ₆₈₂	C ₃₄₁ H ₆₈₄	C ₃₄₂ H ₆₈₆	C ₃₄₃ H ₆₈₈	C ₃₄₄ H ₆₉₀	C ₃₄₅ H ₆₉₂	C ₃₄₆ H ₆₉₄	C ₃₄₇ H ₆₉₆	C ₃₄₈ H ₆₉₈	C ₃₄₉ H ₇₀₀	C ₃₅₀ H ₇₀₂	C ₃₅₁ H ₇₀₄	C ₃₅₂ H ₇₀₆	C ₃₅₃ H ₇₀₈	C ₃₅₄ H ₇₁₀	C ₃₅₅ H ₇₁₂	C ₃₅₆ H ₇₁₄	C ₃₅₇ H ₇₁₆	C ₃₅₈ H ₇₁₈	C ₃₅₉ H ₇₂₀	C ₃₆₀ H ₇₂₂	C ₃₆₁ H ₇₂₄	C ₃₆₂ H ₇₂₆	C ₃₆₃ H ₇₂₈	C ₃₆₄ H ₇₃₀	C ₃₆₅ H ₇₃₂	C ₃₆₆ H ₇₃₄	C ₃₆₇ H ₇₃₆	C ₃₆₈ H ₇₃₈	C ₃₆₉ H ₇₄₀	C ₃₇₀ H ₇₄₂	C ₃₇₁ H ₇₄₄	C ₃₇₂ H ₇₄₆	C ₃₇₃ H ₇₄₈	C ₃₇₄ H ₇₅₀	C ₃₇₅ H ₇₅₂	C ₃₇₆ H ₇₅₄	C ₃₇₇ H ₇₅₆	C ₃₇₈ H ₇₅₈	C ₃₇₉ H ₇₆₀	C ₃₈₀ H ₇₆₂	C ₃₈₁ H ₇₆₄	C ₃₈₂ H ₇₆₆	C ₃₈₃ H ₇₆₈	C ₃₈₄ H ₇₇₀	C ₃₈₅ H ₇₇₂	C ₃₈₆ H ₇₇₄	C ₃₈₇ H ₇₇₆	C ₃₈₈ H ₇₇₈	C ₃₈₉ H ₇₈₀	C ₃₉₀ H ₇₈₂	C ₃₉₁ H ₇₈₄	C ₃₉₂ H ₇₈₆	C ₃₉₃ H ₇₈₈	C ₃₉₄ H ₇₉₀	C ₃₉₅ H ₇₉₂	C ₃₉₆ H ₇₉₄	C ₃₉₇ H ₇₉₆	C ₃₉₈ H ₇₉₈	C ₃₉₉ H ₈₀₀	C ₄₀₀ H ₈₀₂	C ₄₀₁ H ₈₀₄	C ₄₀₂ H ₈₀₆	C ₄₀₃ H ₈₀₈	C ₄₀₄ H ₈₁₀	C ₄₀₅ H ₈₁₂	C ₄₀₆ H ₈₁₄	C ₄₀₇ H ₈₁₆	C ₄₀₈ H ₈₁₈	C ₄₀₉ H ₈₂₀	C ₄₁₀ H ₈₂₂	C ₄₁₁ H ₈₂₄	C ₄₁₂ H ₈₂₆	C ₄₁₃ H ₈₂₈	C ₄₁₄ H ₈₃₀	C ₄₁₅ H ₈₃₂	C ₄₁₆ H ₈₃₄	C ₄₁₇ H ₈₃₆	C ₄₁₈ H ₈₃₈	C ₄₁₉ H ₈₄₀	C ₄₂₀ H ₈₄₂	C ₄₂₁ H ₈₄₄	C ₄₂₂ H ₈₄₆	C ₄₂₃ H ₈₄₈	C ₄₂₄ H ₈₅₀	C ₄₂₅ H ₈₅₂	C ₄₂₆ H ₈₅₄	C ₄₂₇ H ₈₅₆	C ₄₂₈ H ₈₅₈	C ₄₂₉ H ₈₆₀	C ₄₃₀ H ₈₆₂	C ₄₃₁ H ₈₆₄	C ₄₃₂ H ₈₆₆	C ₄₃₃ H ₈₆₈	C ₄₃₄ H ₈₇₀	C ₄₃₅ H ₈₇₂	C ₄₃₆ H ₈₇₄	C ₄₃₇ H ₈₇₆	C ₄₃₈ H ₈₇₈	C ₄₃₉ H ₈₈₀	C ₄₄₀ H ₈₈₂	C ₄₄₁ H ₈₈₄	C ₄₄₂ H ₈₈₆	C ₄₄₃ H ₈₈₈	C ₄₄₄ H ₈₉₀	C ₄₄₅ H ₈₉₂	C ₄₄₆ H ₈₉₄	C ₄₄₇ H ₈₉₆	C ₄₄₈ H ₈₉₈	C ₄₄₉ H ₉₀₀	C ₄₅₀ H ₉₀₂	C ₄₅₁ H ₉₀₄	C ₄₅₂ H ₉₀₆	C ₄₅₃ H ₉₀₈	C ₄₅₄ H ₉₁₀	C ₄₅₅ H ₉₁₂	C ₄₅₆ H ₉₁₄	C ₄₅₇ H ₉₁₆	C ₄₅₈ H ₉₁₈	C ₄₅₉ H ₉₂₀	C ₄₆₀ H ₉₂₂	C ₄₆₁ H ₉₂₄	C ₄₆₂ H ₉₂₆	C ₄₆₃ H ₉₂₈	C ₄₆₄ H ₉₃₀	C ₄₆₅ H ₉₃₂	C ₄₆₆ H ₉₃₄	C ₄₆₇ H ₉₃₆	C ₄₆₈ H ₉₃₈	C ₄₆₉ H ₉₄₀	C ₄₇₀ H ₉₄₂	C ₄₇₁ H ₉₄₄	C ₄₇₂ H ₉₄₆	C ₄₇₃ H ₉₄₈	C ₄₇₄ H ₉₅₀	C ₄₇₅ H ₉₅₂	C ₄₇₆ H ₉₅₄	C ₄₇₇ H ₉₅₆	C ₄₇₈ H ₉₅₈	C ₄₇₉ H ₉₆₀	C ₄₈₀ H ₉₆₂	C ₄₈₁ H ₉₆₄	C ₄₈₂ H ₉₆₆	C ₄₈₃ H ₉₆₈	C ₄₈₄ H ₉₇₀
----------------------	----	-----------------	----------------	-----------------	-------------------------------	-------------------------------	--------------------------------	--------------------------------	--------------------------------	--------------------------------	--------------------------------	--------------------------------	---------------------------------	---------------------------------	---------------------------------	---------------------------------	---------------------------------	---------------------------------	---------------------------------	---------------------------------	---------------------------------	---------------------------------	---------------------------------	---------------------------------	---------------------------------	---------------------------------	---------------------------------	---------------------------------	---------------------------------	---------------------------------	---------------------------------	---------------------------------	---------------------------------	---------------------------------	---------------------------------	---------------------------------	---------------------------------	---------------------------------	---------------------------------	---------------------------------	---------------------------------	---------------------------------	---------------------------------	---------------------------------	---------------------------------	---------------------------------	---------------------------------	---------------------------------	---------------------------------	---------------------------------	---------------------------------	----------------------------------	----------------------------------	----------------------------------	----------------------------------	----------------------------------	----------------------------------	----------------------------------	----------------------------------	----------------------------------	----------------------------------	----------------------------------	----------------------------------	----------------------------------	----------------------------------	----------------------------------	----------------------------------	----------------------------------	----------------------------------	----------------------------------	----------------------------------	----------------------------------	----------------------------------	----------------------------------	----------------------------------	----------------------------------	----------------------------------	----------------------------------	----------------------------------	----------------------------------	----------------------------------	----------------------------------	----------------------------------	----------------------------------	----------------------------------	----------------------------------	----------------------------------	----------------------------------	----------------------------------	----------------------------------	----------------------------------	----------------------------------	----------------------------------	----------------------------------	----------------------------------	----------------------------------	----------------------------------	----------------------------------	----------------------------------	----------------------------------	----------------------------------	----------------------------------	-----------------------------------	-----------------------------------	-----------------------------------	-----------------------------------	-----------------------------------	-----------------------------------	-----------------------------------	-----------------------------------	-----------------------------------	-----------------------------------	-----------------------------------	-----------------------------------	-----------------------------------	-----------------------------------	-----------------------------------	-----------------------------------	-----------------------------------	-----------------------------------	-----------------------------------	-----------------------------------	-----------------------------------	-----------------------------------	-----------------------------------	-----------------------------------	-----------------------------------	-----------------------------------	-----------------------------------	-----------------------------------	-----------------------------------	-----------------------------------	-----------------------------------	-----------------------------------	-----------------------------------	-----------------------------------	-----------------------------------	-----------------------------------	-----------------------------------	-----------------------------------	-----------------------------------	-----------------------------------	-----------------------------------	-----------------------------------	-----------------------------------	-----------------------------------	-----------------------------------	-----------------------------------	-----------------------------------	-----------------------------------	-----------------------------------	-----------------------------------	-----------------------------------	-----------------------------------	-----------------------------------	-----------------------------------	-----------------------------------	-----------------------------------	-----------------------------------	-----------------------------------	-----------------------------------	-----------------------------------	-----------------------------------	-----------------------------------	-----------------------------------	-----------------------------------	-----------------------------------	-----------------------------------	-----------------------------------	-----------------------------------	-----------------------------------	-----------------------------------	-----------------------------------	-----------------------------------	-----------------------------------	-----------------------------------	-----------------------------------	-----------------------------------	-----------------------------------	-----------------------------------	-----------------------------------	-----------------------------------	-----------------------------------	-----------------------------------	-----------------------------------	-----------------------------------	-----------------------------------	-----------------------------------	-----------------------------------	-----------------------------------	-----------------------------------	-----------------------------------	-----------------------------------	-----------------------------------	-----------------------------------	-----------------------------------	-----------------------------------	-----------------------------------	-----------------------------------	-----------------------------------	-----------------------------------	-----------------------------------	-----------------------------------	-----------------------------------	-----------------------------------	-----------------------------------	-----------------------------------	-----------------------------------	-----------------------------------	-----------------------------------	-----------------------------------	-----------------------------------	-----------------------------------	-----------------------------------	-----------------------------------	-----------------------------------	-----------------------------------	-----------------------------------	-----------------------------------	-----------------------------------	-----------------------------------	-----------------------------------	-----------------------------------	-----------------------------------	-----------------------------------	-----------------------------------	-----------------------------------	-----------------------------------	-----------------------------------	-----------------------------------	-----------------------------------	-----------------------------------	-----------------------------------	-----------------------------------	-----------------------------------	-----------------------------------	-----------------------------------	-----------------------------------	-----------------------------------	-----------------------------------	-----------------------------------	-----------------------------------	-----------------------------------	-----------------------------------	-----------------------------------	-----------------------------------	-----------------------------------	-----------------------------------	-----------------------------------	-----------------------------------	-----------------------------------	-----------------------------------	-----------------------------------	-----------------------------------	-----------------------------------	-----------------------------------	-----------------------------------	-----------------------------------	-----------------------------------	-----------------------------------	-----------------------------------	-----------------------------------	-----------------------------------	-----------------------------------	-----------------------------------	-----------------------------------	-----------------------------------	-----------------------------------	-----------------------------------	-----------------------------------	-----------------------------------	-----------------------------------	-----------------------------------	-----------------------------------	-----------------------------------	-----------------------------------	-----------------------------------	-----------------------------------	-----------------------------------	-----------------------------------	-----------------------------------	-----------------------------------	-----------------------------------	-----------------------------------	-----------------------------------	-----------------------------------	-----------------------------------	-----------------------------------	-----------------------------------	-----------------------------------	-----------------------------------	-----------------------------------	-----------------------------------	-----------------------------------	-----------------------------------	-----------------------------------	-----------------------------------	-----------------------------------	-----------------------------------	-----------------------------------	-----------------------------------	-----------------------------------	-----------------------------------	-----------------------------------	-----------------------------------	-----------------------------------	-----------------------------------	-----------------------------------	-----------------------------------	-----------------------------------	-----------------------------------	-----------------------------------	-----------------------------------	-----------------------------------	-----------------------------------	-----------------------------------	-----------------------------------	-----------------------------------	-----------------------------------	-----------------------------------	-----------------------------------	-----------------------------------	-----------------------------------	-----------------------------------	-----------------------------------	-----------------------------------	-----------------------------------	-----------------------------------	-----------------------------------	-----------------------------------	-----------------------------------	-----------------------------------	-----------------------------------	-----------------------------------	-----------------------------------	-----------------------------------	-----------------------------------	-----------------------------------	-----------------------------------	-----------------------------------	-----------------------------------	-----------------------------------	-----------------------------------	-----------------------------------	-----------------------------------	-----------------------------------	-----------------------------------	-----------------------------------	-----------------------------------	-----------------------------------	-----------------------------------	-----------------------------------	-----------------------------------	-----------------------------------	-----------------------------------	-----------------------------------	-----------------------------------	-----------------------------------	-----------------------------------	-----------------------------------	-----------------------------------	-----------------------------------	-----------------------------------	-----------------------------------	-----------------------------------	-----------------------------------	-----------------------------------	-----------------------------------	-----------------------------------	-----------------------------------	-----------------------------------	-----------------------------------	-----------------------------------	-----------------------------------	-----------------------------------	-----------------------------------	-----------------------------------	-----------------------------------	-----------------------------------	-----------------------------------	-----------------------------------	-----------------------------------	-----------------------------------	-----------------------------------	-----------------------------------	-----------------------------------	-----------------------------------	-----------------------------------	-----------------------------------	-----------------------------------	-----------------------------------	-----------------------------------	-----------------------------------	-----------------------------------	-----------------------------------	-----------------------------------	-----------------------------------	-----------------------------------	-----------------------------------	-----------------------------------	-----------------------------------	-----------------------------------	-----------------------------------	-----------------------------------	-----------------------------------	-----------------------------------	-----------------------------------	-----------------------------------	-----------------------------------	-----------------------------------	-----------------------------------	-----------------------------------	-----------------------------------	-----------------------------------	-----------------------------------	-----------------------------------	-----------------------------------	-----------------------------------	-----------------------------------	-----------------------------------	-----------------------------------	-----------------------------------	-----------------------------------	-----------------------------------	-----------------------------------	-----------------------------------	-----------------------------------	-----------------------------------	-----------------------------------	-----------------------------------	-----------------------------------	-----------------------------------	-----------------------------------	-----------------------------------	-----------------------------------	-----------------------------------	-----------------------------------	-----------------------------------	-----------------------------------	-----------------------------------	-----------------------------------	-----------------------------------	-----------------------------------	-----------------------------------	-----------------------------------	-----------------------------------	-----------------------------------	-----------------------------------	-----------------------------------	-----------------------------------	-----------------------------------	-----------------------------------	-----------------------------------	-----------------------------------	-----------------------------------	-----------------------------------	-----------------------------------	-----------------------------------	-----------------------------------	-----------------------------------	-----------------------------------	-----------------------------------	-----------------------------------	-----------------------------------	-----------------------------------	-----------------------------------	-----------------------------------	-----------------------------------	-----------------------------------	-----------------------------------	-----------------------------------	-----------------------------------	-----------------------------------	-----------------------------------	-----------------------------------	-----------------------------------	-----------------------------------	-----------------------------------	-----------------------------------	-----------------------------------	-----------------------------------	-----------------------------------	-----------------------------------	-----------------------------------	-----------------------------------	-----------------------------------	-----------------------------------

Table 5. Temperature effect on coal conversion yields and product distribution (60 minutes, H₂ - 1000 psig)

Conditions	% Yield ⁺	% Toluene insolubles	% Toluene solubles	% Volatile plus gas	Toluene solubles fraction		
					% Pentane insolubles	% Pentane solubles	API gravity
<u>Coal solvation</u>							
GCOS bitumen							
Athabasca deposit							
300° C	2	28.8	69.8	1.4	16.1	83.9	7.9
350° C	5	28.0	69.4	2.6	19.5	80.5	12.8
400°C	15	26.1	65.4	8.5	19.0	81.0	10.7
450°C	27	40.1	20.9	39.0	15.3	84.7	4.4
GCOS coker gas oil							
300°C	0	27.1	71.9	1	0.4	99.6	17.4
350°C	7	29.1	68.9	2	2.0	98.0	15.1
400°C	24	23.6	68.2	8.2	3.1	96.9	18.9
450°C	0	39.2	27.7	33.1	3.0	97.0	8.1
<u>Catalytic hydrogenation</u>							
GCOS bitumen							
Athabasca deposit							
350°C	8	26.2	70.7	3.1	17.0	83.0	13.7
400°C	32	20.8	69.1	10.1	12.5	87.5	12.4
450°C	34	22.6	25.4	52.0	11.8	88.2	1.8
GCOS coker gas oil							
300°C	0	29.6	69.4	1	0.3	99.7	17.4
350°C	7	26.7	71.3	2	1.6	98.4	17.0
400°C	30	20.6	73.9	5.5	1.8	98.2	17.3
450°C	45	16.3	42.3	41.4	4.5	95.5	8.5

⁺ Calculate yield after subtraction of coke formed from the solvent in blank determinations.

Table 6. Time effect on coal conversion yields and product distribution (400° C, H₂ - 1000 psig)

Reaction time	% Yield ⁺	% Toluene insolubles	% Toluene solubles	% Volatile plus gas	Toluene solubles fraction		
					% Pentane insolubles	% Pentane solubles	API gravity
<u>Coal solvation</u>							
GCOS bitumen							
Athabasca deposit							
1/4 hour	10	26.3	68.4	5.3	21.7	78.3	9.2
1 hour	15	26.1	65.4	8.5	19.0	80.9	10.7
2 hours	0	31.6	51.3	17.1	16.1	83.9	9.9
GCOS coker gas oil							
1/4 hour	10	26.8	70.1	3.1	4.2	95.8	15.8
1 hour	24	23.6	68.2	8.2	3.1	96.9	18.9
2 hours	12	25.6	55.7	18.7	6.4	93.6	12.7
<u>Catalytic hydrogenation</u>							
GCOS bitumen							
Athabasca deposit							
1/4	17	24.2	69.2	6.6	17.8	82.2	10.1
1 hour	32	20.8	69.1	10.1	12.5	87.5	12.4
2 hours	31	20.1	66.5	13.4	11.5	88.5	13.1
GCOS coker gas oil							
1/4 hour	17	24.2	72.8	3.0	3.5	96.5	17.9
1 hour	30	20.6	73.9	5.5	1.8	98.2	17.3
2 hours	41	17.4	75.5	7.1	3.8	96.2	18.5

⁺ Calculated yield after subtraction of coke formed from the solvent in blank determinations.

Table 7. Pressure effect on coal conversion yields and product distribution (60 minutes, 400 °C)

	% Yield ^a	% Toluene Insolubles	% Toluene Solubles	% Volatile plus gas	Toluene solubles fraction		
					% Pentane Insolubles	% Pentane Solubles	API gravity
<u>Catalytic hydrogenation</u>							
GCOS bitumen Athabasca deposit							
500	16	24.5	63.3	12.2	17.8	82.2	9.6
1,000	32	20.8	69.1	10.1	12.5	77.5	12.4
1,500	30	21.7	68.3	10.0	15.0	85.0	11.4
2,000	30	21.8	75.0	3.2	14.7	85.3	12.1

Table 8. Gas product distribution derived from processing coal for 60 min. at various temperatures

Temperature	% Relative Composition									
	CO	CO ₂	H ₂ S	CH ₄	C ₂ H ₆	C ₂ H ₄	C ₂ H ₂	C ₃	C ₄ iso	C ₆ nCfr
<u>Coal solution</u>										
GCOS bitumen Athabasca Deposit										
300°C	-	97.8	-	-	-	1.7	-	0.5	-	-
350°C	2.1	74.5	3.6	10.5	-	5.9	-	2.7	-	0.6
400°C	0.6	31.9	7.5	31.6	-	15.4	-	9.8	1.1	2.0
450°C	insufficient sample									
GCOS coker gas oil										
300°C	-	94.0	1.5	-	-	3.8	-	0.6	-	-
350°C	1.6	64.8	2.3	12.7	-	14.6	-	2.9	0.2	0.9
400°C	N.D.									
450°C	N.D.									
<u>Catalytic hydrogenation</u>										
GCOS bitumen Athabasca deposit										
350°C	1.4	55.1	10.3	12.0	-	17.0	-	3.5	-	0.9
400°C	0.7	22.8	24.4	26.0	1.3	13.8	-	8.0	0.9	1.9
450°C	0.3	7.4	7.9	51.9	0.1	19.9	-	9.7	0.9	1.9
GCOS coker gas oil										
300°C	-	95.4	3.7	-	-	-	-	0.9	-	-
350°C	1.7	62.0	17.1	10.9	1.7	2.6	-	3.2	-	0.9
400°C	N.D.									
450°C	0.1	6.1	4.0	56.9	-	20.8	-	9.4	0.9	1.7
N.D.	Not Determined									

Table 9. Gas product distribution derived from processing coal at 400 C° for various times

Reaction Time	% Relative Composition									
	CO	CO ₂	H ₂ S	CH ₄	C ₂ H ₄	C ₂ H ₆	C ₂ H ₂	C ₃	C ₄ iso	C ₄ npar
Coal solvation										
GCOS bitumen Athabasca deposit										
1/4 hour	1.0	44.7	9.9	24.0	-	9.6	-	7.9	0.7	2.1
1 hour	0.6	31.9	7.5	31.6	-	15.4	-	9.8	1.1	2.0
2 hours	2.8	37.7	13.7	24.2	-	10.5	-	8.0	1.0	2.1
GCOS coker gas oil										
1/4 hour	2.9	56.5	3.1	19.8	-	10.1	-	6.2	0.4	1.1
1 hour	N.D.									
2 hours	2.8	23.8	3.4	39.2	0.1	15.7	-	11.0	1.4	1.1
Catalytic hydrogenation										
GCOS bitumen Athabasca deposit										
1/4 hour	0.2	17.0	19.5	27.6	0.4	13.6	-	16.6	2.4	2.9
1 hour	0.7	22.8	24.4	26.0	1.3	13.8	-	8.0	0.9	1.9
2 hours	1.5	23.7	18.4	32.2	-	12.0	-	8.5	1.3	2.3
GCOS coker res oil										
1/4 hour	4.4	44.4	15.6	22.0	-	7.2	-	5.0	0.3	1.0
1 hour	N.D.									
2 hours	2.6	23.5	17.7	34.9	-	12.0	-	7.1	0.7	1.5

Table 10. Gas product distribution derived from processing coal for 60 min. at 400°C under various pressures

Pressure psig	% Relative composition									
	CO	CO ₂	H ₂ S	CH ₄	C ₂ H ₄	C ₂ H ₆	C ₂ H ₂	C ₃	C ₄ iso	C ₄ npar
Catalytic hydrogenation										
GCOS bitumen Athabasca deposit										
500	0.9	33.7	17.6	26.1	-	10.2	-	8.1	1.1	1.3
1,000	0.7	22.8	24.4	26.0	1.3	13.8	-	8.0	0.9	1.9
1,500	3.5	26.2	22.4	26.9	-	10.2	-	7.7	1.0	2.1
2,000	1.2	23.9	21.6	31.5	-	11.1	-	7.6	0.9	0.3

TECHNICAL RISK AS A COST FACTOR IN
COAL LIQUEFACTION: SOME FINANCIAL CONSIDERATIONS

David A. Tillman

Senior Fuel Scientist
Envirosphere Co.
Bellevue, Washington

INTRODUCTION

The U. S. economy is fueled largely by liquid fuels obtained, in no small measure, from unstable sources. The litany of wars, embargoes, and sudden price hikes implies that developing alternative indigenous supplies of liquid fuel is a national economic security issue. Liquid fuels derived from coal are among the alternatives available.

Coal liquids must replace petroleum products in existing applications when they enter the marketplace. That point of entry is almost unique [1-3]. Coal liquids must replace oil directly, for domestic oil supplies are declining. This is also unique in the energy supply history of this country [4-5]. Thus the entry of coal liquids into the economy is fraught with uncertainties caused by unusual conditions.

Uncertainties in the marketplace exist; however a technical base for the development of a coal liquids industry has been developed. Generically four approaches have been pursued: pyrolysis, solvent extraction, catalytic hydrogenation, and indirect liquefaction. Of these, indirect liquefaction is being practiced commercially in countries outside the United States [6].

The existence of a technical base does not imply that coal liquefaction is a mature technology. Rather, it shows that there is a significant gap between what is technologically available and what is economically available. This gap can be attributed to the efficiencies, the capital costs, and the financial risks of such systems. Those financial risks are substantially influenced by the magnitude of the investments and the status of the technology.

This financial gap has not always been recognized in the literature. In order to show the influence of this risk-related issue on coal liquefaction costs and market potentials, the following

considerations are addressed here: (1) a review of previous cost estimating practices, (2) an evaluation of U.S. investment practice related to innovative processes, and (3) the influence of those factors on the costs of coal liquids.

In 1976 a major coal liquids economics symposium was held by the American Chemical Society. In this symposium a common set of economic assumptions were employed. The 1976 ACS symposium, and the values in Table 1 used in that meeting, represents a major step in unifying coal liquefaction economics. However these assumptions do not lead to a solid financial analysis of coal liquefaction plants, and for the following reasons: (1) they intertwine the "what to finance" with "how to finance" decisions; (2) they mask the fact that cash flow, not profit, supports a corporation; and (3) they do not incorporate the influence of technical risk into the discount rate.

The first defect argues that corporations will view new technologies with the same investment ground rules as existing technologies. Corporations are risk averse, however, and prefer to invest in improved existing systems rather than higher risk new systems [8]. Higher rates of discount are required to attract capital into new projects. The second and third deficiencies are violations of the principles of financial analysis [10]. The use of any or all of these three assumptions leads to overly optimistic product cost values.

Given these problems, it is useful to reexamine the discount rate used in calculating coal liquid costs, adjust the accounting procedures to separate "what to finance" from "how to finance," and analyze costs in a way to maximize cash flow. With these adjustments, order of magnitude price estimates may be made and, more importantly, the influences of risk and experience on product costs can be made.

THE DISCOUNT RATE AND COAL LIQUID COSTS

The nominal discount rate is composed of three elements as shown in formula (1):

$$DR = I + M + R \quad (1)$$

Where I = the inflation rate, M = the riskless cost of money (sometimes referred to as the premium for early availability of funds), and R = the premium for total investment risk [10]. Risk can be broken down further into several components as shown in formula (2):

$$R = f(R_e, R_b, R_f, R_t) \quad (2)$$

Where R_e = economic risk (e.g., the risk of a recession), R_b = business

risk, R_f = financial risk (e.g., degree of leverage) and R_t = technological risk. For most firms, the R_e term is uncontrollable and is not isolated. R_t is usually subsumed in business risk if no major innovation is contemplated, where the major innovation will influence the capital structure.

Calculating the Discount Rate

Each major industry has its own appropriate nominal discount rate reflecting the financial investments of debt and equity participants in that industry. While several models exist for calculating the discount rate, the Modigliani-Miller (M-M) theorem is sufficient for these purposes. The model is shown in equation (3) from Haley and Schall [11].

$$DR = \theta K_d + (1 - \theta) K_e \quad (3)$$

Where θ = the proportion of debt, K_d = the cost of debt (including tax effects) and K_e = the cost of equity capital. K_d is taken as the yield-to-maturity on bonds multiplied by $1-TR$ where TR = the Tax Rate, fractional basis. K_e can be calculated by several techniques varying in sophistication. Again, due to the imprecise nature of discount rate estimation in the face of technological risk, the simplistic approach is taken here and shown in formula (4).

$$K_e = D/P + G \quad (4)$$

Where D = expected dividends, P = stock price, and G = the expected growth rate of the (stock) investment over its useful life.

The M-M model applies to traditional investments and is based upon the principle that, while increasing the debt fraction decreases the apparent discount rate, it increases the degree of leverage, the financial risk and hence the cost of equity capital. Based upon the above equations, Tables 2 and 3 are presented, giving the estimated discount rates for Gulf, Exxon, and Mobil Oil. Growth estimates are based on 10-year earnings/share ratios. For subsequent analysis, the nominal rate of 15% is used since it shows the approximate 1:3 debt/equity ratio common to the energy industry [12] and is the median case calculated.

Table 2 presents the capital structure for Exxon, Gulf, and Mobil--the three companies chosen to develop the discount rate for this industry. Significant is the absence of preferred stock in these companies. Also significant to note is that there is heavy reliance on common stock. Thus the growth issue arises; and it is

complicated by varying expectations concerning the decontrol of petroleum prices.

The Influence of Risk on the Discount Rate

The financial literature is replete with citations concerning the influence of business and financial risk on the discount rate. The typical relationship shown is essentially linear and is referred to as the "Security Market Line" shown in Fig. 1.

Technical risk and/or uncertainty is less well-treated in the literature than business/financial risk. Technical risk, however, is critical to new energy investment evaluation [13]. Its influence can be evaluated by analogy to traditional business/financial risk assessments.

Empirical studies have addressed the risk issue, including reports by technical Micro Economic Associates [14] and Robert R. Nathan Associates [15]. The former deals largely with the influence of risks on supplies and prices; and the latter shows rates of return obtained on innovations in U.S. industry since 1940. Pre-tax private internal rates of return (IRR) ranged from negative to 157% over a broad spectrum innovations on a real dollar basis.

Two petroleum industry innovations, one in extraction and one in processing, showed pre-tax IRR values of 50 to 56% in the Nathan Associates study. This is slightly higher than the median value of 34 to 38%. Given standard economic assumptions, after tax rates of return can be calculated at ~20% on average and ~30% in the petroleum industry. It should be noted that the petroleum related investments were made in 1942 and 1949. However, a mining related innovation introduced in 1964 had a pre-tax IRR of 54%. These IRR values are not discount rates per se, but they give some clue to investor expectations. Thus, resource industry innovations may generally require the higher discount rates.

The risk-adjusted discount rate also is a function of some learning curve concerning the new technology. Those extractive industry innovations which first earned ~30% after taxes now require ~15%. The initial parts of the investment learning curve, both technically and financially, relate to the process of going from concept development and bench scale research to commercial technologies through process development units and then pilot plants. Swabb [16] identifies the preferred succeeding step from pilot plant to commercial technology as a pioneer plant, to be owned and operated by the private industry as a commercial facility followed by the design and construction of succeeding commercial plants. The pioneer plant

is critical in this approach as it demonstrates plant reliability, product output, environmental protection safeguards, and commercial viability. It reduces business risk to manageable levels.

If one accepts the Schwabb argument, then the discount rate for the pioneer plant may be nominally ~30%. The lower limit is, of course, nominally 15%. The upper limit, however, remains essentially undefined. Further, the number of commercial plants required to go from 30% to 15%, is also undefined.

Similar learning curves have been posited for capital cost estimates [17, 18]. Such curves take the form of sensitivity analysis parameters. The analogy between capital cost and discount rate estimation is imperfect, both sets of data deal with investment uncertainties as perceived by boards of directors. Despite these uncertainties, a 30% discount rate is used here for pioneer plants, and a 15% discount rate is used for mature plants.

The empirical technical risk adjustment made here is analogous to an unusual business risk taken. Before the passage of the Public Utility Regulatory and Policies Act (PURPA), industries entering cogeneration ventures perceived the following risks: (1) would they be regulated as utilities; (2) would utilities purchase surplus power from them; and (3) would utilities sell them power as needed at a reasonable cost. Frequently after-tax rates of return demanded by cogenerators were 30% [19]. Again it is an imperfect analogy. The investment community is consistent--manufacturing industry. The broad investment arena is energy. The cogeneration technology, however, is mature. Thus this risk adjustment is only one more indicator of investor behavior.

CALCULATED COSTS OF COAL LIQUIDS UNDER UNUSUAL AND NORMAL RISK CONDITIONS

Remaining are the tasks of estimating the initial costs of coal liquids and the price reductions possible as investor corporations gain commercial experience in coal liquefaction. Accomplishing these evaluations requires making some accounting assumptions. It then involves calculating fuel costs based on the systems selected.

Accounting Conventions and Assumptions

In the projecting of synthetic fuel costs, certain conventions play an important role: (1) the selection of a depreciation method; and (2) the selection of a dollar basis.

Three depreciation methods exist: straight line, sum-of-the-years digits, and double declining balance. In general, the latter two accelerated systems generate more favorable cash flows (depending upon the capital structure of the industry). The double declining balance method generates particularly high depreciation values in the first few years. Thus, it is used here.

Depreciation may be taken over a variety of time periods. To maximize cash flow, and the contribution of depreciation to net present value, the shortest possible depreciation period is preferred. The Internal Revenue Service [20] gives a minimum of 13 years for petroleum refineries; and this value is assumed to hold for coal liquefaction plants.

Depreciation is the major area of capital recovery meriting documentation. Historical statistics can be used to develop assumptions for cost increases over time. These are shown in Table 4. These values are used in constructing proforma statements.

System and Product Costs

Two systems have been selected for analysis here: (1) methanol synthesis and (2) solvent extraction. Methanol is advanced frequently as a technology of immediate application [21, 22]. Solvent extraction is considered one of the leading candidates for boiler fuels production [23]. Both systems are described generically in Sliepcevich et al. [24]. Table 5 presents the significant capital cost and product output parameters for each unit. The cost values have been updated to 1980 dollars from the original publication by use of the chemical engineering plant cost index as reported in the Engineering News Record [25].

Both the methanol and solvent extraction plants were estimated to cost $\$1 \times 10^9$ in 1977, and are now estimated to cost $\$1.3 \times 10^9$. After removal of the 20% investment tax credit, these capital costs are $\$1.04 \times 10^9$. If one assumes a 13-year amortization period, the risky investment with a discount rate of 30% must generate an annual after-tax cash flow of $\$322 \times 10^6$. If the technology were considered by investors to be mature, that after-tax cash flow requirement would be $\$178 \times 10^6$. The differential is particularly significant since investment tax credits and depreciation are calculated without regard to technological maturity. Thus the $\$144 \times 10^6$ must be made up entirely with after-tax profits.

From these data, modified proforma statements have been constructed for both technologies assuming: (1) instantaneous construction and startup and (2) constant after-tax cash flows. These

are optimistic assumptions but they do not affect the analysis of financial risk reduction seriously, since they are constant relative to the variable discount rate. Table 6 is the proforma statement for selected years of the risky solvent extraction plant. Table 7 is the proforma statement for the same years assuming a mature technology. Values are in nominal (inflated) dollars.

It is significant to note that the high risk plant must be profitable from the start. The mature plant can sustain losses during the first year without jeopardizing the cash flow stream. Depreciation is for more significant to the mature plant than the high risk pioneer plant. Similar proforma statements can be constructed for methanol plants. Revenue streams can then be deflated to 1980 dollars by the following formula:

$$D_t = 1.064^t \quad (8)$$

Where D = deflator and t = the year of operation. From these values Table 8 is constructed showing the approximate cost of fuels from pioneer plants and mature plants. In both cases the gaining of financial experience carries a cost savings of about \$10/bbl of oil equivalent.

What is significant here is not the \$40/bbl or \$60/bbl value. These are best guesses based upon available information from pilot plants. Nobody knows what coal liquids will actually cost. Rather, it is the cost reduction associated with investor experience which is significant. Cost savings of \$1-2/10⁶ Btu are substantial. These result from a reduction in the discount rate as risks and uncertainties are reduced.

CONCLUSION

Substantial fuel cost savings, then, are available from corporation investment experience in coal liquefaction facilities. These savings are in the vicinity of \$10/bbl or \$1-2/10⁶ Btu. These savings also should be pursued. These substantial price reductions may be achieved when investors advance along their own learning curve. That learning curve equates the relationship of expected product price and plant performance to achieved product price and plant performance; and translates that relationship plus market acceptance of the product into a risk factor and an appropriate discount rate. Large savings in fuel costs can be achieved only when investors have advanced sufficiently to reduce their perceptions of liquefaction risk and uncertainty.

REFERENCES

1. Hottel, H. C. and J. B. Howard. 1971. New Energy Technology: Some Facts and Assessments. MIT Press, Cambridge, Mass.
2. Frey, J. W. and H. C. Ide. 1946. A History of the Petroleum Administration for War: 1941-1945. U.S. Government Printing Office, Washington, D.C.
3. National Materials Advisory Board. 1975. Problems and Legislative Opportunities in the Basic Materials Industry. National Academy of Sciences, Washington, D.C.
4. Tillman, D. A. 1978. Wood as an Energy Resource. Academic Press, New York.
5. Enger, H., W. Dupree, and S. Miller. 1975. Energy Perspectives: A presentation of major energy and energy-related data. U.S. Department of the Interior, Washington, D.C.
6. Smith, I. H. and G. J. Werner. 1976. Coal Conversion Technology. Noyes Data Corp., Park Ridge, N.J.
7. Pelofsky, A. H. 1977. Preface, in Synthetic Fuels Processing: Comparative Economics (Pelofsky, A. H. ed.), Marcel Dekker, New York, iii-v.
8. Perry, H. 1979. Synthetic Fuels Commercialization Testimony before the House Committee on Science and Technology, Sept. 12.
9. Bierman, H., and S. Smidt. 1971. The Capital Budgeting Decision. Macmillan, New York.
10. Schall, L. D., and C. W. Haley. 1977. Introduction to Financial Management. McGraw-Hill, New York.
11. Haley, C. W., and L. D. Schall. 1979. The Theory of Financial Decisions. McGraw-Hill, New York.
12. Haas, J. E., E. J. Mitchell, and B. K. Stone. 1974. Financing the Energy Industry. Ballinger, Cambridge, Mass.
13. Tillman, D. A. 1980. A financial analysis of silvicultural fuel farms on marginal lands. Ph.D. Dissertation, College of Forest Resources, University of Washington, Seattle, Wash.

14. Microeconomic Associates. 1978. Effect of Risk on Prices and Quantities of Energy Supplies. Electric Power Research Institute, Palo Alto, Calif.
15. Robert R. Nathan Assoc. 1978. Net Rates of Return on Innovations: Final Report. Vol. 1. Technical Report. Washington, D.C. (for the National Science Foundation).
16. Swabb, L. E. 1978. Liquid Fuels from Coal: From R & D to an Industry. Science 199(4329), 619-622.
17. Adams, M. R., C. W. Knudsen, and C. W. Draffin. 1977. Economic Evaluation by ERDA of Alternative Fossil Energy Technologies, in Synthetic Fuels Processing: Comparative Economics (Pelofsky, A. H., ed). Marcel Dekker, New York.
18. Beath, B. C. 1979. Guidelines for Economic Evaluation of Coal Conversion Processes. The Engineering Societies Commission on Energy, Washington, D.C.
19. Stobaugh, R. and D. Yergin (eds.). 1979. Energy Future: Report of the Energy Project at the Harvard Business School. Random House, New York.
20. Internal Revenue Service. 1977. Tax Information on Depreciation. Department of the Treasury, Washington, D.C.
21. Perry, H. 1978. Clean fuels from coal, in Advances in Energy Systems and Technologies, Vol. 1 (Auer, P., ed.), Academic Press, New York.
22. Stokes, C. A. 1979. Synthetic Fuels at the Crossroads. Technology Review, Aug/Sept. 25-33.
23. Whitaker, R. 1978. Scaling up coal liquids. EPRI Journal 3 (7) 6-13.
24. Slipecevich, C. M. et al. 1977. Assessment of Technology for the Liquefaction of Coal. National Research Council/National Academy of Sciences, Washington, D.C.
25. Anon. 1980. Builders' construction cost indexes. Engineering News Record 205(25):77.

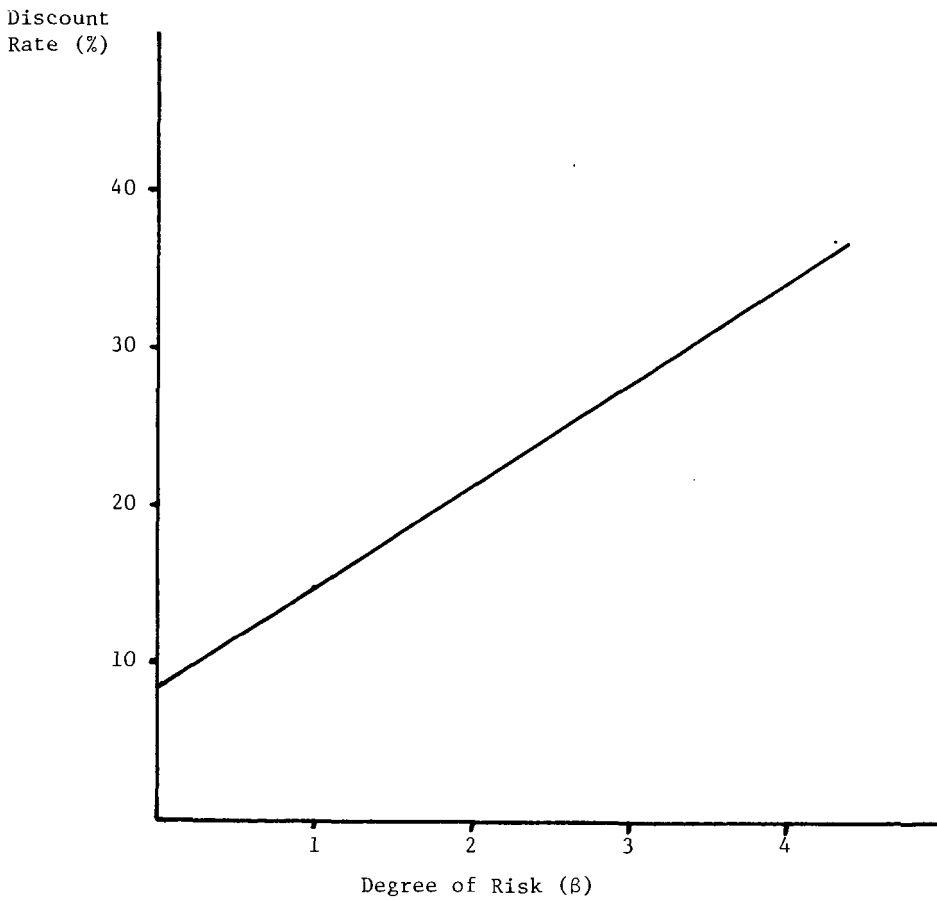


Figure 1. The discount rate, or cost of money, as a function of the degree of risk associated with the investment. This curve is known as the Security Market Line.

TABLE 1. Financial Assumptions for the 1976 American Chemical Society Meeting on Synthetic Fuel Economics

Parameter	Value
Project life	20 years
Cost of capital	10 percent
Depreciation	Straight line
Base Return on Investment ^a	15 percent

^aNot specified but reaquently used.
Source: [7]

TABLE 2. The Capital Structure of Three Petroleum Companies, 1979

Capital Instrument	Company		
	Gulf	Exxon	Mobil
Debt	.191	.112	.261
Preferred stock	-0-	-0-	-0-
Common stock	.809	.888	.739
Total	1.00	1.00	1.00

TABLE 3. The Cost of Capital for Three Petroleum Companies (in %)

Capital Instrument	Capital Cost Contribution by Company		
	Gulf	Exxon	Mobil
Debt portion	0.97 ^a	0.54 ^b	1.18 ^c
Common equity portion	11.6 ^d	16.3 ^e	14.0 ^f
Total	12.6	16.8	15.2

^a .191 x .570 x .089 x 100 = 0.97; .089 = Yield to Maturity on bonds.

^b .112 x .553 x .087 x 100 = 0.54; .087 = Yield to Maturity on bonds.

(Continued next page.)

c $.261 \times .524 \times .086 \times 100 = 1.18$; $0.86 =$ Yield to Maturity on bonds.

Second term in all above calculations = $1 - TR$ for domestic operations. Thus the tax effect of interest is accounted for in the discount rate calculation.

$$d \quad \frac{2.05}{30.75} + .076 = .143; .143 \times .809 = .116$$

$$e \quad \frac{4}{56.5} + .112 = .183; .183 \times .888 = .163$$

$$f \quad \frac{2.40}{42.625} + .135 = .190; .190 \times .739 = 14.0$$

General formula for d, e, f, is $\frac{D_e}{P} + G = K_{ceq}$ as defined as follows:

The cost of common equity capital is determined by $D_e/P + G_e = K_{ceq}$ where $D_e =$ expected dividend, $P =$ price, and $G_e =$ expected growth and $K_{ceq} =$ capital cost, common equity.

Sources: Annual Reports, 1978; Standard and Poor's Bond Guide, August, 1979; WSJ, August 28; Value Line.

TABLE 4. Real Price Increases 1968-1978

Good/Service	10 Yr Nominal Rate (%)	10 Yr Real Rate (%)
All goods and Services (CPI)	6.4	-0-
Labor		
Utilities	8.4	2.0
Chemical manufacturing	8.3	1.9
Fuels and Energy		
Coal	11.7	5.3
Electricity	9.3	2.9
Supplies		
Chemicals (Industrial)	8.3	1.9
Miscellaneous supplies	6.0	-0.4
Services	7.0	0.6

Sources: U. S. Census Bureau, 1978; U.S. Census Bureau, 1974; U.S. Bureau of Labor Statistics, 1980.

TABLE 5. Cost and Output Parameters for Selected Solvent Extraction and Methanol Plants

Parameter	Technology	
	Solvent extraction	Methanol
Plant size	50 x 10 ³ bbl/day 325 x 10 ⁹ Btu/day	11,300 tons/day 230 x 10 ⁹ Btu/day
Thermal efficiency	64%	46%
1977 capital cost total	\$0.9 - 1.15 x 10 ⁹	\$0.85 - 1.2 x 10 ⁹
1977 capital cost/bbl/day	\$16.5 - 21.5 x 10 ³	\$23 - 30 x 10 ³
Median 1980 capital cost (gross)	\$1.3 x 10 ⁹	\$1.3 x 10 ⁹
1980 investment tax credit	\$260 x 10 ⁶	\$260 x 10 ⁶

Source: [24].

TABLE 6. Pro Forma Statement for the Solvent Extraction Plant
30% Discount Rate (Values in \$ x 10⁶)

Cost/Income Stream	Year		
	1	5	13
Revenue	655	988	1677
Operating cost			
Fuel	223	347	841
Labor	6	8	15
Chemicals and supplies	14	18	31
Water and utilities	2	2	3
Maintenance	68	94	177
Taxes and insurance	16	20	37
Depreciation	200	103	27
Earnings before taxes	226	406	546
Income tax (46%)	104	187	251
Net income after taxes	122	219	295
Depreciation	200	103	27
Cash flow	322	322	322

Sources: Table 5 and [24].

TABLE 7. Pro Forma Statement for the Solvent Extraction Plant - 15% Discount Rate (Values in \$ x 10⁶)

Cost/Income Stream	Year		
	1	5	13
Revenue	507	731	1411
Operating cost			
Fuel	223	347	841
Labor	6	8	15
Chemicals and supplies	14	18	31
Water and utilities	2	2	3
Maintenance	68	94	177
Taxes and insurance	16	20	37
Depreciation	200	103	27
Earnings before taxes	(22)	139	280
Income tax (46%)	-0-	64	129
Net income after taxes	(22)	75	151
Depreciation	200	103	27
Cash flow	178	178	178

Sources: Table 5 and [24].

TABLE 8. Levelized Fuel Costs for Pioneer and Mature Coal Conversion Plants (in 1980 Dollars)

Coal Liquefaction System	Fuel Cost			
	Pioneer Plant		Mature Plant	
	\$/10 ⁶ Btu	\$/bbl	\$/10 ⁶ Btu	\$/bbl
Solvent extraction	8	50	7	40
Methanol	10	60	8	50

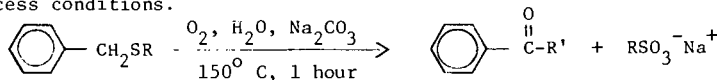
SYNTHETIC POLYMERS AS MODELS FOR COAL IN A DESULFURIZATION PROCESS

Thomas E. Schmidt, Thomas G. Squires and Clifford G. Venier

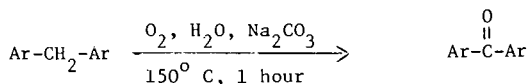
Ames Laboratory*, Iowa State University, Ames, Iowa 50011

Oxydesulfurization processes use air or oxygen to remove sulfur from coal for the purpose of converting high sulfur coal into an environmentally acceptable solid fuel (1). The desulfurization is mainly from the conversion of pyritic sulfur into sulfate and its removal when the coal is recovered from the aqueous slurry of the process (2). Because evidence for the removal of organic sulfur from coal could revitalize the now dormant status of oxydesulfurization as a method of coal beneficiation, we have been investigating the ability of these processes to degrade organic sulfur functions.

A direct comparison of a coal's organic sulfur content before and after process treatment is fraught with uncertainty due to the confusion in distinguishing the various forms of sulfur in coal (3). Therefore, our evaluation of the Ames Process, which employs oxygen and 0.2 M aqueous sodium carbonate at 200 psi total pressure and 150° C, has been based on the use of model compounds (4). In these investigations, the organic sulfur functional groups exhibited one of three kinds of behavior: direct autoxidation of the sulfur, indirect oxidation of the sulfur via autoxidation of an adjacent, benzylic C-H bond; and no reaction. Thiols and disulfides were directly oxidized to sulfonates which were stable under process conditions (i.e. no carbon-sulfur bond cleavage). Model compounds containing a benzylic sulfide function gave products (Equation 1) via a reaction pathway which is analogous to the autoxidation of benzylic C-H's in diarylmethanes (Equation 2). Other sulfides were recovered unchanged after one hour under Ames Process conditions.



R = methyl or phenyl, R' = H or OH



The further evaluation of the Ames Process with model compounds has been aimed at considering the relation between desulfurization and the autoxidative degradation of the substrate as a whole.

The evaluation of oxydesulfurization processes using simple model compounds is well suited for determining the reactivity of particular functional groups, but does not speak to effects on that reactivity when such are part of an extended hydrocarbon matrix. The influence of the proximate environment on the oxidation of sulfur functions is expected to be based on factors such as:

- 1) inhibition to mass transport of reagents or oxidation products;
- 2) competitive reactivity by hydrocarbon functions; and
- 3) intramolecular propagation of autoxidation.

In order to devise a model substrate for process evaluation in which sulfur is incorporated in a hydrocarbon matrix while maintaining the ability to describe the results in terms of functional group reactivity, we have prepared a series of synthetic polymers which meet the requirements outlined below :

*Operated for the U.S. Department of Energy by Iowa State University under Contract No. W-7405-Eng-82. This research was supported by the Assistant Secretary for Fossil Energy, Office of Coal Mining, WPAS-AA-75-05-05.

- 1) a high carbon, hydrogen and sulfur content,
- 2) a predictable average structure, and
- 3) sufficient crosslinking to impart insolubility.

Such polymers simulate some of the physical properties of coal and allow the recovery of the hydrocarbon content of the model as a solid product, which procedure is a basis of oxydesulfurization processes.

Materials

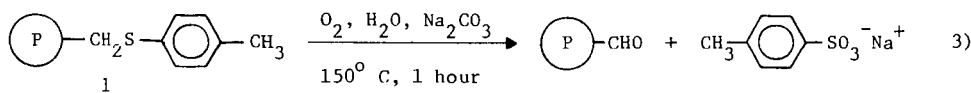
The modification, outlined in Figure 1, of chloromethylated polystyrene beads (Biobeads S-X1, 200-400 mesh, BioRad Laboratories, Richmond, CA) provides a convenient entry to several polymers meeting the above requirements as well as being comparable one with another. The preparation of a formaldehyde condensation polymer (Figure 2), which is closer than polystyrene to the H/C ratio of coals and is high in diarylmethane functions, was also carried out although this polymer is less defined as to its average size and structure. Similar condensation polymers, without sulfur, had previously been proposed as models for coal (5).

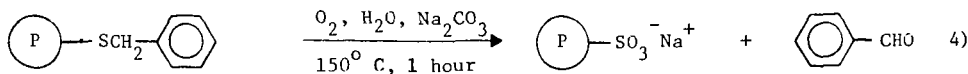
Experimental

The procedure by which the synthetic polymers were subjected to the Ames Process is described here. The dry polymer, 0.6 to 1.8 g, and 100 ml of 0.2 M aqueous sodium carbonate were placed in a 300 ml autoclave, which was flushed three times with nitrogen at 80 psi pressure, and the sealed autoclave was heated to the operating temperature. When the temperature had reached 150° C, oxygen was added to a total pressure of 200 psi and the autoclave was vented until the pressure was about 100 psi. The addition of oxygen was repeated twice, then the sealed autoclave was stirred at 1500 rpm for 1 h. while maintaining the temperature at 150 ± 10° C. In the case of these polymers, no significant amount of material was lost by the venting procedure. After cooling to room temperature the residual pressure (70 to 90 psi) was vented. The solid was collected by filtration, using 400 ml of distilled water to rinse the autoclave and wash the solid. The solid was successively washed with 30 ml portions of methanol, THF and benzene, then dried under reduced pressure and 80 to 90° C for at least five h. prior to weighing, recording the IR spectrum (KBr pellet) and submitting a sample for elemental analysis (elemental analyses were performed by Galbraith Laboratories, Knoxville, TN). The residue obtained by evaporation of the combined organic solvents exhibited PMR and IR spectra characteristic of polystyrene. In the case of (4-polystyryl)methyl 4-tolyl sulfide (1), sodium 4-toluenesulfonate in the residue of the aqueous phase was measured by its integral intensities in the PMR spectrum relative to *t*-BuOH as an internal standard. In the case of benzyl (4-polystyryl) sulfide (2), the aqueous phase was extracted with dichloromethane and benzaldehyde was found to be present in the extract in a yield of 19 % based on the amount of sulfur in 2.

Results

The effect of the Ames Process on the synthetic polymers was monitored by the degree of solubilization and the elemental analysis of the solid product. For polystyrenes, the formation of soluble polymers is a measure of the extent of autoxidation of the polystyryl backbone (6); this degradation will have no significant effect on the S/C ratio of the recovered solids. It is only when a C-S bond is more susceptible to autoxidative cleavage than the polymer backbone that a marked change in the S/C ratio can occur. This behavior is exhibited by polymers 1 (Table 1) and 2 (Table 2) which contain the benzylic sulfide function. The decrease in the S/C ratio in recovered polymer 1 and the increase in this ratio for recovered polymer 2 is explained by the facile autoxidation reactions shown in Equations 3 and 4.





While the extent of desulfurization and polymer solubilization of 1 over four seemingly identical runs (Table 1) were quite variable, there is a correlation between the two types of degradation, i.e. more desulfurization was accompanied by more solubilization. That radical initiation of autoxidation is important for both processes was shown by the fact that the inclusion of a specific initiator, 2,2'-azobis (2-methylpropionitrile) (AIBN), increased both desulfurization and solubilization of polymer 1. In contrast, the use of AIBN with 7 was counterproductive with respect to desulfurization. This result is entirely consistent with our earlier findings that DBT is inert to Ames Process conditions and with our postulate that C-S bond cleavage must be initiated by autoxidation of an α -H.

When coal is subjected to an oxydesulfurization process, indigenous labile functions can presumably initiate autoxidation. It has been reported for example, that the pyridine soluble portion of coal contains substances which promote the air oxidation of coal at 100^o C (7). To test whether a pyridine extract of coal could initiate the autoxidation of 1, we added such an extract to 1 under the conditions of the Ames Process. This result is reported in Table 1 and leads to the conclusion that the extract was not an effective initiator of autoxidation under these conditions.

Table 2 contains sulfur functions which are inert to the process conditions, i.e. DBT, DBTO₂ and ethyl phenyl sulfone; and, in these systems, autoxidation was not accompanied by desulfurization. This is especially evident with the condensation polymer 7, which is perhaps a better model for coal than polystyrene (8). The ability of the Ames Process to oxidize fluorene (4) suggested that 7 should undergo autoxidation. This was established on the basis of the degree of solubilization, the presence of carbonyl functions in the recovered solid (as detected by IR, 1715 cm⁻¹) and the incorporation of oxygen in the solid.

Conclusions

Although the Ames Process was designed to oxidize and remove sulfur from coal, these reaction conditions promote autoxidation of hydrocarbon functions as well, and the relative rates of hydrocarbon oxidation and organic sulfur removal are determined by the particular structure of each. Benzylic sulfides were the only case examined where C-S bond cleavage was significant precisely because of its greater susceptibility to autoxidation relative to the hydrocarbon part of the polymer. When incorporated into a hydrocarbon polymer, benzylic sulfides were found to be less reactive under the process conditions than the monomer benzyl phenyl sulfide (4). There is no indication that the hydroperoxides, which are formed by autoxidation of labile C-H bonds, react with sulfides to produce sulfoxides or sulfones under these conditions.

In this evaluation of the Ames Process with polymer models, we have shown that:

- 1) only benzylic sulfides undergo preferential C-S bond cleavage;
- 2) this cleavage is a radical process analogous to hydrocarbon autoxidation;
- 3) conditions which accelerate the oxidative cleavage of these C-S bonds will also increase the rate of degradation of the hydrocarbon matrix;
- 4) as expected, the rate of reaction of the benzylic C-S bond is attenuated when the sulfide is incorporated into an insoluble polymer.

Figure 1. Synthesis of Modified Polystyrenes for Use as Coal Models.

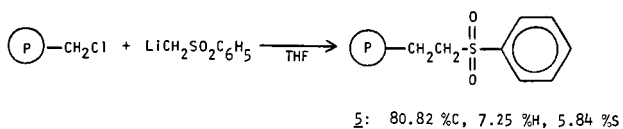
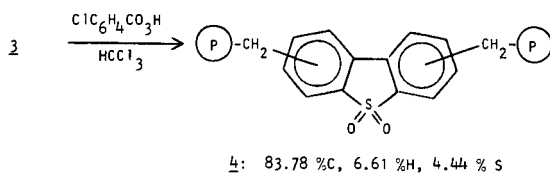
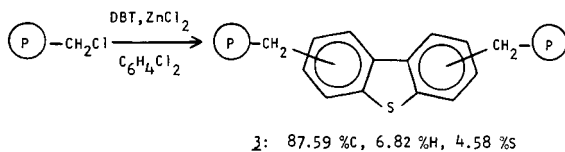
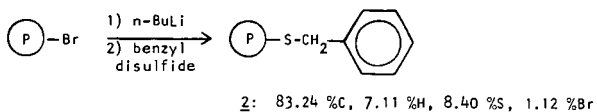
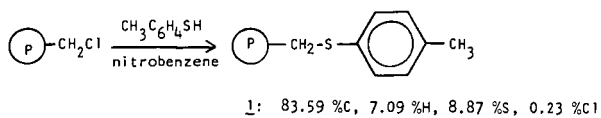


Figure 2. Hypothetical Structure for DBT/Fluorene/Formaldehyde Copolymer (7).

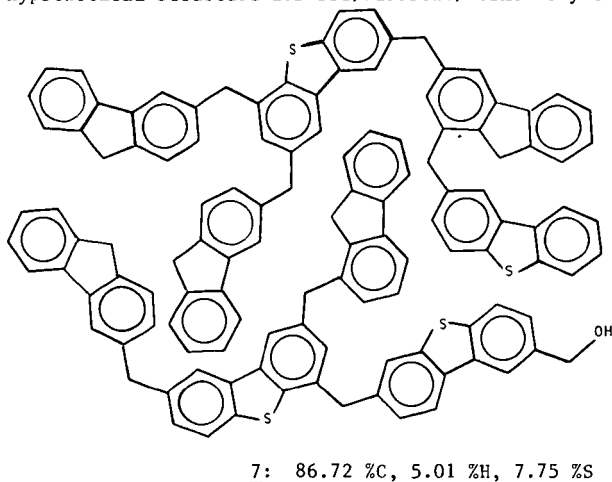


TABLE 1. Effect of Ames Process on (4-Polystyryl)methyl 4-Tolyl Sulfide (1).^a

Initial Wgt.	Recovered as a Solid ^b				% CH ₂ -S ^c Cleavage	4-Tolyl Sulfonate	Soluble ^d Polymer
	Weight	Carbon	Sulfur	ΔS/C			
0.91 g	84 %	81 %	57 %	-30 %	37 %	22 %	4.5 %
0.91	92	90	76	-16	21	28	2.7
1.14	93	91	76	-17	22	18	1.7
0.60	92	93	92	- 1	2	0.3	0
average of four	90	89	75	-16	20	17	2.2
1.00 ^e	89	88	76	-13	17		-
0.74 ^f	86	83	54	-34	42		9.3

TABLE 2. Effect of Ames Process on Some Synthetic Polymers.^a

Polymer	Initial Wgt.	Recovered as a Solid ^b				Soluble ^d Polymer
		Weight	Carbon	Sulfur	ΔS/C	
Polystyrene ^g	1.59 g	96 %	96 %	-	-	2.3 %
Polystyrene ^{g,h}	1.50	95	-	-	-	0.7
<u>2</u>	0.62	87	84	98 %	+17 %	3.2
<u>3</u>	0.78	96	96	97	+ 1	1.4
<u>4</u>	0.73	104	101	102	+ 1	1.0
<u>5</u>	1.16	94	95	96	+ 1½	0
<u>7</u>	1.06	89	87	88	+ 2	9.4
<u>7</u> ^f	0.90	95	92	95	+ 5	4.0

a) See Figures 1 and 2 for the structures of the polymers.

b) Presented as a percentage of the corresponding original values.

c) This is based on the loss of sulfur relative to the polystyryl carbon, which is the total carbon less the carbon due to the 4-tolyl groups, and is calculated as $100\% - 100\% \left(\frac{S_p C_i - 7S_p S_i}{S_i C_p - 7S_p S_i} \right)$ where S_p is the moles per unit weight of sulfur in the solid product, S_i is the moles of sulfur in the initial polymer, C_i is the moles of carbon in the initial polymer and C_p is the moles of carbon in the solid product.

d) Residue after evaporation of the organic solvents as a percentage of the initial weight.

e) Pyridine extract of an Ill. No. 6 coal, 0.1 g, was added to this run; the presence of the extract masked detection of soluble polymer.

f) With 0.16 g of AIBN added and oxygen added before heating the autoclave.

g) Biobeads S-X1, 200-400 mesh, prewashed with benzene and MeOH.

h) N₂ atmosphere only instead of O₂; elemental analysis not obtained.

REFERENCES

1. (a) S. Friedman, R.B. LaCount and R.P. Warzinski, in Coal Desulfurization, T.D. Wheelock, ed., A.C.S. Symposium Series, 64, 164-172 (1977); (b) S. Sareen, ibid., 173-181; (c) C.Y. Tai, G.V. Graves and T.D. Wheelock, ibid., 182-197.
2. T.D. Wheelock, R.T. Greer, R. Markuszewski and R.W. Fisher, Advanced Development of Fine Coal Desulfurization and Recovery Technology, Annual Technical Progress Report, Oct. 1, 1976-Sept. 30, 1977, submitted to the U.S. Department of Energy, Ames Laboratory, Iowa State University, Document No. IS-4363, March, 1978.
3. B. Paris, in Coal Desulfurization, T.D. Wheelock, ed., A.C.S. Symposium Series, 64, 22-31 (1977).
4. T.G. Squires, C.G. Venier, L.W. Chang and T.E. Schmidt, ACS Div. Fuel Chem., PREPRINTS, 26, No. 1, 50-55 (1981).
5. (a) P. Wolfs, D. Van Krevelen and H. Waterman, Brennstoff-Chemie, 40, 215-222, (1959); (b) L. Lazrov and S. Angelov, Fuel, 59, 55-58 (1979).
6. L. Dulog and K.-H. David, Die Makromolekulare Chemie, 145, 67-85 (1971).
7. V.A. Sukhov, et.al., Solid Fuel Chemistry (trans. of Khim. Tverd. Topl.), 10, (3), 96-100 (1976).
8. K.-D. Gundermann, G. Fledler and I. Knoppel, Brennstoff-Chemie, 29, 23-27 (1976).

PRODUCT YIELD AND HYDROGEN CONSUMPTION SELECTIVITY
TESTS FOR COAL LIQUEFACTION CATALYST DEVELOPMENT*

H. P. Stephens

Sandia National Laboratories, Albuquerque, New Mexico 87185

INTRODUCTION

Because hydrogenation of coal to liquid products (oils) is accompanied by distributions of complex by-product mixtures (IOM, preasphaltenes, asphaltenes and gases) which change as a function of reaction variables (time, temperature and pressure) and reactor configuration, the determination of selectivity relationships for coal liquefaction catalysts has been a difficult and time-consuming task involving numerous experiments to adequately describe catalyst performance over a range of conditions. This paper describes a method for analyzing the experimental results of coal liquefaction reactions which may be applied to a number of aspects of coal liquefaction research and process control, including: rapid selectivity and performance screening for catalysts; correlation of laboratory results with process parameters; and optimization of product yield for plant process conditions. Catalyst selectivity and performance screening will be emphasized here.

A primary goal of catalyst development for direct coal liquefaction is to maximize the yield of distillate products while minimizing the conversion to by-product hydrocarbon gases which unprofitably consume much of the hydrogen. Selectivity relationships for direct coal liquefaction catalysts have been difficult to determine and accurately describe, not only because of the complexity of the reaction mixtures, but also because of the difficulty of comparing the results of experiments performed at different times and temperatures or with different types of reactors. Imprecision in control of experimental variables such as temperature and contact time often causes significant differences in conversions for experiments for which the mean variables were designed to be nominally the same. Thus selectivity comparisons based on conversions at constant time and temperature are not entirely reliable.

The approach to selectivity relationships described in this paper is based on 1) a ternary product distribution diagram with a hyperbolic relation

$$y = \frac{x(c-x)}{a+bx} \quad 1)$$

between product and by-product conversions and 2) a hydrogen consumption diagram which relates the product conversion to the fraction of hydrogen consumed by the production of hydrocarbon gases. Each of these diagrams correlates, on a single curve, product distributions from reactions carried out over a wide range of experimental parameters, including temperature, time and different reactors.

Waterman first used ternary product distribution diagrams with reaction paths represented by

$$y = \frac{x(1-x)}{a+bx} \quad 2)$$

* This work supported by the U.S. Department of Energy.

to describe the catalytic hydroisomerization of paraffin wax (1) and later demonstrated their application to the characterization of many other complex chemical processes (2). Although the technique has been used to describe other hydrogenation processes (2,3), application to direct coal liquefaction has been unexplored. The results and analysis of direct coal liquefaction experiments described in this paper demonstrate the general applicability of ternary and hydrogen consumption diagrams to selectivity tests for coal liquefaction catalyst development.

EXPERIMENTAL

Materials

Liquefaction reactions were performed with Illinois No. 6 coal, SRC-II heavy distillate from the Ft. Lewis pilot plant (1:2 coal:solvent, by weight) and high purity hydrogen. An extensively used commercial HDS catalyst, American Cyanamid 1442A, an alumina supported CoMo formulation, was tested to establish base-line selectivity relationships. The catalyst extrudates were ground to a -200 mesh powder and added to the reaction feed slurry on a 5 weight percent coal basis. This quantity of CoMo/alumina was equivalent to 0.15% Co and 0.45% Mo. To test the utility of the selectivity relationships, additional microreactor experiments were performed with 0.3% Mo as molybdenum naphthenate (6% solution of molybdenum in naphthenic acid, obtained from Research Organic/Research Inorganic, Inc.), along with a control experiment with the equivalent amount of naphthenic acid alone.

Apparatus and Procedure

Two types of reactor systems were utilized, 30 cm³ batch microreactors (4), and a one-liter autoclave (5). For the low to moderate conversion range, microreactor experiments were performed at 1000 psig cold charge hydrogen pressure and over a wide range of times, $t = 0.5$ to 80 min, and temperatures, $T = 350^\circ$ to 425°C . Two autoclave experiments were conducted at 1000 psig and 425°C for 30 and 120 min to obtain data for high conversions. Temperatures and pressures were accurately recorded during the course of each experiment. Following the heating period of each experiment, the reaction vessel was quenched to ambient temperature, the resulting pressure was recorded, a gas sample was taken, and the product slurry was quantitatively transferred to a flask and subsampled for analysis.

Product Analysis

Gas samples were analyzed for mole percentages of CO, CO₂, H₂S and C₁-C₄ hydrocarbons with a Hewlett-Packard 5710A gas chromatograph, which was calibrated with standard mixtures of hydrocarbon gases and H₂S in hydrogen, obtained from Matheson Gas Products. Hydrogen in the samples was obtained by difference as the remainder of the product gas mixture. The quantity of each gas produced was calculated from the mole percent in the gas sample and the post-reaction vessel temperature T and pressure P using an ideal gas law calculation:

$$n_i = \frac{PV}{RT} f_i \quad 3)$$

$$w_i = FW_i n_i \quad 4)$$

where n_i = number of moles of component i
 f_i = mole fraction of i in the gas sample = mole %/100
 V = gas volume of reactor
 w_i = weight of i
 FW_i = the formula weight of i

Hydrogen consumed during the reaction was obtained as the difference between the initial charge and hydrogen remaining after the reactor was quenched.

The reaction product slurry was analyzed for insols, preasphaltenes, asphaltenes, and oils by tetrahydrofuran (THF) solubility and high performance liquid chromatography (HPLC). A 0.2 gm subsample was mixed with about 50 ml of THF, filtered to obtain the weight of insols, and brought to 100 ml with additional THF. Chromatograms of 5 μ l aliquots of the filtrate were obtained with a Waters Assoc. Model 6000A solvent delivery system equipped with a Model 440 uv absorbance detector. Separations of the solution into three fractions, preasphaltenes, asphaltenes, and oils, were effected on 100 A micro-syragal gel permeation columns. The uv absorbance response factors for the product separations were determined using standards prepared by dissolving known amounts of preasphaltenes, asphaltenes and oils obtained by soxhlet separation of whole liquid product from preparatory liquefaction experiments (6). Peak height measurement and response factors were used to calculate the percentages of preasphaltenes, asphaltenes and oils for the THF soluble product. All yield and conversion data were calculated on a dry mineral matter-free (dmmf) coal basis, which included a correction for the conversion of pyrite content of the coal to pyrrhotite.

RESULTS AND DISCUSSION

Process Course and Selectivity

Two ternary diagrams of product/by-product distributions for the coal liquefaction experiments previously described are shown in Figures 1 and 2. Conversion data for the various experiments are represented by the following symbols-- ● Co/Mo catalyzed; ■ Mo-naphthenate catalyzed; and □ naphthenic acid blank. In Figure 1, asphaltene conversion is plotted against oil conversion (both wt % dmmf basis) and in Figure 2, the sum of mole percent oil and asphaltene conversion is plotted vs mole percent hydrocarbon gas conversion. Because of the large difference between molecular weight of gases (CH_4 to C_4H_{10} -- 16-58) and other products (e.g., oils--200 to 400), the mole percent basis is used to more precisely represent the ternary diagrams involving hydrocarbon gases. For the purpose of calculating mole percentages, average molecular weights of 2400, 1200, 600 and 300 were assumed for the fractions of IOM, preasphaltenes, asphaltenes and oils. These values approximately correspond to the middle of the molecular weight distribution ranges for these fractions (7). Moles of gases produced were experimentally determined as previously described.

Figures 1 and 2 illustrate several general observations which can be made about the coal liquefaction process. First, although the liquefaction process is complex, involving myriad chemical species, its course can be quantitatively described by simple diagrams relating groups of compounds which react in similar and predictable manners.

These diagrams may roughly be considered the kinetic analog of equilibrium phase diagrams in which the number of components of a system is the smallest number of independently variable constituents. The composition of the liquefaction reaction mixture is given by the fractions explicitly represented by the x and y axes, and a remainder portion represented by the length of a horizontal tie line from a point on the curve to the diagonal axis connecting the x and y axes. For Figure 1, asphaltene and oil conversion are given by the y and x axis and preasphaltene, IOM and gases by the tie line. Second, the hyperbolic relationships for the conversion of the fractions shown in the figures represent unique reaction paths for the Co/Mo catalyzed reactions, over a wide range of operating conditions--time, temperature and reactor type. Deviations from this hyperbola represent conditions which change the process course, for example, the onset of competing pyrolysis reactions at high temperatures which form coke and gas. This indicates that the selectivity for a coal liquefaction catalyst, with respect to product groups, may be uniquely described by hyperbolic relationships. Support for this hypothesis is given by the analysis of the selectivity for a set of two unidirectional, consecutive reactions for which the selectivity may be described by relative concentrations given by hyperbolic equations of one constant (2, 8).

The utility of ternary diagrams and hyperbolic relationships exemplified by Figures 1 and 2 is that they may be used to rapidly screen for catalyst selectivity. Once hyperbolic relations are derived for a baseline catalyst, the selectivity of another catalyst may be screened by comparison of its product/by-product distributions for one or two experiments with the hyperbola of the baseline catalyst. It can be seen in Figure 1 that the point for the Mo naphthenate experiment falls below the curve for Co/Mo but above the blank experiment. This indicates that the order of asphaltene to oil selectivity is:

Blank < Mo-naphthenate < Co/Mo.

In Figure 2, the sum of the coal conversion products, oils and asphaltenes, are plotted as a function of unwanted by-product hydrocarbon gas conversion. Again, the Mo-naphthenate point falls between the Co/Mo curve and the blank. Thus Mo-naphthenate, at the concentration used is not as selective for asphaltene and oil conversion as Co/Mo, but does promote a better product/by-product ratio than the non-catalyzed experiment.

Hydrogen Consumption Diagram

Another useful relationship developed to determine the efficiency or selectivity of a hydrogenation catalyst with respect to process hydrogen consumption is illustrated in Figure 3, a plot of the sum of oil and asphaltene conversion (wt %, dmmf) as a function of the fraction of hydrogen consumed by production of hydrocarbon gases (the ratio of the weight of hydrogen in the hydrocarbon gases to the hydrogen consumed). Again, a wide range of experimental conditions for hydrogenation of coal catalyzed by Co/Mo can be represented by a single curve. This diagram provides a more significant selectivity test than the hyperbolic correlations in that it relates directly to a primary goal of catalyst development for direct coal liquefaction--maximizing the yield of distillate products with respect to hydrogen consumption. Figure 3 illustrates that hydrogenation efficiency of Co/Mo-catalyzed conversion of coal to oil and asphaltenes sharply

decreases above conversions of about 80%. Points representing experiments for other catalysts falling below the Co/Mo curve indicate that these catalysts are less efficient than Co/Mo with respect to hydrogen consumption. The point representing the Mo-naphthenate experiment falls close to the Co/Mo curve indicating an efficiency nearly equal to Co/Mo, while the blank experiment (naphthenic acid) shows that non-catalyzed coal conversion is much less efficient in hydrogen consumption.

REFERENCES

1. F. Breimer, H. I. Waterman and A. B. R. Weber, *J. Inst. Petroleum*, 43, 297 (1957).
2. H. I. Waterman, C. Bodhouwer and D. Th. A. Huibers, "Process Characterization", Elsevier, New York, 1960.
3. L. C. Doelp, W. Brenner, and A. H. Weiss, *I&EC Proc. Des. Dev.* 4, 92 (1965).
4. M. G. Thomas and D. G. Sample, "Catalyst Characterization in Coal Liquefaction", SAND-80-0123, Sandia National Laboratories, June 1980.
5. B. Granoff, et al., "Chemical Studies on the Synthoil Process: Mineral Matter Effects," SAND-78-1113, Sandia National Laboratories, June 1978.
6. A. W. Lynch, Sandia National Laboratories, personal communication, 1981.
7. D. D. Whitehurst, M. Farcasiu and T. O. Mitchell, "The Nature and Origin of Asphaltenes in Processed Coals," EPRI AF-252, February 1976.
8. A. H. Weiss, "Considerations in the Study of Reaction Sets," *Catalysis Reviews* 5, 1972.

Key to Figures

Number	Symbol	Reactor	Catalyst	T(°C)	t(min)
1	●	Micro	Co/Mo	350	15
2	●	"	"	375	15
3	●	"	"	425	0.5
4	●	"	"	400	15
5	●	"	"	425	10
6	●	"	"	425	15
7	●	"	"	425	40
8	●	"	"	425	80
9	●	Autoclave	"	425	30
10	●	"	"	425	120
11	■	Micro	Mo-Naphth	425	30
12	□	"	Blank	425	30

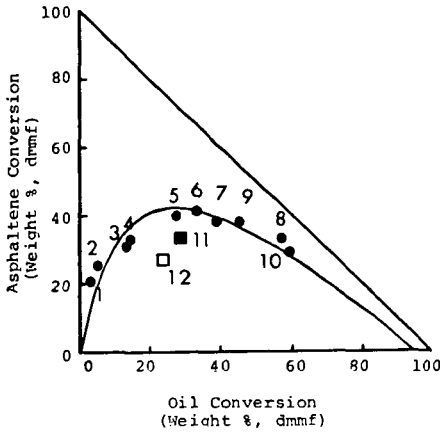


Figure 1. Ternary diagram of asphaltene vs. oil conversion. The curve, given by the equation

$$y = \frac{x(95-x)}{16.9+1.00x}$$

represents the process course for the Co/Mo catalyzed experiments.

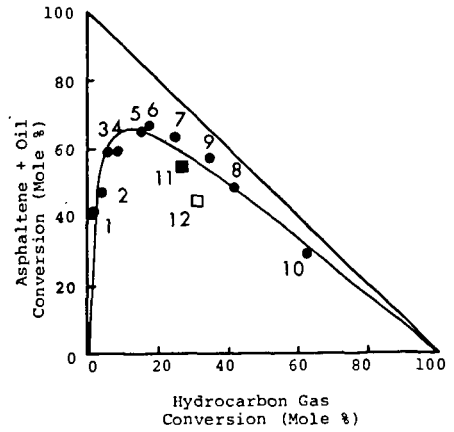


Figure 2. Ternary diagram of the sum of asphaltene and oil conversion vs. hydrocarbon gas conversion. The curve is given by the equation

$$y = \frac{x(100-x)}{2.35+1.15x}$$

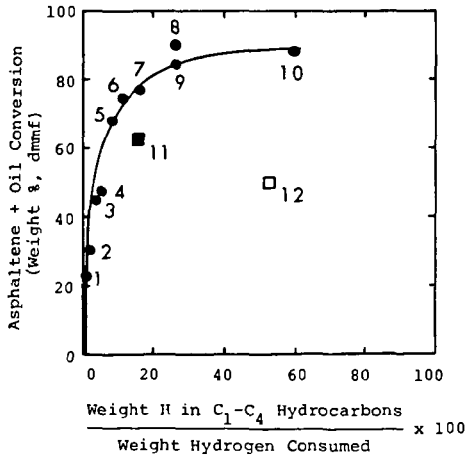


Figure 3. Hydrogen consumption diagram for direct coal liquefaction experiments. Curve represents Co/Mo catalyzed experiments.

The Effect of Pressure and Gas Composition
on the Fluidity of Pittsburgh No. 8 Coal

M. S. Lancet
F. A. Sim

Conoco Coal Development Company
Research Division
Library, PA 15129

INTRODUCTION

The Gieseler method⁽¹⁾ of measuring the fluidity of coal has long been a parameter used by the steel industry for the evaluation of coke oven feedstocks. This analytical technique in which the rotational speed of a rabble arm stirrer held in a packed sample of ground coal is measured as it is twisted with a known torque while the sample is heated through the plastic range, is a measure of the pseudo viscosity of the molten or semi-molten coal.

The interest in recent years in the gasification of Eastern U.S. bituminous coals has led to concern over potential coking and handling problems of these coals as they are fed to the gasifier. Conoco's experience with the gasification of two highly fluid Eastern coals during the DOE sponsored Technical Support Program for the British Gas/Lurgi slagging gasifier project suggested that these coals demonstrate significantly different coking and fluidity properties under gasifier conditions than they do at standard atmospheric conditions. Hence Conoco began a program for the evaluation of gasifier feedstocks which includes examining the coking properties at simulated gasifier conditions.

As a part of this overall program Conoco has designed and built a pressurized Gieseler Plastometer in which it is possible to measure the fluidity of coals in atmospheres of any desired composition and at total pressures up to 450 psig. The initial series of tests in this apparatus, reported here, is a study of the effect of nitrogen and hydrogen pressure on the fluidity of a Pittsburgh No. 8 seam coal. Nitrogen was chosen as an "inert" gas to examine only the effect of total pressure while hydrogen - probably the most reactive gas in a gasifier - was chosen as a first approximation to a gasifier gas.

EXPERIMENTAL

Apparatus

The basic apparatus consists of a Standard Instrumentation Model P-11R research version Gieseler Plastometer with the measuring head and solder pot mounted in a pressure vessel and the associated electronics located externally. Figure 1 is a design drawing of the apparatus. The pressure vessel is fabricated from a 30" long, 10" dia schedule 40 pipe, capped at the bottom and flanged at the top. A solder pot rests on a perforated steel plate at the bottom and the measuring head and crucible assembly are suspended from the top flange. A sight gauge is provided to insure proper alignment during the lowering of the crucible into the solder pot.

Electrical leads are passed into the pressure shell through conax pressure seal fittings. The vessel is pressurized through a half inch inlet port and the pressure is monitored during a run via a 0-600 psig pressure indicator. The vessel has a pressure relief valve set at approximately 550 psig to insure against accidental over pressurization. Figure 2 is a flow diagram for the pressurized Gieseler plastometer at Conoco Coal Development Company.

Procedure

The coal is sampled, ground and packed into the crucible in the standard manner.⁽¹⁾ The packed crucible assembly is then connected to the measuring head and the whole assembly is lowered, along with the attached top flange, into the pressure vessel. When the flange is flush with the top the crucible is at the proper position in the solder bath which is preheated to 320°C. After lowering, the flange is sealed and the vessel evacuated. The vessel is pressurized with the desired gas and, as soon as the solder pot temperature recovers to 320°C, the run is begun.

The sample is heated at a constant rate, normally 3°C/min, and the rotation of the rabble arm stirrer is constantly monitored and is printed out each minute. The unit of dial divisions per minute (DDPM) which is actually 100 times the rotational speed in RPM are the standard Gieseler fluidity units.

As the coal sample is heated it begins to soften and the stirrer begins to rotate. The point at which this occurs is called the softening temperature, T_S . Further heating the sample leads to an increase of the stirrer rotation until the maximum rate is reached at the temperature of maximum fluidity, T_M . Finally as the temperature of the coal is raised past T_M the fluidity begins to decrease until the temperature of resolidification, T_R , is reached. At this point all stirrer rotation stops and the sample is normally fully coked.

At the end of a run the vessel is depressurized and the sample, crucible and head assembly are removed for cleaning. A complete run requires about 1.5-2 hours.

Results and Discussion

The coal used in this work was from Montour No. 4 mine and is a high volatile, highly caking Eastern U.S. bituminous coal from the Pittsburgh No. 8 seam. The run of mine (ROM) coal was screened at 3/4" and only the washed +3/4" lumps were used in this work. The coal was stored in a sealed plastic bag and was ground for the Gieseler work just prior to use. Table 1 shows the proximate and ultimate analyses of this coal together with the energy content, the standard Gieseler fluidity and Free Swelling Index (FSI).

A total of 44 runs were made in this study, 23 with prepurified nitrogen and 21 with hydrogen. The results of these experiments are given in Table 2. The fluidity given at each point is the average of the maximum fluidity value from at least two runs and for the unpressurized cases, four runs. The agreement between duplicate runs was always better than $\pm 10\%$.

Since the maximum fluidity obtainable at standard Gieseler conditions of 1.40 oz.in (141 gm.cm) of torque is about 28,000 most of the data obtained here were at lower torque settings of either 0.45 oz.in (45 g.cm) or 0.30 oz.in (30 g.cm). All the data reported in terms of the standard torque value. This value was obtained by multiplying the measured fluidity by the ratio of standard torque to the torque value actually used (i.e., 3.11 or 4.67 for the two cases in this work). When duplicate runs were made using the different torque settings the agreement between the corrected fluidities was as good as that obtained for duplicate runs at the same torque setting. This suggests that, at least in the case of highly fluid coals, a coal in its plastic state may resemble a Newtonian liquid.

If it is possible to treat this coal as a Newtonian liquid we can, by calibration of our plastometer crucible and stirrer with viscosity standards, estimate the viscosity of the coal in its plastic state. Such calibration gives

the following relationship between "pseudo" viscosity, η (poise) and fluidity, F (DDFM).

$$\log_{10} \eta = -\log_{10} F + 7.257 \quad 1)$$

This suggests that the apparent viscosity of the Montour No. 4 coal used in this work, at the temperature of its maximum fluidity, lies between about 170 and 2000 poise.

Figure 3, a plot of the data in Table 2 clearly shows the effect that pressure has on the maximum fluidity of this particular coal. Initially, the fluidity is increased quite rapidly by raising the pressure of both hydrogen and nitrogen, however, while the effect is seen to continue almost linearly for the hydrogen pressure, the nitrogen pressure has only a limited effect above about 100 psig. These efforts are consistent with those observed by Kaiho and Toda⁽²⁾ who made a similar study for the medium fluidity, weakly caking Akabira coal. The initial large increase in maximum fluidity with pressure is probably due to the retarded rate of volatile evolution. With the more volatile and hence presumably less viscous components held in the "plastic" coal longer, an increase in maximum fluidity is logical.

Another, although seemingly less likely, possibility for the increased fluidity is the increased dissolution of the gas used and/or coal gases in the coal liquids which may lead to a decrease in the viscosity of the coal system and hence to an increase in the fluidity. The higher fluidities observed with nitrogen vs. hydrogen in the range 0-150 psig may be an experimental artifact caused by slightly lower heating rates for the hydrogen cases due to the higher thermal conductivity of hydrogen. It is known that heating rate is directly related to the fluidity of certain coals.⁽³⁾

As the pressure of the inert gas, nitrogen, is further increased, the leveling off of the fluidity may be due to approaching the limits of the effect of pressure alone on fluidity. Possibly pressures of 100-150 psig are sufficient to retard the escape of volatiles until the plastic coal has reached its temperature of maximum fluidity. Above these pressures it appears that any additional volatiles which are trapped have little effect on the fluidity.

The much more dramatic effect of hydrogen pressure on the maximum fluidity, Figure 3, is probably due to reactions between the hydrogen and components in the coal as well as the retardation of volatile escape. This observed hydrogen effect is, of course, consistent with the liquefaction of coal by very high pressures (\approx 2000 psig) of hydrogen at approximately the temperature of maximum fluidity.

While the pressure has a major effect on the maximum fluidity of the coal it shows almost no relation to the temperature of maximum fluidity. Also no effect of pressure on the softening point or the resolidification temperature was observed. Throughout this work the softening temperature was $360 \pm 5^\circ\text{C}$, the solidification temperature was $475 \pm 5^\circ\text{C}$ and the temperature of maximum fluidity was $435 \pm 5^\circ\text{C}$.

REFERENCES

1. Standard Method of Test for Plastic Properties of Coal by the Constant-Torque Gieseler Plastometer. ASTM Designation: D 2639-71.
2. Kaiho, M. and Toda, Y., Change in the Thermoplastic Properties of Coal Under Pressure of Various Gases. FUEL 58, 397 (May, 1979).
3. Van Krevelen, D. W., Huntjens, F. J., and Dormans, H. N. M., "Chemical Structures and Properties of Coal I VI--Plastic Behavior on Heating," Fuel 35, 462 (1955).

TABLE 1.

Analysis of Montour No. 4 Coal

<u>Proximate Analysis</u>		
Moisture	(%)	1.69
Ash	(%)	6.97
Volatile Matter	(%)	38.79
<u>Ultimate Analysis (Dry Basis)</u>		
C	(%)	76.81
H	(%)	5.16
N	(%)	1.73
S	(%)	1.35
O (By Diff.)	(%)	7.98
<u>Ultimate Analysis (MAF)</u>		
C	(%)	82.67
H	(%)	5.55
N	(%)	1.86
S	(%)	1.46
O (By Diff.)	(%)	8.46
<u>Energy Content (Dry Basis)</u>		
HHV (Btu/lb)		14,110
Free Swelling Index		7-1/2
Fluidity (DDPM)		9300

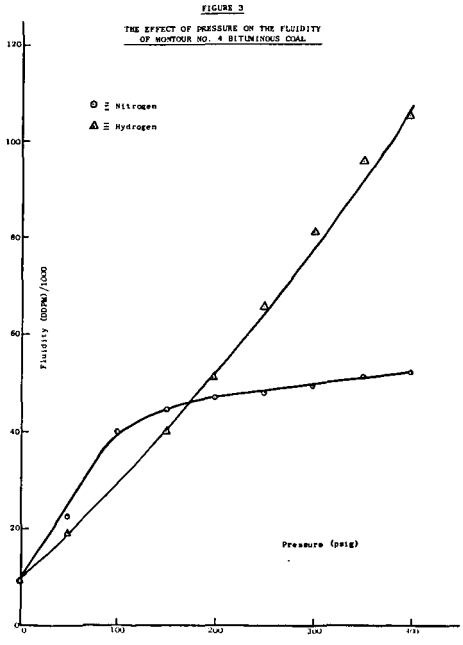
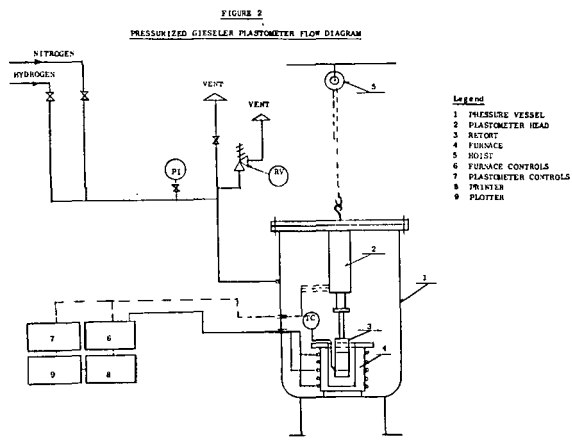
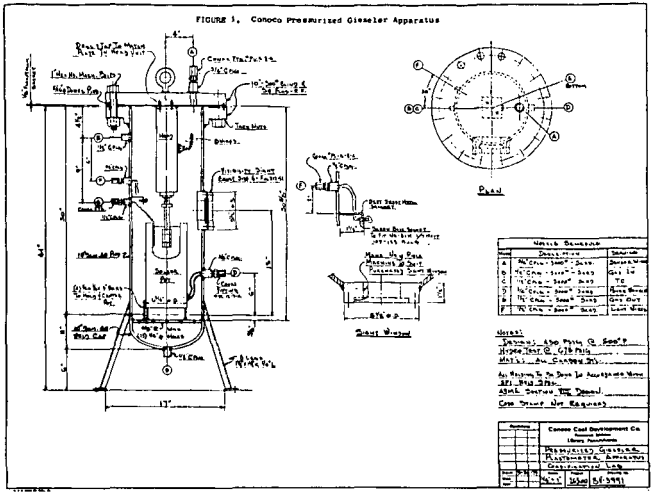
TABLE 2

Fluidity of Montour No. 4 Coal in Nitrogen and Hydrogen Atmospheres

<u>Gas</u>	<u>Pressure (psig)</u>	<u>Fluidity⁽¹⁾</u>
Nitrogen	0	9,300
	50	22,300
	100	38,800
	150	44,600
	200	46,800
	250	48,100
	300	49,100
	350	51,200
	400	51,900
Hydrogen	0	9,400
	50	19,400
	100	34,700
	150	40,000
	200	51,100
	250	65,900
	300	80,800
	350	95,100
	400	104,900

(1) Fluidity rounded to nearest 100 DDPM based on average of at least 2 measurements.

All runs at $3 \pm .1^\circ\text{C}/\text{min}$ heating rate.



DIFFUSION OF IONS INTO COAL: METHOD OF MEASUREMENT,
ORDER OF MAGNITUDE AND DIRECTIONAL EFFECTS

By: Attar, A. and Warren, D.

Dept. Chem. Eng., N.C.S.U., Raleigh, N.C. 27650

1. INTRODUCTION

Incorporation of metal ions from solution into the coal structure is becoming a useful method to achieve high contact between the coal surface and the metal ions. However, no data were found in the literature relative to the diffusivity of ions in coal. In this work, preliminary results are reported on the rate of diffusion of ions into coal and on the rate of leaching of ions from coal.

The main results found are that: 1) the diffusivity of ions varies in different directions of a vitrinite particle, relative to the direction of the bedding, and 2) the diffusion coefficient of calcium ions is of the order of 10^{-12} cm²/sec in the direction of the bedding and 10^{-13} cm²/sec in the direction perpendicular to the bedding.

2. EXPERIMENTAL

The coal particles to be examined were hot pressed (70°C, 15000 psi) in polymethyl metacrylate stubs, 3/4" in diameter and 3/8 - 1/2" thick. The stubs were cut through the coal particles and the exposed surfaces were polished under petroleum ether, using cloths 220, 400 and 600 successively. Finishing was done using 0.3 micron alumina powder in petroleum ether. The polished surface was sputtered with carbon and grounded with silver paint.

The surfaces were scanned using a 20000 Volt electron beam and the K_{α} x-rays from the calcium were collected within ± 2 eV. The resolution between the Ca (K_{α}) lines and the K (K_{β}) lines appears to be adequate to allow separation of the calcium.

Scanning of the coal surface was done at the rate of 3 microns/minute and plotted at either 3 microns/inch or 16 microns/inch. The total counts of x-rays were integrated and printed every 20 seconds.

3. MODES OF CALCIUM PENETRATION

The results that are obtained are a signal proportional to the number of atoms of calcium in a segment of volume of the coal specimen, with a shape of a droplet of tear, with an average length of about 6-10 microns and a diameter of 3-5 microns near the surface. This volume will be heretofore titled the "probe volume." Obviously, the signal obtained will not resolve differences in concentrations of calcium associated with features smaller than the probe volume and consequently the signal is only an average measure of the calcium present in the probe volume in all forms. A special mathematical method is being developed to "deconvolute" the signal in order to resolve finer features.

The main modes by which calcium could have penetrated into the coal are:

1. Penetration of Ca^{+2} through pores.
2. Diffusion of Ca^{+2} ions into the solid matrix and forming a Ca-containing intercolate.

Figure 1 shows the form of the signal expected when penetration of Ca occurs into the solid, through a pore oriented parallel to the direction of travel of the beam and through a pore presented perpendicular to the direction of travel of the beam. Since the diffusion coefficient in liquid is substantially larger than in solid, a relatively low incorporation occurs via the micropores ($r < 0.01$ M) and most of the calcium incorporation occurs via the mesopores and the macropores.

Several models can be used to interpret the experimental results. First, the models and their solutions will be described and then data will be presented and interpreted.

3.1 Effective Diffusion through a Thin Layer of Solid

In the case of a thin layer the unidirectional model is applicable.

Thus:

$$\frac{\partial c}{\partial t} = D_s \frac{\partial^2 c}{\partial x^2}, \quad (1)$$

$$c(0, x) = 0, \quad (2)$$

$$c(t, 0) = c_0, \quad (3)$$

and

$$c(t, \infty) = 0. \quad (4)$$

The solution is:

$$\frac{c}{c_0} = \operatorname{erfc} \left(\frac{x}{2\sqrt{D_s t}} \right). \quad (5)$$

x is the distance from the surface, D_s is the effective diffusivity coefficient, and t is the penetration time. The concentration at (x, t) is c and c_0 is the concentration near the surface. The error function complementary, erfc , is defined by:

$$\operatorname{erfc}(z) = 1 - \frac{2}{\sqrt{\pi}} \int_0^z e^{-u^2} du. \quad (6)$$

Obviously:

$$\int_0^\infty e^{-u^2} du = \frac{\sqrt{\pi}}{2} \quad (7)$$

was used to normalize the distributions.

Equation (5) is useful to interpret data for diffusion through a thin layer of solid or effective diffusivity through heterogeneous features smaller than the depth of penetration.

3.2 Effective Diffusion Through a Pore Full with Liquid

$$\frac{\partial c}{\partial t} = D_L \frac{\partial^2 c}{\partial x^2}, \quad (8)$$

$$c(0, t) = c_0, \quad (9)$$

$$c(x, 0) = 0, \quad (10)$$

$$\frac{\partial c}{\partial x}(\ell, t) = 0. \quad (11)$$

The solution is:

$$\frac{c}{c_0} = 1 - \sum_{n=1}^{\infty} \frac{4e^{-\lambda_n^2 D_L t}}{(2n-1)\pi + (-1)^{n+1}} \sin \lambda_n x \quad (12)$$

$$\lambda_n = \frac{(2n-1)\pi}{2\ell}. \quad (13)$$

The total material diffused after time t is:

$$M = - \int_0^t D \left(\frac{\partial c}{\partial x} \right)_{x=0} A dt = + 4Dc_0 \int_0^t \sum_{n=1}^{\infty} \frac{e^{-\lambda_n^2 D_L t} \lambda_n}{(2n-1)\pi + (-1)^{n+1}} dt$$

$$= - 4Dc_0 \sum_{n=1}^{\infty} \frac{1 - e^{-\lambda_n^2 D_L t}}{[(2n-1)\pi + (-1)^{n+1}] \lambda_n D_L}. \quad (14)$$

The use of equation (14) is not immediately obvious since the total area of pore mouth/unit mass, A , is not readily available and because λ_n depends on the distribution of pore lengths.

4. TESTS PERFORMED

The experimental tests performed can be divided into two classes:

- A. Tests used to develop the method.
- B. Tests on samples exposed to calcium acetate solution at room temperature and atmospheric pressures.

4.1 Method Development

The method that has been developed was described in the previous section. The possibility of inaccurate results due to overlap of consecutive scanning intervals should be addressed. Since the beam is about 4 microns in diameter and a printout is generated every twenty seconds, each printout represents counts taken over 4 microns diameter beam which moved 1 micron. Thus, the second printout will include counts taken from some of the calcium atoms which contributed to the first counts. In addition, since the electron beam damages the surface to some extent, the results may be distorted. The data show, however, that in three Ca curves almost on the same coal surface path, forward, backward and forward again, very little distortion occurred over about 200 microns.

4.2 Incorporation Tests

Samples of vitrinite from an Illinois #6 (Monterey Mine) and of the Colberg seam (W. Va.) were:

1. Leached with HCl 2:1 per 20 min.
2. Mixed with 0.05M calcium acetate solution at room temperature for 78 hours, dried and stored under nitrogen until fixed in the polymer.

The results on the HCl treated samples had a large statistical error built into them but show that:

1. Leaching of calcium occurs through a boundary layer.
2. The thickness of the leached layer is different in different directions of the seam.

For each leaching, the governing equation is:

$$\frac{c}{c_0} = \operatorname{erf} \left(\frac{x}{2\sqrt{D_e t}} \right) \quad (15)$$

The data collected for the first fourteen microns near the surface and the background information are tabulated in Table 1. In accord with equation (15), a plot of $x/(2\sqrt{D_e t})$ vs. x should give a straight line, with slope of $1/(2\sqrt{D_e t})$. The line will not necessarily intersect with the origin, since there is uncertainty relative to the exact location of the surface of the particle. Figure 2 shows that the slope of the line is 806.4 cm^{-1} which corresponds to $D_e = 1.68 \cdot 10^{-12} \text{ cm}^2/\text{sec}$ since the leaching time was 78 hours. Similar calculations for scans in different directions yielded values of D_e in the range of $10^{-9} - 10^{-13} \text{ cm}^2/\text{sec}$. However, it appears that $10^{-12} \text{ cm}^2/\text{sec}$ can be considered a representative number for this coal.

Many samples of coal were treated for periods of 1 hour to 5 days with excess solution of 0.05M calcium acetate in water. The samples were fixed in polymethyl methacrylate base, sputtered with carbon and analyzed as before. The data seem to indicate two modes of penetration of calcium: (A) by diffusion through the surface, and (B) by filling up of pores. Schematically, the calcium signal shows three types of behavior as the electron beam travels from the outside of the particle in (A) gradual decrease in calcium concentration in accord with the diffusion through the surface, i.e., $\operatorname{erfc} [x/(2\sqrt{Dt})]$; (B) large and reasonably fixed level of signal, corresponding to scanning along a pore; and (C) a Gaussian-shaped peak, corresponding to traveling across a pore.

Table 1. HCl leached coal

Distance from Coal Surface (microns)	Counts	$\frac{c}{c_0} = \frac{110}{c_0}$	$\text{erf}^{-1}\left(\frac{c}{c_0}\right) = \frac{x}{2\sqrt{D_e t}}$
-4	2	0.018	-
-3	1	0.009	-
-2	1	0.009	-
-1	3	0.027	-
0	3	0.027	-
+1	10	0.091	0.091
2	12	0.019	0.098
3	13	0.118	0.105
4	20	0.182	0.163
5	36	0.327	0.298
6	47	0.427	0.398
7	52	0.473	0.447
8	69	0.627	0.630
9	74	0.673	0.695
10	71	0.645	0.654
11	77	0.700	0.738
12	86	0.782	0.873
13	73	0.664	0.863
14	96	0.873	1.085

The results of scans of a sample of coal from the Colberg seam, West Virginia, in two orthogonal directions are described below. The data for the first 21 microns are given in Tables 2 and 3. Figure shows that the penetration in the vertical direction is much slower but more uniform than penetration in the horizontal direction. The effective diffusivity coefficient in the vertical direction is about two orders of magnitude smaller than in the horizontal direction.

Table 2. Scanning of Colberg seam coal in the direction of the grain

Distance from Surface (microns)	Counts	$\frac{c}{c_0} (c_0=1973)$	$\text{erfc}^{-1}\left(\frac{c}{c_0}\right)$
-2	1005	0.5094	-
-1	1019	0.5165	-
Coal Particle →	1973	1.0000	-
Surface	1	1860	0.9427
	2	1755	0.8899
	3	1520	0.7704
	4	1336	0.6771
	5	1139	0.5773
	6	941	0.4769
	7	818	0.4146
	8	725	0.3675
	9	566	0.2869
	10	591	0.2995
	11	461	0.2336
	12	442	0.2240
	13	444	0.2250
	14	424	0.2149

Table 3. Scanning of Colberg seam coal perpendicular to the direction of the grain

Distance from Surface (microns)	Counts	$\frac{c}{c_0}$ ($c_0=1973$)	$\operatorname{erfc}^{-1}\left(\frac{c}{c_0}\right)$
-21	60	0.1881	-
-20	61	0.1912	-
-19	74	0.2319	
-18	61	0.1912	
-17	71	0.2226	
-16	80	0.2508	
-15	93	0.2915	
-14	80	0.2508	
-13	106	0.3323	
-12	141	0.4420	
-11	166	0.9204	
-10	166	0.5204	
- 9	184	0.5768	
- 8	217	0.6802	
- 7	205	0.6426	
- 6	253	0.7931	
- 5	278	0.8715	
- 4	271	0.8495	
- 3	282	0.8840	
- 2	260	0.8150	
- 1	278	0.8715	
0	319	1.0000	0.0000
1	264	0.8276	0.1580
2	281	0.7555	0.2210
3	301	0.9436	0.0510
4	262	0.8213	0.1590
5	238	0.7461	0.2280
6	234	0.7335	0.2480
7	235	0.7367	0.2481
8	223	0.6990	0.2750
9	209	0.6552	0.3150
10	239	0.7492	0.2280
11	232	0.7272	0.2460
12	209	0.6552	0.3150
13	175	0.5486	0.4310
14	221	0.6928	0.2790
15	202	0.6332	0.3380
16	224	0.7072	0.2750

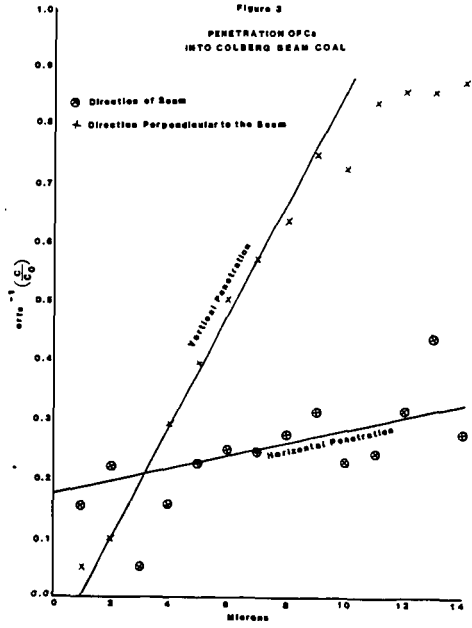
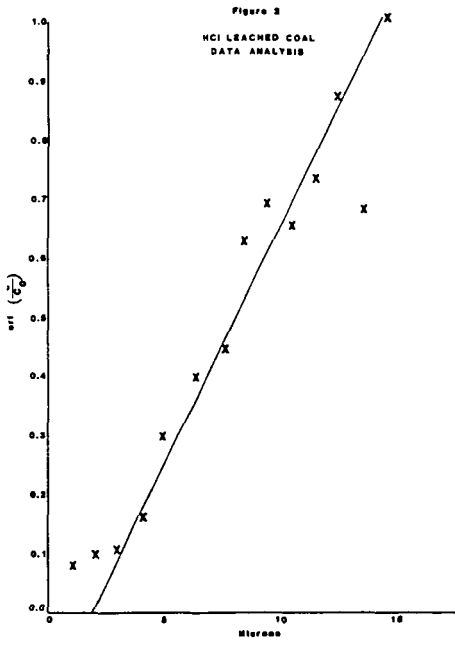
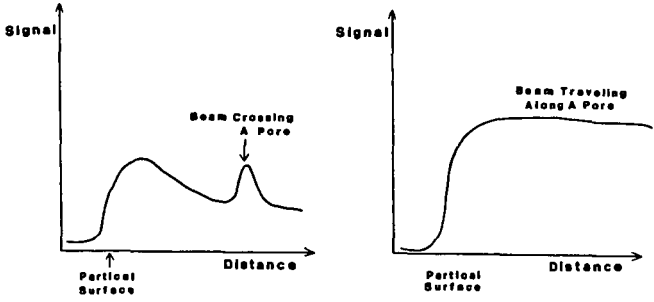
5. CONCLUSIONS

The main objectives of this study were achieved:

1. A method has been developed which allows examination of the penetration of calcium ions into coal.
2. The method was applied to study the penetration of calcium into coals.

The data show that calcium penetrates into coal in two main modes: via pores and via regular diffusion. The diffusivity coefficient in the horizontal direction relative to the seam is $10^2 - 10^3$ times larger than in the vertical direction. In the horizontal direction it is $10^{-8} - 10^{-11}$ cm²/sec while in the vertical direction it is of the order of $10^{-12} - 10^{-13}$ cm²/sec. $D_{\text{bedding}} = 7.6 \cdot 10^{-11}$ cm²/sec. $D_{\text{vertical}} = 9.7 \cdot 10^{-13}$ cm²/sec.

Figure 1
EFFECT OF DIFFERENT FEATURES
ON THE PROBE SIGNAL



Effect of Composition on Freezing Points of Model Hydrocarbon Fuels

W. A. Affens, J. M. Hall, S. Holt, R. N. Hazlett

Naval Research Laboratory, Washington, D. C. 20375

INTRODUCTION

Freezing Points of Jet Fuels

Jet aircraft are frequently exposed to low operating temperatures and it is essential that their fuels not freeze in these environments. Plugging of filters, pumpability, and related fuel system operational problems are dependent on freezing point, and for this reason, jet fuel specifications include requirements for maximum freezing point. Commercial jet fuel (Jet A, Aviation Turbine Fuel, ASTM D 1655-80), for example, is required not to freeze above -40°C . Military jet fuels, because of world wide operations, have even lower temperature requirements. The maximum acceptable freezing points for Air Force fuels (JP-4 and JP-8 Aviation Turbine Fuels, MIL-T-5624L and MIL-T-83133A respectively) are -58° and -50°C ; and the Navy's JP-5, (MIL-T-5624L, High Flash Point Aviation Turbine Fuel) has a maximum of -46°C .

The low temperature properties of a jet fuel (freezing point, pour point, viscosity), as well as some of its other properties, are controlled by the nature and concentrations of its components (chemical composition). Unfortunately, many components of a fuel which tend to lower freezing point (smaller hydrocarbons of higher vapor pressure), will also lower the flash point. In the case of JP-5, because of its relatively high minimum requirement for flash point (60°C) for reasons of ship safety, and its low maximum requirement for freezing point (-46°C), it is not always practical to produce JP-5 from all available crudes. These restraints limit the amount of JP-5 which can be produced from a barrel of crude oil and the problem exists for both conventional JP-5 (from petroleum) and for JP-5 from syncrudes.

Freezing Point and Composition

It has been known that molecular size and symmetry play an important part in the phenomenon of crystallization from solution and that this also applies to solutions of hydrocarbons. Dimitroff et al (1,2), studying the effect of composition on several types of fuels, found that the saturate fraction exerted the greatest influence on raising the freezing point and that the presence and amount of high-temperature freezing hydrocarbons had a major influence. They reported that in some cases the aromatic fraction was important and that in general all hydrocarbons play a part in fuel crystallization. Petrovic and Vitorovic (3) found a correlation between the sum of the concentrations of the three largest straight chain alkanes and freezing point in the jet fuels which they studied. Antoine reported on studies of 32 samples of jet

fuel derived from oil shale and coal syncrudes (4) and concluded that the concentrations of the long straight chain molecules in the fuels exert influence on the freezing point but are not the complete controlling factor. Solash et al (5) at this laboratory investigated jet fuels derived from various sources and reported that the freezing points were related to the amount of the largest n-alkane present (but not the total n-alkane concentration) in these fuels. These findings were not in agreement with the correlation of Petrovic and Vitorovic. Solash et al plotted $\log(\text{mol}\% C_{16})$ vs. the reciprocal freezing point of 11 fuels and found reasonable adherence to a solubility plot. They concluded that the freezing point of a fuel is not a simple function of fuel composition and that much more work must be done before a coherent theory of freezing point can be developed for multi-component mixtures.

It was decided to extend our freezing point studies to model hydrocarbon fuel mixtures, with emphasis on the higher n-alkanes, in order to learn more concerning the effect of composition on freezing point.

EXPERIMENTAL

Defining Freezing Point

"Freezing Point," as applied to jet fuels and related mixtures, is defined by the ASTM (6) as "...that temperature at which crystals of hydrocarbons formed on cooling disappear when the temperature of the fuel is allowed to rise". This, of course, is really a "melting point," since "freezing point" is the temperature at which crystals start to crystallize out. However, the two phenomena take place at almost equivalent temperatures, and the term "freezing point" will be used here because of its wide use in the fuel literature.

Determination of Freezing Point

Freezing points were determined by the ASTM method D2386 for aviation fuels (7) with some modifications. Temperature readings were made by means of a thermocouple (Type "J") - potentiometer-recorder system, and liquid nitrogen was used as the refrigerant. Stirring was done mechanically.

Hydrocarbons

The hydrocarbons used were 99% pure grade. The decalin (decahydronaphthalene) was found to consist of 62.7% (w/w) of the trans isomer and 37.3% cis isomer by gas chromatography. The "Isopar-M" kerosene consisted of a relatively high boiling, low freezing, narrow-cut isoparaffinic solvent whose average molecular weight was 191 (8).

RESULTS AND DISCUSSION

n-Alkanes in Isopar-M

Solutions of six n-alkanes ($C_{12} - C_{17}$) in Isopar-M at various concentrations (mol %) were prepared and their freezing points (T_m) determined. Reciprocal freezing points ($1/T_m$) vs log of concentrations are plotted in Figure 1 for each alkane. The temperature scale (ordinate) of the graph is reversed in order to show temperature increase going up the graph. It is seen in the figure that the data points fit the straight lines fairly well so that there is good adherence to a typical solubility plot (ideal freezing point curve). The lines shown in the graph were derived by means of a linear regression treatment of the data and are a best fit of the data. From their slopes and intercepts, heats (ΔH_m) and entropies (ΔS_m) of fusion and extrapolated freezing points ($T_{m,0}$) of the pure alkanes were calculated by means of the Van't Hoff ideal solubility equation (9-12), and the thermodynamic relationship between ΔS_m , ΔH_m and $T_{m,0}$ (13).

$$\ln X = - \frac{\Delta H_m}{RT_m} + \frac{\Delta H_m}{RT_{m,0}} \quad 1)$$

$$\Delta S_m = \frac{\Delta H_m}{T_{m,0}} \quad 2)$$

where R is the gas constant, and X represents molar concentration. This approximate equation, which describes the variation of freezing point with concentration, is based on several simplifying assumptions including that ΔH_m is independent of temperature, and that Raoult's law is obeyed. Derived freezing point data from the Isopar-M solutions are shown in Table I with literature values of pure n-alkanes (13, 14) shown for comparison.

It is seen in the table that the experimentally derived and literature $T_{m,0}$ values are in good agreement, but this is not always the case for ΔH_m and ΔS_m . For ΔH_m and ΔS_m , the agreement is good only for the even carbon numbered alkanes, but there is poor agreement for the odd numbered compounds. It has long been known (9) that freezing and melting point data of pure compounds in some homologous series often exhibit the phenomenon of "alternation". In these series, such as the n-alkanes, with each additional CH_2 group, alternately small and large increases in a given property are observed (9). This can be seen for each of the three properties in Table I for both the literature data for the pure alkanes, and the values derived from the Isopar-M solution freezing points. It has been shown (9) for the higher members of a homologous series, that ΔH_m and ΔS_m values fall on two linear curves when plotted against carbon number. In this work, the odd and the even carbon numbered alkane data also form two separate straight lines respectively when ΔH_m or ΔS_m are plotted against carbon number. There was, however, a much wider variation between the odd and even data points for the literature values than between that of the experimentally derived points in this study.

Solvent Effect

In a second set of freezing point experiments, the effect of solvent was investigated. Solutions were prepared for *n*-tetradecane, *n*-hexadecane, and naphthalene in different solvents and at several concentrations. In the case of *n*-hexadecane, some mixed solvents were also used and their compositions are shown in Table II. Freezing point data were plotted in the same manner as that of the alkanes in Isopar-M. Some of the *n*-hexadecane data for single solvents are shown in Figure 2. It is seen in the figure that the straight lines plotted fit the data fairly well for these four plots and this was also true for the other solutions. The solvent effect experimental data (T_m and X) were also treated by linear regression and the derived T_m^o freezing point data are shown in Table III. For each of the three solutes, the solvents are listed in order of increasing ΔH_m . Literature data (13, 14) for the pure solutes are included in the table for comparison. An examination of Figure 2 and Table III shows considerable variation in the derived data for each of the solutes in the different solvents. When a solid dissolves in a liquid and an ideal solution is formed, the process may be considered equivalent to melting of the pure solute at the lowered temperature at which solution is taking place, and the ideal solubility equation implies this concept (9-12). From the ideal solubility equation (or from the solubility plots in Figures 1 and 2), it follows that relative solubility bears an inverse relationship with T_m . At a given concentration, for a relatively good solvent, solution (melting) will take place at a lower temperature than that of a relatively poorer solvent. Similarly, at a given temperature, it can be shown that solubility increases with decreasing ΔH_m for systems which obey the ideal solubility equation. In general, both T_m^o and ΔH_m are approximate measures of relative solubility. For example, in Figure 2, it is seen that decalin (the lowest curve in the figure) is a relatively better solvent for *n*-hexadecane than secondary butyl benzene (the upper curve). The data in Table III also illustrate this concept. For C_{14} , in the three solvents shown in the table, *n*-heptane and Isopar-M are good solvents, and secondary butyl benzene, an aromatic compound, the poorest. The T_m^o for C_{14} in Isopar-M (280°K) is the same as that of the literature value for the pure C_{14} (279°K) within experimental error. For C_{16} in individual solvents, *n*-heptane, decalin and Isopar-M appear to be relatively good solvents, and secondary butyl benzene the poorest. The T_m^o values derived for decalin (289°K) and Isopar-M (290°K) solutions are the same as that of pure C_{16} within experimental error, but the *n*-heptane result (295°K) seems to be high. For C_{16} in mixed solvents, Solutions A, B and C are relatively good solvents, and Solution G the poorest. As seen in Table II, Solutions A, B and C consist chiefly of Isopar-M or Isopar-M and decalin which were shown above to be relatively good solvents for C_{16} . Again, the aromatic (Solution G) was the poorest. For naphthalene, as might be expected, Table III shows that secondary butyl benzene is a better solvent than Isopar-M. The T_m^o derived from the secondary butyl benzene solutions (374°K), however, is much higher than that of pure naphthalene (354°K). The naphthalene data are limited, however, to only two solvents at a limited number of concentrations.

Tertiary Solutions

In order to observe possible interaction between n-alkanes in a common solvent and its effect on freezing point, solutions of n-C₁₃ and n-C₁₆ in Isopar-M were prepared at several concentrations. Standard freezing point plots of $1/T_m$ vs. $\log n-C_{13}$ at several constant C₁₆ concentrations are shown in Figure 3. The 0% C₁₆ line in the graph is the curve for C₁₃ in Isopar-M from Figure 1. It is seen in the figure that the 0.17% C₁₆ data points fall on a parallel straight line, but at somewhat lower temperatures than that of the pure C₁₃ line. However, a change is observed for higher C₁₆ concentrations. The 0.42% C₁₆ curve consists of two lines of opposite slopes. The section of the curve above about 3% C₁₃ falls on the 0.17% C₁₆ line. The 0.84% and 1.69% C₁₆ data follow the pattern of the 0.42% C₁₆ curve but with decreasing slopes. The 4.25% C₁₆ line is horizontal, showing that changes in C₁₃ concentration have no effect, and that the C₁₆ has "taken over" the control of freezing point.

Two interesting observations were noted in Figure 3. First, for C₁₆ concentrations of 0.42, 0.84, and 1.69% C₁₆, addition of C₁₃ at the lower C₁₃ concentrations causes a reduction of freezing point. The second observation, which was unexpected, is that certain combinations of C₁₃ and C₁₆ in Isopar-M freeze at lower temperatures than that of the same concentration of either alkane alone in the same Isopar-M base stock. For example, the freezing point of 1.04% C₁₃ and 0.17% C₁₆ in Isopar-M was 207°K, whereas the freezing point of 1.04% C₁₃ (C₁₆ = 0) was 209°K and that of 0.17% C₁₆ (C₁₃ = 0) was 225°K. A similar solution of 3.11% C₁₃ + 0.42% C₁₆ froze at 218°K, whereas the freezing points of the single alkanes in Isopar-M were 221°K and 233°K respectively for 3.11% C₁₃ and 0.42% C₁₆.

The data in Figure 3 suggest that there has been interaction between the C₁₃ and C₁₆ in their mutual influence on the freezing points in Isopar-M solutions.

The freezing point-concentration plots for C₁₃ and C₁₆ in Isopar-M (Figure 1) show relatively close adherence to the ideal solubility equation suggesting a minimum of interaction between the individual solutes and solvent for either alkane. But, when together in the same solution, their mutual behavior is unexpected. The mutual solubility of two compounds is a qualitative measure of the extent of the interaction between their molecules, varying from simple departure from ideal behavior to actual compound formation between the two substances (12). In some cases, it is possible to explain deviations from ideality. Most commonly, the explanation is based on association to form dimers or trimers; compound formation between solute and solvent; or possibly dissociation of the solute to form two or more molecules (11). The last of these possible explanations (dissociation), however, would not be expected to apply to solutions of alkanes in hydrocarbon solvents. Another possible explanation is that the two alkanes form a eutectic type mixture. In the case of the C₁₃-C₁₆ in Isopar-M behavior, this is now under investigation. It is hoped that by isolating the crystals which form during freezing, and identifying them, an explanation of this behavior might be forthcoming. This work is still in progress.

SUMMARY AND CONCLUSIONS

A study was made of the effect of composition on the freezing points of model hydrocarbon jet fuel type mixtures. Solutions of higher n-alkanes (C_{12} - C_{17}) in several solvents were emphasized. Freezing points (T_m) of solutions of single alkanes were found to conform with the Van't Hoff ideal solubility equation. From the slopes and intercepts of plots of concentration ($\ln X$) vs $1/T_m$, heats (ΔH_m) and entropies (ΔS_m) of fusion, and extrapolated freezing points of pure alkanes ($T_{m,0}$) were derived. For an isoparaffinic base solvent (Isopar-M), the derived $T_{m,0}$ values were in good agreement with the literature values for the pure alkanes. For ΔH_m and ΔS_m , only the even carbon numbered alkanes exhibited values similar to literature data for the pure compounds. This alternating behavior for the n-alkanes series has been observed for melting point and other properties of the pure compounds. For alkanes in other solvents, considerable solubility effect was noticed. For C_{14} and C_{16} , decalin and Isopar-M were found to be relatively good solvents but aromatic compounds, such as butyl benzenes, were relatively poor. For naphthalene, butyl benzene was a better solvent than Isopar-M. For mixtures of C_{13} and C_{16} in Isopar-M, significant changes or reversals of slope were observed for $1/T$ plotted against $\ln X$ (C_{13} concentration) at various C_{16} concentrations, and this suggested interaction between the two alkane solutes. C_{16} had the predominant effect in $C_{13} + C_{16}$ solutions in Isopar-M. Above about 4% C_{16} , changes in C_{13} concentration had no observable effect.

REFERENCES

1. Dimitroff, E., Gray, Jr., J. T., Meckel, N. T., and Quillian, Jr., R. D., 7th World Petroleum Congress, Mexico City, April 1967, Individual Paper No. 47.
2. Dimitroff, E. and Dietzman, H. E., American Chemical Society, Petroleum Division, Preprints, 14, B-132 (1969).
3. Petrovic, K. and Vitorovic, D., J. Inst. Pet. 59, 20 (1973).
4. Antoine, A. C., "Evaluation of the Application of Some Gas Chromatographic Methods for the Determination of Properties of Synthetic Fuels," NASA Technical Memorandum 79035, November 1978.
5. Solash, J., Hazlett, R. N., Hall, J. M. and Nowack, C. J., Fuel, 57, 521 (1978).
6. American Society for Testing and Materials, Compilation of ASTM Standard Definitions, 4th Ed, 1979.
7. American Society for Testing and Materials, "Freezing Point of Aviation Fuels," ASTM D 2386-67.
8. Humble Oil and Refining Co., Isopar-M, Data Sheet DG-1P, 1968.
9. Cines, M. R., "Solid-Liquid Equilibria of Hydrocarbons," Chap. 8, Physical Chemistry of the Hydrocarbons, A. Farkas, Ed., Academic Press, New York, 1950, pp. 315-362.

10. Williams, A. G., "An Introduction to Non-Electrolyte Solutions," Wiley, New York 1967.
11. Skau, E. L. and Wakeham, H., "Determination of Melting and Freezing Temperatures," Chap. III, Physical Methods of Organic Chemistry, Techniques of Organic Chemistry, A. Weissberger, Ed., Vol. I, Part I., Interscience, New York, 1949, pp. 49-105.
12. Vold, R. D. and Vold, M. J., "Determination of Solubility," Chap. VII, Physical Methods of Organic Chemistry, Techniques of Organic Chemistry, A. Weissberger, Ed., Vol. I, Part I, Interscience, New York 1949, pp. 297-308.
13. Rossini, F., Pitzer, K. S., Arnett, R. L., Braun, R. M. and Pimentel, G. C., "Selected Values of Physical and Thermodynamic Properties of Hydrocarbons and Related Compounds," Amer. Petrol. Instit. Research Project 44, Carnegie Press, Carnegie Inst. of Technol., Pittsburgh, 1953.
14. American Chemical Society, "Physical Properties of Chemical Compounds," Volumes I and II, Advances in Chemistry Series #15 and 22, Amer. Chem. Soc., Washington, D. C. 1955, 1959.

Table I - Freezing Point Data - n-Alkanes in Isopar-M

n-Alkane	Heat of Fusion ΔH_m (Kcal/Mole)		Entropy of Fusion ΔS_m (Cal/Mol-deg.)		Freezing Point* $T_{m,o}$ (°K)	
	Exp.	Lit.	Exp.	Lit.	Exp.	Lit.
C-12	8.8	8.80	33.1	33.4	266	264
C-13	8.9	6.81	33.4	25.4	267	268
C-14	10.5	10.77	37.3	38.6	280	279
C-15	11.4	8.27	40.5	29.2	281	283
C-16	12.7	12.75	43.7	43.8	291	291
C-17	13.2	9.68	44.6	32.8	296	295

* - Extrapolated to 100%

Table II - Composition of Mixed Solvent (% w/w)

Solution	Isopar-M	Decalin	Tetralin	Butyl Benzene		
				(normal)	(secondary)	(tertiary)
A	40	40	-	-	20	-
B	40	40	20	-	-	-
C	80	-	20	-	-	-
D	80	-	-	-	20	-
E	80	-	-	6.7	6.7	6.7
F	50	25	-	-	-	25
G	-	-	-	33.3	33.3	33.3

Table III - Freezing Point Data - Solvent Effect

Solute	Solvent	Heat of Fusion, ΔH_f (Kcal/Mole) [†]	Entropy of Fusion, ΔS_f (Cal/Mole-Deg)	Freezing Point* $T_{m,0}$ (°K)
$n-C_{14}H_{30}$	$n-C_7H_{16}$	9.3	32.8	283
"	Isopar-M	10.5	37.3	280
"	sec-Butyl Benzene	11.3	39.0	291
"	(Liter.)	10.77	38.6	279
$n-C_{16}H_{34}$	$n-C_7H_{16}$	11.2	37.9	295
"	Decalin	11.9	41.3	289
"	Isopar-M	12.7	43.7	291
"	sec-Butyl Benzene	14.3	47.8	300
"	(Liter.)	12.75	43.8	291
"	Solution A	12.0	41.2	291
"	" B	12.4	42.6	290
"	" C	12.4	42.4	292
"	" D	12.6	42.8	294
"	" E	12.7	43.1	294
"	" F	12.7	43.4	293
"	" G	13.3	44.7	298
Naphthalene	sec-Butyl Benzene	3.9	10.4	374
"	Isopar-M	4.7	11.4	413
"	(Liter.)	4.32	12.21	354

* - Extrapolated to 100%

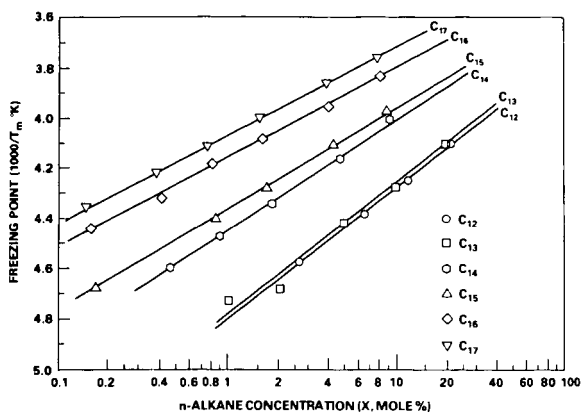


Figure 1 — Freezing Point vs Concentration — *n*-Alkanes in Isopar-M

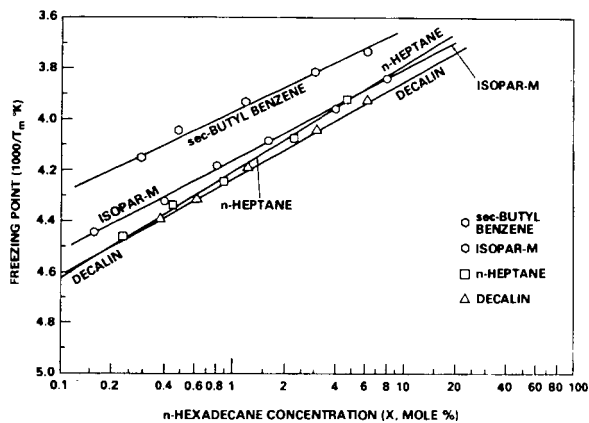


Figure 2 — Freezing Point vs Concentration — *n*-Hexadecane in Several Solvents

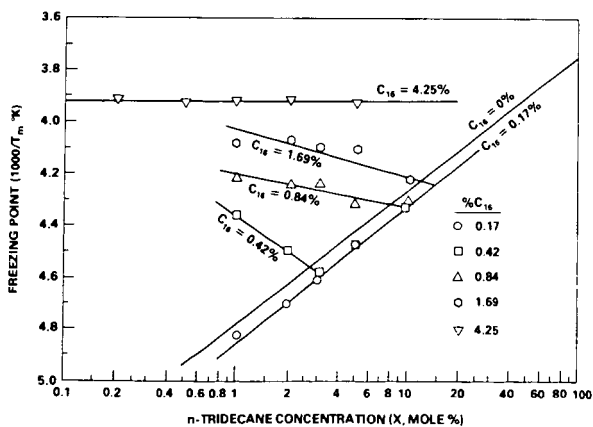


Figure 3 — Freezing Point vs *n*-Tridecane Concentration — *n*-Tridecane + *n*-Hexadecane in Isopar-M

Low-Rank Coals -- A Resource Not Fully Exploited

Irving Wender, Chemical and Petroleum
Engineering Department, University
of Pittsburgh, Pittsburgh, Pa. 15261

Total recoverable reserves of low-rank coals (subbituminous and lignite) are estimated in the hundreds of billions of tons. Almost all of this resource is located west of the Mississippi. Although increasing amounts of these coals are being used for utility purposes, less than 5% is cleaned prior to burning; probably larger amounts should be cleaned. The fact that these coals are not caking coals makes them suitable for use in certain gasifiers and the first plants for the conversion of coal to synthetic fuels will likely arise in the west. Historically coal science has largely been confined to the study of bituminous coals and there are several so-called models of 82-83% carbon coals. The structures of low-rank coals, however, remains largely a mystery. The constitution of low-rank coals, including oxygen functionality, and the effects of their mineral and moisture contents on reactivity and end use will be discussed.

PREMIUM TRANSPORTATION FUELS FROM SYNGAS. G. Alex Mills, Department of Energy, A-118, Germantown, Washington, D.C. 20545

There is an essential need for synthetic liquid transportation fuels. Indirect liquefaction involving coal derived syngas has gained new interest because of new discoveries in the catalytic synthesis of liquids from CO+H₂. Catalytic improvements have been made in the manufacture of CH₃OH and higher alcohols. Also, higher engine efficiency is made possible by a combination of high compression ratio and catalytic decomposition of alcohol to provide a gaseous fuel to the engine using heat otherwise wasted.

Conversion of CH₃OH over ZSM-5 zeolite catalyst to high octane gasoline is remarkable. Also, beginning with CO+H₂ mixtures, of special interest is the application of catalyts having dual functions (metal + acid) in combination with shape selective zeolites for control of both chemical composition and product molecular size. Further, the addition of a shift function to the hydrocarbon synthesis function makes possible the water gas shift in-situ in the reactor, thus permitting the use of syngas of low H₂/CO ratios, although with problems in simultaneous optimization of aromatization and shift reactions.

The Mechanism of Carbon Oxidation

Ralph T. Yang and Chor Wong
Department of Chemical Engineering
State University of New York at Buffalo
Amherst, New York 14260

Oxidation of single crystal graphite is being studied with the technique of etch-decoration and transmission electron microscopy, which was developed by Hennig et al. and Thomas et al. On the basal or (0001) plane, the carbon atoms surrounding the vacancy are the active sites, which are to be gasified and a circular pit is developed. Two sets of results have been obtained: (a) the rate of C removal per active site depends directly on the population density of the active sites; and (b) for low active-site densities, C removal continues for a prolonged period of time after O_2 is cut off from the gas phase.

Hundreds of crystals have been studied, which contained vacancies from 0.1 to 60 per μm^2 . The turnover frequency decreases with increasing vacancy density and levels off at a high density. For example, at 650°C and 0.2 atm O_2 (in Ar), the rate is 0.9 C/C/s for a vacancy density of $1/\mu m^2$; 0.6 C/C/s for $10/\mu m^2$; and levels off at about 0.5 C/C/s.

In the argon purge experiments, rates are measured during the purge after 10 min. of reaction with O_2 . The pit size is more than doubled during argon purge for surfaces with small vacancy densities, whereas no gasification occurs during argon purge with high vacancy densities.

Gasification of C on the edge sites with O_2 involves two independent processes: (a) direct collision by O_2 from gas phase (which follows the Langmuir-Hinshelwood mechanism), and (b) reaction with oxides which are chemisorbed on the basal sites and subsequently migrate to the active sites. Preliminary calculations indicate that the amount of chemisorbed oxide is 0.4 O per basal carbon for the surfaces with low vacancy densities, and that the surface diffusion coefficient is on the order of 10^{-11} cm^2/s , both at 650°C.

Catalysis in Coal Liquefaction

Sol W. Weller
State University of New York
at Buffalo

Efficient catalysts, useful at a level less than 1%, can play an important role in the primary liquefaction of coal. Most of our present knowledge of efficient catalysts derives from empirical catalyst screening performed decades ago. By contrast, our understanding of the organic chemistry of coal is advancing at an exponential rate. This understanding will permit formulation of reaction mechanisms that are more soundly based than the ad hoc mechanisms suggested in the past. Still to be tackled is the question of determining the precise role of multifunctional, efficient catalysts in the many reaction steps that occur during coal liquefaction. This paper presents an eclectic consideration of catalyst systems involving tin, molybdenum, or iron which are known to be effective in coal liquefaction in small concentration. Some of the topics to be discussed are the importance of catalyst distribution, the fate of catalyst components during liquefaction, and the chemical role played by the catalyst in accelerating the reactions occurring in liquefaction. The last problem is the least understood and presents the greatest challenge for future research.